1

The Crystal Chemistry of Sulfate Minerals

Frank C. Hawthorne
Department of Geological Sciences
University of Manitoba
Winnipeg, Manitoba, Canada R3T 2N2

Sergey V. Krivovichev and Peter C. Burns
Department of Civil Engineering and Geological Sciences
156 Fitzpatrick Hall, University of Notre Dame
Notre Dame, Indiana 46556

INTRODUCTION

Sulfur is the fifteenth most abundant element in the continental crust of the Earth (260 ppm), and the sixth most abundant element in seawater (885 ppm). Sulfur (atomic number 16) has the ground-state electronic structure $[Ne]3s^2 3p^4$, and is the first of the group VIB elements in the periodic table (S, Se, Te, Po). In minerals, sulfur can occur in the formal valence states S^{2-}, S^0, S^{4+}, and S^{6+}, corresponding to the *sulfide* minerals, *native sulfur*, the *sulfite* minerals, and the *sulfate* minerals. In the sulfide minerals, S^{2-} functions as a simple anion (e.g. $CuFeS_2$, chalcopyrite) and as a compound S_2 anion (e.g. FeS_2, pyrite). In the sulfosalts, S^{2-} functions as a component of a complex anion (e.g. AsS_3 in tennantite, $Cu_{12}As_4S_{13}$). In the sulfite minerals, S^{4+} has four valence electrons available for chemical bonding, and occurs in triangular pyramidal coordination with O. In the sulfate minerals, S^{6+} has six valence electrons available for bonding, and occurs in tetrahedral coordination with O. In addition, there are the *thiosulfate* minerals, in which S is in the hexavalent state, but is coordinated by three O^{2-} anions and one S^{2-} anion. Chemists frequently write the thiosulfate group as S_2O_3; however, we write it as SO_3S to emphasize that one of the S atoms is an anion and is involved in a tetrahedral group. Although the focus of this chapter is the sulfate minerals, we will deal also with the sulfite and thiosulfate minerals, as they occur in the same types of geochemical environments.

CHEMICAL BONDING

We adopt a pragmatic approach to matters involving chemical bonding. We use bond-valence theory (Brown 1981) and its developments (Hawthorne 1985a, 1994, 1997) to consider structure topology and hierarchical classification of structures, and we use molecular-orbital theory to consider aspects of structural energetics, stereochemistry and spectroscopy of sulfate minerals. These approaches are compatible, as bond-valence theory can be considered as a simple form of molecular-orbital theory (Burdett and Hawthorne 1993; Hawthorne 1994).

STEREOCHEMISTRY OF SULFATE TETRAHEDRA IN MINERALS

The variation of S–**Ø** (**Ø**: unspecified anion) distances and **Ø**–S–**Ø** angles is of great interest for several reasons:

(1) mean bond-length and empirical cation and anion radii play a very important role in systematizing chemical and physical properties of crystals;

(2) variations in individual bond-lengths give insight into the stereochemical behavior of structures, particularly with regard to the factors affecting structure stability;

1529-6466/00/0040-0001$10.00 DOI: 10.2138/rmg.2000.40.1

(3) there is a range of stereochemical variation beyond which a specific oxyanion or cation-coordination polyhedron is not stable; it is of use to know this range, both for assessing the stability of hypothetical structures (calculated by DLS [Distance Least-Squares] refinement) and for assessing the accuracy of experimentally determined structures.

Here, we examine the variation in S–**Ø** distances in minerals and review previous work on polyhedral distortions in SO_4 tetrahedra. Data for 206 (SO_4) tetrahedra were taken from 112 refined crystal structures with $R \leq 6.5\%$ (for a definition of R, see Ladd and Palmer 1994) and standard deviations of ≤0.005 Å on S–O bond-lengths. Ionic radii are from Shannon (1976).

The symbol ⟨ ⟩ signifies a mean value; thus ⟨S–O⟩ is the mean value of the four S–O distances in a sulfate tetrahedron. A grand ⟨ ⟩ value is the mean of a series of mean values; thus a grand ⟨S–O⟩ distance is the mean of a series of ⟨S–O⟩ distances.

Variation in ⟨S–Ø⟩ distances

The variation in ⟨S–O⟩ distances is shown in Figure 1a. The grand ⟨S–O⟩ distance is

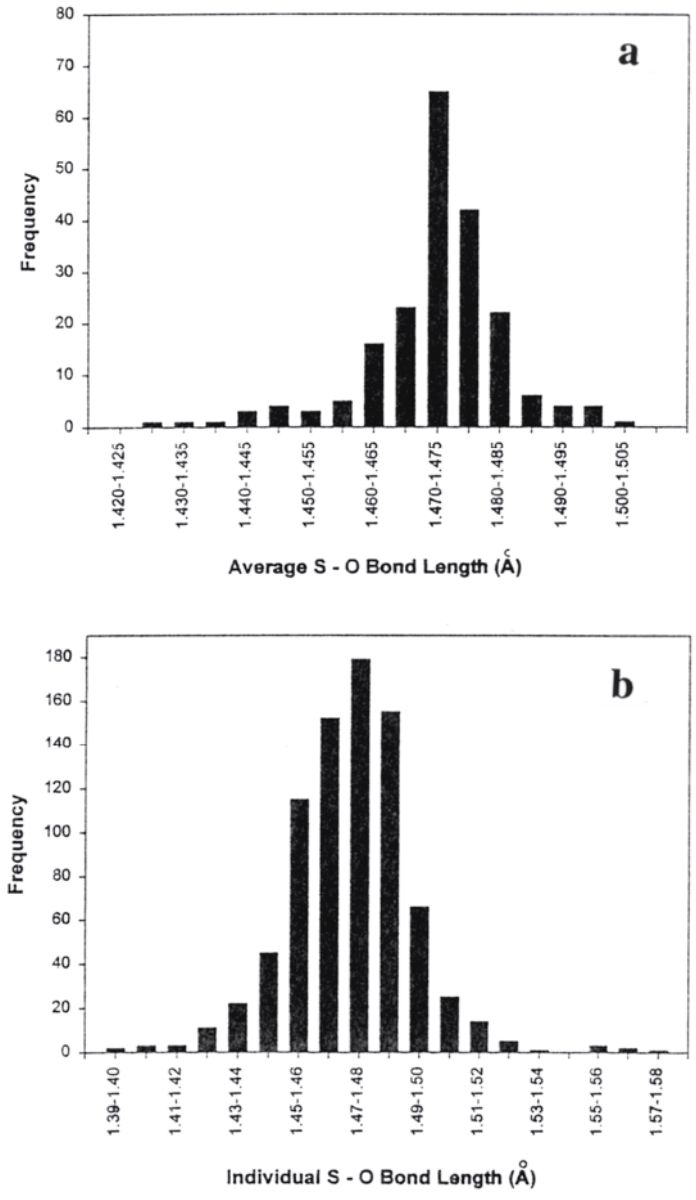

Figure 1. (a) Variation in mean S–O distance (n = 206), ⟨S–O⟩, in minerals containing (SO_4) tetrahedra; (b) variation in S–O distance (n = 824) in minerals containing SO_4 tetrahedra.

1.473 Å, the minimum and maximum ⟨S–O⟩ distances are 1.430 and 1.501 Å, respectively, and the range of variation is 0.071 Å. Shannon (1976) lists the radius of $^{[4]}S$ as 0.12 Å and the radius of $^{[3.25]}O^{2-}$ as 1.36 Å (assuming a mean anion-coordination number of 3.25); the sum of the constituent radii is thus 0.12 + 1.360 = 1.48 Å, in accord with the grand ⟨S–O⟩ distance of 1.473 Å. Brown and Shannon (1973) showed that variation in ⟨*M*–O⟩ (*M* = cation) distance can correlate with bond-length distortion Δ(= Σ[l(o)–l(m)]/l(m); l(o) = observed bond-length, l(m) = mean bond-length) when the bond-valence curve of the constituent species shows a strong curvature, and when the range of distortion is large. There is no significant correlation between ⟨S–O⟩ and Δ; this is in accord with the small degree of curvature of the bond-valence curve for S–O given by Brown (1981).

Variation in S–O distances

The variation in S–O distances is shown in Figure 1b; the grand mean S–O distance is 1.473 Å. The minimum and maximum observed S–O distances are 1.394 and 1.578 Å, respectively, and the range of variation is 0.173 Å; the distribution follows a skewed Gaussian curve. According to the bond-valence curve for S^{6+}–O (the universal curve for second-row elements) from Brown (1981), the range of variation in S–O bond-valence is 1.13–1.92 vu (valence units).

General polyhedral distortion in sulfate minerals

As noted above, there is no general correlation between ⟨S–O⟩ and bond-length distortion. However, as pointed out by Griffen and Ribbe (1979), there are two ways in which polyhedra may distort (i.e. depart from their holosymmetric geometry): (1) the central cation may displace from its central position (bond-length distortion); (2) the anions may displace from their ideal positions (edge-length distortion); Griffen and Ribbe (1979) designated these two descriptions as BLDP (Bond-Length Distortion Parameter) and ELDP (Edge-Length Distortion Parameter), respectively. Figure 2 shows the variation in both these parameters for the second-, third-, and fourth-period (non-transition) elements in tetrahedral coordination. Some general features of interest (Griffen and Ribbe 1979) are apparent from Figure 2:

(1) A BLDP value of zero only occurs for an ELDP value of zero; presuming that ELDP is a measure also of the O–*T*–O angle variation (*T* is a tetrahedrally coordinated cation), this is in accord with the idea that variation in orbital hybridization (associated with variation in O–*T*–O angles) must accompany variation in bond-length.

(2) Large ranges of BLDP are associated with small ranges of ELDP, and vice versa. The variation in mean ELDP correlates very strongly with the grand mean tetrahedral-edge length for each period (Fig. 3).

Griffen and Ribbe (1979) suggested that the smaller the tetrahedrally coordinated cation, the more the tetrahedron of anions resists edge-length distortion because the anions are in contact, whereas the intrinsic size of the interstice is larger than the cation which can easily vary its cation–oxygen distances by 'rattling' within the tetrahedron.

$S^{6+} \leftrightarrow T^{n+}$ substitution in minerals and its influence on (S,*T*)–O distances

In most sulfate structures, there is no cation substitution at the tetrahedrally coordinated S site. However, there are a few exceptions. Vergasovaite, $Cu_3O[(SO_4)((Mo,S)O_4)]$, is the only known mineral with $Mo^{6+} \leftrightarrow S^{6+}$ substitution. In this mineral, one of two tetrahedrally coordinated sites is occupied by both S and Mo, with a Mo:S ratio of about 3:1 (Berlepsch et al. 1999). Recently, Krivovichev et al. (unpublished results) studied a crystal of vergasovaite with the formula $Cu_3O[(SO_4)(MoO_4)]$, i.e. one site

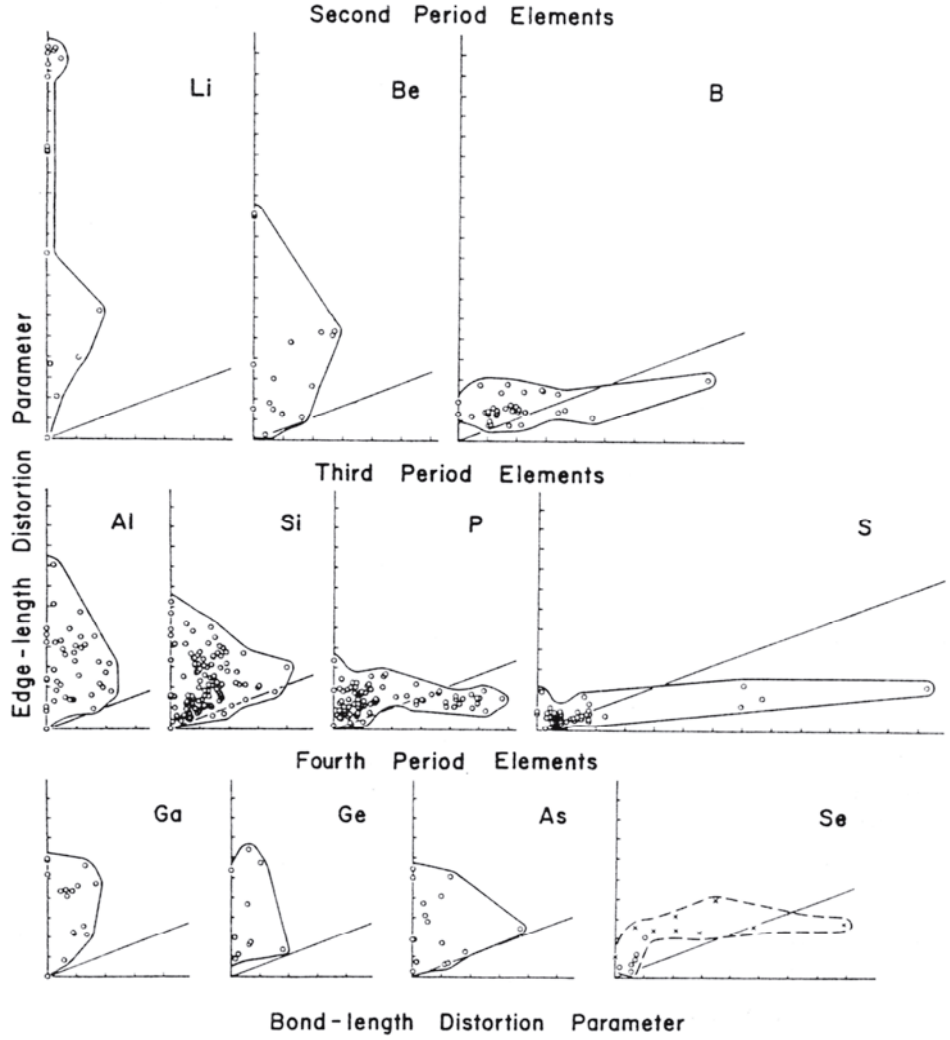

Figure 2. Variation in BLDP (Bond-Length Distortion Parameter) and ELDP (Edge-Length Distortion Parameter) for second-, third-, and fourth-period non-transition elements in tetrahedral coordination by oxygen (after Griffen and Ribbe 1979).

contained only Mo. The ⟨(Mo,S)–O⟩ distance reported by Berlepsch et al. (1999) is 1.715 Å, whereas the crystal studied by Krivovichev et al. has a ⟨Mo–O⟩ of 1.753 Å.

There are two minerals with proven $Cr^{6+} \leftrightarrow S^{6+}$ substitution. In hashemite, $Ba[(Cr,S)O_4]$ (Duesler and Foord 1986; Pasero and Davoli 1987), the Cr:S ratio is about 9:1, although a broad range of Cr^{6+}–S^{6+} substitution is known for its synthetic analogs. Carlosruizite, $K_6(Na,K)_4Na_6Mg_{10}\{(Se,S,Cr)O_4\}_{12}(IO_3)_{12}(H_2O)_{12}$ (Konnert et al. 1994), a Se analog of fuenzalidaite, is an interesting example of a structure in which Se^{6+}, S^{6+}, and Cr^{6+} occur at the same tetrahedrally coordinated site. There are twelve tetrahedrally coordinated cations in the unit formula of carlosruizite: 6.4 Se, 4.4 S, and 1.2 Cr. The mean ⟨(Se,S,Cr)–O⟩ is 1.588 Å, whereas the expected $^{[4]}$Se–O distance is about 1.63 Å. Heterovalent $P^{5+} \leftrightarrow S^{6+}$ isomorphism has been observed in woodhouseite, $Ca[Al_3(OH)_6((S_{0.5}P_{0.5})O_4)_2]$ (Kato 1977) and svanbergite, $Sr[Al_3(OH)_6((S_{0.5}P_{0.5})O_4)_2]$ (Kato and Miura 1977). Cahill et al. (submitted) determined the structure of mitryaevaite, $[Al_5(PO_4)_2\{(P,S)O_3(O,OH)\}_2F_2(OH)_2(H_2O)_8](H_2O)_{6.56}$, with $P^{5+} \leftrightarrow S^{6+}$ substitution at one of the tetrahedrally coordinated sites. The charge-balance mechanism in this structure can be described by the scheme: $[P^{5+}O_3(OH)]^{2-} \leftrightarrow [SO_4]^{2-}$. Beudantite, $Pb(Fe,Al)_3[(As,S)O_4]_2(OH)_6$ (Szymanski 1988), is an example of $As^{5+} \leftrightarrow S^{6+}$ heterovalent

Table 1. S–O and S–OH bond lengths in $SO_3(OH)$ groups in sulfate minerals.

Mineral	Formula	S–O (Å)	<S–O> (Å)	S–OH (Å)	Reference
matteuccite	$Na(HSO_4)(H_2O)$	1.446, 1.447, 1.458	1.450	1.578	Catti et al. (1975)
mercallite	$K(HSO_4)$	1.441, 1.443, 1.467	1.450	1.574	Payan and Haser (1976)
		1.438, 1.444, 1.475	1.452	1.565	Payan and Haser (1976)
letovicite	$(NH_4)_3H(SO_4)_2$*	1.455, 1.460, 1.461	1.459	1.529	Leclaire et al. (1985)

* in letovicite, the H atom is disordered over two positions

substitution; the tetrahedrally coordinated site contains 53.5% As and 46.5% S, with a ⟨(As,S)–O⟩ distance of 1.605 Å.

Hydrogen bonding in sulfate minerals

In general, each O atom in an (SO_4) tetrahedron receives ~1.5 vu (valence units) from the bond involving the S atom. The O–H bond of an hydroxyl group commonly has a bond valence of ~0.8 vu, and the acceptor anion receives ~0.2 vu. However, the bonds may be more symmetric, depending on local bond-valence requirements, and symmetrical hydrogen bonds, although rare, do occur: donor and acceptor anions each receive ~0.5 vu. The O atoms of (SO_4) tetrahedra commonly accept hydrogen bonds, consistent with their bond-valence requirements. Mercallite, $K(HSO_4)$ (Payan and Haser 1976), may contain an example of a symmetrical hydrogen bond. However, the H atom involved has a site-occupancy of 0.5, and the O···H distances are 1.66 and 1.85 Å instead of 1.2–1.3 Å that is typical for symmetrical hydrogen bonds.

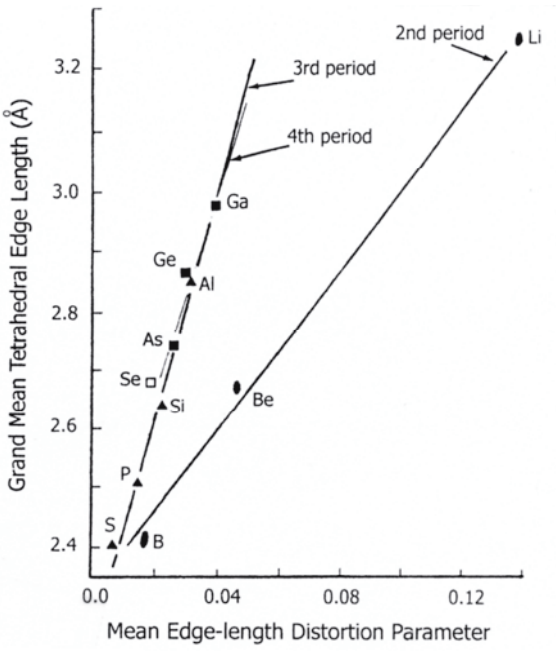

Figure 3. Variation in grand mean tetrahedral edge-length with mean ELDP for the second-, third- and fourth-period elements of the periodic table; redrawn from Griffen and Ribbe (1979).

The sulfate minerals mercallite, letovicite, and matteuccite involve sulfate tetrahedra that contain an hydroxyl group, i.e. acid-sulfate groups: $SO_3(OH)$. Owing to bond-valence requirements, the S–OH bond must be significantly longer than is typical for S–O bonds. The S–OH bond should have ~1.2 vu, which corresponds to an S–OH distance of ~1.58 Å (according to the curve of Brown 1981). The remaining S–O bonds in the tetrahedron must shorten to provide sufficient bond-valence to the cation. Table 1 lists S–O and S–OH bond lengths in mercallite, letovicite, and matteuccite. The observed bond lengths are in good agreement with bond-valence considerations. Kemnitz et al. (1996a) noted that S–O bonds are ~0.1 Å shorter than S–OH bonds in alkali-metal and ammonium hydrogen sulfates. The cation polyhedra, hydrogen-bonding systems, and other crystal-chemical aspects of alkali-metal hydrogen sulfates are reviewed by Kemnitz et al. (1996a,b).

Table 2. Thiosulfate compounds.

Formula				Cation/S_2O_3 Ratio	Reference
Na_2		S_2O_3		2	Teng et al. (1984)
Na_2		S_2O_3	$(H_2O)_{2/3}$	2	Hesse et al. (1993)
Na_2		S_2O_3	$(H_2O)_5$	2	Uraz and Armağan (1977)
Na_3	Au^{1+}	$(S_2O_3)_2$	$(H_2O)_2$	2	Ruben et al. (1974)
[1]K_2		S_3O_6		1	Christidis and Rentzeperis (1985)
K_2	S^{2+}	$(S_2O_3)_2$	$(H_2O)_{3/2}$	1.5	Marøy (1971)
Mg		S_2O_3	$(H_2O)_6$	1	Elerman et al. (1983)
Ni^{2+}		S_2O_3	$(H_2O)_6$	1	Elerman et al. (1978)
Cd		S_2O_3	$(H_2O)_2$	1	Baggio et al. (1997)
Ba		S_2O_3	H_2O	1	Aka et al. (1980)
Ba	Te^{2+}	$(S_2O_3)_2$	$(H_2O)_3$	1	Gjerrestad and Marøy (1973)

[1] contains $O_3S^{6+}–S^{2-}–S^{6+}O_3$ group

STEREOCHEMISTRY OF THIOSULFATE TETRAHEDRA

The thiosulfate group consists of a central S^{6+} cation surrounded by four anions, three O^{2-} and one S^{2-}, arranged at the vertices of a tetrahedron (Fig. 4); this group is conventionally written as S_2O_3, but it is much more informative to write it as ($S^{6+}O_3S^{2-}$). As sidpietersite, $Pb^{2+}_4(S^{6+}O_3S^{2-})O_2(OH)_2$ (Cooper and Hawthorne 1999), is the only thiosulfate mineral for which structural data are available, here we examine stereochemical variations in some synthetic thiosulfate compounds. These are listed in Table 2; all are refined to *R* indices between 2 and 9%, and provide us with 23 distinct thiosulfate groups.

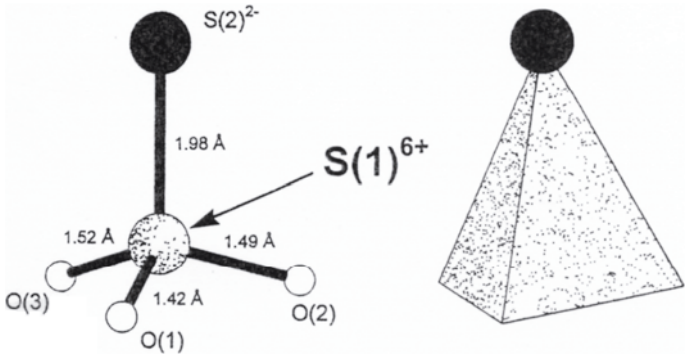

Figure 4. The thiosulfate group in sidpietersite shown as atoms (left) and as a tetrahedron (right) in which the S^{2-} anion is identified as a large black circle, S^{6+} is the random-dot-shaded circle, and O^{2-} are the unshaded circles.

Variation in ⟨S–Ø⟩ distances

The variation in $\langle S^{6+}–O\rangle$ distances in thiosulfate structures is shown in Figure 5a. The grand $\langle S^{6+}–O\rangle$ distance in thiosulfate compounds is 1.459 Å, the minimum and maximum $\langle S^{6+}–O\rangle$ distances are 1.429 and 1.476 Å, respectively, and the range of variation is 0.047 Å. The grand $\langle S^{6+}–S^{2-}\rangle$ distance is 2.038 Å, the minimum and maximum $S^{6+}–S^{2-}$ distances are 1.965 and 2.123 Å, respectively (Fig. 5b), and the range of variation is 0.158 Å. The grand $\langle S^{6+}–O\rangle$ distance of 1.459 Å is fairly close to the sum of the empirical radii of Shannon (1976) for $^{[4]}S^{6+}$ and $^{[3.25]}O^{2-}$: 0.12 + 1.360 = 1.480 Å ([3.25] is an average value for the coordination of O in sulfate minerals). However, there is no reason that the $\langle S^{6+}–O\rangle$ distance should be equal to the sum of the constituent radii as there is another ligand in the

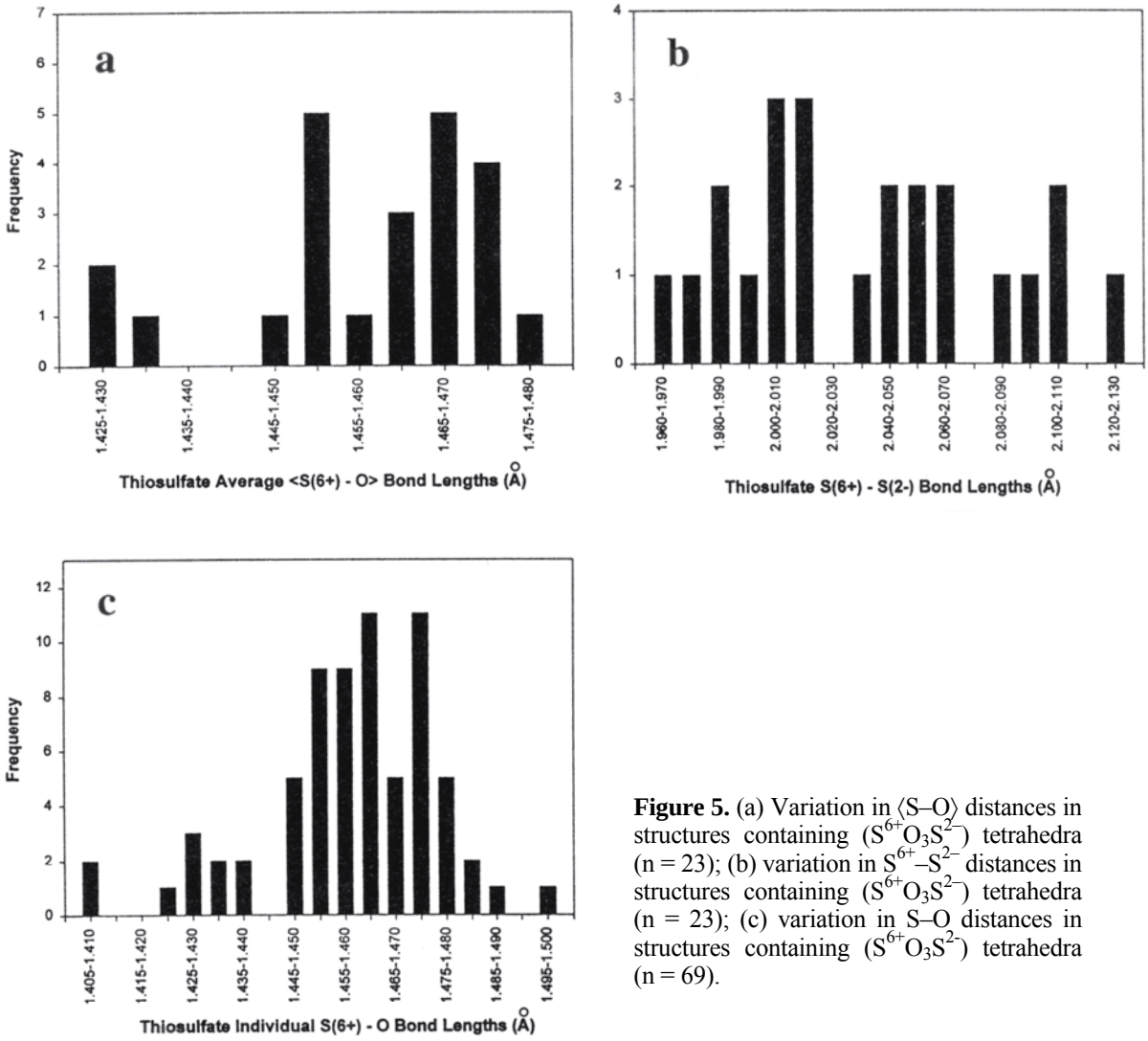

Figure 5. (a) Variation in ⟨S–O⟩ distances in structures containing ($S^{6+}O_3S^{2-}$) tetrahedra (n = 23); (b) variation in S^{6+}–S^{2-} distances in structures containing ($S^{6+}O_3S^{2-}$) tetrahedra (n = 23); (c) variation in S–O distances in structures containing ($S^{6+}O_3S^{2-}$) tetrahedra (n = 69).

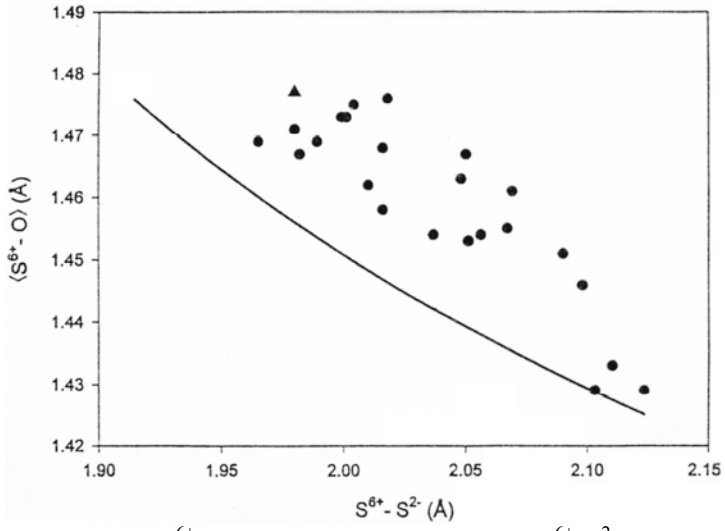

Figure 6. The ⟨S^{6+}–O⟩ distance as a function of S^{6+}–S^{2-} distance in thiosulfate groups from the synthetic compounds listed in Table 1 and sidpietersite (black triangle). The curve shows the relation for ideal bond-valence satisfaction at the central S^{6+} cation.

coordination polyhedron: S^{2-}. According to the valence-sum rule (Brown 1981; Hawthorne 1994, 1997), there should be an inverse relation between $\langle S^{6+}–O\rangle$ and $S^{6+}–S^{2-}$ in thiosulfate groups; Figure 6 shows this to be the case. The data for sidpietersite lie on the general trend, albeit near the lower end of the range of $S^{6+}–S^{2-}$ distances. The curve in Figure 6 shows ideal agreement with the valence-sum rule calculated using the observed ⟨S–O⟩ distances. There is reasonable agreement between the slope of the curve and that of the data, but the curve is displaced approximately 0.02 Å below the trend of the data. The bond-valence curve for S^{6+}–O can be considered as reliable. The value reported by Brese and O'Keeffe (1991) is the same as that reported by Brown (1981), and gives close-to-ideal bond-valence sums at S^{6+} in (SO_4) groups. The problem, therefore, is likely to be with the $S^{6+}–S^{2-}$ bond-valence curve of Brese and O'Keeffe (1991).

Variation in S–O distances

The variation in S^{6+}–O distances is shown in Figure 5c; the grand ⟨S–O⟩ distance is 1.459 Å. The minimum and maximum observed S–O distances are 1.408 and 1.497 Å, respectively, and the range of variation is 0.089 Å. According to the bond-valence curve for S^{6+}–O (the universal curve for second-row elements) from Brown (1981), the range of variation in S–O bond-valence is 1.41 to 1.83 vu. According to the bond-valence curve for $S^{6+}–S^{2-}$ (from Brese and O'Keeffe 1991), the variation in $S^{6+}–S^{2-}$ bond-valence is 0.87 to 1.33 vu.

The formal valences of S in the thiosulfate group

On the basis of XANES spectroscopy, Vairavamurthy et al. (1993) proposed that the valences of S in thiosulfate are 5^+ and 1^- instead of the conventionally assigned 6^+ and 2^-. This proposal may be tested in a very simple manner using structural data for sidpietersite and bond-valence theory. The bond-valence incident at the O anions of the thiosulfate group, from the rest of the structure, is calculated independent of the formal charges of S in the structure. The valence-sum rule (Brown 1981) states that the sum of the bond valences at an atom is equal to the magnitude of the formal valence of that atom. Hence the difference between the formal valence of oxygen (O^{2-}) and the sum of the bond valence incident at that oxygen (exclusive of the S–O bond) gives the bond valence of the S–O bond. Summing the bond valences thus calculated for the S–O bonds gives a value of 4.83 vu. If the formal charge on S^{6+} were actually 5^+, the bond-valence for the $S^{6+}–S^{2-}$ bond would be 0.17 vu. This result seems unlikely from several perspectives. First, the four long $Pb–S^{2-}$ bonds would be required to supply 0.83 vu, at a mean $Pb^{2+}–S^{2-}$ bond-valence of 0.21 vu. This requirement is not in accord with the incident bond-valence sums around the Pb sites, as it would require a bond-valence sum around one specific Pb site of ~2.36 vu. Second, it is unlikely that the thiosulfate group would be a prominent complex in aqueous solutions at a range of pH (and Eh) values if it were defined by such a weak $S^{6+}–S^{2-}$ bond. Third, it seems intuitively unlikely that a group involving such a weak bond would occur with such reproducible stereochemistry in a range of structures. Thus it does not seem possible that the formal valences of S in the thiosulfate group are 5^+ and 1^-.

STEREOCHEMISTRY OF FLUOROSULFATE TETRAHEDRA

The fluorosulfate group consists of a central S^{6+} cation surrounded by four anions, three O^{2-} and one F^-, arranged at the vertices of a tetrahedron: $(SO_3F)^-$. Reederite-(Y), ideally $Na_{15}Y_2(CO_3)_9(SO_3F)Cl$ (Grice et al. 1995), is the only known fluorosulfate mineral, and fortunately, structural data are available. Here, we examine stereochemical variations in 16 synthetic fluorosulfate compounds. These are listed in Table 3; all are refined to *R* indices between 2 and 9%, and provide us with 27 distinct fluorosulfate groups.

Table 3. Fluorosulfate compounds.

Cs	Sb^{5+}	$(SO_3F)_6$	Zhang et al. (1996)	(H_3O)	(SO_3F)	Mootz & Bartmann (1991)
Cs_2	Pt	$(SO_3F)_6$	Zhang et al. (1996)	H	(SO_3F)	Bartmann & Mootz (1990)
Cs	Au	$(SO_3F)_4$	Zhang et al. (1996)	I_2	$(SO_3F)_2$	Birchall et al. (1990)
Cs	H	$(SO_3F)_2$	Zhang et al. (1996)	Se_{10}	$(SO_3F)_2$	Collins et al. (1986)
Cs		(SO_3F)	Zhang et al. (1996)	(S_4N_4)	$(SO_3F)_2$	Gillespie et al. (1981a)
Ir	$(CO)_3$	$(SO_3F)_6$	Wang et al. (1996)	(S_6N_4)	$(SO_3F)_2$	Gillespie et al. (1981b)
Pd	$(CO)_2$	$(SO_3F)_2$	Wang et al. (1994)	Li	(SO_3F)	Zak & Kosicka (1978)
Sn		$(SO_3F)_2$	Adams et al. (1991)	$(XeF)_2(AsF_6)$	(SO_3F)	Gillespie et al. (1977)
Au_2		$(SO_3F)_6$	Willner et al. (1991)	(XeF)	(SO_3F)	Bartlett et al. (1972)
				NH_4	(SO_3F)	O'Sullivan et al. (1970)

Variation in S–Ø distances

The variations in S–O and S–F distances are shown in Figure 7. The ⟨S–O⟩ distance is 1.428 Å and the ⟨S–F⟩ distance is 1.540 Å. These values, and the distribution within Figure 7, are what one expects from bond-valence considerations. As the formal charge of F is 1^-, the S–F bond-valence must be ≤1 vu; hence the mean bond-valence of the S–O bonds must be ≥ (6 – 1)/3, i.e. ≥ 1.67 vu. This value translates into a maximum ⟨S–O⟩ distance of 1.440 Å, in accord with the observed ⟨S–O⟩ distance of 1.428 Å for SO_3F groups; this value also compares with the grand ⟨S–O⟩ value of 1.473 Å for SO_4 groups. For the bond-valence requirements at the central cation to be satisfied, one would expect an inverse relation between the S–F and ⟨S–O⟩ distances; however, this is not the case, as the data show only random scatter. According to the bond-valence curve for S^{6+}–O (Brown 1981), the range of S–O bond-valence is 1.33–2.56 vu. The latter value is not physically realistic; the maximum possible bond-valence of an S–O bond is 2.0 vu, which translates into a minimum possible S–O distance of 1.38 Å. Inspection of Figure 7 shows that five S–O values are less than this minimum possible distance, and hence must be in error.

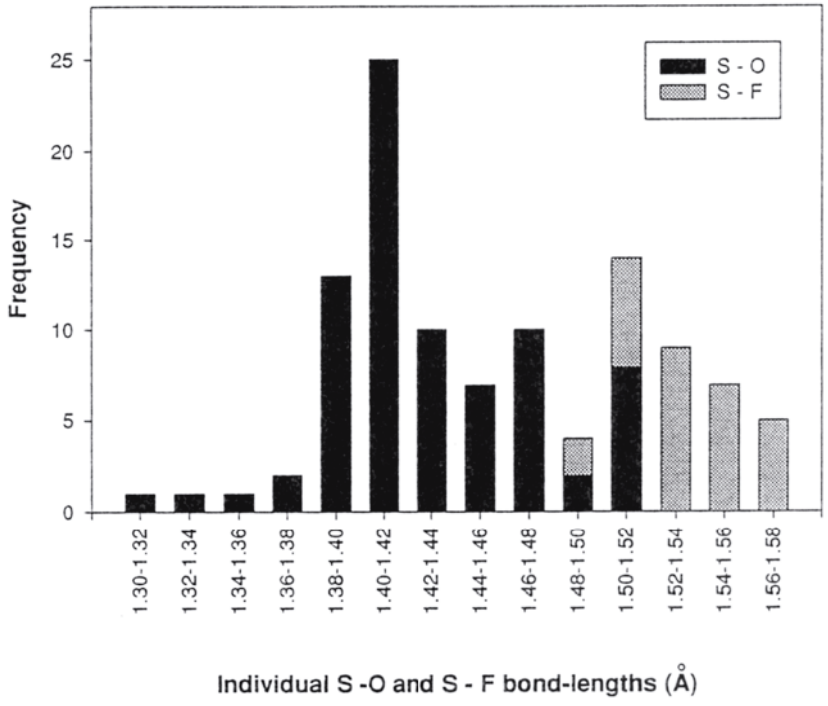

Figure 7. Histogram of S–O and S–F distances in fluorosulfate structures.

MOLECULAR-ORBITAL STUDIES OF SO_4 POLYHEDRA

Molecular-orbital (MO) calculations have been used by theoretical chemists for many years, primarily to predict geometries, energetics, and stabilities of molecules. MO methods are based on quantum mechanics, and range from empirical and semi-empirical methods, which include an experimentally determined component, to *ab-initio* methods, which include no experimentally determined parameters (for a summary of these methods, see Tossel and Vaughan 1992). MO methods have been applied with considerable success to the study of small molecules, and available computational sophistication and power have permitted application of MO methods to mineralogically relevant problems for the past two decades (Gibbs 1982).

Sulfate minerals have been the topic of a considerable number of MO calculations. To date, all MO calculations for these structures have been done using molecular clusters that are designed to be an approximation of the local environment in a structure; many long-range effects in a periodic structure are ignored by such calculations. The calculations for sulfate minerals involve various MO methods [extended Hückel (Bartell et al. 1970; Gibbs et al. 1972), Hartree-Fock self-consistent field (HF SCF) (Lindsay and Gibbs 1988; Ramondo et al. 1991; Sliznev and Solomonik 1996; Hill et al. 1997), density functional theory (DFT) (McKee 1996a,b; Wang et al. 1999)] applied to small clusters that model both individual (SO_4) polyhedra, and larger clusters that allow examination of such structural aspects as S–O–S bond angles, S–O bond lengths, and polyhedral linkages.

The role of 3*d*-orbitals in bonding in sulfates

Cruickshank (1961) stressed the role of 3*d*-orbitals in bonds between second-row elements and oxygen or nitrogen. Later, this hypothesis in its original form was criticized by Bartell et al. (1970) and finally rejected [see Cruickshank (1985) for an extensive review]. However, *ab initio* studies show that it is essential to include *d*-functions in the basis sets used for calculations involving third-row elements, and that the 3*d*-functions strengthen (and shorten) the S–O bonds significantly (Cruickshank 1985; Cruickshank and Eisenstein 1985, 1987).

Stability of the $(SO_4)^{2-}$ tetrahedron

Calculations have shown that an isolated $(SO_4)^{2-}$ tetrahedron is not stable (Boldyrev and Simons 1994): additional ions or molecules are essential to stabilize the tetrahedron (McKee 1996a,b; Wang et al. 1999). Four (H_2O) molecules and $(SO_4)^{2-}$ form relatively stable $(SO_4(H_2O)_4)^{2-}$ anions in the gas phase (Blades and Kebarle 1994). The equilibrium geometry of the $(SO_4(H_2O)_4)^{2-}$ cluster has been calculated by McKee (1996a,b) using DFT. The S–O distances obtained were 1.521 and 1.531 Å, values that are longer than those observed in crystals.

(H_2SO_4) and ($H_2S_2O_7$) clusters: prediction of equilibrium geometry

Lindsay and Gibbs (1988) and Hill et al. (1997) studied the minimum-energy geometries of (H_2SO_4) and ($H_2S_2O_7$) clusters (Fig. 8). These clusters contain three different types of oxygen atoms: O_{nbr}: non-bridging oxygen atoms bonded to S atoms only; O_{br}: bridging oxygen atoms bonded to two S atoms in the ($H_2S_2O_7$) cluster; OH: oxygen atoms bonded to both S and H atoms. Table 4 gives a comparison of the geometric parameters calculated by Lindsay and Gibbs (1988) and Hill et al. (1997), and the parameters observed in crystal structures of H_2SO_4 (Kemnitz et al. 1996c) and $H_2S_2O_7$ (Hoenle 1991). Data in Table 4 show good agreement between calculated and observed geometries. Note that S–OH distances are ~0.1 Å longer than S–O_{nbr} distances, consistent with the findings of Kemnitz et al. (1996a) for alkali-metal hydrogen sulfates.

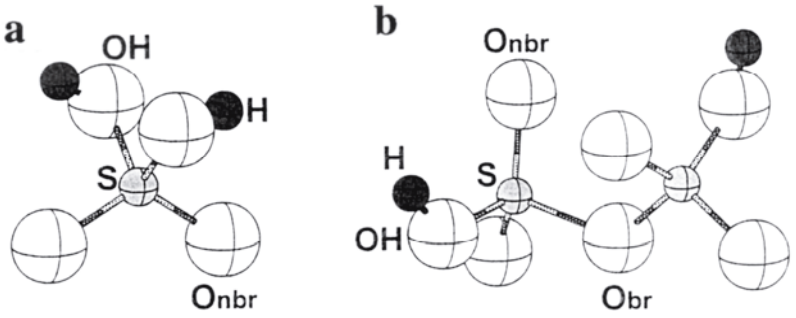

Figure 8. (H_2SO_4) and ($H_2S_2O_7$) clusters studied by the HF SCF method by Lindsay and Gibbs (1988) and Hill et al. (1997).

Table 4. Geometric parameters (Å and °) for H_2SO_4 and $H_2S_2O_7$ clusters: comparison of observed and calculated geometries.

Parameter	MO [6–31G**][1]	MO [6–311++G**][2]	Crystal[3]
		H_2SO_4	
S–O	1.411	1.411	1.426
S–OH	1.569	1.557	1.537
HO–S–OH	101.8	not given	105.2
HO–S–O	107.4	not given	110.7, 105.9
O–S–O	123.5	not given	117.9
		$H_2S_2O_7$	
$S–O_{br}$	1.623	1.609	1.618
$S–O_{nbr}$	1.405	1.397	1.412
S–OH	1.553	1.547	1.524
$S–O_{br}–S$	125.6	not given	122.1
$O_{br}–S–OH$	95.8	not given	102.8
$O_{br}–S–O_{nbr}$	108.1	not given	105.6
$O_{nbr}–S–O_{nbr}$	123.3	not given	122.2
$O_{nbr}–S–OH$	109.1	not given	109.2

[1] Lindsay and Gibbs (1988); [2] Hill et al. (1997); [3] H_2SO_4 (Kemnitz et al. 1996a,b), $H_2S_2O_7$ (Hoenle 1991) (only mean bond lengths and angles are given)

Lindsay and Gibbs (1988) calculated the deformation energies of the bridging $S–O_{br}–S$ angle in $H_2S_2O_7$. All geometric parameters of the cluster were fixed, and single-point energy calculations were done at 20° intervals for $S–O_{br}–S$ from 100 to 180°. Lindsay and Gibbs (1988) observed an energy minimum at $\theta = 125.6°$, with ΔE = -64.500 kJmol^{-1}. For comparison, the analogous parameters (θ_{min} and ΔE) for silicates and phosphates obtained by O'Keeffe et al. (1985) are 141.0° and -13.600 kJmol^{-1}, and 145.0° and -9.373 kJmol^{-1}, respectively. This is in good agreement with experimental data on synthetic polysulfates that show a narrower range of bridging S–O–S angles than phosphates or silicates. For this reason, Lindsay and Gibbs (1988) suggested that sulfate glasses are unlikely to adopt structures based on polymerized sulfate tetrahedra.

Bond angles in $(SO_4)^{2-}$ tetrahedra

Observed stereochemistries in (TO_4) groups indicate that there is considerable variation in O–*T*–O angles in crystals. Molecular orbitals can be envisaged as combinations of atomic orbitals *via* overlap, and hence the resulting bond-overlap populations are expected to be affected by variation in O–*T*–O angles, an idea that was confirmed for silicates by

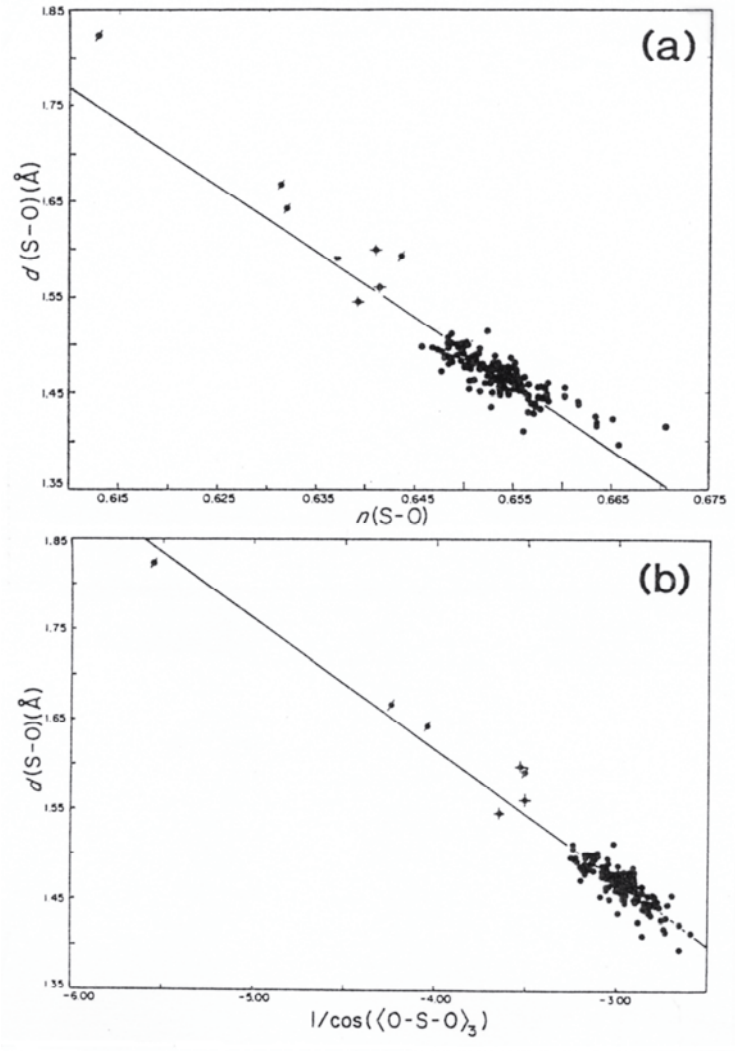

Figure 9. (a) Variation in observed S–O bond-length, d(S–O), with Mulliken bond-overlap population calculated for a constant bond-length of 1.49 Å and the observed O–S–O angles in selected sulfate structures; (b) variation in observed S–O bond-length as a function of $1/\cos\langle O–S–O_3\rangle$ in selected sulfate structures; points with a single / involve bridging anions in condensed sulfates, points with a + in-volve donor anions in acid-sul-fate groups (after Louisnathan et al. 1977).

Louisnathan and Gibbs (1972a). Louisnathan and Gibbs (1972b) and Louisnathan et al. (1977) examined sulfate structures (primarily minerals) from this perspective, and showed that observed ⟨S–O⟩ bond-lengths are highly correlated with Mulliken bond-overlap populations (Fig. 9a). In these calculations, the S–O bond-lengths were fixed at 1.49 Å (in order to prevent inducing such a correlation through the connection of bond-overlap population to bond length) and the observed O–S–O angles were used. In this way, the effect of variations in O–S–O angles was examined while the S–O distances in the calculations were fixed. Louisnathan et al. (1977) showed that observed S–O bond-lengths are very strongly correlated with O–S–O angles (Fig. 9b) *via* the expression $1/\cos(\langle O–S–O\rangle_3)$, where $\langle O–S–O\rangle_3$ is the mean value of the three O–S–O angles involving the S–O bond under consideration. These correlations rationalize the variations in stereochemistry of the (SO_4) group in minerals: the final configuration is a compromise between connectivity and bonding requirements, and correlated adjustment of both S–O distances and O–S–O angles is the molecular-orbital mechanism whereby this is achieved.

Alkali metal–sulfate clusters

Wang et al. (1999) used DFT to study $M^+(SO_4)^{2-}$ and $[M^+(SO_4)^{2-}]_2$ (M = Na, K) alkali-metal sulfate-ion pairs. The results for $Na^+(SO_4)^{2-}$ and $K^+(SO_4)^{2-}$ are particularly interesting, as several K- and Na-sulfate minerals are known. In general, the calculations show that the most stable $M^+(SO_4)^{2-}$ configurations are those in which the M^+ cations are

bonded to three O atoms of the (SO_4) tetrahedron (face-sharing of S and $M\emptyset_n$ coordination polyhedra). The $M^+(SO_4)^{2-}$ configuration, with the M^+ cation bonded to two O atoms, has a higher energy. The difference between face- and edge-sharing configurations is 0.48 kcal·mol^{-1} for M = Na, and 3.30 kcal·mol^{-1} for M = K. This is consistent with the structures of Na- and K-sulfate minerals. Whereas face-sharing between K_n polyhedra and (SO_4) tetrahedra is common (e.g. arcanite, glaserite, etc.), in Na sulfates (e.g. thenardite), edge-sharing between Na_n polyhedra and (SO_4) tetrahedra dominates.

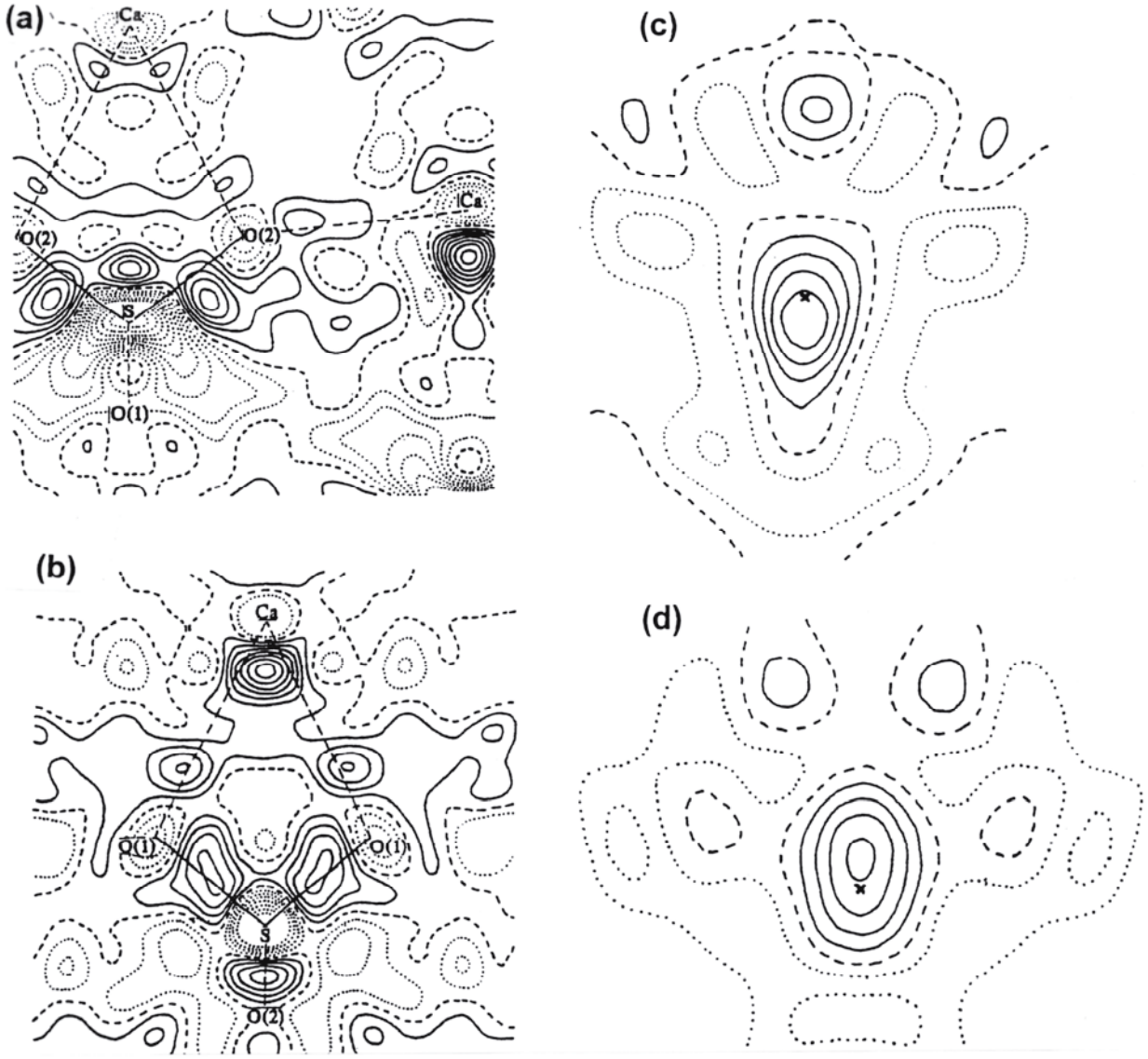

Figure 10. Dynamic deformation-density distribution in anhydrite (after Kirfel and Will 1980). (a) in the mirror plane (010) at y = 0; (b) in the mirror plane (100) at x = 1/4 ; (c) and (d) difference densities in planes halfway between S and O atoms and normal to the S–O bonds. Levels at 0.1 e·Å^{-3}, zero lines broken, negative contours dotted.

Experimental studies of electron density

Kirfel and Will (1980) studied the room-temperature electron-density distribution in anhydrite, $CaSO_4$, with special attention to the charge distribution within and around the $(SO_4)^{2-}$ anion. The $(SO_4)^{2-}$ anion in anhydrite has *mm*2 point symmetry, with oxygen atoms on the mirror planes. Figure 10 shows the dynamic deformation-density distribution in the sulfate group. Kirfel and Will (1980) suggested several explanations for the features in the

deformation electron-density maps. Figure 10a shows the mirror plane on (010) that contains the O(2)–S–O(2) bond angle. The peak > 0.50 e $Å^{-3}$ between the S and O(2) atoms, evidently associated with π-bond overlap, is shifted toward a line connecting the S and Ca atoms. This may be due to Coulombic forces involving the adjacent Ca cation. The two symmetrical S–O(2) peaks are connected by a band of positive deformation density that has a maximum on the bisectrix of the O(2)–S–O(2) bond angle. Kirfel and Will (1980) associated this maximum with interaction of the $3d_z$ orbital of S with the $2p$ orbitals of the O(2) atoms according to the π-bond model for sulfate suggested by Cruickshank (1961). However, there is no maximum on the bisectrix of the O(1)–S–O(1) bond angle (Fig. 10b) where π-bond peaks are also connected by a band of positive deformation density. Figures 10c and 10d depict deformation densities in planes halfway between the S and O atoms and normal to the S–O bonds. It is evident that the π-bond charge accumulations deviate significantly from ideal cylindrical symmetry. According to Kirfel and Will (1980), this shows that the electron-density distribution within the (SO_4) tetrahedron is affected by external bonding conditions, i.e. by attractive Coulombic forces from Ca cations in the case of anhydrite. Similar results were also reported by Christidis et al. (1983) for monoclinic $Fe_2(SO_4)_3$.

Theoretical studies of electron densities

Hill et al. (1997) studied minimum-energy geometries and electron-density distributions for (H_2SO_4) and $(H_2S_2O_7)$ clusters at the HF SCF level with a 6–311++G** basis set. Topological analysis of the electron-density distribution showed that bond critical points between S and O atoms are 0.549 and 0.545 Å away from the S atom in (H_2SO_4) and $(H_2S_2O_7)$ clusters, respectively. The electron density at bond critical points for S–O bonds are 2.200 and 2.246 $e \cdot Å^{-3}$ for the (H_2SO_4) and $(H_2S_2O_7)$ clusters, respectively. Analysis of the theoretical electron-density distribution allowed Hill et al. (1997) to characterize the S–O bonds in terms of their covalency. Applications of various theoretical criteria (see Hill et al. 1997) showed that S–O bonds in sulfates are predominantly covalent, as expected from the relative electronegativities, χ, of S and O atoms (χ_S = 2.44; χ_O = 3.50; Allred and Rochow 1958).

Models of chemical bonding

In this chapter, we couch several of our arguments in terms of bond-valence theory (Brown and Shannon 1973; Brown 1981; Hawthorne 1992, 1994, 1997). Louisnathan et al. (1977) examined the relation between the MO and bond-valence approaches. Brown and Shannon (1973) showed how to calculate the relative covalency of a bond using the bond-valence approach. Louisnathan et al. (1977) showed that, for the (SO_4) group, this covalency is strongly correlated (Fig. 11) with the electrical charge of the O atom, calculated using a fixed S–O distance of 1.49 Å, the observed O–S–O angles, and extended Hückel MO theory. This explicit connection between MO theory and bond-valence theory for the (SO_4) group is in accord with later arguments concerning the similarity of these two approaches (Burdett and Hawthorne 1993; Hawthorne 1994, 1997).

HIERARCHICAL ORGANIZATION OF CRYSTAL STRUCTURES

Ideally, the physical, chemical, and paragenetic characteristics of a mineral should arise as natural consequences of its crystal structure and the interaction of that structure with the environment in which it occurs. Hence, an adequate structural hierarchy of minerals should provide an epistemological basis for the interpretation of the role of minerals in Earth processes. We have not yet reached this stage for any major class of minerals, but significant advances have been made. For example, Bragg (1930) classified the major rock-forming silicate minerals according to the geometry of polymerization of

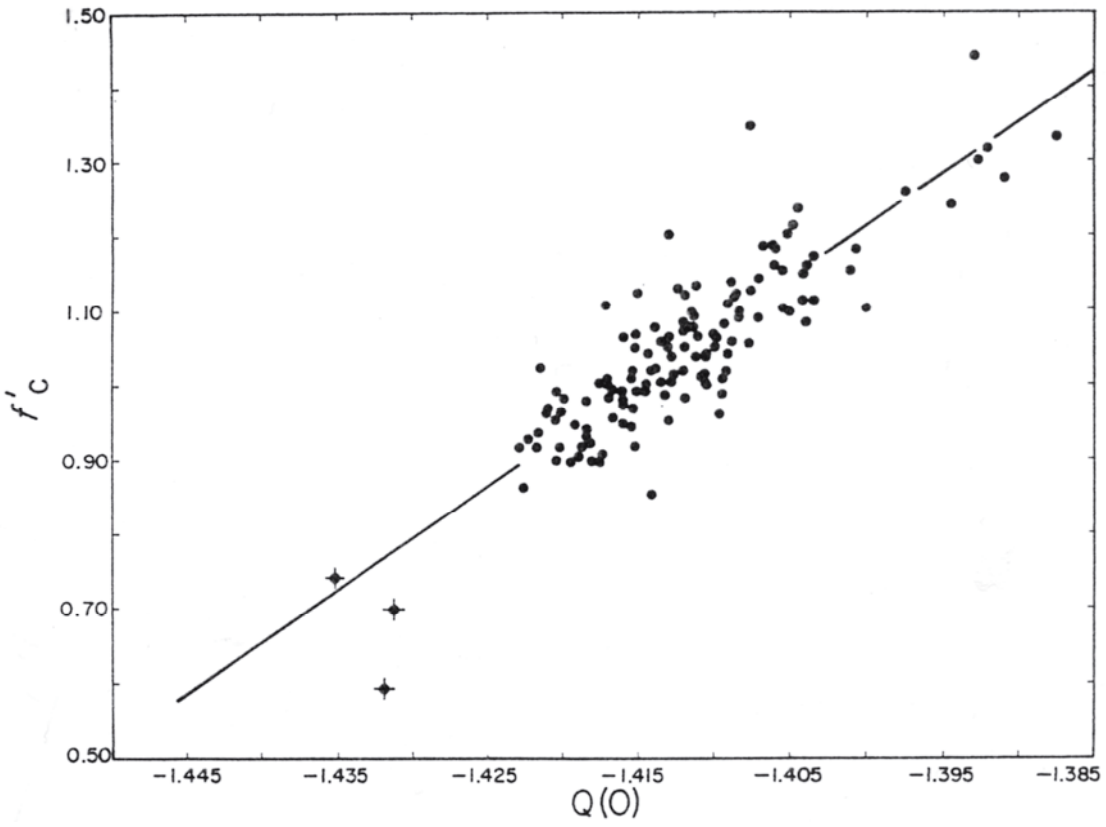

Figure 11. Variation in covalency, *f ′c*, of an S–O bond, calculated according to the method of Brown and Shannon (1973), with the electric charge of the constituent O anion, Q(0), calculated for a constant bond-length of 1.49 Å and observed O–S–O angles; symbols as in Figure 9 (after Louisnathan et al. 1977).

$(Si,Al)O_4$ tetrahedra, and this scheme was extended by Zoltai (1960) and Liebau (1985); it is notable that the scheme parallels Bowen's reaction series (Bowen 1928) for silicate minerals in igneous rocks. Much additional insight can be derived from such structural hierarchies, particularly with regard to controls on bond topology (Hawthorne 1983a, 1994) and mineral paragenesis (Moore 1965, 1970, 1973; Hawthorne 1984; Hawthorne et al. 1987).

Hawthorne (1983a) proposed that structures be ordered or classified according to the polymerization of those cation coordination polyhedra with higher bond-valences. Higher bond-valence polyhedra polymerize to form *homo-* or *heteropolyhedral clusters* that constitute the *fundamental building block (FBB)* of the structure. The *FBB* is repeated, commonly polymerized, by translational symmetry operators to form the *structural unit*, a complex (typically anionic) polyhedral array (not necessarily connected), the excess charge of which is balanced by the presence of *interstitial* species (usually large, low-valence cations; Hawthorne 1985a). The possible modes of cluster polymerization are (1) unconnected polyhedra; (2) finite clusters; (3) infinite chains; (4) infinite sheets; and (5) infinite frameworks.

All structural classifications of sulfate minerals have considered sulfate-mineral structures as based on heteropolyhedral structural units. In their crystal-chemical classification, Bokii and Gorogotskaya (1969) subdivided 70 sulfate minerals into two large groups: (1) minerals with isolated (SO_4) tetrahedra, and (2) (SO_4) tetrahedra linked to other cation polyhedra. The sulfate minerals of both groups were subdivided into finite-cluster, infinite-chain, infinite-sheet, and infinite-framework structures. Sabelli and Trosti-

Ferroni (1985) classified sulfate minerals into the same four categories and provided a general scheme that included the ~200 mineral species known at that time. Rastsvetaeva and Pushcharovsky (1989) considered ~600 sulfate minerals and inorganic compounds and classified them on the basis of mixed-anion radicals (~heteropolyhedral structural units) (Sandomirsky and Belov 1984). Pushcharovsky et al. (1998) considered the main structural subdivisions and structural formulae of sulfate minerals within the framework of the structural classification suggested by Lima-de-Faria (1994) and recommended by the Subcommittee on the Nomenclature of the Inorganic Structure Types of the International Union of Crystallography Commission on the Crystallographic Nomenclature (Lima-de-Faria et al. 1990).

POLYMERIZATION OF SO_4 AND OTHER $T\O_4$ TETRAHEDRA

Bond valence is a measure of the strength of a chemical bond, and, in a coordination polyhedron, can be approximated by the formal valence divided by the coordination number. Thus, in an SO_4 group, the mean bond-valence is 6/4 = 1.5 vu. The valence-sum rule (Brown 1981) states that the sum of the bond valences incident at an atom is equal to the magnitude of the formal valence of that atom. Thus, any oxygen atom linked to the central S^{6+} cation receives ~1.50 vu from the S^{6+} cation, and hence must receive ~0.50 vu from other coordinating cations. There are several ways in which this bond-valence requirement may be satisfied:

(1) The oxygen atom is bonded to another tetrahedrally coordinated cation; this method is not common in minerals as most tetrahedrally coordinated cations have sufficiently large bond-valences that such an S–O–*T* linkage violates the valence-sum rule. This argument is not completely satisfactory, as even synthetic polymerized sulfates exist. For example, $K_2S_2O_7$ has been synthesized (Lynton and Truter 1960); it has an S–O distance of 1.642 Å, far longer than any S–O distance recorded in minerals (Fig. 1), and is presumably unstable under natural Earth conditions. Nevertheless, lopezite, $K_2Cr_2O_7$, is a mineral with O bridging two hexavalent cations (Cr^{6+}), a configuration similar to that in $K_2S_2O_7$, so the reason for the absence of the latter configuration is not completely clear.

Similarly, the sulfate oxyanion does not polymerize with any of the common tetrahedral oxyanions in minerals [e.g. (PO_4), (AsO_4), (VO_4), (SiO_4), (AlO_4)] because the ideal bond-valence sums incident at the bridging anion would significantly exceed 2 vu. This is not the case for the (BeO_4) and (LiO_4) groups; polymerization of these groups with (SO_4) would give ideal bond-valence sums incident at the bridging anion of 1.50 + 0.50 = 2.00 vu and 1.50 + 0.25 = 1.75 vu, respectively. Nevertheless, these arrangements have not been observed in minerals.

(2) The oxygen atom is bonded to additional octahedrally coordinated cations; this mechanism is extremely common in minerals. Di- and tri-valent octahedrally coordinated cations have ideal bond-valences of 0.33 and 0.50 vu, respectively, and hence there are several different types of linkage that are compatible with the valence-sum rule, e.g. 1.50 + 0.50 = 2.00 vu; 1.50 + 2 × 0.33 = 2.16 vu (small to moderate deviations from the valence-sum rule are compensated by antipathetic variations in the bond lengths).

(3) The oxygen atom bonds to additional higher-coordinated alkali and/or alkaline-earth cations; this mechanism is also common in minerals. Mono- and di-valent cations have bond valences in the ranges of 0.08-0.15 and 0.17-0.29 vu, respectively, and hence there are many types of linkage compatible with the valence-sum rule, e.g. 1.50 + 3 × 0.15 = 1.95 vu; 1.50 + 2 × 0.25 = 2.00 vu.

(4) The oxygen atom is bonded to additional octahedrally coordinated and higher-

coordinated alkali and/or alkaline-earth cations; this is also common in minerals.

(5) The oxygen atom may act as a hydrogen-bond acceptor.

Most sulfate minerals consist of (SO_4) tetrahedra polymerizing with MO_n polyhedra, and hence we will organize their structures on this basis.

A STRUCTURAL HIERARCHY FOR SULFATE MINERALS

There are ~370 sulfate-mineral species, and structural information is available for ~80% of them. About 140 sulfate-mineral structure-types are known, and these are considered here.

The utility of this approach for consideration of the minerals with single tetrahedral oxyanions (sulfates, phosphates, arsenates, vanadates, borates) has been shown by Hawthorne (1985a, 1986, 1990, 1992, 1994, 1997), Hawthorne et al. (1996), Burns et al. (1995), Grice et al. (1999), Eby and Hawthorne (1993), and Schindler et al. (2000a,b). It should be noted, however, that most of the minerals considered in the above works are based on structural units involving polymerization of ($M\emptyset_6$) octahedra (M = divalent or trivalent cation: Mg^{2+}, Fe^{2+}, Mn^{2+}, Zn^{2+}, Al^{3+}, Fe^{3+}, etc.) and ($T\emptyset_4$) tetrahedra (T = pentavalent or hexavalent cation: As^{5+}, P^{5+}, V^{5+}, S^{6+}, Cr^{6+}, Mo^{6+}, etc.). However, numerous sulfate minerals do not contain divalent- or trivalent-cation octahedra; hence we must introduce additional categories of structures. Thus, we subdivide the sulfate minerals into the following groups: (1) sulfates with divalent- and trivalent-metal octahedra; (2) sulfates with non-octahedral cation polyhedra and Na sulfates; (3) sulfates with anion-centered tetrahedra.

The structure diagrams presented here generally have the following shading patterns: (SO_4) tetrahedra are shaded with pale gray, colorless or narrow-spaced lines, octahedra and higher coordinations are shaded with dark gray or wide-spaced lines; H atoms are shown as small shaded circles; H bonds are shown by dotted lines.

STRUCTURES BASED ON SULFATE TETRAHEDRA AND DIVALENT AND/OR TRIVALENT CATION OCTAHEDRA

Graphical representation of octahedral–tetrahedral structures

The majority of minerals have structures that are based on complex anions built by polymerization of octahedra and tetrahedra. To analyze the connectivity of the octahedral–tetrahedral structures, Hawthorne (1983a) considered polyhedral clusters from a graph-theoretic viewpoint. Polyhedra are represented by the chromatic vertices of a labelled graph in which different colors (e.g. black and white) represent coordination polyhedra of different type. Linking of polyhedra can be denoted by the presence of an edge or edges between vertices representing linked polyhedra. The number of edges between vertices denotes the number of atoms common to both polyhedra. Thus, no edge between two vertices represents disconnected polyhedra (Fig. 12a), one edge between two vertices represents corner-sharing between two polyhedra (Fig. 12b), two edges between two vertices represents edge-sharing between two polyhedra (Fig. 12c), and three edges between two vertices represents triangular-face-sharing (Fig. 12d). The octahedra and tetrahedra are denoted as white and black vertices, respectively. Figure 12e shows the polyhedral cluster $[M_2(T\emptyset_4)_2\emptyset_8]$ and its graphical representation (M = octahedrally coordinated cation; T = tetrahedrally coordinated cation; Ø = unspecified ligand); round brackets and curly brackets denote a polyhedron or a group, e.g. (SO_4), (H_2O); square brackets denote linked polyhedra, e.g. $[M(TO_4)_2\emptyset_4]$.

Moving from polyhedral representation to graphical representation, geometrical

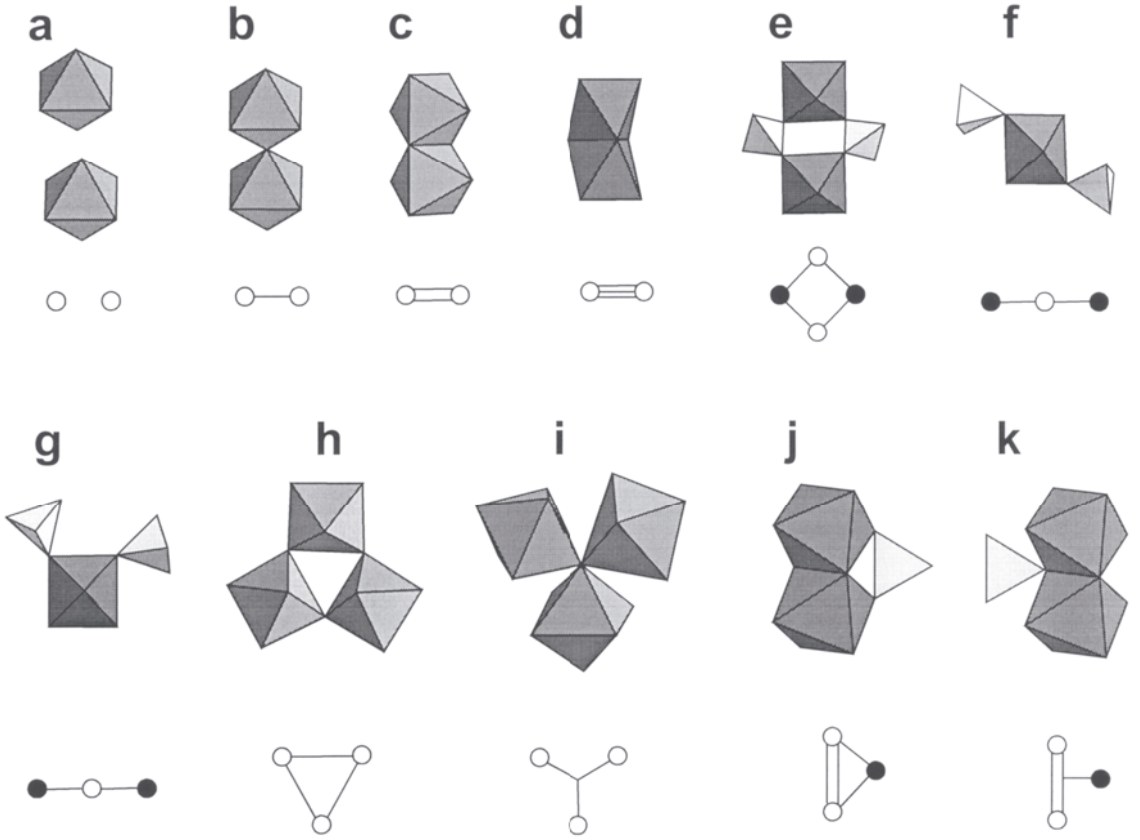

Figure 12. Examples of graphical representation of octahedral–tetrahedral clusters (see text for details).

information is lost. This is illustrated in Figures 12f and 12g, which show two different possible arrangements of the corner-linked cluster $[M(T\text{Ø}_4)_2\text{Ø}_4]$. Both of these clusters are described by identical graphs; such clusters are called *geometrical isomers*. Information on geometrical isomerism is lost in the graphical representation; examples are shown in Figures 12h to 12k. In some cases, we can distinguish between these configurations by allowing (more than two) edges in the graph to intersect without forming a vertex (e.g. Figs. 12i, 12k). Although these modifications do not follow conventional notation, they are useful in representing different structures (e.g. Hawthorne et al. 1996), and are used here.

The octahedral–tetrahedral structural units can be arranged according to the dimension of their polymerization: (a) unconnected (isolated) polyhedra; (b) finite clusters; (c) infinite chains; (d) infinite sheets; (e) infinite frameworks.

Structures with unconnected SO_4 groups

The graphs of this class of structures are shown in Figures 13a and 13b; they consist of white vertices and isolated black and white vertices. Sulfate minerals of this class are given in Tables 5 and 6, and their structures are shown in Figures 14-19. In these minerals, sulfate tetrahedra and ($M\text{Ø}_6$) octahedra are linked together by hydrogen bonding and/or by large low-valence interstitial cations. In the minerals of the **hexahydrite group** (Table 5), $\{M^{2+}(H_2O)_6\}(SO_4)$ (Fig. 14a), and **retgersite**, $\{Ni(H_2O)_6\}(SO_4)$ (Fig. 14b), the (SO_4) tetrahedra and $\{M^{2+}(H_2O)_6\}$ octahedra are linked by hydrogen bonding only; this involves linkage from donor ligands of the octahedra to acceptor ligands of the tetrahedra, together with weak hydrogen bonding between ligands of different octahedra. The minerals of the **epsomite group**, $\{M^{2+}(H_2O)_6\}(SO_4)(H_2O)$, M = Mg, Zn, Ni (Fig. 14c), and the **melanterite group**, $\{M^{2+}(H_2O)_6\}(SO_4)(H_2O)$, M = Fe^{2+}, Co, Mn^{2+}, Cu^{2+}, Zn (Fig.

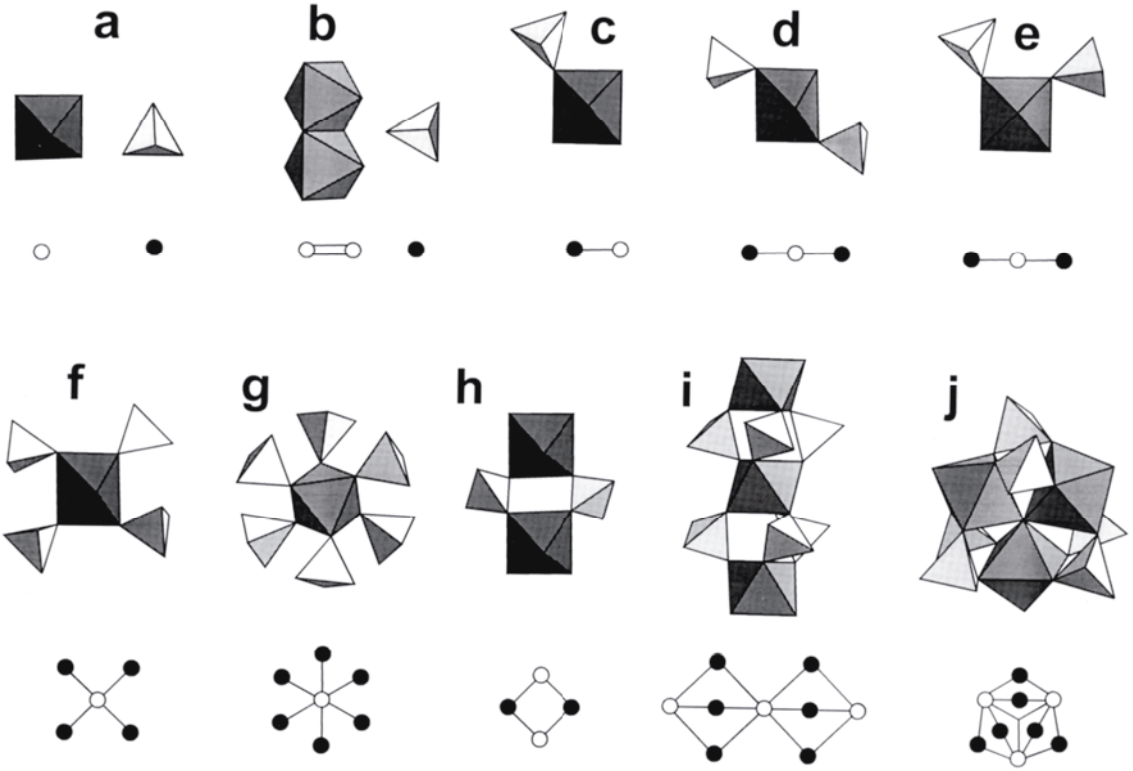

Figure 13. Finite octahedral–tetrahedral clusters in the sulfate minerals and their graphs.

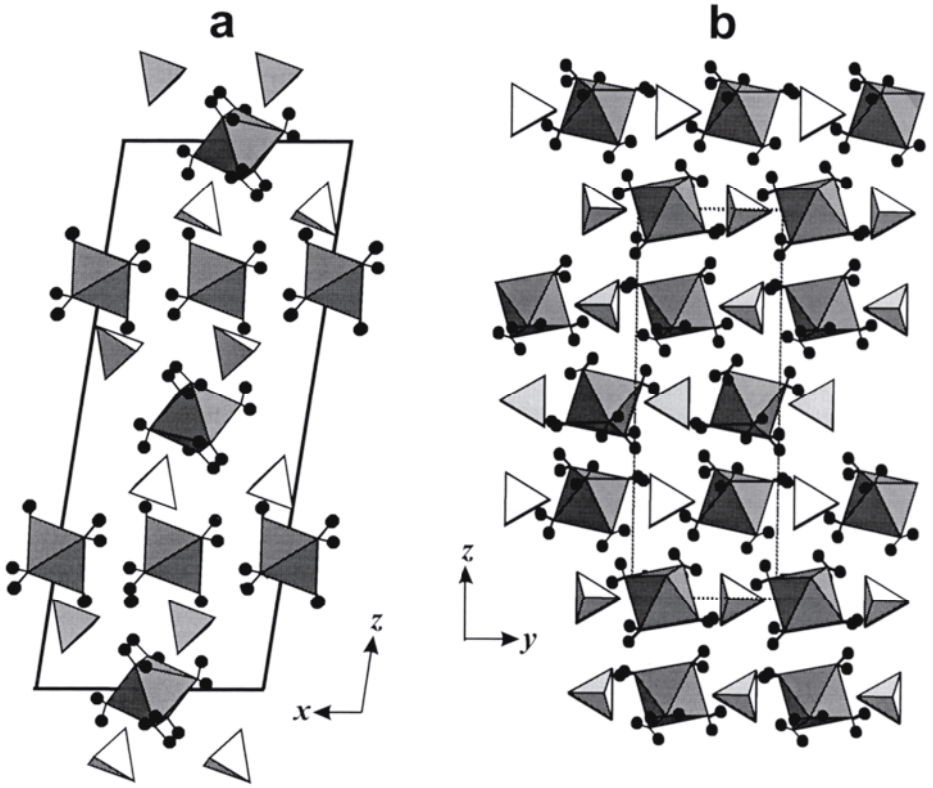

Figure 14. The structures of sulfate minerals with isolated (SO_4) tetrahedra and ($M\emptyset_6$) octahedra: (a) hexahydrite; (b) retgersite.

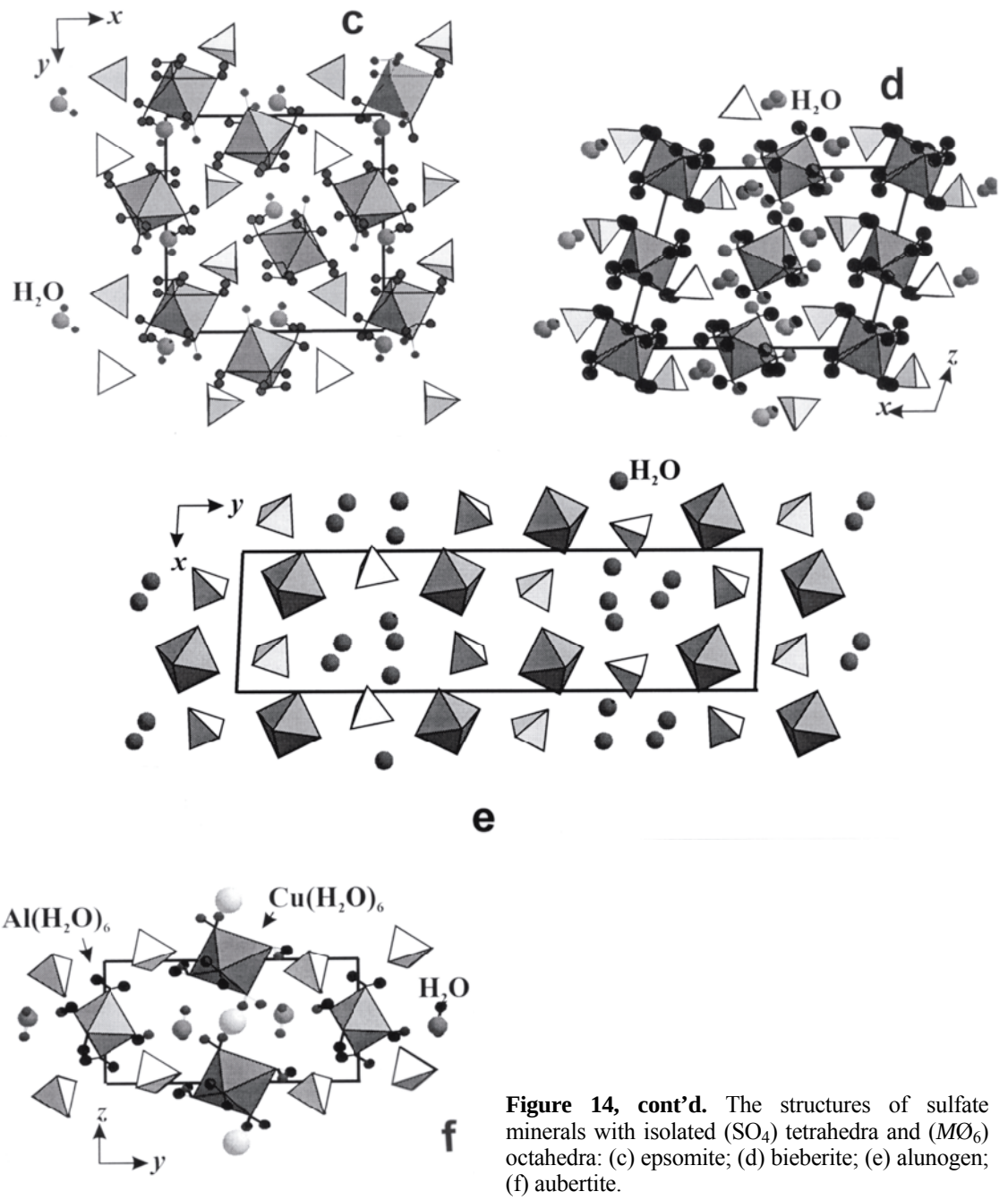

Figure 14, cont'd. The structures of sulfate minerals with isolated (SO_4) tetrahedra and ($M\emptyset_6$) octahedra: (c) epsomite; (d) bieberite; (e) alunogen; (f) aubertite.

14d), are characterized by (H_2O) in addition to that required to coordinate the M^{2+} cations (Table 5). In the melanterite group, there is direct hydrogen bonding between octahedra and tetrahedra, and there is also hydrogen bonding through the additional interstitial (H_2O) (acting as both a hydrogen-bond donor and a hydrogen-bond acceptor) to both tetrahedral and octahedral ligands. In the epsomite group, the pattern of hydrogen bonding is slightly different; there is direct hydrogen bonding between octahedra and tetrahedra, weak hydrogen bonding between adjacent octahedra, and hydrogen bonding through inter -stitial (H_2O) to both octahedra and tetrahedra. In **alunogen**, $\{Al(H_2O)_6\}_2(SO_4)_3(H_2O)_{4.4}$ (Fig. 14e), there are interstitial (H_2O) groups linking tetrahedra and octahedra together through additional hydrogen bonds. In the structure of **aubertite**, $\{Cu^{2+}(H_2O)_6\}\{Al(H_2O)_6\}(SO_4)_2Cl(H_2O)_2$ (Fig. 14f), hydrogen bonding between octa-hedra and tetrahedra involves interstitial Cl as well as (H_2O) groups.

Table 5. Sulfate minerals with isolated (SO_4) tetrahedra and ($M\phi_6$) octahedra with the general formula $(M\phi_6)_p(SO_4)_q(H_2O)_r$ (r = 0–5).*

Name	Formula	a (Å)	b (Å)	c (Å)	α (°)	β (°)	γ (°)	S. G.	Fig.	Ref.
		$(M\phi_6)(SO_4)$								
hexahydrite	$\{Mg(H_2O)_6\}(SO_4)$	10.110	7.212	24.410	–	98.3	–	$C2/c$	14a	[1]
bianchite	$\{Zn(H_2O)_6\}(SO_4)$	10.10	7.20	24.49	–	98.3	–	$C2/c$	14a	(2)
chvaleticeite	$\{Mn^{2+}(H_2O)_6\}(SO_4)$	10.05	7.24	24.3	–	98.0	–	$C2/c$	14a	(2)
ferrohexahydrite	$\{Fe^{2+}(H_2O)_6\}(SO_4)$	10.08	7.28	24.59	–	98.4	–	$C2/c$	14a	(2)
moorhouseite	$\{Co(H_2O)_6\}(SO_4)$	10.03	7.23	24.23	–	98.4	–	$C2/c$	14a	(2)
nickelhexahydrite	$\{Ni(H_2O)_6\}(SO_4)$	9.880	7.248	24.171	–	98.5	–	$C2/c$	14a	[3]
retgersite	$\{Ni(H_2O)_6\}(SO_4)$	6.783	a	18.288	–	–	–	$P4_12_12$	14b	[4]
		$(M\phi_6)_p(SO_4)_q(H_2O)_r$								
epsomite	$\{Mg(H_2O)_6\}(SO_4)(H_2O)$	11.887	12.013	6.861	–	–	–	$P2_12_12_1$	14c	[5]
goslarite	$\{Zn(H_2O)_6\}(SO_4)(H_2O)$	11.799	12.050	6.822	–	–	–	$P2_12_12_1$	14c	(2)
morenosite	$\{Ni(H_2O)_6\}(SO_4)(H_2O)$	11.768	12.021	6.758	–	–	–	$P2_12_12_1$	14c	[6]
melanterite	$\{Fe^{2+}(H_2O)_6\}(SO_4)(H_2O)$	14.072	6.503	11.041	–	105.6	–	$P2_1/c$	14d	[7]
bieberite	$\{Co(H_2O)_6\}(SO_4)(H_2O)$	14.048	6.494	10.925	–	105.2	–	$P2_1/c$	14d	[8]
mallardite	$\{Mn^{2+}(H_2O)_6\}(SO_4)(H_2O)$	14.15	6.50	11.06	–	105.6	–	$P2_1/c$	14d	(2)
boothite	$\{Cu^{2+}(H_2O)_6\}(SO_4)(H_2O)$	13.89	6.50	10.64	–	105.6**	–	–	14d	(2)
zinc-melanterite	$\{Zn(H_2O)_6\}(SO_4)(H_2O)$	14.04	6.51	10.99	–	105.3†	–	–	14d	(2)
alunogen	$\{Al(H_2O)_6\}_2(SO_4)_3(H_2O)_{4.4}$	7.245	26.975	6.061	90.0	97.7	91.9	$P\bar{1}$	14e	[9]
aubertite	$\{Cu^{2+}(H_2O)_6\}\{Al(H_2O)_6\}(SO_4)_2Cl(H_2O)_2$	6.282	13.192	6.26	91.8	94.7	82.5	$P\bar{1}$	14f	[10]
magnesioaubertite	$\{Mg(H_2O)_6\}\{Al(H_2O)_6\}(SO_4)_2Cl(H_2O)_2$	6.31	13.20	6.29	91.7	94.5	82.6	$P\bar{1}$	14f	[2]
svyazhinite	$\{Mg(H_2O)_6\}\{Al(H_2O)_6\}(SO_4)_2F(H_2O)_2$	6.217	13.306	6.255	90.05	93.3	82.03	$P\bar{1}$	14f	(2)

* M = Cu^{2+}, Fe^{2+}, Ni, Mg, Zn, Mn^{2+}, Co, Al; ϕ = O, OH, H_2O, F, Cl. ** From morphological axial ratios assuming isomorphism with melanterite. † From re-indexing of the powder-diffraction pattern of Liu Tiegeng et al. (1995).

A reference in square brackets (e.g., [1]) indicates that a structure has been refined; a reference in round brackets [e.g., (2)] indicates a structure has not been refined. *References*: [1] Zalkin et al. (1964), [2] Gaines et al. (1997), [3] Ptasiewicz-Bak et al. (1983), [4] Stadnicka et al. (1987), [5] Calleri et al. (1984),[6] Iskhakova et al. (1991), [7] Baur (1964), [8] Kellersohn et al. (1991), [9] Menchetti and Sabelli (1974), [10] Ginderow and Cesbron (1979)

Table 6. Sulfate minerals with isolated (SO_4) tetrahedra and ($M\emptyset_6$) octahedra.*

Name	Formula	*a* (Å)	*b* (Å)	*c* (Å)	β (°)	S. G.	Fig.	Ref.
picromerite	$K_2\{Mg(H_2O)_6\}(SO_4)_2$	9.072	12.212	6.113	104.8	$P2_1/a$	15a	[1]
boussingaultite	$(NH_4)_2\{Mg(H_2O)_6\}(SO_4)_2$	9.316	12.596	6.198	107.1	$P2_1/a$	15a	[2]
cyanochroite	$K_2\{Cu^{2+}(H_2O)_6\}(SO_4)_2$	9.066	12.130	6.149	104.4	$P2_1/a$	15a	[3]
mohrite	$(NH_4)_2\{Fe^{2+}(H_2O)_6\}(SO_4)_2$	9.170	12.419	6.297	106.7	$P2_1/a$	15a	[4]
nickel-boussingaultite	$(NH_4)_2\{Ni(H_2O)_6\}(SO_4)_2$	6.244	12.469	9.195	107.0	$P2_1/c$	15a	[5]
lonecreekite	$(NH_4)\{Fe^{3+}(H_2O)_6\}(SO_4)_2(H_2O)_6$	12.302	*a*	*a*	–	$Pa\bar{3}$	15b	(6)
potassium alum	$K\{Al(H_2O)_6\}(SO_4)_2(H_2O)_6$	12.157	*a*	*a*	–	$Pa\bar{3}$	15b	[7]
sodium alum	$Na\{Al(H_2O)_6\}(SO_4)_2(H_2O)_6$	12.213	*a*	*a*	–	$Pa\bar{3}$	15b	[8]
tschermigite	$(NH_4)\{Al(H_2O)_6\}(SO_4)_2(H_2O)_6$	12.248	*a*	*a*	–	$Pa\bar{3}$	15b	[9]
tamarugite	$Na\{Al(H_2O)_6\}(SO_4)_2$	7.353	25.225	6.097	95.2	$P2_1/a$	15c,d	[10]
amarillite	$Na\{Fe^{3+}(H_2O)_6\}(SO_4)_2$	8.419	10.841	12.472	95.5	$C2/c$	15c,d	[11]
mendozite	$Na\{Al(H_2O)_6\}(SO_4)_2(H_2O)_5$	21.75	9.11	8.300	92.5	$C2/c$	15g	[12]
kalinite	$K\{Al(H_2O)_6\}(SO_4)_2(H_2O)_5$	19.92	9.27	8.304	98.8	$C2/c$	15g	(6)
chukhrovite	$Ca_4F\{AlF_6\}_2(SO_4)(H_2O)_{12}$	16.710	*a*	*a*	–	$Fd\bar{3}$	16a-d	[18]
chukhrovite-(Ce)	$(Ca,Ce,Nd)_4F\{AlF_6\}_2(SO_4)(H_2O)_{10}$	16.800	*a*	*a*	–	$Fd\bar{3}$	16a-d	[19]
ettringite	$Ca_6\{Al(OH)_6\}_2(SO_4)_3(H_2O)_{26}$	11.260	*a*	21.480	–	$P31c$	16e,f,g	[13]
bentorite	$Ca_6\{Cr^{3+}(OH)_6\}_2(SO_4)_3(H_2O)_{26}$	22.35	*a*	21.41	–	$P6_3/mmc$	16e,f,g	(6)
charlesite	$Ca_6\{Al(OH)_6\}_2(SO_4)_2\{B(OH)_4\}(H_2O)_{26}$	11.16	*a*	21.21	–	$P31c$	16e,f,g	(6)
sturmanite	$Ca_6\{Fe^{3+}(OH)_6\}_2(SO_4)_2\{B(OH)_4\}(H_2O)_2$	11.16	*a*	21.79	–	$P31c$	16e,f,g	(6)
jouravskite	$Ca_3\{Mn^{4+}(OH)_6\}(SO_4)(CO_3)(H_2O)_{12}$	11.060	*a*	10.500	–	$P6_3$	16e,f,g	[14]
thaumasite	$Ca_3\{Si(OH)_6\}(SO_4)(CO_3)(H_2O)_{12}$	11.04	*a*	10.390	–	$P6_3$	16e,f,g	[15]
despujolsite	$Ca_3\{Mn^{4+}(OH)_6\}(SO_4)_2(H_2O)_3$	8.560	*a*	10.760	–	$P\bar{6}2c$	16e,f,h	[16]
fleischerite	$Pb_3\{Ge(OH)_6\}(SO_4)_2(H_2O)_3$	8.867	*a*	10.875	–	$P\bar{6}2c$	16e,f,h	[17]
schaurteite	$Ca_3\{Ge(OH)_6\}(SO_4)_2(H_2O)_3$	8.525	*a*	10.803	–	$P\bar{6}2c$	16e,f,h	(6)

* $M = Cu^{2+}$, Fe^{2+}, Ni, Mg, Zn, Al, Fe^{3+}, Cr^{3+}, Mn^{4+}, Si, Ge

References: [1] Kannan and Viswamitra (1965), [2] Maslen et al. (1988), [3] Robinson and Kennard (1972), [4] Figgis et al. (1992), [5] Tahirov et al. (1994), (6) Gaines et al. (1997), [7] Larson and Cromer (1967), [8] Cromer et al. (1967), [9] Abdeen et al. (1981), [10] Robinson and Fang (1969), [11] Li et al. (1990), [12] Fang and Robinson (1972), [13] Moore and Taylor (1970), [14] Granger (1969), [15] Zemann and Zobetz (1981), [16] Gaudefroy et al. (1968), [17] Otto (1975), [18] Mathew et al. (1981), [19] Bokii and Gorogotskaya (1965)

In the minerals of the **picromerite group** (Table 6), e.g. **cyanochroite**, $K_2\{Cu^{2+}(H_2O)_6\}(SO_4)_2$, the $\{M^{2+}(H_2O)_6\}$ and (SO_4) groups are linked by K into sheets parallel to (100) (Fig. 15a), which are linked together by hydrogen bonding from the octahedral ligands to the acceptor anions of the sulfate group. The structure of **sodium alum**, $Na\{Al(H_2O)_6\}(SO_4)_2(H_2O)_6$, consists of $\{Al(H_2O)_6\}$, $\{Na(H_2O)_6\}$, and (SO_4) groups linked by hydrogen bonding (Fig. 15b). All (H_2O) groups are coordinated to cations; any additional (H_2O) in a structure of this type would entail (H_2O) held in the structure solely by hydrogen bonding. In the structure of **tamarugite**, $Na\{Al(H_2O)_6\}(SO_4)_2$ (Fig. 15c,d), Na is octahedrally coordinated by oxygen atoms of the (SO_4) tetrahedra. The two (NaO_6) octahedra share an edge to form $[Na_2O_{10}]$ dimers that are linked through (SO_4) groups to form infinite chains along [001]. Figures 15e,f show the chain and its graph, respectively. A similar situation occurs in the structure of **mendozite**,

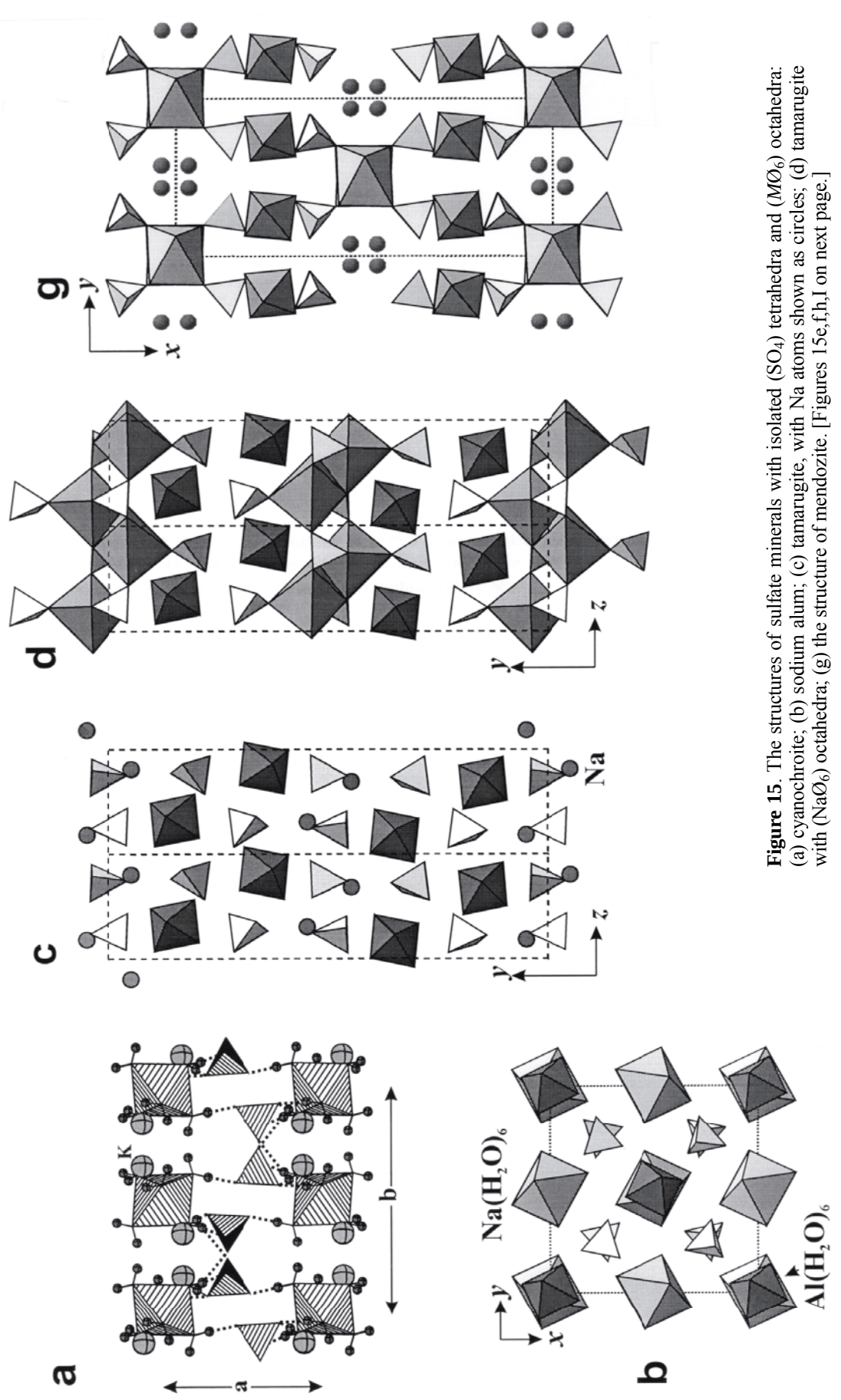

Figure 15. The structures of sulfate minerals with isolated (SO_4) tetrahedra and ($M\emptyset_6$) octahedra: (a) cyanochroite; (b) sodium alum; (c) tamarugite, with Na atoms shown as circles; (d) tamarugite with ($Na\emptyset_6$) octahedra; (g) the structure of mendozite. [Figures 15e,f,h,I on next page.]

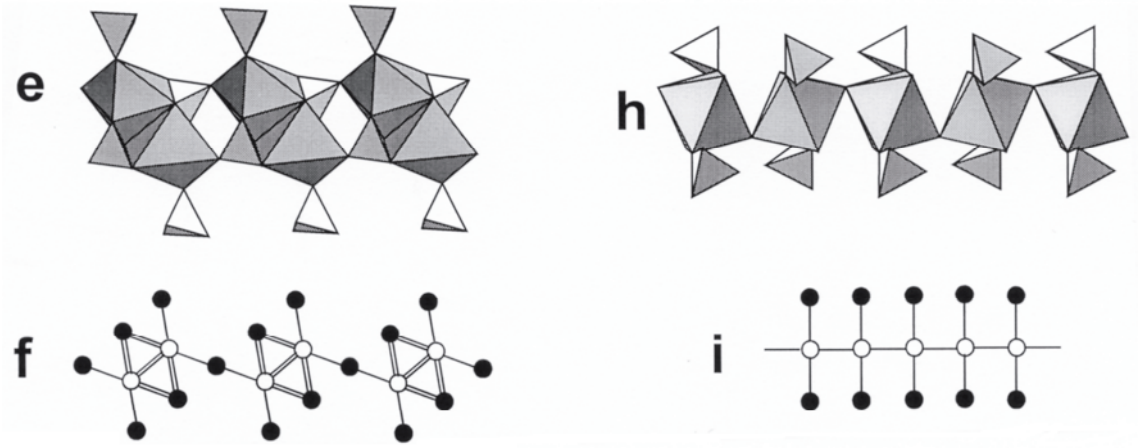

Figure 15, cont'd. The structures of sulfate minerals with isolated (SO_4) tetrahedra and ($M\emptyset_6$) octahedra: (e) the chain of ($Na\emptyset_6$) octahedra and (SO_4) tetrahedra in tamarugite; (f) the graph of the chain in tamarugite; (h) the chain of ($Na\emptyset_6$) octahedra and (SO_4) tetrahedra in mendozite; (i) the graph of the chain in mendozite.

$Na\{Al(H_2O)_6\}(SO_4)_2(H_2O)_5$ (Fig. 15g), where corner-sharing $\{NaO_4(H_2O)_2\}$ octahedra form infinite $[Na\emptyset_5]$ chains that are parallel to [001] and are decorated by (SO_4) tetrahedra (Figs. 15h,i). Note that these chains are topologically identical to the $[M\emptyset_5]_0$ chains described by Moore (1970) as 7-Å chains, although their repeat distance is longer (~8.3 Å, Table 6) because of the size of Na. In the structure of **chukhrovite**, $Ca_4F\{AlF_6\}_2(SO_4)(H_2O)_{12}$, four ($Ca\emptyset_7$) polyhedra share one F atom to form, together with four (AlF_6) octahedra, the rather complex cluster shown in Figure 16a. These clusters are linked together to form a framework with (SO_4) tetrahedra in the cavities (Fig. 16c). An alternative description is that the structure is built from (FCa_4) tetrahedra (Fig. 16b), (AlF_6) octahedra, (SO_4) tetrahedra, and (H_2O) groups (Fig. 16d).

The structures of the minerals of the **ettringite**, $Ca_6\{Al(OH)_6\}_2(SO_4)_3(H_2O)_{26}$, and **fleischerite**, $Pb^{2+}{}_3\{Ge(OH)_6\}(SO_4)_2(H_2O)_3$, **groups** (Table 6) are based on the column (Fig. 16e) formed by edge-sharing of $\{Mn(OH)_6\}$ octahedra with triplets of ($Ca\emptyset_8$) polyhedra (Fig. 16f) girdling the column at intervals along [001]. The columns are isolated in the minerals of the ettringite group (Fig. 16g); intercolumn linkage is provided by hydrogen bonding *via* the (SO_4) tetrahedra in the interstices between the columns. The columns are linked into a three-dimensional framework directly *via* (SO_4) tetrahedra in the minerals of the fleischerite group (Fig. 16h).

Structures with finite clusters of polyhedra

Sulfate minerals based on finite clusters of octahedra and tetrahedra are listed in Table 7; Figures 13c-j show all the cluster types and their graphs.

In **creedite**, $Ca_3[Al_2(OH)_2F_8](SO_4)(H_2O)_2$, and **jurbanite**, $[Al_2(OH)_2(H_2O)_8](SO_4)_2 \cdot (H_2O)_2$, there is an octahedral edge-sharing dimer of the form $[Al_2\emptyset_{10}]$. In creedite, linkage between the octahedral clusters, (SO_4) tetrahedra, and (H_2O) groups is provided by Ca cations (Figs. 16i,j), whereas linkage of structural subunits in jurbanite is provided by hydrogen bonding only (Fig. 17a). Creedite and jurbanite can be considered as transitional between the unconnected-polyhedra structures and the finite-cluster structures because of the connectivity of the octahedra.

The structures of **minasragrite**, $[V^{4+}O(SO_4)(H_2O)_4](H_2O)$, and **xitieshanite**, $[Fe^{3+}(H_2O)_4\,Cl(SO_4)](H_2O)_2$, are based on a simple corner-sharing cluster of a tetrahedron and an octahedron (Fig. 13c). These clusters are linked by hydrogen bonding

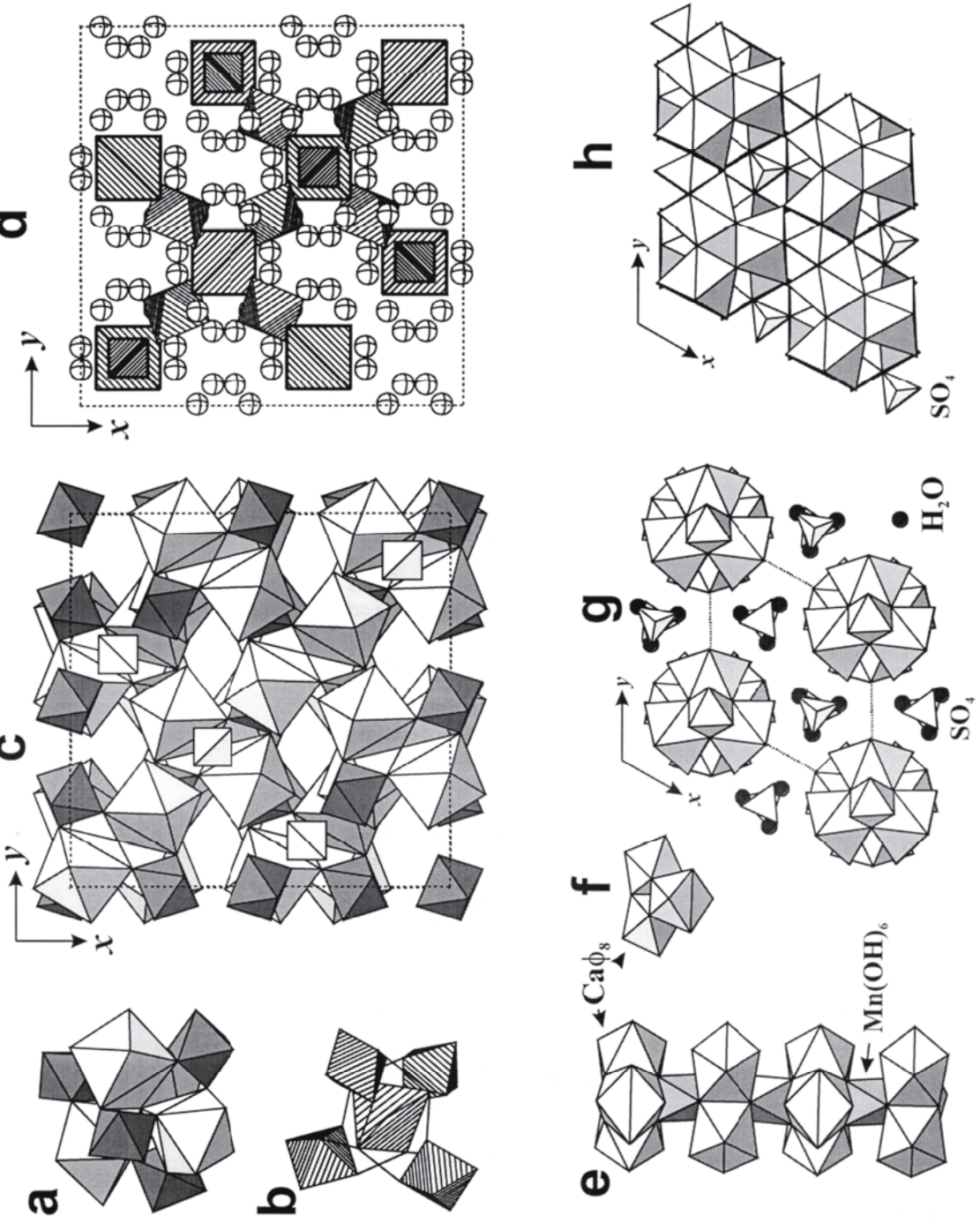

Figure 16. (a) The cluster of four ($CaØ_7$) polyhedra and (AlF_6) octahedra in chukhrovite; (b) the same cluster shown as an (FCa_4) tetra-hedron surrounded by four (AlF_6) octahedra; (c) the linkage of clusters, shown in Figure 14a, into a framework in chukhrovite; (d) repre-sentation of the structure of chukhrovite as (FCa_4) tetra-hedra (large tetrahedra), (AlF_6) octahedra, (SO_4) tetra-hedra (small tetrahedra), and (H_2O) groups (circles); (e) the column of ($MØ_6$) octahedra and triplets of ($CaØ_8$) polyhedra in the minerals of the ettringite and fleischerite groups; (f) the triplet of ($CaØ_8$) polyhedra in ettringite and fleischerite; the columns are (g) isolated in the minerals of the ettringite group, and (h) linked into a framework in the minerals of the fleischerite group.

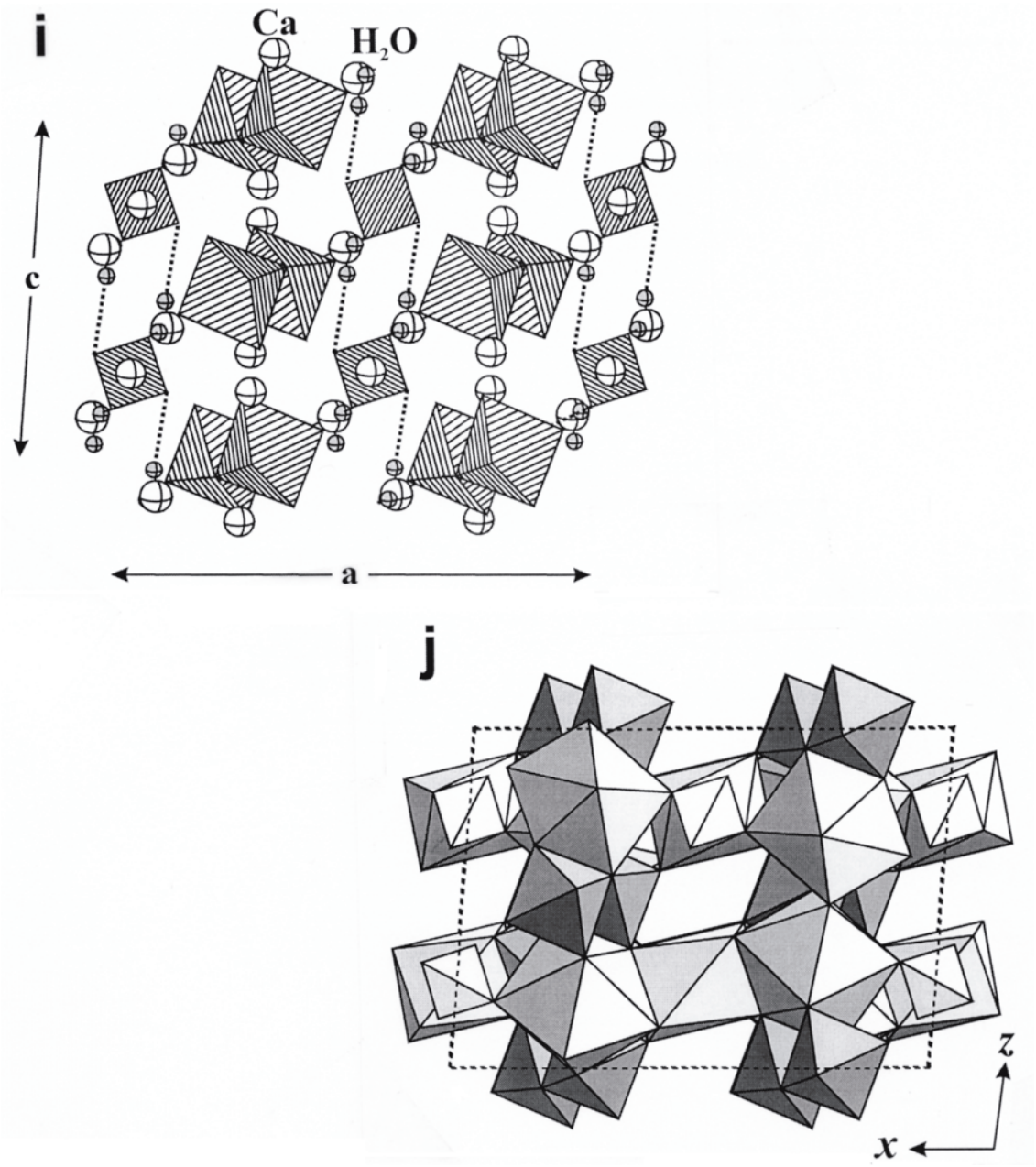

Figure 16, cont'd. (i) the structure of creedite with Ca atoms shown as circles; (j) polyhedral view of the structure of creedite.

through interstitial (H_2O) groups (Fig. 17b). The **blödite-group** minerals, $Na_2[M^{2+}(H_2O)_4(SO_4)_2]$, the **leonite-group** minerals, $K_2[M^{2+}(H_2O)_4(SO_4)_2]$, **chenite**, $(Pb^{2+}{}_4(OH)_2[Cu^{2+}(OH)_4(SO_4)_2]$ (Fig. 18a), and related minerals (Table 7) are based on the simple *trans* $[M(T\O_4)_2\O_4]$ cluster (Fig. 13d, 17c) that is also a constituent in phosphate minerals (e.g. anapaite, $Ca_2[Fe^{2+}(PO_4)_2(H_2O)_4]$ and schertelite, $(NH_4)_2[Mg(PO_3OH)_2(H_2O)_4]$. In **blödite**, these clusters are linked through edge-sharing octahedral $[Na_2\O_{10}]$ dimers into sheets parallel to (001) (Fig. 17d,e) in which the clusters are arranged at the vertices of a plane centered rectangular lattice. Intersheet linkage occurs *via* the interstitial alkali cations and hydrogen bonding, as shown in Figure 17d. In the leonite-group mineral **mereiterite**, $K_2[Fe^{2+}(H_2O)_4(SO_4)_2]$, there are sheets of unconnected *trans* $[M(T\O_4)\O_4]$ clusters (as in blödite, Fig. 17d) parallel to (001) that are linked by interstitial K and a network of hydrogen bonds (Fig. 17f). In **chenite**, (SO_4) tetrahedra are

Table 7. Sulfate minerals with finite clusters of (SO_4) tetrahedra and ($M\emptyset_6$) octahedra.*

Name	Formula	*a* (Å)	*b* (Å)	*c* (Å)	β (°)	S. G.	Graph	Fig.	Ref.
creedite	$Ca_3[Al_2(OH)_2F_8](SO_4)(H_2O)_2$	13.936	8.606	9.985	94.4	*C*2/*c*	13c	16i,j	[1]
jurbanite	$[Al_2(OH)_2(H_2O)_8](SO_4)_2(H_2O)_2$	8.396	12.479	8.155	101.9	$P2_1/n$	13c	17a	[2]
minasragrite	$[V^{4+}O(SO_4)(H_2O)_4](H_2O)$	6.976	9.716	12.902	110.9	$P2_1$/c	13d	–	[3]
blödite	$Na_2[Mg(H_2O)_4(SO_4)_2]$	11.03	8.140	5.490	100.7	$P2_1/a$	13c	17c,d	[5]
nickelblödite	$Na_2[Ni(H_2O)_4(SO_4)_2]$	10.87	8.07	5.46	100.7	$P2_1/a$	13e	17c,d	(6)
changoite	$Na_2[Zn(H_2O)_4(SO_4)_2]$	11.077	8.249	5.532	100.2	$P2_1/a$	13e	17c,d	(7)
leonite	$K_2[Mg(H_2O)_4(SO_4)_2]$	11.769	9.539	9.889	95.3	*C*2/*m*	13e	17f	[8]
mereiterite	$K_2[Fe^{2+}(H_2O)_4(SO_4)_2]$	11.841	9.553	9.942	94.9	*C*2/*m*	13e	17f	[9]
chenite[1]	$Pb^{2+}_4(OH)_2[Cu^{2+}(OH)_4(SO_4)_2]$	5.791	7.940	7.976	97.7	$P\bar{1}$	13e	18a,b	[10]
römerite[2]	$[Fe^{3+}(SO_4)_2(H_2O)_4]_2[Fe^{2+}(H_2O)_6]$	6.463	15.309	6.341	90.5	$P\bar{1}$	13f	18c	[11]
halotrichite	$[Fe^{2+}(SO_4)(H_2O)_5]\{Al(H_2O)_6\}_2(SO_4)(H_2O)_5$	6.179	24.29	20.51	101.0	$P2_1/c$	13f	18d	(6)
pickeringite	$[Mg(SO_4)(H_2O)_5]\{Al(H_2O)_6\}_2(SO_4)(H_2O)_5$	6.17	24.2	20.8	95.0	$P2_1/c$	13f	18d	(6)
bilinite	$[Fe^{2+}(SO_4)(H_2O)_5]\{Fe^{3+}(H_2O)_6\}_2(SO_4)(H_2O)_5$	6.208	24.333	21.255	100.3	$P2_1/c$	13f	18d	(6)
apjohnite	$[Mn^{2+}(SO_4)(H_2O)_5]\{Al(H_2O)_6\}_2(SO_4)(H_2O)_5$	6.198	24.347	21.266	100.3	$P2_1/c$	13f	18d	[12]
dietrichite	$[Zn(SO_4)(H_2O)_5]\{Al(H_2O)_6\}_2(SO_4)(H_2O)_5$	6.24	24.434	21.379	100.1	$P2_1/c$	13f	18d	(6)
wupatkiite	$[Co(SO_4)(H_2O)_5]\{Al(H_2O)_6\}_2(SO_4)(H_2O)_5$	6.189	24.234	21.204	100.3	$P2_1/c$	13f	18d	(6)
quenstedtite[3]	$[Fe^{3+}(H_2O)_4(SO_4)_2][Fe^{3+}(H_2O)_5(SO_4)](H_2O)_2$	6.184	23.600	6.539	101.7	$P\bar{1}$	13d,f	19a	[13]
polyhalite[4]	$K_2Ca_2[Mg(SO_4)_4(H_2O)_2]$	11.69	16.330	7.600	90.0	$F\bar{1}$	13g	19b,c	[14]
leightonite	$K_2Ca_2[Cu^{2+}(SO_4)_4(H_2O)_2]$	11.67	16.52	7.492	–	*Fmmm*	13g	–	(6)
rozenite	$[Fe^{2+}(SO_4)(H_2O)_4]$	5.97	13.640	7.980	90.4	$P2_1/n$	13i	19d	[15]
starkeyite	$[Mg(SO_4)(H_2O)_4]$	5.922	13.604	7.905	90.8	$P2_1/n$	13i	19d	[16]
ilesite	$[Mn^{2+}(SO_4)(H_2O)_4]$	5.94	13.76	8.01	90.8	$P2_1/n$	13i	19d	(6)
aplowite	$[Co(SO_4)(H_2O)_4]$	5.952	13.576	7.908	90.5	$P2_1/n$	13i	19d	[17]
boyleite	$[Zn(SO_4)(H_2O)_4]$	5.95	13.60	7.96	90.3	$P2_1/n$	13i	19d	(6)
ungemachite	$K_3Na_8[Fe^{3+}(SO_4)_6](NO_3)_2(H_2O)_6$	10.898	*a*	24.989	–	$R\bar{3}$	13h	19e,f	[18]
humberstonite	$K_3Na_6(Na,Mg)_2[Mg(SO_4)_6](NO_3)_2(H_2O)_6$	10.906	*a*	24.395	–	$R\bar{3}$	13h	19e,f	[19]
coquimbite	$[Fe^{3+}_3(SO_4)_6(H_2O)_6]\{Fe^{3+}(H_2O)_6\}(H_2O)_6$	10.922	*a*	17.084	–	$P\bar{3}1c$	13j	19g	[20]
paracoquimbite	$[Fe^{3+}_3(SO_4)_6(H_2O)_6]\{Fe^{3+}(H_2O)_6\}(H_2O)_6$	10.926	*a*	51.300	–	$R\bar{3}$	13j	19g	[21]
metavoltine	$K_2Na_6[Fe^{3+}_3O(SO_4)_6(H_2O)_3]\{Fe^{2+}(H_2O)_6\}(H_2O)_6$	9.575	*a*	18.170	–	*P*3	13k	19h	[22]

* $M = Fe^{2+}$, Ni, Mg, Cu^{2+}, Mn^{2+}, Zn, Al, V^{3+}, Fe^{3+} [1] α = 112.0°; γ = 100.4°; [2] α = 90.5°; γ = 85.2°; [3] α = 94.2°; γ = 96.3; [4] α = 91.6°; γ = 91.9

References: [1] Giuseppetti and Tadini (1983), [2] Sabelli (1985a), [3] Tachez et al. (1979), [4] Zhou et al. (1988), [5] Rumanova and Malitskaya (1959), Hawthorne (1985b), (6) Gaines et al. (1997), (7) Schlüter et al. (1999), [8] Jarosch (1985), [9] Giester and Rieck (1995), [10] Hess et al. (1988), [11] Fanfani et al. (1970), [12] Menchetti and Sabelli (1976b), [13] Thomas et al. (1974), [14] Schlatti et al. (1970), [15] Baur (1960), [16] Baur (1962), [17] Kellersohn (1992), [18] Groat and Hawthorne (1986), [19] Burns and Hawthorne (1994), [20] Fang and Robinson (1970a), [21] Robinson and Fang (1971), [22] Giacovazzo et al. (1976a)

linked to Jahn-Teller-distorted $\{Cu^{2+}(OH)_4O_2\}$ octahedra *via* apical (and therefore weak) bonds. The strongest bonding in chenite is within sheets parallel to the $(\bar{1}10)$ plane and is formed by Pb^{2+} and Cu^{2+} cations and $(OH)^-$ groups (Fig. 18a). The structure of the sheet (Fig. 18b) can be described as based on $\{(OH)Pb^{2+}_3\}$ and $[(OH)Cu^{2+}Pb^{2+}_2]$ triangular pyramids or $\{Pb^{2+}(OH)_3\}$ triangular pyramids, $[Pb^{2+}(OH)_4]$ tetragonal pyramids, and $[Cu^{2+}(OH)_4]$ squares.

The structures of **römerite**, $[Fe^{3+}(SO_4)_2(H_2O)_4]_2\{Fe^{2+}(H_2O)_6\}$, and the minerals of the **halotrichite group**, $[M^{2+}(SO_4)(H_2O)_5]\{M^{3+}(H_2O)_6\}_2(SO_4)(H_2O)_5$, are also based on the $[M(T\emptyset_4)_2\emptyset_4]$ cluster, but in the *cis* rather than the *trans* arrangement (Fig. 13e). In addition to this cluster, römerite contains isolated $\{Fe^{2+}(H_2O)_6\}$ octahedra (Fig. 18c), and these elements are linked by hydrogen bonding both between unconnected octahedra and

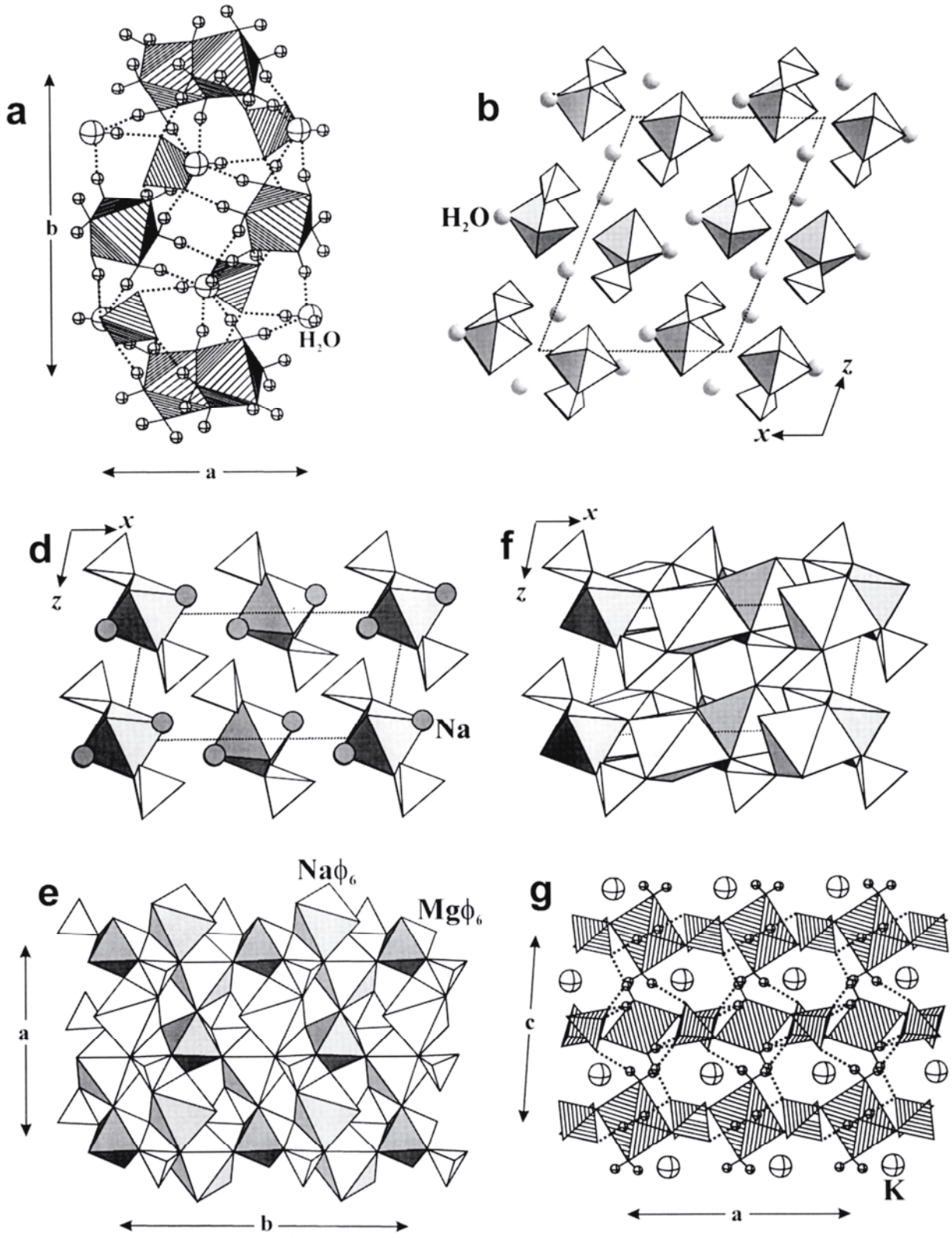

Figure 17. The structures of (a) jurbanite; (b) xitieshanite; (c) blödite, shown as $[Mg(H_2O)_4(SO_4)_2]$ clusters and Na atoms; (d,e) blödite as a framework of ($MgØ_6$) octahedra, ($NaØ_6$) octahedra, and (SO_4) tetrahedra; (f) mereiterite.

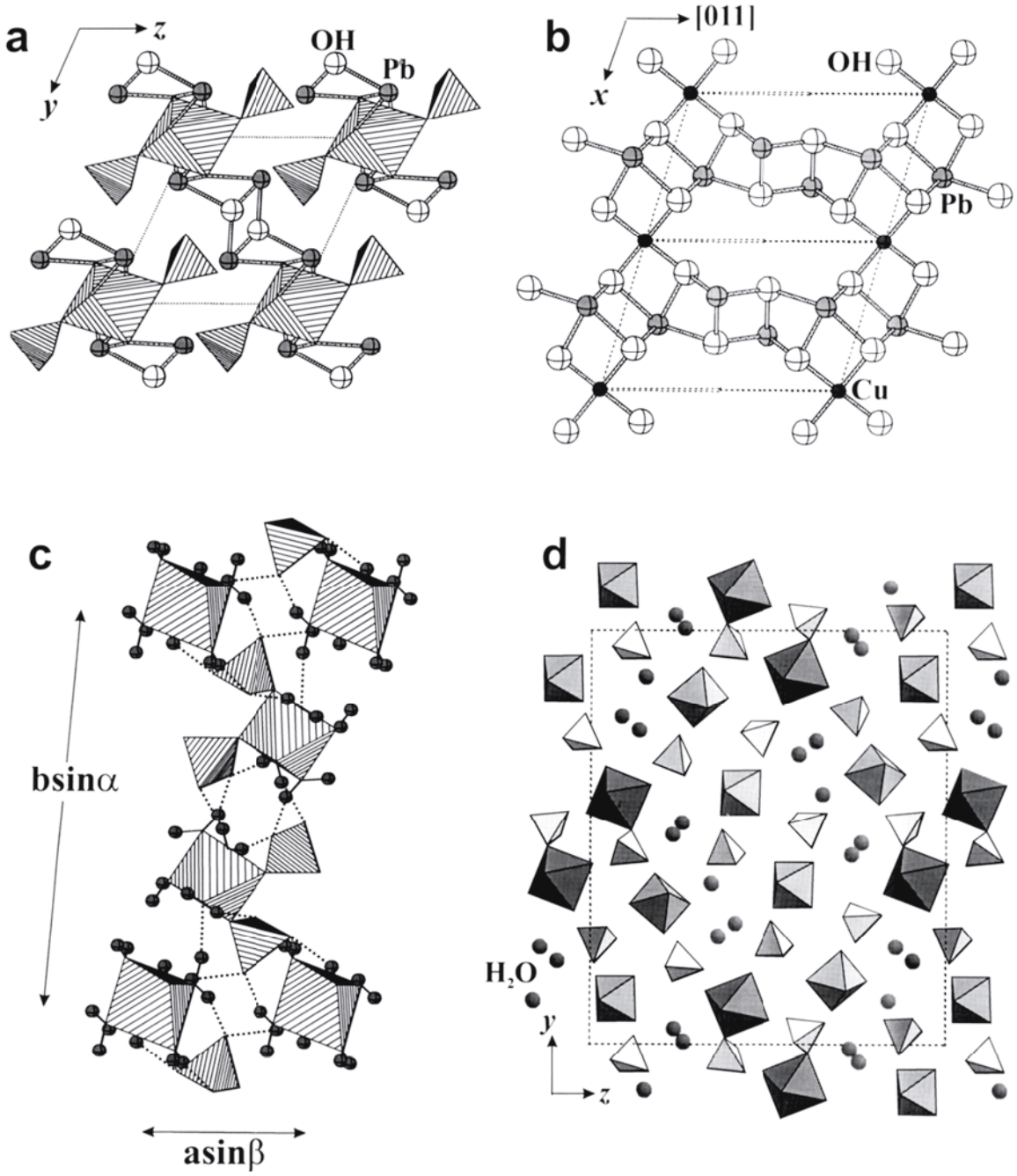

Figure 18. The structures of (a) chenite, based on $[Cu(OH)_4(SO_4)_2]$ clusters, Pb atoms, and (OH)-anions; (b) the sheet of Pb and Cu atoms and (OH)-groups in chenite; (c) römerite; (d) apjohnite.

tetrahedra, and between octahedra and tetrahedra of the same $[M(TO_4)_2Ø_4]$ cluster. **Apjohnite**, a mineral of the halotrichite group, contains isolated $[Mn^{2+}(SO_4)_2(H_2O)_4]$ clusters, $\{Al(H_2O)_6\}$ octahedra, (SO_4) tetrahedra, and (H_2O) groups (Fig. 18d) linked solely by hydrogen bonding. The structure of **quenstedtite**, $[Fe^{3+}(H_2O)_4(SO_4)_2][Fe^{3+}(H_2O)_5(SO_4)](H_2O)_2$, consists of *cis* $[M(TØ_4)_2Ø_4]$ clusters, $[M(TØ_4)Ø_5]$ clusters, and (H_2O) groups. The clusters are arranged in layers parallel to (010). There are layers of $[M(TO_4)Ø_5]$ clusters either side of $y = 0$, and layers of $[M(TO_4)_2Ø_2]$ clusters either side of $y = 1/2$. Like layers are linked directly *via* hydrogen bonds, with donor groups in one layer and acceptor groups in the other layer. Unlike layers are linked *via* hydrogen bonding that involves intermediary (H_2O) groups (at $y \sim \pm 1/4$) that do not bond to any cations

(Fig. 19a). In **polyhalite**, $K_2Ca_2[Mg(SO_4)_4(H_2O)_2]$, the fundamental $[M(TO_4)_4Ø_2]$ cluster is an ($MgØ_6$) octahedron that shares four of its vertices with four (SO_4) tetrahedra (Fig. 13f). These clusters are arranged in sheets parallel to (010) (Fig. 19b) and are linked into a framework by Ca and K cations (Fig. 19c). **Leightonite**, $K_2Ca_2[Cu^{2+}(SO_4)_4(H_2O)_2]$, has the same stoichiometry as polyhalite, the cell dimensions of these two minerals are similar, and both have an *F*-centered unit cell. However, leightonite is reported as orthorhombic and polyhalite as triclinic with $\alpha \approx \beta \approx \gamma \approx 90°$ (Table 7). The difference in symmetry between these two structures is not understood.

The structures of the minerals of the **rozenite group**, e.g. **aplowite**, $[Co(SO_4)(H_2O)_4]$, are based on the $[M_2(TØ_4)_2Ø_8]$ cluster (Fig. 13h), linked solely by hydrogen bonds both within and between adjacent clusters (Fig. 19d). The structure of **ungemachite**, $K_3Na_8[Fe^{3+}(SO_4)_6](NO_3)_2(H_2O)_6$, is based on the $[M(TØ_4)Ø_6]$ cluster shown in Figure 13g. In his work on glaserite-related structures, Moore (1973) called such a cluster *a pinwheel*. The $[Fe(SO_4)_6]$ pinwheels in ungemachite, together with triangular-prismatic-coordinated Na cations, NO_3 groups, and K cations, form layers parallel to (001) (Fig. 19e). Each $[FeØ_6]$ octahedron shares two faces with $\{NaO_3(H_2O)_3\}$ octahedra to form a linear octahedral trimer parallel to [001] (Fig. 19f). The only interlayer linkage is provided by hydrogen bonds from (H_2O) groups of the $\{NaO_3(H_2O)_3\}$ octahedra to sulfate groups of neighboring layers. The structures of **coquimbite**, $[Fe^{3+}{}_3(SO_4)_6(H_2O)_6]$-$\{Fe^{3+}(H_2O)_6\}(H_2O)_6$, and its polytype, **paracoquimbite**, $[Fe^{3+}{}_3(SO_4)_6(H_2O)_6]$-$\{Fe^{3+}(H_2O)_6\}(H_2O)_6$, are based on the $[M_3(TO_4)_6]$ cluster shown in Fig. 13j, isolated $\{Fe^{3+}(H_2O)_6\}$ octahedra, and (H_2O) groups. The $[M_3(TO_4)_3]$ clusters are oriented with their long axis parallel to [001]. The $\{Fe^{3+}(H_2O)_6\}$ octahedra lie in the plane at $z = 0$ and 1/2 (Fig. 19g), forming layers of octahedra that are connected into sheets by hydrogen bonds; thus coquimbite and paracoquimbite are polytypic. **Metavoltine**, $K_2Na_6[Fe^{3+}{}_3O(SO_4)_6(H_2O)_3]_2\{Fe^{2+}(H_2O)_6\}(H_2O)_6$, is built from a complex but elegant $[M_3(TØ_4)_6Ø_4]$ cluster (Fig. 13j) that also occurs in the structures of **Maus's salts** (Scordari et al. 1994 and references therein). These clusters form layers parallel to (001) at z = 1/4 and 3/4 (Fig. 19h), and are linked in the plane of the layer by K. Linkage between the layers occurs *via* hydrogen bonds through layers of (H_2O) groups at z ~0 and 1/2 and involving the isolated $\{Fe^{2+}(H_2O)_6\}$ groups.

Structures with infinite chains

The graphs of chains of octahedra and tetrahedra that occur in sulfate minerals are shown in Figure 20; sulfate minerals based on these chains are listed in Table 8.

The structure of **aluminite**, $[Al_2(OH)_4(H_2O)_3](SO_4)(H_2O)_4$, is based on chains of edge-sharing octahedra (Fig. 21a) that extend along [100] and are linked to (SO_4) groups by hydrogen bonds involving (H_2O) groups. There are two types of H_2O groups in aluminite: (1) those bonded to cations; (2) those not bonded to cations (Fig. 21b). The latter are held in the structure solely by hydrogen bonds, and serve to propagate bonding from hydrogen-bond donors attached to one cation to hydrogen-bond acceptors attached to another cation out-of-range of direct hydrogen bonding. Aluminite is the only known example of an undecorated chain of octahedra in sulfate minerals. In all other minerals based on chains, ($MØ_6$) octahedra and ($TØ_4$) tetrahedra link together by sharing common vertices.

The structures of the **chalcanthite-group** minerals, $[M^{2+}(H_2O)_4(SO_4)](H_2O)$, are based on the $[M(TO_4)Ø_4]$ chain with alternating corner-sharing octahedra and tetrahedra (Fig. 21c). The chains extend along [110] and are cross-linked by hydrogen bonds between the octahedral (H_2O) ligands and the tetrahedral ligands. In addition, there is an (H_2O) group that is not directly bonded to a cation; this acts as both a hydrogen-bond

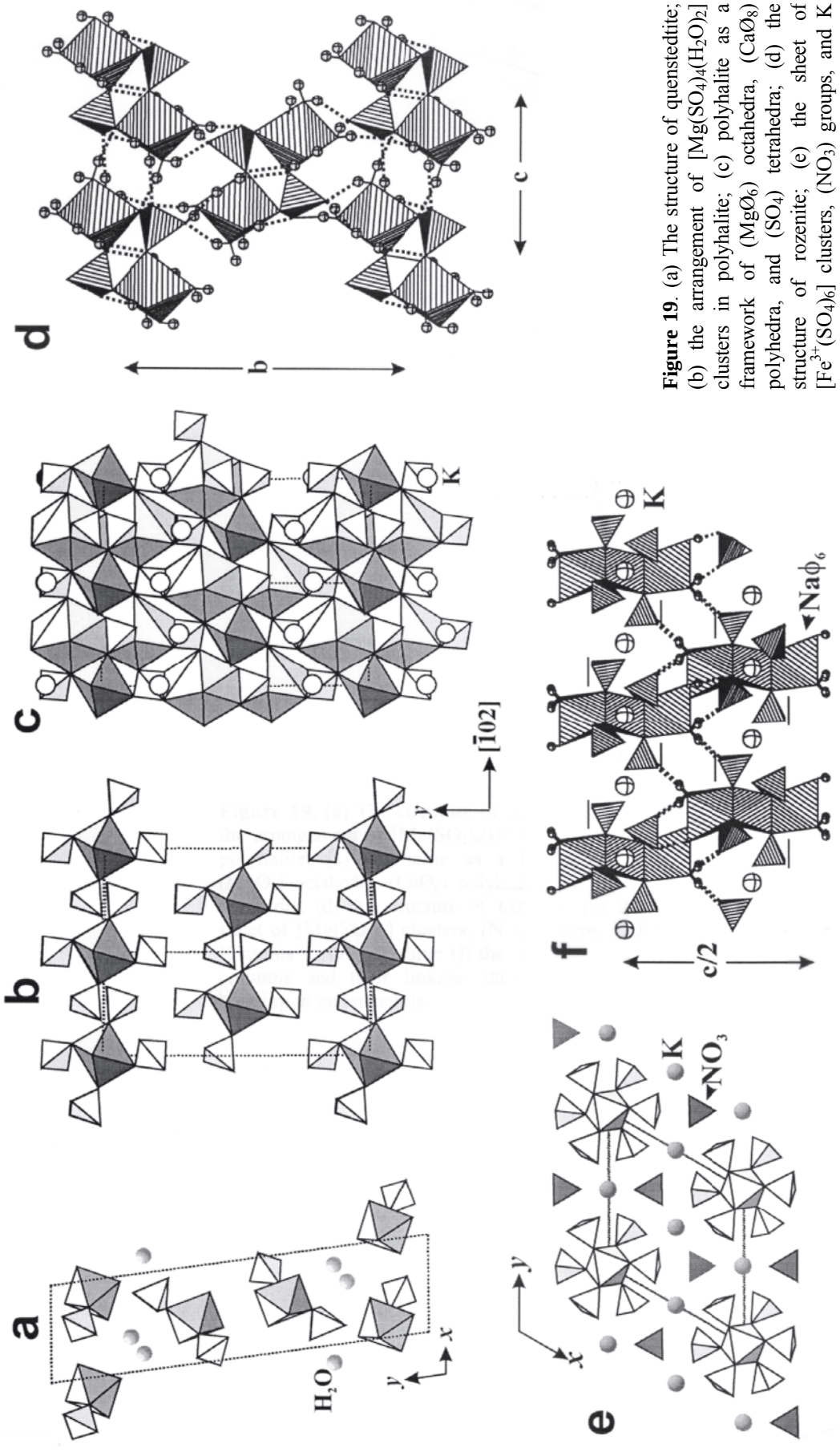

Figure 19. (a) The structure of quenstedtite; (b) the arrangement of $[Mg(SO_4)_4(H_2O)_2]$ clusters in polyhalite; (c) polyhalite as a framework of ($MgØ_6$) octahedra, ($CaØ_8$) polyhedra, and (SO_4) tetrahedra; (d) the structure of rozenite; (e) the sheet of $[Fe^{3+}(SO_4)_6]$ clusters, (NO_3) groups, and K atoms in ungemachite; (f) the arrangement of columns and their linkage through hydrogen bonding in ungemachite.

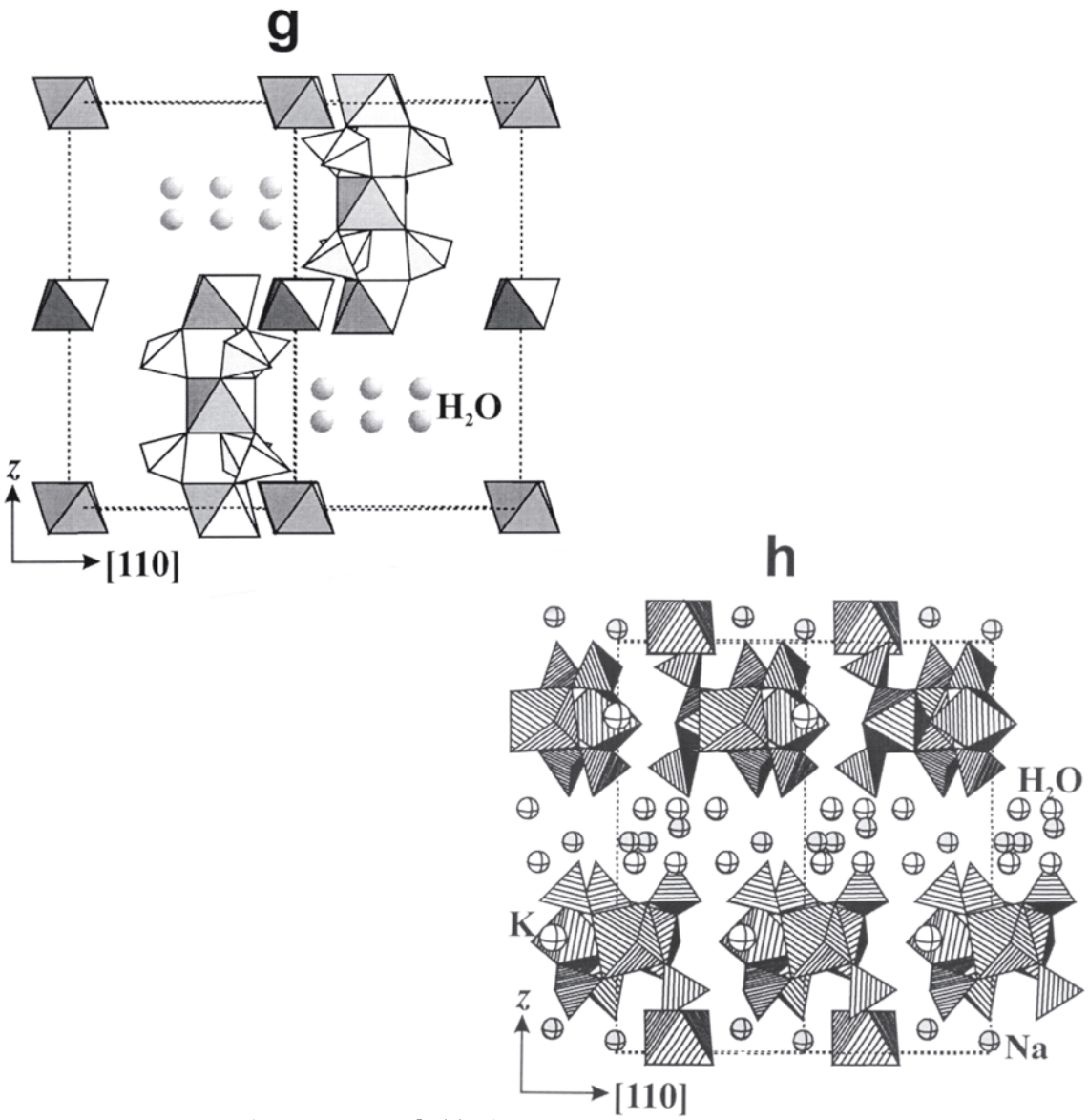

Figure 19, cont'd. (g) The structure of coquimbite, and (h) the structure of metavoltine.

acceptor and donor, promoting linkage along and between the chains (Fig. 21d). This $[M(TO_4)]$ chain also occurs in the structures of the arsenate minerals liroconite, $Cu^{2+}{}_2[Al(AsO_4)(OH)_4](H_2O)_4$, and brassite, $[Mg\{AsO_3(OH)\}(H_2O)_4]$.

The $[M(T\O_4)\O_3]$ chain is the basis of **butlerite**, $[Fe^{3+}(OH)(H_2O)_2(SO_4)]$, **parabutlerite**, $[Fe^{3+}(OH)(H_2O)_2(SO_4)]$, and **uklonskovite**, $Na[MgF(H_2O)_2(SO_4)]$. In this chain (Figs. 20c, 21e), the tetrahedra alternate along the chain and link to *trans* vertices of the octahedra. This is a 7-Å chain in the terminology of Moore (1970); the repeat distance of the chains is approximately 7 Å, and this is usually apparent in the cell dimensions of minerals containing these chains. In butlerite and parabutlerite, the $[Fe^{3+}(SO_4)(OH)(H_2O)_2]$ chains are linked solely by hydrogen bonds, as there are no interstitial cations (Figs. 21e to 21g). The chains are extremely similar in these dimorphous minerals, and the principal structural difference is in the relative disposition of adjacent

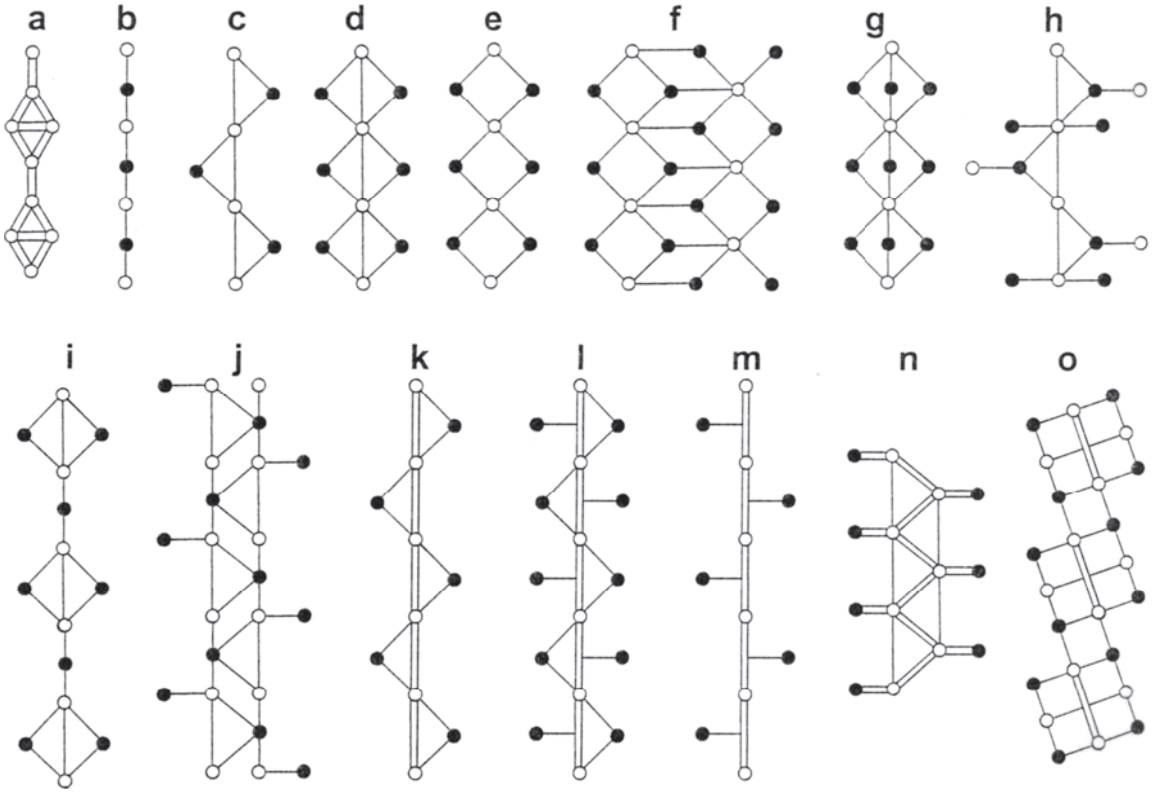

Figure 20. Graphs of octahedral–tetrahedral chains in the structures of sulfate minerals; octahedra are white, tetrahedra are black. See text for details.

chains (see Hawthorne 1990 for details). Uklonskovite consists of topologically identical $[Mg(SO_4)(OH)(H_2O)_2]$ chains, linked by [8]-coordinated Na (Fig. 21h). Hydrogen bonding provides additional linkage from an octahedral ligand in one chain to a tetrahedral ligand in the adjacent chain.

Fibroferrite, $[Fe^{3+}(OH)(H_2O)_2(SO_4)](H_2O)_3$, is a magnificent structure (Fig. 22a,b). The $[M\emptyset_5]$ vertex-sharing chain of octahedra with *cis*-corner-sharing octahedra is unusual; chains of this stoichiometry usually link through *trans* octahedral vertices (e.g. Fig. 21e). The chain in fibroferrite links *via cis* octahedral vertices, thus accounting for its helical configuration (Fig. 22a). This chain is closely related to the chain in butlerite, parabutlerite, and uklonskovite (Fig. 19c) in that they are geometrical isomers and have the same graph (Fig. 20c). Adjacent chains link both by direct hydrogen-bonding between chains, and by a hydrogen-bonding network involving (H_2O) groups not linked to any cations (Fig. 22b). The structures of **sideronatrite**, $Na_2[Fe^{3+}(OH)(SO_4)_2](H_2O)_3$, and **metasideronatrite**, $Na_4[Fe^{3+}{}_2(OH)_2(SO_4)_4](H_2O)_3$, are based on the chain that has the graph shown in Figure 20d; this is the type-VII 7 Å chain of Moore (1970). These minerals show considerable disorder in terms of the relations between adjacent chains in their structures (Scordari 1981c). This chain topology is also present in the phosphate mineral tancoite, $Na_2LiH[Al(PO_4)_2(OH)]$ (Hawthorne 1983b). The structures of the **botryogen group**, $[M^{2+}Fe^{3+}(OH)(H_2O)_6(SO_4)_2](H_2O)$, are also based on the 7 Å chain of the form $[M(TO_4)_2\emptyset]$ (type-I according to Moore 1970). The chain in botryogen links to a $(Mg\emptyset_6)$ octahedron through one of its vertices (Fig. 22c). The packing of the chains in the structure is shown in Figure 22d; interchain linkage involves only hydrogen bonding.

The chain in **kröhnkite**, $Na_2[Cu^{2+}(H_2O)_2(SO_4)_2]$, can be described as based on *cis* $[M(TO_4)_2\emptyset_4]$ clusters (Fig. 13e) polymerized by corner-sharing between polyhedra (Fig. 20e, 22e). The chains are linked together by interstitial Na and hydrogen bonds from

Table 8. Sulfate minerals with chains of (SO_4) tetrahedra and ($M\phi_6$) octahedra.*

Name	Formula	*a* (Å)	*b* (Å)	*c* (Å)	α (°)	β (°)	γ (°)	S. G.	Graph	Fig.	Ref.
aluminite	$[Al_2(OH)_4(H_2O)_3](SO_4)(H_2O)_4$	7.440	15.583	11.700	–	110.2	–	$P2_1/c$	20a	21a,b	[1]
chalcanthite	$[Cu^{2+}(H_2O)_4(SO_4)](H_2O)$	6.141	10.736	5.986	82.3	107.4	102.7	$P\bar{1}$	20b	21c,d	[2]
pentahydrite	$[Mg(H_2O)_4(SO_4)](H_2O)$	6.314	10.565	6.030	81.1	109.8	105.1	$P\bar{1}$	20b	21c,d	[3]
siderotil	$[Fe^{2+}(H_2O)_4(SO_4)](H_2O)$	6.26	10.63	6.06	92.1	110.2	102.9	$P\bar{1}$	20b	21c,d	(4)
jokokuite	$[Mn^{2+}(H_2O)_4(SO_4)](H_2O)$	6.37	10.77	6.13	98.8	110.0	102.2	$P\bar{1}$	20b	21c,d	(4)
butlerite	$[Fe^{3+}(OH)(H_2O)_2(SO_4)]$	6.500	7.370	5.840	–	108.4	–	$P2_1/m$	20c	21e,f	[5]
parabutlerite	$[Fe^{3+}(OH)(H_2O)_2(SO_4)]$	7.380	20.130	7.220	–	–	–	$Pmnb$	20c	21g	[6]
uklonskovite	$Na[MgF(H_2O)_2(SO_4)]$	7.202	7.214	5.734	–	113.2	–	$P2_1/m$	20c	21h	[7]
fibroferrite	$[Fe^{3+}(OH)(H_2O)_2(SO_4)](H_2O)_3$	24.177	*a*	7.656	–	–	–	$R\bar{3}$	20c	22a,b	[8]
botryogen	$[MgFe^{3+}(OH)(H_2O)_6(SO_4)_2](H_2O)$	10.526	17.872	7.136	–	100.1	–	$P2_1/n$	20h	22c,d	[9]
zincobotryogen	$[ZnFe^{3+}(OH)(H_2O)_6(SO_4)_2](H_2O)$	10.517	17.847	7.133	–	100.1	–	$P2_1/n$	20h	22c,d	[10]
kröhnkite	$Na_2[Cu^{2+}(H_2O)_2(SO_4)_2]$	5.807	12.656	5.517	–	108.3	–	$P2_1/c$	20e	22e,f	[11]
krausite	$K[Fe^{3+}(H_2O)_2(SO_4)_2]$	7.920	5.146	9.014	–	102.8	–	$P2_1/m$	20f	22g,h	[12]
sideronatrite	$Na_2[Fe^{3+}(OH)(SO_4)_2](H_2O)_3$	7.290	20.560	7.170	–	–	–	$Pnn2$	20d	–	[13]
metasideronatrite	$Na_4[Fe^{3+}{}_2(OH)_2(SO_4)_4](H_2O)_3$	7.357	16.002	7.102	–	–	–	$Pbnm$	20d?	–	(14)
ferrinatrite	$Na_3[Fe^{3+}(SO_4)_3](H_2O)_3$	15.566	*a*	8.690	–	–	–	$P\bar{3}$	20g	23a,b	[15]
copiapite	$[Fe^{3+}{}_2(OH)(H_2O)_4(SO_4)_3]_2\{Fe^{2+}(H_2O)_6\}(H_2O)_6$	7.390	18.213	7.290	93.7	102.1	99.3	$P\bar{1}$	20i	23c,d	[16]
magnesiocopiapite	$[Fe^{3+}{}_2(OH)(H_2O)_4(SO_4)_3]_2\{Mg(H_2O)_6\}(H_2O)_6$	7.370	18.890	7.240	91.3	102.4	99.0	$P\bar{1}$	20i	23c,d	[17]
cuprocopiapite	$[Fe^{3+}{}_2(OH)(H_2O)_4(SO_4)_3]_2\{Cu^{2+}(H_2O)_6\}(H_2O)_6$	7.31	18.15	7.25	92.5	102.3	100.4	$P\bar{1}$	20i	23c,d	(4)
ferricopiapite	$[Fe^{3+}{}_2(OH)(H_2O)_4(SO_4)_3]_2\{(Fe^{3+}{}_{0.67}\square_{0.33})(H_2O)_5\}(H_2O)_6$	7.390	18.213	7.290	93.7	102.2	99.3	$P\bar{1}$	20i	23c,d	(18)
calciocopiapite	$[Fe^{3+}{}_2(OH)(H_2O)_4(SO_4)_3]_2\{Ca(H_2O)_6\}(H_2O)_6$	7.44	18.79	7.22	94.7	104.7	102.2	$P\bar{1}$	20i	23c,d	(4)
zincocopiapite	$[Fe^{3+}{}_2(OH)(H_2O)_4(SO_4)_3]_2\{Zn(H_2O)_6\}(H_2O)_6$	7.33	18.72	7.35	91.5	102.1	98.7	$P\bar{1}$	20i	23c,d	(4)
aluminocopiapite	$[Fe^{3+}{}_2(OH)(H_2O)_4(SO_4)_3]_2\{Al_{0.67}\square_{0.33})(H_2O)_6\}(H_2O)_6$	7.251	18.161	7.267	94.0	102.2	98.0	$P\bar{1}$	20i	23c,d	(19)
destinezite	$[Fe^{3+}{}_2(OH)(H_2O)_5(PO_4)(SO_4)](H_2O)$	9.570	9.716	7.313	98.7	107.9	63.9	$P\bar{1}$	20j	23e,f	[20]
linarite	$Pb^{2+}[Cu^{2+}(OH)_2(SO_4)]$	9.701	5.650	4.690	–	102.7	–	$P2_1/m$	20k	23g,h	[21]

wherryite	$Pb^{2+}_7[Cu^{2+}(OH)(SO_4)(SiO_4)]_2(SO_4)_2$	20.789	5.787	9.142	–	91.2	–	$C2/m$	20l	23i,j	[22]
tsumebite	$Pb^{2+}_2[Cu^{2+}(OH)(PO_4)(SO_4)]$	7.85	5.80	8.70	–	111.5	–	$P2_1/m$	20l	–	[23]
arsentsumebite	$Pb^{2+}_2[Cu^{2+}(OH)(AsO_4)(SO_4)]$	7.84	5.92	8.85	–	112.6	–	$P2_1/m$	20l	–	[4]
caledonite	$Pb^{2+}_5[Cu^{2+}_2(OH)_6(SO_4)_2](SO_4)(CO_3)$	20.089	7.146	6.560	–	–	–	$Pmn2_1$	20m	24a,b	[24]
chlorothionite	$K_2[Cu^{2+}Cl_2(SO_4)]$	7.732	6.078	16.292	–	–	–	$Pnma$	20n	24c,d	[25]
amarantite	$[Fe^{3+}_2O(H_2O)_4(SO_4)_2](H_2O)_3$	8.976	11.678	6.698	95.7	90.4	97.2	$P\bar{1}$	20o	24e,f	[26]
hohmannite	$[Fe^{3+}_2O(H_2O)_4(SO_4)_2](H_2O)_4$	9.148	10.922	7.183	90.3	90.8	104.4	$P\bar{1}$	20o	24e,g	[27]

* M = Cu, Fe, Ni, Mg, Zn, Mn, Co, Al; ϕ = O, OH, H_2O, F, Cl

References: [1] Sabelli and Ferroni (1978), [2] Bacon and Titterton (1975), [3] Baur and Rolin (1972), [4] Gaines et al. (1997), [5] Fanfani et al. (1971), [6] Borene (1970), [7] Sabelli (1985b), [8] Scordari (1981a), [9] Süsse (1968), [10] Hexiong and Pingqiu (1988), [11] Hawthorne and Ferguson (1975a), [12] Effenberger et al. (1986), [13] Scordari (1981b), (14) Scordari et al. (1982), [15] Scordari (1977), Mereiter (1976), [16] Fanfani et al. (1973), [17] Süsse (1970), (18) Bayliss and Atencio (1985), (19) Jolly and Foster (1967), [20] Peacor et al. (1999a), [21] Effenberger (1987), [22] Cooper and Hawthorne (1994), [23] Fanfani and Zanazzi (1967), [24] Giacovazzo et al. (1973), [25] Giacovazzo et al. (1976b), [26] Süsse (1967), Giacovazzo and Menchetti (1969), [27] Scordari (1978)

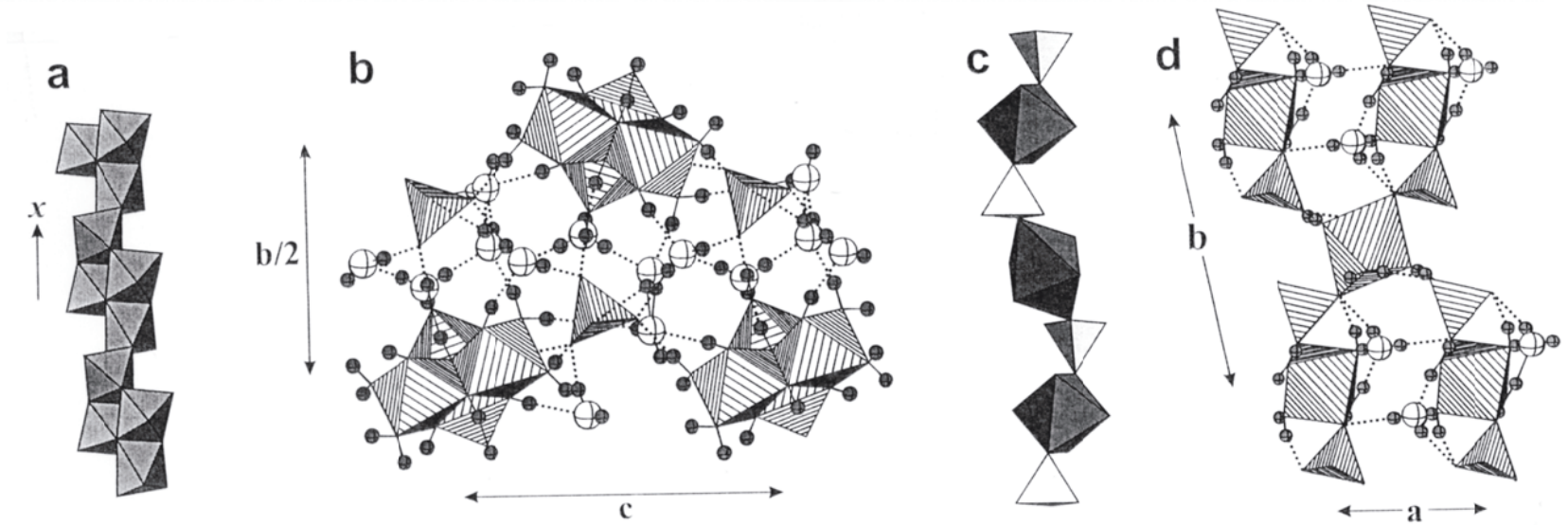

Figure 21. (a) The chain of edge-sharing ($AlØ_6$) octahedra in aluminite; (b) the linkage of octahedral chains, (SO_4) tetrahedra, and (H_2O) groups through hydrogen bonds (shown as dashed lines) in aluminite; (c) the chain of alternating corner-sharing octahedra and tetrahedra in the minerals of the chalcanthite group; (d) interchain linkage to (SO_4) tetrahedra and (H_2O) groups through hydrogen bonds (shown as dashed lines) in chalcanthite.

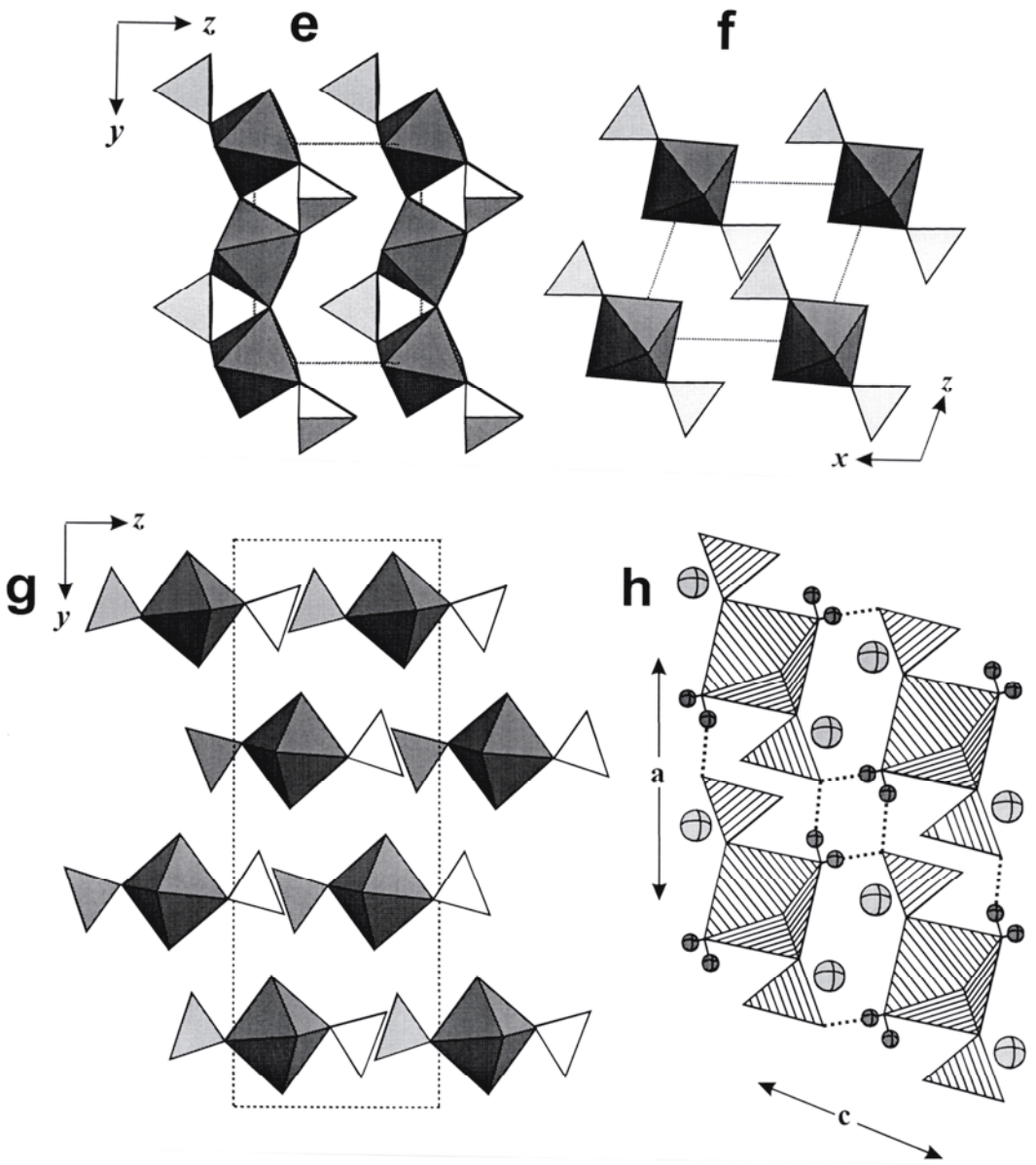

Figure 21, cont'd. (e) the $[M(TO_4)Ø_3]$ chains extending along *y* in butlerite; (f) packing of $[M(TO_4)Ø_3]$ chains in butlerite; (g) packing of $[M(TØ_4)Ø_3]$ chains in parabutlerite; (h) the hydrogen bonds between adjacent $[M(TØ_4)Ø_3]$ chains in uklonskovite (Na atoms are shown as large circles).

octahedral donor ligands to tetrahedral acceptor ligands (Fig. 22f). This type of $[M(TO_4)_2Ø_4]$ chain is common in arsenate and phosphate minerals, and is the basis of the minerals of the brandtite, $Ca_2[Mn^{2+}(AsO_4)_2(H_2O)_2]$, talmessite, $Ca_2[Mg(AsO_4)_2(H_2O)_2]$, and fairfieldite, $Ca_2[Mn^{2+}(PO_4)_2(H_2O)_2]$, groups (Hawthorne 1985a). **Krausite**, $K[Fe^{3+}(H_2O)_2(SO_4)_2]$, is based on a ribbon of double kröhnkite chains (Figs. 20f, 22g) linked by interstitial K (Fig. 22h). This ribbon also occurs as a fragment of the sheet that is the basis of the structure of ransomite.

Ferrinatrite, $Na_3(H_2O)_3[Fe^{3+}(SO_4)_3]$, is based on a chain consisting of octahedra linked by corner-sharing with tetrahedra such that all octahedron vertices link to tetrahedra, and half the tetrahedron vertices link to octahedra (Fig. 23a); the graph of this arrangement is shown in Figure 20g. This chain is closely related to the finite cluster in coquimbite and paracoquimbite (Fig. 13i). These columns occur at the vertices of a 3^6 plane net (Fig. 23b),

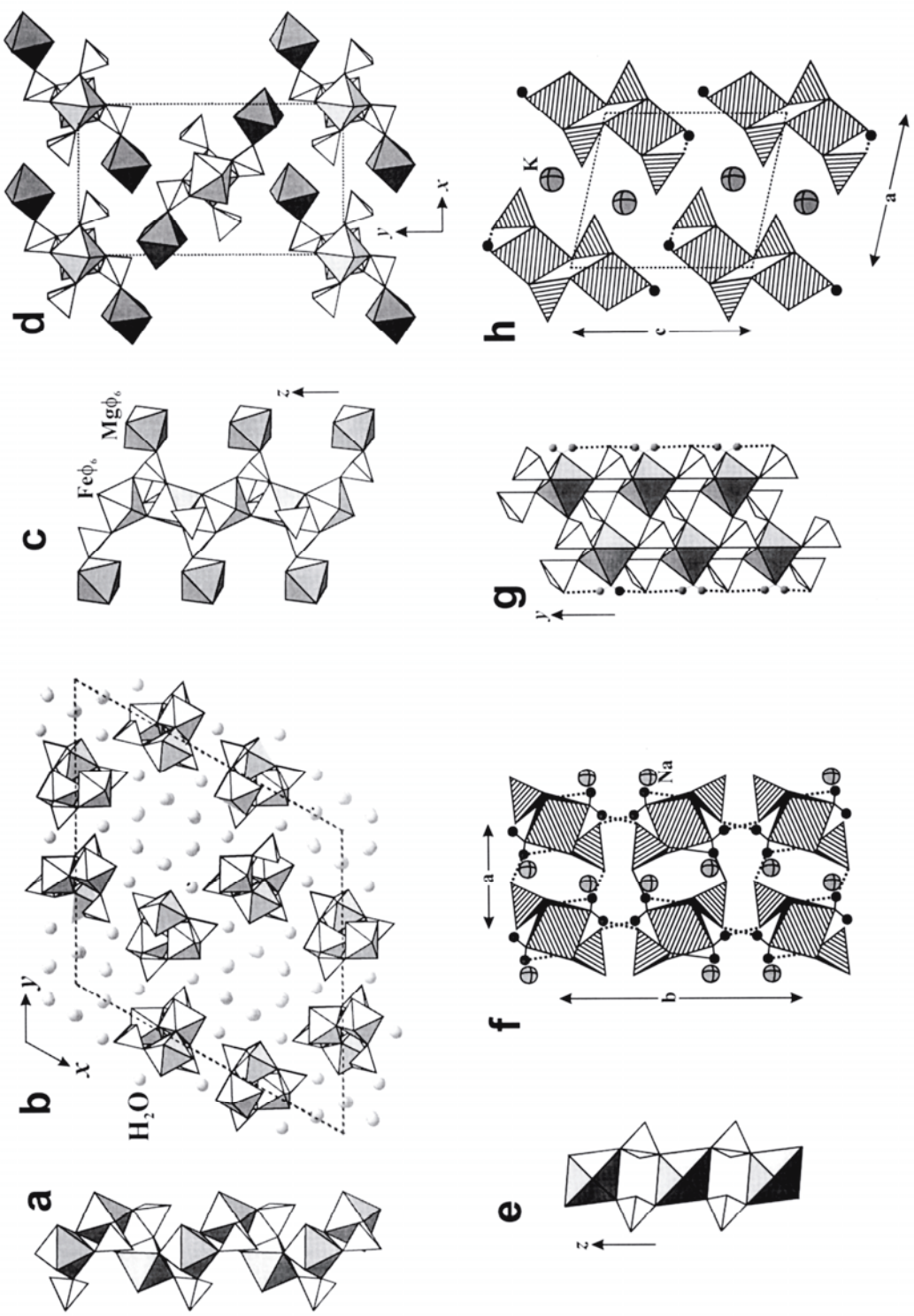

Figure 22. (a) The chain of *cis*-corner-sharing octahedra (decorated with tetrahedra) in fibroferrite; (b) the arrangement of chains and (H_2O) groups in fibroferrite; (c) the open-branched octahedral–tetrahedral chain in botryogen; (d) packing of chains in the botryogen structure; (e) the $[M(TO_4)_2Ø_4]$ chain in kröhnkite; (f) packing of $[M(TO_4)_2Ø_4]$ chains in kröhnkite; (g) the double-kröhnkite-like ribbon in krausite; (h) packing of ribbons in the structure of krausite.

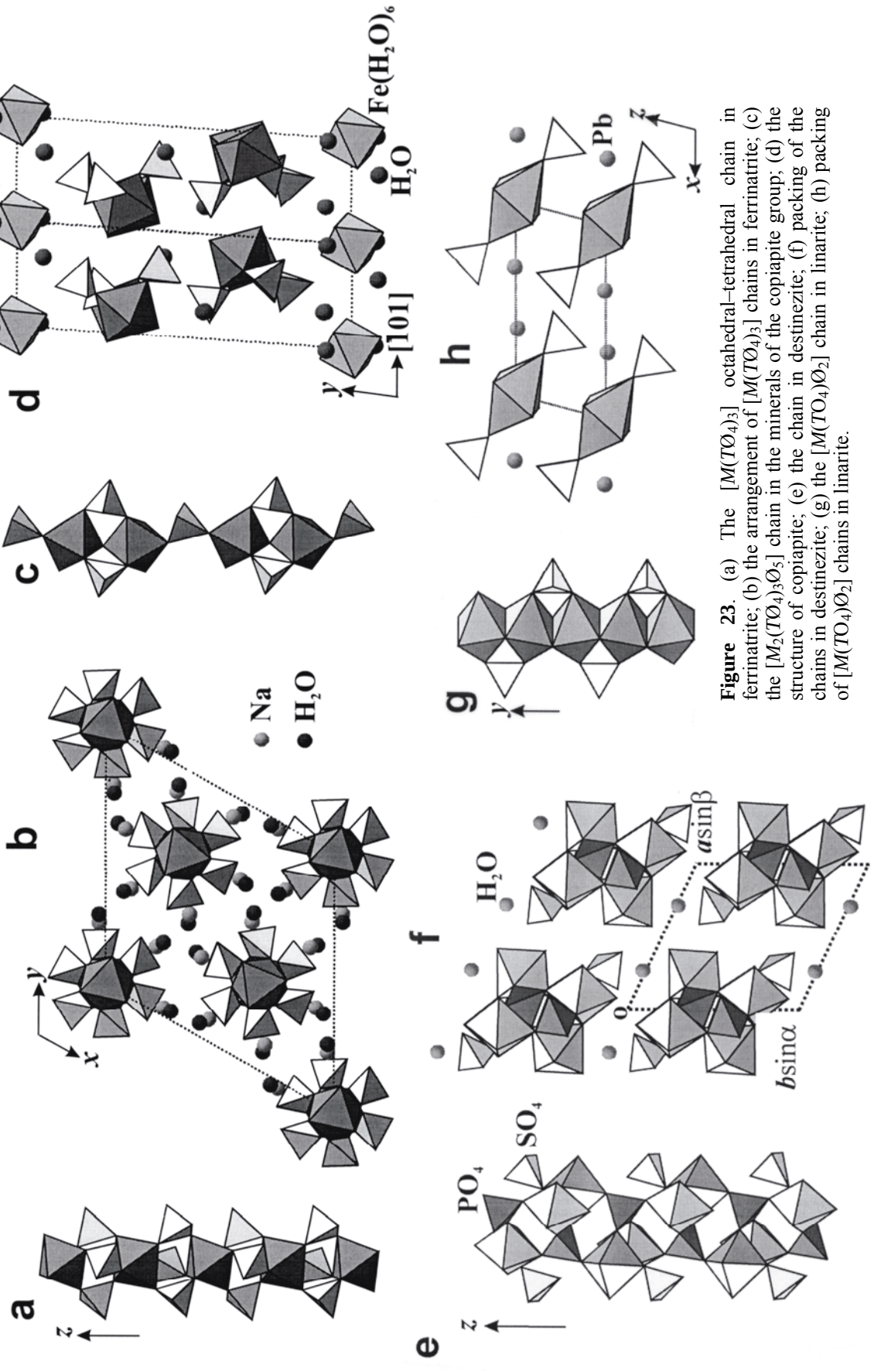

Figure 23. (a) The $[M(T\emptyset_4)_3]$ octahedral–tetrahedral chain in ferrinatrite; (b) the arrangement of $[M(T\emptyset_4)_3]$ chains in ferrinatrite; (c) the $[M_2(T\emptyset_4)_3\emptyset_5]$ chain in the minerals of the copiapite group; (d) the structure of copiapite; (e) the chain in destinezite; (f) packing of the chains in destinezite; (g) the $[M(TO_4)\emptyset_2]$ chain in linarite; (h) packing of $[M(TO_4)\emptyset_2]$ chains in linarite.

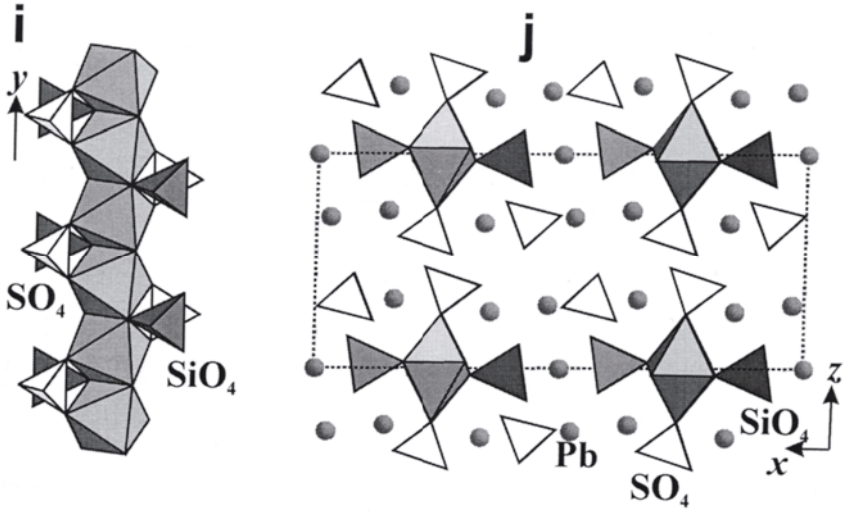

Figure 23, cont'd. (i) the $[M(TO_4)_2Ø]$ chain in wherryite; (j) packing of $[M(TO_4)_2Ø]$ chains in wherryite.

and are linked by interstitial Na and (H_2O) groups.

In the **copiapite-group** minerals, $[Fe^{3+}{}_2(OH)(H_2O)_4(SO_4)_3]_2\{M^{2+}(H_2O)_6\}(H_2O)_6$, corner-sharing $[M_2(TO_4)_2Ø_7]$ clusters link through additional tetrahedra to form infinite $[M_2(TO_4)_3Ø_5]$ chains (Fig. 20i) that extend along [101] (Fig. 23c,d). These chains are linked together by hydrogen bonds involving unconnected $\{Fe^{2+}(H_2O)\}$ octahedra and interstitial (H_2O) groups. There is some question as to the chemical formulae of ferricopiapite and aluminocopiapite. In Table 8, these two minerals are written with the unconnected $\{M(H_2O)_6\}$ octahedra as $M = (Fe^{3+}{}_{0.67}\,❑_{0.33})$ and $(Al_{0.67}❑_{0.33})$, as per Fanfani et al. (1973). However, these formulae seem unlikely from a bond-valence perspective. Formulae have also been written as $[Fe^{3+}{}_4O(OH)(H_2O)_8(SO_4)_6]\{Fe^{3+}(H_2O)_6\}(H_2O)_6$, but it is not clear that this fits with the available crystal-structure data; more structural work is needed. The $[M_2(TO_4)_2Ø_7]$ cluster is the basis of an extensive hierarchy of (mainly phosphate) structures (Hawthorne 1979). The structure of **destinezite**, $[Fe^{3+}{}_2(OH)(H_2O)_5(PO_4)(SO_4)](H_2O)$, is based on the complex chain shown in Figure 23e; the connectivity of this chain is clearly represented by its graph given in Figure 20j. The chains in destinezite and copiapite are somewhat related; this is most easily seen by comparison of their graphs (Fig. 20i,j). First, break one of the o–t linkages in graph 20i; next, fuse two of these modified graphs *via* o–t linkage: the result is the graph of Figure 20j. The chains in destinezite extend along [001] (Fig. 23e) and are linked solely by hydrogen bonding both directly and through intermediate (H_2O) groups (Fig. 23f).

The chain shown in Figure 23g is the basis of the structure of **linarite**, $Pb^{2+}[Cu^{2+}(OH)_2(SO_4)]$; octahedra share two *trans* edges to form an $[MØ_4]$ chain that is decorated by flanking tetrahedra that adopt a staggered arrangement either side of the chain (Fig. 20k). In projection, the chains are arranged at the vertices of a primitive monoclinic lattice (Fig. 23h), and are linked primarily by [9]-coordinated Pb^{2+}. The $[M(TO_4)Ø_2]$ can be recognized as a parent chain for many other octahedral–tetrahedral structures. The structure of **wherryite**, $Pb^{2+}{}_7[Cu^{2+}(OH)(SO_4)(SiO_4)]_2(SO_4)_2$ (Fig. 22i,j), is based on linarite chains that are decorated by (SiO_4) tetrahedra (Figs. 20l, 23i). The $[M(TO_4)_2Ø]$ chains extend along the *c* axis and pack at the vertices of a primitive orthogonal plane lattice (Fig. 23j).

There are additional (SO_4) groups in wherryite that do not link to the ($Cu^{2+}Ø_6$) octahedra; the chains and the isolated (SO_4) tetrahedra are linked by [7]- and [8]-coordinated Pb^{2+} cations (Fig. 23j). The chain shown in Figure 23i is a common constituent of oxysalt minerals, occurring in brackebuschite-, fornacite- and vaquelinite-group minerals (Hawthorne 1990). Among these groups, only **tsumebite**, $Pb^{2+}{}_2[Cu^{2+}(OH)(PO_4)(SO_4)]$, and **arsentsumebite**, $Pb^{2+}{}_2[Cu^{2+}(OH)\ (AsO_4)(SO_4)]$, are sulfate minerals. In the structure of tsumebite, $[Cu^{2+}(OH)(PO_4)(SO_4)]$, chains extend along the *b* axis, giving the typical ~5.5 Å repeat, and are cross-linked by [9]-coordinated Pb^{2+} cations. The structure of **caledonite**, $Pb^{2+}{}_5[Cu^{2+}{}_2(OH)_6(SO_4)_2](SO_4)(CO_3)$, is based on an $[M(TO_4)Ø_3]$ chain of edge-sharing octahedra decorated by (SO_4) tetrahedra (Fig. 24a). Note that the chain corresponds to the graph of Figure 20m. Thus both the chains shown in Figures 23g and 24a correspond to Figure 20k; these chains are geometrical isomers and hence have the same graph. As in wherryite, there are additional (SO_4) tetrahedra in the structure of caledonite and linkage is provided by [8]- and [9]-coordinated Pb^{2+} (Fig. 24b).

The $[M(TO_4)Ø_2]$ chain in **chlorothionite**, $K_2[Cu^{2+}Cl_2(SO_4)]$, is extremely unusual in that it involves edge-sharing between sulfate tetrahedra and divalent-metal octahedra (Fig. 24c); this type of edge-sharing seems to be much more common in Cu^{2+} minerals than in other divalent-metal oxysalts. Moreover, the stoichiometry of the chain of octahedra is $[MO_4]$, but the shared edges on an octahedron are *cis* instead of the more usual *trans* (compare Figs. 24a and 24c), which also leads to second-nearest-neighbor octahedra sharing vertices; this is more easily apparent in the graph of the $[M(TO_4)Ø_2]$ chain in Figure 20n. The chains are cross-linked by [6]-coordinated K, an unusually low coordination number for K (Fig. 24d).

The structures of **amarantite**, $[Fe^{3+}{}_2O(H_2O)_4(SO_4)_2](H_2O)_3$, and **hohmannite**, $[Fe^{3+}{}_2O(H_2O)_4(SO_4)_2](H_2O)_4$, are based on the chain shown in Figure 24e (its graph is given in Figure 20o). Two octahedra share an edge to form an $[M_2Ø_{10}]$ dimer. Two additional octahedra link to either end of the shared edges of the dimer to form an $[M_4Ø_{20}]$ tetramer. Two tetrahedra link between corners of adjacent octahedra, and further link adjacent decorated tetramers to form the complex chain shown in Figures 24e and 20o. The structures of amarantite and hohmannite (Figs. 24f, and 24g respectively) differ with regard to the amount of interstitial (H_2O) groups, which results in different packing of the chains.

Structures with infinite sheets

The sulfate minerals with infinite sheets can be subdivided into two groups: (a) minerals with brucite-like sheets, and (b) other minerals.

The structures belonging to the first group (Table 9) are based on sheets of octahedra closely related to the sheet of octahedra in brucite, $Mg(OH)_2$. The first examples are the minerals of the **hydrotalcite group**, ideally $[M^{2+}{}_6M^{3+}{}_2(OH)_{16}](TO_n)(H_2O)_m$, where TO_n = (CO_3) in hydrotalcite itself and (SO_4) in many other minerals of this group (Table 9). A key feature of this group is the substitution of M^{3+} cations for M^{2+} cations within the brucite-like sheet, as this makes the sheet positively charged, rather than negatively charged as is the case for the structural unit in most minerals. Thus, the interstitial species of the minerals in this group require a net negative charge, which is the reason for the presence of interstitial $(SO_4)^{2-}$ and $(CO_3)^{2-}$ groups in these minerals. Many of these minerals are poorly crystalline because of extensive stacking disorder. However, this is not so for **shigaite**, $Na[AlMn^{2+}{}_2(OH)_6]_3\ (SO_4)_2(H_2O)_{12}$, the structural unit of which is a sheet of edge-sharing ($Mn^{2+}Ø_6$) and ($AlØ_6$) octahedra (Fig. 25a). These sheets are held together by hydrogen bonding involving $\{Na(H_2O)_6\}$ octahedra, (SO_4) tetrahedra, and (H_2O) groups located in the interlayer (Figs. 25b,c). This group shows a large diversity in interlayer species, and the relations of adjacent sheets cause significant variation in unit-cell parameters. Bookin and

Dri inerals and
sho
ani

tetr

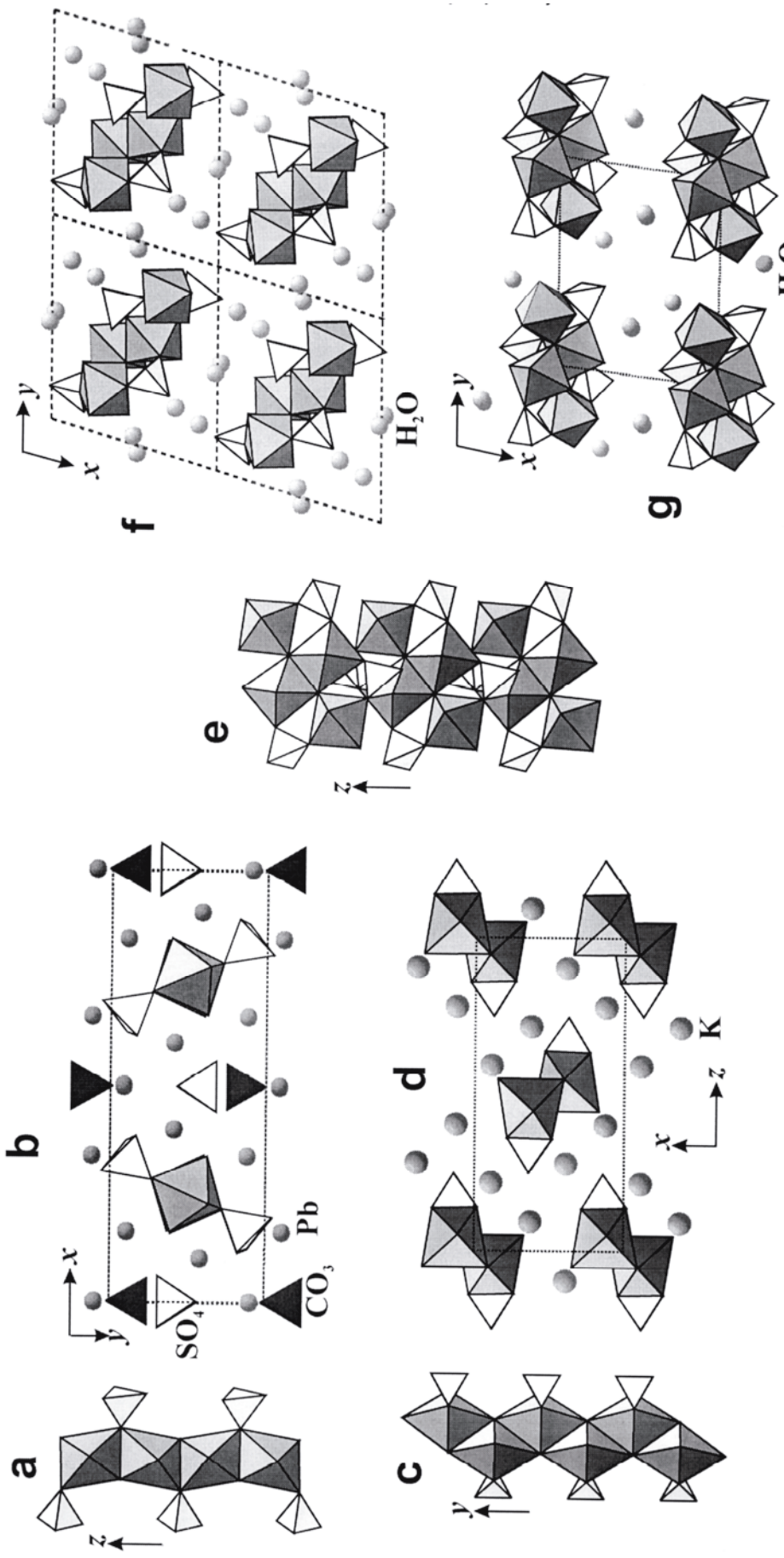

Figure 24. (a) the $[M(T\emptyset_4)\emptyset_3]$ chain in caledonite; (b) packing of chains and the interstitial species in caledonite; (c) the $[M(T\emptyset_4)\emptyset_2]$ chain in chlorothionite; (d) packing of chains in chlorothionite; (e) the complex $[M_2(T\emptyset_4)_2\emptyset_5]$ chain in amarantite; (f,g) the arrangement of chains in (f) amarantite and (g) hohmannite.

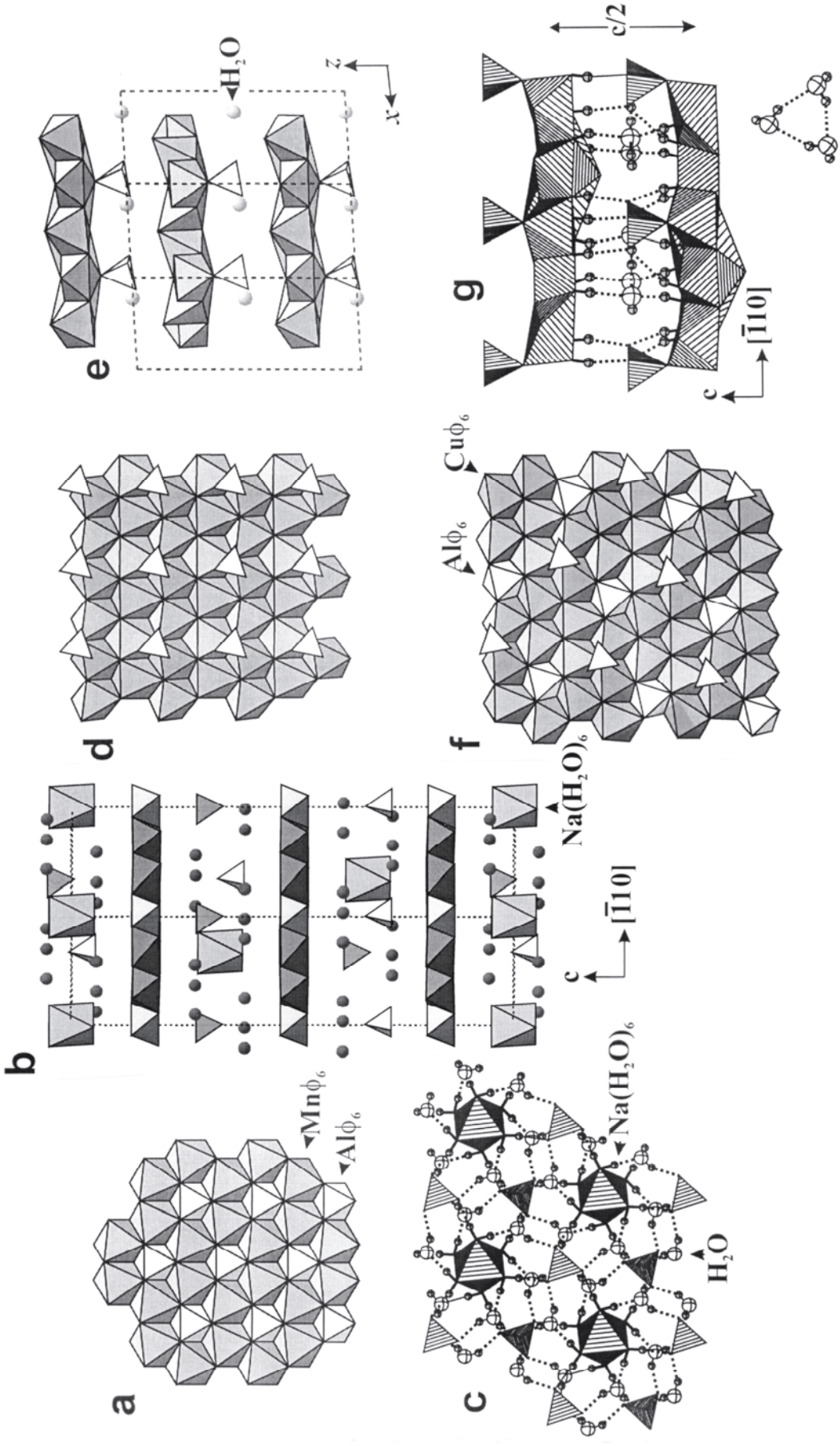

Figure 25. (a) The octahedral sheet in shigaite; (b) the structure of shigaite viewed in the plane of the sheets (circles are H_2O groups); (c) the interlayer species in shigaite projected down [001], with hydrogen bonds shown as dashed lines; (d) the one-side decorated octahedralBtetrahedral sheet in wroewolfeite; (e) the structure of wroewolfeite viewed in the plane of the sheet; (f) the one-sided decorated sheet in spangolite; (g) the structure of spangolite viewed in the plane of the sheet.

Table 9. Sulfate minerals with brucite-like octahedral ($M\emptyset_2$) sheets.

Name	Formula	*a* (Å)	*b* (Å)	*c* (Å)	β (°)	S. G.	Fig.	Ref.
honessite	$[Ni_6Fe^{3+}_2(OH)_{16}](SO_4)(H_2O)_4$	3.083	*a*	26.71	–	*R*3*m*	–	(1)
hydrohonessite	$[Ni_6Fe^{3+}_2(OH)_{16}](SO_4)(H_2O)_7$	3.09	*a*	10.80	–	?	–	(1)
glaucocerinite	$[Zn_5Al_3(OH)_{16}](SO_4)_{1.5}(H_2O)_9$	3.057	*a*	32.52	–	?	–	(1)
woodwardite	$[Cu^{2+}_4Al_2(OH)_{12}](SO_4)(H_2O)_{2-4}$	3.00	*a*	27.3	–	?	–	(1)
hydrowoodwardite	$[Cu^{2+}_{1-x}Al_x(OH)_2](SO_4)_{x/2}(H_2O)_n$ $x < 0.67$, $n > \sim 3x/2$	3.07	*a*	31.9	–	$R\bar{3}m$	–	(2)
carrboydite	$(Ni,Cu^{2+})_{14}Al_9(OH)_{43}(SO_4,CO_3)_6(H_2O)_7$	9.14	*a*	10.34	–	?	25a,b,c	(1)
motukoreaite	$Na_{0.6}[Mg_{5.6}Al_{3.4}(OH)_{18}](SO_4,CO_3)_2(H_2O)_{12}$	9.172	*a*	33.510	–	$R\bar{3}m$	25a,b,c	[3]
shigaite	$Na[AlMn^{2+}_2(OH)_6]_3(SO_4)_2(H_2O)_{12}$	9.512	*a*	33.074	–	$R\bar{3}$	25a,b,c	[4]
wermlandite	$[Mg_7(Al,Fe^{3+})_2(OH)_{18}](Ca,Mg)(SO_4)_2(H_2O)_{12}$	9.303	*a*	22.570	–	$P\bar{3}c$	25a,b,c	[5]
mountkeithite	$(Mg,Ni)_{11}(Fe^{3+},Cr^{3+})_3(OH)_{24}(SO_4,CO_3)_{3.5}(H_2O)_{11}$	10.698	*a*	22.545	–	?	25a,b,c	(1)
kuzelite	$[Ca_4Al_2(OH)_{12}](SO_4)(H_2O)_6$	5.759	*a*	26.795	–	$R\bar{3}$	25a,b,c	[6]
langite	$[Cu^{2+}_4(OH)_6(H_2O)(SO_4)](H_2O)$	7.118	6.034	11.209	90	*Pc*	–	[7]
posnjakite	$[Cu^{2+}_4(OH)_6(H_2O)(SO_4)](H_2O)$	10.578	6.345	7.863	118.0	*Pa*	–	[8]
wroewolfeite	$[Cu^{2+}_4(OH)_6(H_2O)(SO_4)](H_2O)$	6.045	5.646	14.337	93.4	*Pc*	25d,e	[9]
spangolite	$[Cu^{2+}_6Al(OH)_{12}Cl(SO_4)](H_2O)_3$	8.254	*a*	14.354	–	*P*31*c*	25e,f	[10]
schulenbergite	$[Cu^{2+}_7(OH)_{10}(SO_4)_2(H_2O)_2](H_2O)$	8.211	*a*	7.106	–	$P\bar{3}$	26a	[11]
devilline	$Ca(H_2O)_3[Cu^{2+}_4(OH)_6(SO_4)_2]$	20.870	6.135	22.191	102.7	$P2_1/c$	26b	[12]
lautenthalite	$Pb(H_2O)_3[Cu^{2+}_4(OH)_6(SO_4)_2]$	21.642	6.040	22.544	108.2	$P2_1/c$	26b	(13)
campigliaite	$Mn(H_2O)_4[Cu^{2+}_4(OH)_6(SO_4)_2]$	21.707	6.098	11.245	100.3	*C*2	26c	[14]
ktenasite	$Zn(H_2O)_6[Cu^{2+}_4(OH)_6(SO_4)_2]$	5.589	6.166	23.751	95.6	$P2_1/c$	26d	[15]
niedermayrite	$Cd(H_2O)_4[Cu^{2+}_4(OH)_6(SO_4)_2]$	5.543	21.995	6.079	92.04	$P2_1/c$	26e	[16]
chalcophyllite	$[Cu^{2+}_9Al(OH)_{12}(H_2O)_6(AsO_4)_2](SO_4)_{1.5}(H_2O)_{12}$	10.756	*a*	28.678	–	$R\bar{3}$	28a,b	[17]
mooreite	$[Mg_9Zn_4Mn^{2+}_2(OH)_{26}](SO_4)_2(H_2O)_8$	11.147	20.350	8.202	92.7	$P2_1/a$	27c,d	[18]
lawsonbauerite	$[(Mn^{2+},Mg)_9Zn_4(OH)_{22}](SO_4)_2(H_2O)_8$	10.50	9.64	16.41	95.2	$P2_1/c$	–	[19]
torreyite	$[(Mg,Mn^{2+})_9Zn_4(OH)_{22}](SO_4)_2(H_2O)_8$	10.619	9.292	16.486	95.4	$P2_1/c$	–	(1)
christelite[1]	$Zn(H_2O)_4[Zn_2Cu^{2+}_2(OH)_6(SO_4)_2]$		6.336	10.470	90.06	$P\bar{1}$	–	[20]
serpierite	$Ca(H_2O)_3[Cu^{2+}_4(OH)_6(SO_4)_2]$	22.186	6.25	21.853	113.4	*C*2/*c*	–	[21]
orthoserpierite	$Ca(H_2O)_3[Cu^{2+}_4(OH)_6(SO_4)_2]$	22.10	6.20	20.39	–	$Pca2_1$	–	(1)
namuwite	$[(Zn,Cu^{2+})_4(OH)_6(H_2O)(SO_4)](H_2O)_3$	8.331	*a*	10.54	–	$P\bar{3}$	–	[22]
gordaite	$[Zn_4(OH)_6Cl(SO_4)]\{Na(H_2O)_6\}$	8.356	*a*	13.025	–	$P\bar{3}$	27e,f	[23]
bechererite	$[Zn_7Cu^{2+}(OH)_{13}\{(SiO(OH)_3\}(SO_4)]$	8.319	*a*	7.377	–	*P*3	27g	[24]
ramsbeckite	$[(Cu^{2+},Zn)_{15}(OH)_{22}(SO_4)_4](H_2O)_6$	16.088	15.576	7.102	90.22	$P2_1/a$	27h,i	[25]

[1] α = 94.32°, γ = 90.27° *References*: (1) Gaines et al. (1997), (2) Witzke (1999), [3] Rius and Plana (1986), [4] Cooper and Hawthorne (1996b), [5] Rius and Allmann (1984), [6] Allmann (1977), Pollmann et al. (1997), [7] Galy et al. (1984), [8] Mellini and Merlino (1979), [9] Hawthorne and Groat (1985), [10] Hawthorne et al. (1993), Merlino et al. (1992), [11] Mumme et al. (1994), [12] Sabelli and Zanazzi (1972), (13) Medenbach and Gebert (1993), [14] Menchetti and Sabelli (1982), [15] Mellini and Merlino (1978), [16] Giester et al. (1998), [17] Sabelli (1980), [18] Hill (1980), [19] Treiman and Peacor (1982), [20] Adiwidjaja et al. (1996), [21] Sabelli and Zanazzi (1968), [22] Groat (1996), [23] Adiwidjaja et al. (1997), [24] Hoffmann et al. (1997), Giester and Rieck (1996), [25] Effenberger (1988)

produces sheets that are the basis of many Cu^{2+} and Zn sulfate minerals. A detailed consideration of the bond topology of these structures and other possible structural arrangements is given by Hawthorne and Schindler (2000). A key feature of these structures is the local bond-valence requirement that three Cu–$\emptyset_{apical}$ bonds must meet at a single anion if an (SO_4) or (H_2O) group is also to attach to that anion. The disposition of the various Cu–$\emptyset_{apical}$ bonds gives rise to different types of sheets. One-side-decorated sheets occur in the structures of the polymorphs **wroewolfeite**, $[Cu^{2+}_4(OH)_6(H_2O)(SO_4)](H_2O)$ (Fig. 25d,e), **langite**, $[Cu^{2+}_4(OH)_6(H_2O)(SO_4)](H_2O)$, and **posnjakite**, $[Cu^{2+}_4(OH)_6(H_2O)(SO_4)](H_2O)$, as well as **spangolite**, $[Cu^{2+}_6Al(OH)_{12}Cl(SO_4)](H_2O)_3$ (Fig. 25f,g). The sheets are linked through hydrogen bonds involving interlayer (H_2O) groups. In spangolite, these (H_2O) groups form the

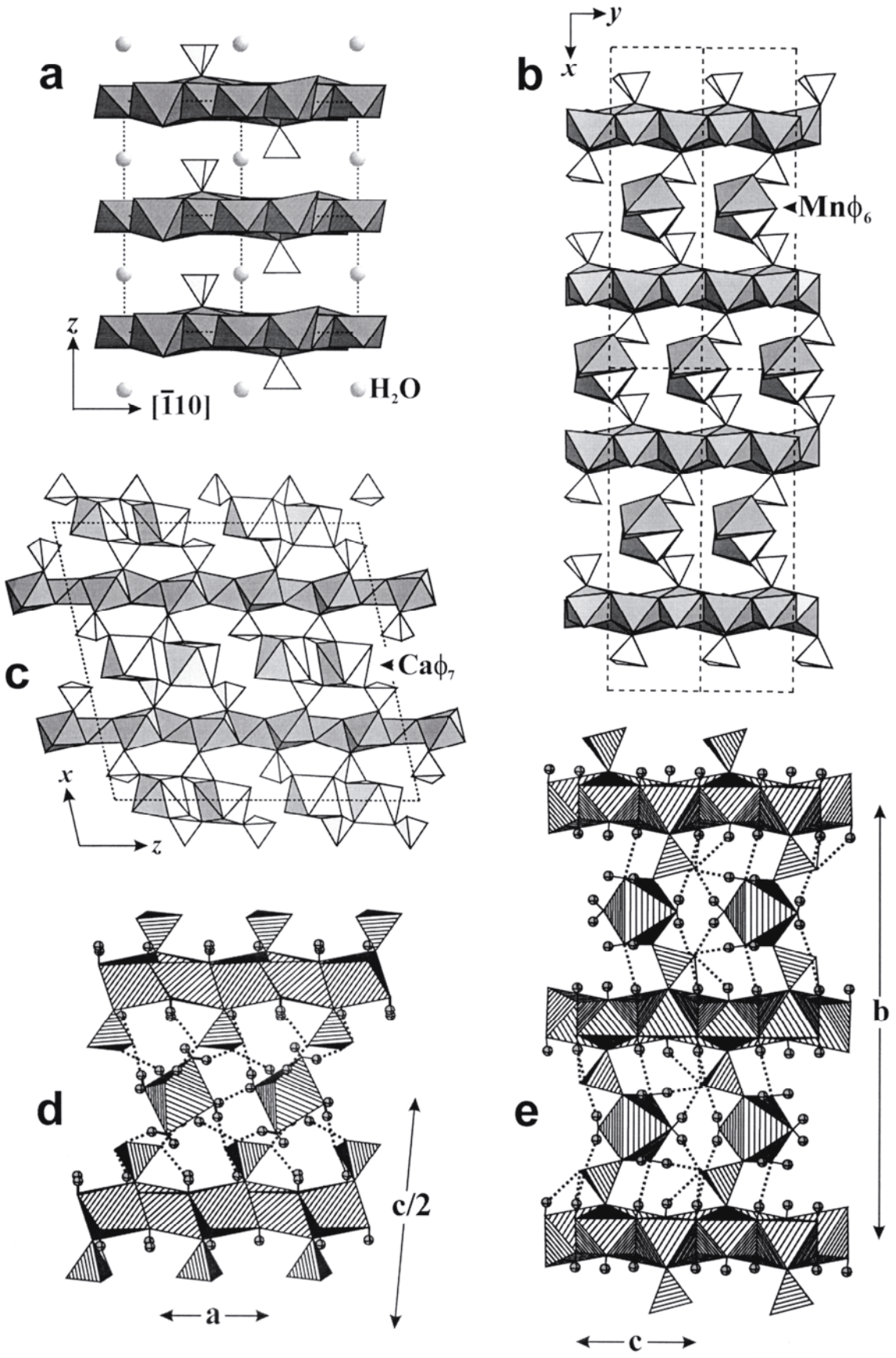
a
z
[$\bar{1}$10]
H_2O
b
y
x
Mnϕ_6
c
Caϕ_7
x
z
d
c/2
a
e
b
c

Figure 26 (opposite page). The structures of (a) schulenbergite; (b) devilline; (c) campigliaite; (d) ktenasite; (e) niedermayrite.

H-bonded cluster $(H_2O)_3$ shown in Figure 25g. Two-sided tetrahedral decoration of the brucite-like sheet occurs in the structures of **schulenbergite**, $[(Cu^{2+},Zn)_7(OH)_{10}(SO_4)_2(H_2O)_2](H_2O)$ (Fig. 26a), **devilline**, $Ca(H_2O)_3[Cu^{2+}_4(OH)_6(SO_4)_2]$ (Fig. 26b), **cam-pigliaite**, $Mn^{2+}(H_2O)_4[Cu^{2+}_4(OH)_6(SO_4)_2]$ (Fig. 26c), **ktenasite**, $Zn(H_2O)_6$-$[(Cu^{2+},Zn)_4(OH)_6(SO_4)_2]$ (Fig. 26d), **niedermayrite**, $Cd(H_2O)_4[Cu^{2+}_4(OH)_6(SO_4)_2]$ (Fig. 26e), **christelite**, $Zn(H_2O)_4[Zn_2Cu^{2+}_2(OH)_6(SO_4)_2]$, and **serpierite**, $Ca(H_2O)_3$-$[(Cu^{2+},Zn)_4(OH)_6(SO_4)_2]$. Among these minerals, only schulenbergite contains no interlayer cations; in other structures, the interlayer cations (Ca, Zn, Mn^{2+}, Cd, Pb^{2+}) provide additional linkage between the sheets (devilline, campigliaite, niedermayrite, serpierite) or form unconnected polyhedra which are held in the structure by hydrogen bonds only (ktenasite; Fig. 26d). The hydrogen bonding is essential in linking the sheets together in these minerals (Fig. 26). It is probable that numerous other minerals of this motif await discovery.

If some octahedral sites in the brucite-like sheet are vacant, the resultant holes are usually capped by tetrahedra above and/or below the plane of the sheet. Figure 27a shows the octahedral-tetrahedral sheet in **chalcophyllite**, $[Cu^{2+}_9Al(OH)_{12}(H_2O)_6(AsO_4)_2](SO_4)_{1.5}$-$(H_2O)_{12}$. In this mineral, the octahedral vacancies are capped by (AsO_4) tetrahedra, and (SO_4) groups occur in the interlayer, together with (H_2O) groups, providing hydrogen bonding between adjacent sheets (Fig. 27b). In the structures of **mooreite**, $[Mg_9Zn_4Mn^{2+}_2(OH)_{26}]$ $(SO_4)_2(H_2O)_8$, and **lawsonbauerite**, $[(Mn^{2+},Mg)_9Zn_4(OH)_{22}]$-$(SO_4)_2(H_2O)_8$, the octahedral vacancies are capped by $(ZnØ_4)$ tetrahedra above and below the plane of the sheet (Fig. 27c). The free vertices of these tetrahedra connect to interlayer $(MØ_6)$ octahedra (M = Mg, Mn^{2+}) that link the structure in the third dimension (Fig. 27d). In the structures of **namuwite**, $[(Zn,Cu^{2+})_4(OH)_6$-$(H_2O)(SO_4)](H_2O)_3$, **gordaite**, $[Zn_4(OH)_6Cl(SO_4)][Na(H_2O)_6]$, **bechererite**, $[Zn_7Cu^{2+}(OH)_{13}\{SiO(OH)_3\}(SO_4)]$, and **ramsbeckite**, $[(Cu^{2+},Zn)_{15}(OH)_{22}(SO_4)_4]$-$(H_2O)_6$, the octahedral-tetrahedral sheets with vacant octahedral positions are decorated by attached $(TØ_4)$ tetrahedra (T = S, Si). Linkage between sheets is provided by hydrogen bonding involving interlayer (H_2O) groups (namuwite) or both interlayer (H_2O) groups and $\{Na(H_2O)_6\}$ octahedra (gordaite; Figs. 27e,f), or by corner-sharing of tetrahedra of adjacent sheets (bechererite and ramsbeckite, Figs. 27g and 27h,i, respectively). The structure of gordaite is closely related to the structure of $Ca[Zn_8(SO_4)_2(OH)_{12}Cl_2](H_2O)_9$, a new phase discovered on slag dumps at Val Varenna, Italy, in association with bechererite (Burns et al. 1998).

The structures of other sulfate minerals based on infinite sheets are listed in Tables 10 and 11. Some of their graphs are given in Figure 28. Note that some sheets cannot be represented as planar graphs.

The structures of minerals in the **alunite supergroup**, $(M^+,M^{2+})[M^{3+}_3(OH)_6(TO_4)_2]$; M^+ = K, Na, Ag^+, Tl^+, (NH_4), (H_3O); M^{2+} = Ca, Pb^{2+}, Sr, Ba; M^{3+} = Al, Fe^{3+}, Ga; T = S, As, P; (Lengauer et al. 1994; Jambor 1999; Dutrizac and Jambor, this volume) are based on octahedral-tetrahedral sheets (Fig. 28a, 29a). The crystallographic information on the minerals of this group is listed in Table 10. Octahedra occur at the vertices of a 6^3 plane net, forming six-membered rings with the octahedra linked by sharing corners. At the junction of three six-membered rings is a three-membered ring, and one set of apical vertices of those three octahedra link to a tetrahedron. The resultant sheets are held together by interstitial cations and hydrogen bonds (Fig. 29b). Ballhorn et al. (1989) and Kolitsch et al. (1999) suggested the minerals of the alunite supergroup as potential host structures for the long-term immobilization of radioactive fission-products and heavy toxic metals. This suggestion has a reasonable structural basis, as the interstitial cation is encapsulated

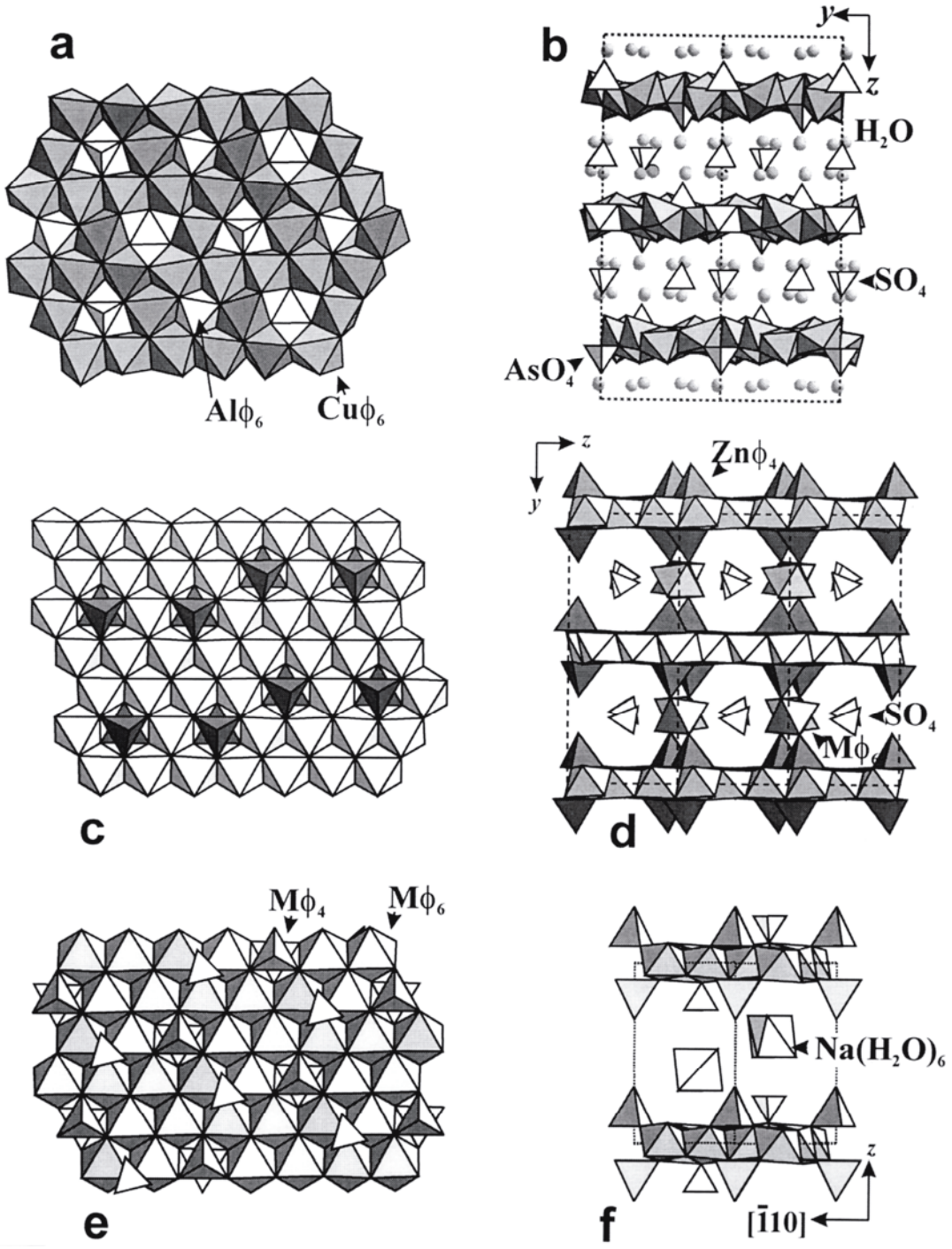

Figure 27. The octahedral–tetrahedral sheets in (a) chalcophyllite and (c) mooreite; the structures of (b) chalcophyllite and (d) mooreite viewed in the plane of the sheet; the octahedral–tetrahedral sheet in (e) gordaite; the structure of (f) gordaite.

between adjacent octahedral-tetrahedral sheets.

The structure of **felsöbányaite**, $[Al_4(OH)_{10}(H_2O)](SO_4)(H_2O)_3$, ("basaluminite") is based on the octahedral sheet shown in Figure 29c. Eight octahedra share edges to form a 2×4 cluster, and these clusters link by sharing an octahedral edge to form a zigzag ribbon that extends along [010]. These ribbons link by sharing corners with ribbons at different layers to form an interrupted sheet of edge- and corner-sharing octahedra. The resultant

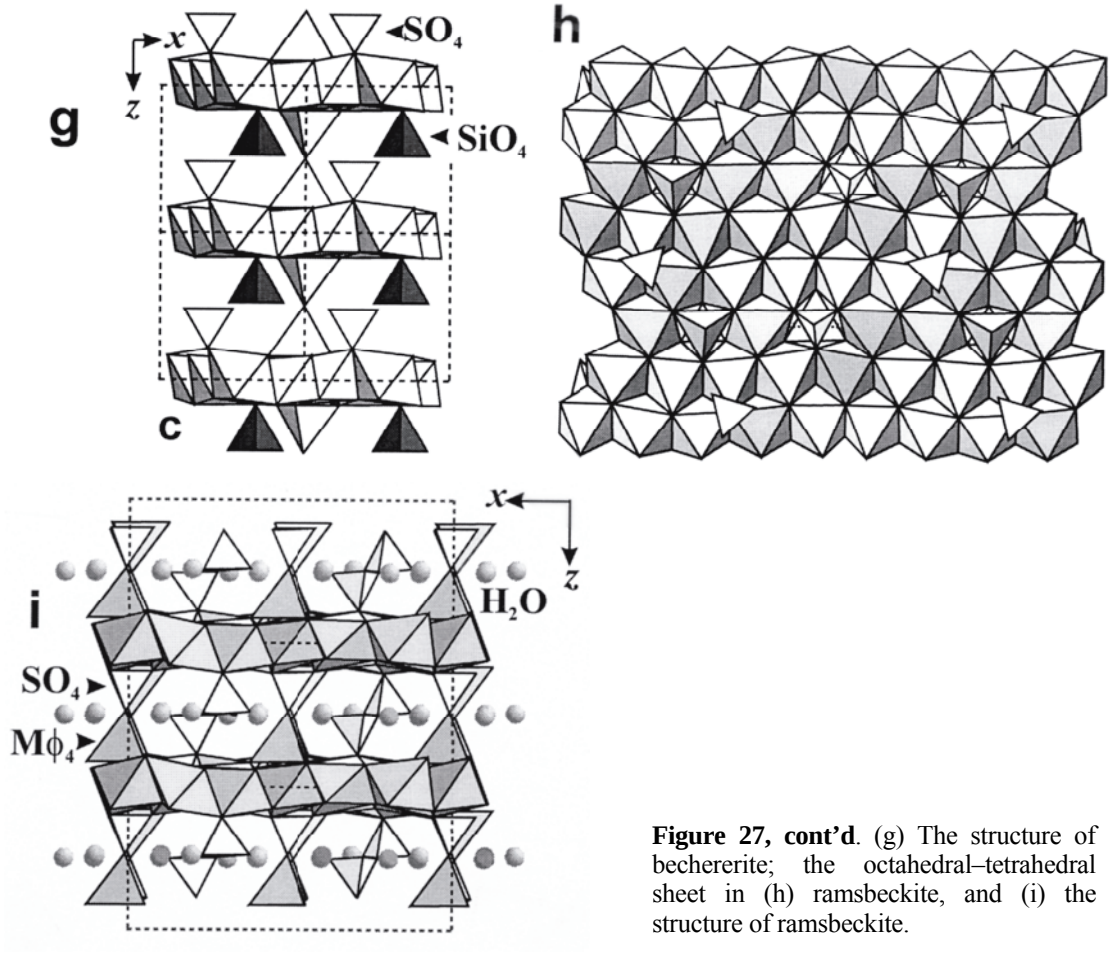

Figure 27, cont'd. (g) The structure of bechererite; the octahedral–tetrahedral sheet in (h) ramsbeckite, and (i) the structure of ramsbeckite.

sheet (Fig. 29c) is parallel to ($\bar{1}01$); the (SO_4) tetrahedra and (H_2O) groups occur in the interlayer (Fig. 29d).

The structure of **kornelite**, $[Fe^{3+}{}_2(H_2O)_6(SO_4)_3](H_2O)_{1.25}$, is based the sheet shown in Figure 29e (its graph is shown in Figure 28b). The sheet consists of fragments of a *trans*-linked $[M(TO_4)Ø_4]$ chain that link to other fragments *via* a *cis* linkage. The open modulated sheets are linked by hydrogen bonds through (H_2O) groups in the interlayer (Fig. 29f). The sheet in **rhomboclase**, $(H_5O_2)[Fe^{3+}(H_2O)_2(SO_4)_2]$, has the simple graph shown in Figure 28c. This sheet is based on finite polyhalite-like clusters linked in two dimensions (Fig. 29g). Rhomboclase possesses an extended hydrogen-bonding scheme involving interstitial $(H_5O_2)^+$ dimers (Fig. 29h). In **vanthoffite**, $Na_6[Mg(SO_4)_4]$, glaserite-ungemachite pinwheels link to form thick slabs parallel to (100) (Fig. 30a); linkage between the slabs is provided by Na in the interlayer (Fig. 30b). **Yavapaite**, $K[Fe^{3+}(SO_4)_2]$, is based on the sheet shown in Figure 30c. The $[M(TO_4)_2]$ sheet can be described as a coalescence, *via* corner-sharing, of kröhnkite-like $[M(TO_4)Ø_2]$ chains; this $[M(TO_4)_2]$ sheet also occurs in merwinite, $Ca_3[Mg(SiO_4)_2]$, and brianite, $Na_2Ca[Mg(PO_4)_2]$. Interstitial [10]-coordinated K links the sheets together (Fig. 30d). The structure of **natrochalcite**, $Na[Cu^{2+}{}_2(OH)(H_2O)(SO_4)_2]$, is based upon sheets consisting of linarite-like chains linked by corner-sharing of tetrahedra of the chain with the octahedra of adjacent chains (Fig. 30e). Intersheet linkage is provided by interstitial Na and by hydrogen bonds; Giester and Zemann (1987) have argued that the hydrogen-bearing interstitial species should be written as $(H_3O_2)^-$. **Goldichite**, $K[Fe^{3+}(H_2O)_2(SO_4)_2](H_2O)_2$, consists of sheets based on an $[M_2(TO_4)_4Ø_6]$ cluster that links into a thick corrugated slab (Fig. 30g,h) by sharing corners between octahedra and

Table 10. Sulfate minerals with $[M_3(OH)_6(SO_4)_2]$ sheets.*

Name	Formula	*a* (Å)	*c* (Å)	S. G.	Fig.	Ref.
alunite	$K[Al_3(OH)_6(SO_4)_2]$	7.020	17.223	$R\bar{3}m$	29a,b	[1]
ammonioalunite	$(NH_4)[Al_3(OH)_6(SO_4)_2]$	7.013	17.885	$R\bar{3}m$	29a,b	(2)
natroalunite	$Na[Al_3(OH)_6(SO_4)_2]$	6.990	16.905	$R\bar{3}m$	29a,b	[3]
jarosite	$K[Fe^{3+}_3(OH)_6(SO_4)_2]$	7.315	17.224	$R\bar{3}m$	29a,b	[1]
ammoniojarosite	$(NH_4)[Fe^{3+}_3(OH)_6(SO_4)_2]$	7.325	17.374	$R\bar{3}m$	29a,b	(2)
natrojarosite	$Na[Fe^{3+}_3(OH)_6(SO_4)_2]$	7.3346	16.747	$R\bar{3}m$	29a,b	(2)
argentojarosite	$Ag[Fe^{3+}_3(OH)_6(SO_4)_2]$	7.348	16.551	$R\bar{3}m$	29a,b	(2)
hydronium jarosite	$(H_3O)[Fe^{3+}_3(OH)_6(SO_4)_2]$	7.347	16.994	$R\bar{3}m$	29a,b	(2)
beaverite	$Pb[(Fe,Cu,Al)_3(OH)_6(SO_4)_2]$	7.205	16.994	$R\bar{3}m$	29a,b	[4]
dorallcharite	$Tl[Fe^{3+}_3(OH)_6(SO_4)_2]$	7.330	17.663	$R\bar{3}m$	29a,b	[5]
osarizawaite	$Pb[(Al,Cu,Fe^{3+})_3(OH)_6(SO_4)_2]$	7.075	17.248	$R\bar{3}m$	29a,b	[6]
schlossmacherite	$(H_3O),Ca[Al_3(OH)_6(SO_4,AsO_4)_2]$	6.998	16.67	$R\bar{3}m$	29a,b	(2)
woodhouseite	$Ca[Al_3(OH)_6(PO_4)(SO_4)]$	6.993	16.386	$R\bar{3}m$	29a,b	[7]
svanbergite	$Sr[Al_3(OH)_6(PO_4)(SO_4)]$	6.992	16.567	$R\bar{3}m$	29a,b	[8]
hinsdalite	$Pb[Al_3(OH)_6(PO_4)(SO_4)]$	7.029	16.789	$R\bar{3}m$	29a,b	[9]
beudantite	$Pb[Fe^{3+}_3(OH)_6(AsO_4)(SO_4)]$	7.315	17.035	$R\bar{3}m$	29a,b	[10]
hidalgoite	$Pb[Al_3(OH)_6(AsO_4)(SO_4)]$	7.0706	16.975	$R\bar{3}m$	29a,b	(2)
kemmlitzite	$Sr[Al_3(OH)_6(AsO_4)(SO_4)]$	7.027	16.51	$R\bar{3}m$	29a,b	(2)
plumbojarosite	$Pb[Fe^{3+}_3(OH)_6(SO_4)_2]_2$	7.306	33.675	$R\bar{3}m$	–	[11]
minamiite	$(Ca_{1-x}Na_{2-x}\square_{1-x})[Al_3(OH)_6(SO_4)_2]$	6.981	33.490	$R\bar{3}m$	–	[12]
huangite	$Ca[Al_3(OH)_6(SO_4)_2]_2$	6.983	33.517	$R\bar{3}m$	–	(13)
walthierite	$Ba[Al_3(OH)_6(SO_4)_2]_2$	6.992	34.443	$R\bar{3}m$	–	[13]
corkite	$Pb^{2+}[Fe^{3+}_3(OH)_6(PO_4)(SO_4)]$	7.280	16.821	$R3m$	–	[14]
gallobeudantite	$Pb^{2+}[Ga_3(OH)_6(AsO_4)(SO_4)]$	7.225	17.03	$R3m$	–	[15]

* M = Fe, Al, Ga

References: [1] Menchetti and Sabelli (1976a), (2) Lengauer et al. (1994), [3] Okada et al. (1982), [4] Breidenstein et al. (1992), [5] Balic Zunic et al. (1994), [6] Giuseppetti and Tadini (1980), [7] Kato (1977), [8] Kato and Miura (1977), [9] Kolitsch et al. (1999), [10] Szymanski (1988), [11] Szymanski (1985), [12] Ossaka et al. (1982), [13] Li et al. (1992), [14] Giuseppetti and Tadini (1987), [15] Jambor et al. (1996)

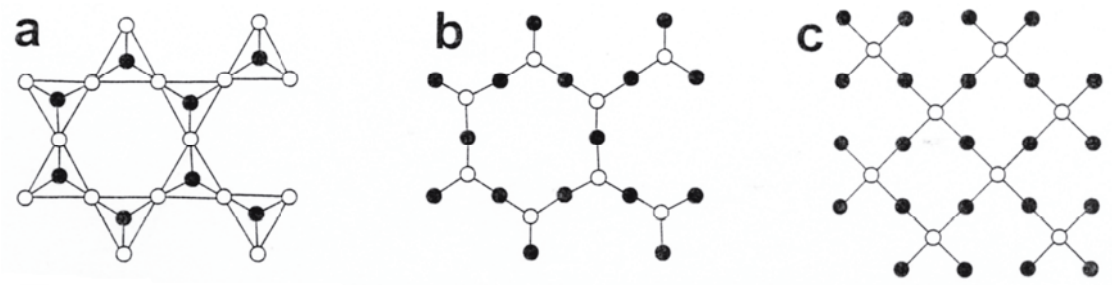

Figure 28. Graphs of the octahedral–tetrahedral sheets in the structures of sulfate minerals.

Continued next page → → →

Table 11. Sulfate minerals with sheets of (SO_4) tetrahedra and ($M\phi_6$) octahedra.

Name	Formula	*a* (Å)	*b* (Å)	*c* (Å)	β (°)	S. G.	Graph	Fig.	Ref.
felsöbányaite	$[Al_4(OH)_{10}(H_2O)](SO_4)(H_2O)_3$	13.026	10.015	11.115	104.3	$P2_1$	–	29c,d	[1]
kornelite	$[Fe^{3+}{}_2(H_2O)_6(SO_4)_3](H_2O)_{1.25}$	14.300	20.120	5.425	96.8	$P2_1/n$	36b	29e,f	[2]
rhomboclase	$(H_5O_2)[Fe^{3+}(H_2O)_2(SO_4)_2]$	9.724	18.333	5.421	–	*Pnma*	36c	29g,h	[3]
vanthoffite	$Na_6[Mg(SO_4)_4]$	9.797	9.217	8.199	113.5	$P2_1/c$	36d	30a,b	[4]
yavapaite	$K[Fe^{3+}(SO_4)_2]$	8.152	5.153	7.877	94.9	$C2/m$	36e	30c,d	[5]
natrochalcite	$Na[Cu^{2+}{}_2(OH)(H_2O)(SO_4)_2]$	8.809	6.187	7.509	118.7	$C2/m$	36f	30e,f	[6]
goldichite	$K[Fe^{3+}(H_2O)_2(SO_4)_2](H_2O)_2$	10.387	10.486	9.086	101.7	$P2_1/c$	36g	30g,h	[5]
slavikite	$Na[Fe^{3+}{}_5(H_2O)_6(OH)_6(SO_4)_6]$ $[Mg(H_2O)_6]_2(SO_4)(H_2O)_{15}$	12.200	*a*	35.130	–	$R\bar{3}$	36h	31a,b	[7]
guildite	$[Cu^{2+}Fe^{3+}(OH)(H_2O)_4(SO_4)_2]$	9.786	7.134	7.263	–	$P2_1/m$	36i	31c,d	[8]
ransomite	$[Cu^{2+}Fe^{3+}{}_2(SO_4)_4(H_2O)_6]$	4.811	16.217	10.403	–	$P2_1/c$	–	31e,f	[9]
poughite	$[Fe^{3+}{}_2(H_2O)_3(TeO_3)_2(SO_4)]$	9.660	14.200	7.86	–	$P2_1nb$	–	32a,b	[10]
fuenzalidaite	$K_6(Na,K)_4Na_6$ $[Mg_{10}(H_2O)_{12}(IO_3)_{12}(SO_4)_{12}]$	9.4643	*a*	27.336	–	$P\bar{3}c$	–	32c,d, e	[11]

$M = Fe^{2+}$, Ni, Mg, V, Zn, Al, Fe^{3+}

References: [1] Farkas and Pertlik (1997), [2] Robinson and Fang (1973), [3] Mereiter (1974), [4] Fischer and Hellner (1964), [5] Graeber and Rosenzweig (1971), [6] Giester and Zemann (1987), [7] Süsse (1973), [8] Wan et al. (1978), [9] Wood (1970),[10] Pertlik (1971), [11] Konnert et al. (1994)

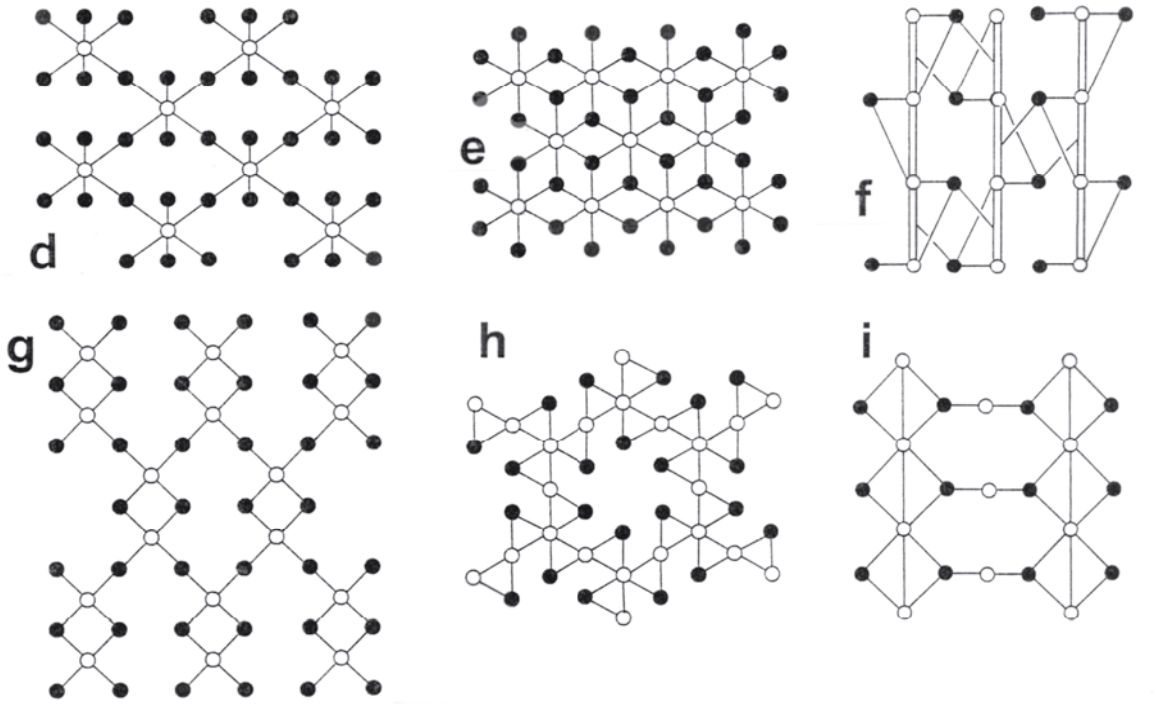

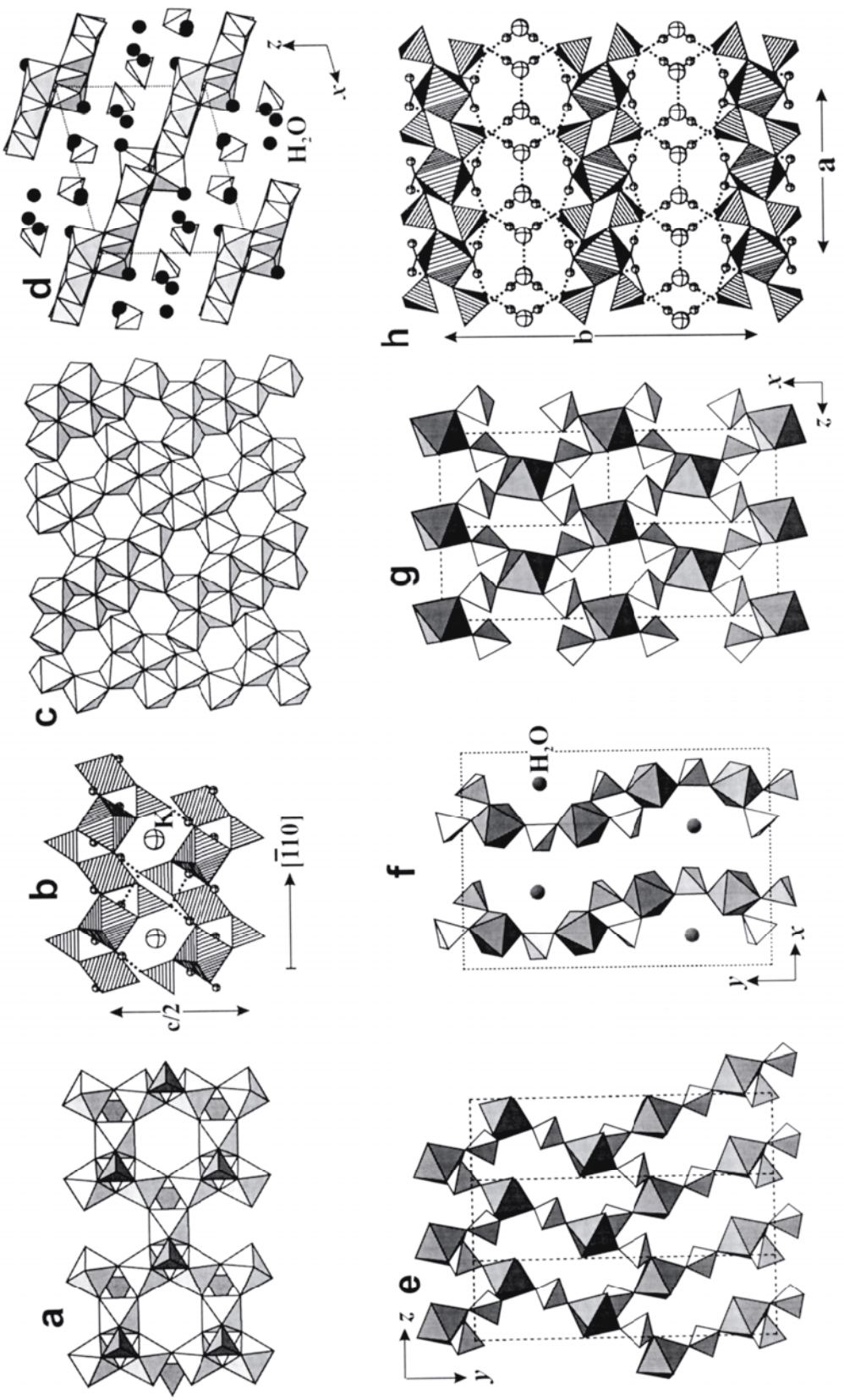

Figure 29. (a) The octahedral–tetrahedral sheet in the minerals of the alunite supergroup; (b) the structure of alunite; (c) the octahedral sheet in felsöbányaite; (d) the structure of felsöbányaite projected down [010]; (e) the $[M_2(T\Phi_4)_3\Phi_6]$ sheet in kornelite; (f) the structure of kornelite projected down [001]; (g) the $[M(T\Phi_4)_2\Phi_2]$ sheet in rhomboclase; (h) the intersheet species and hydrogen-bond network in rhomboclase.

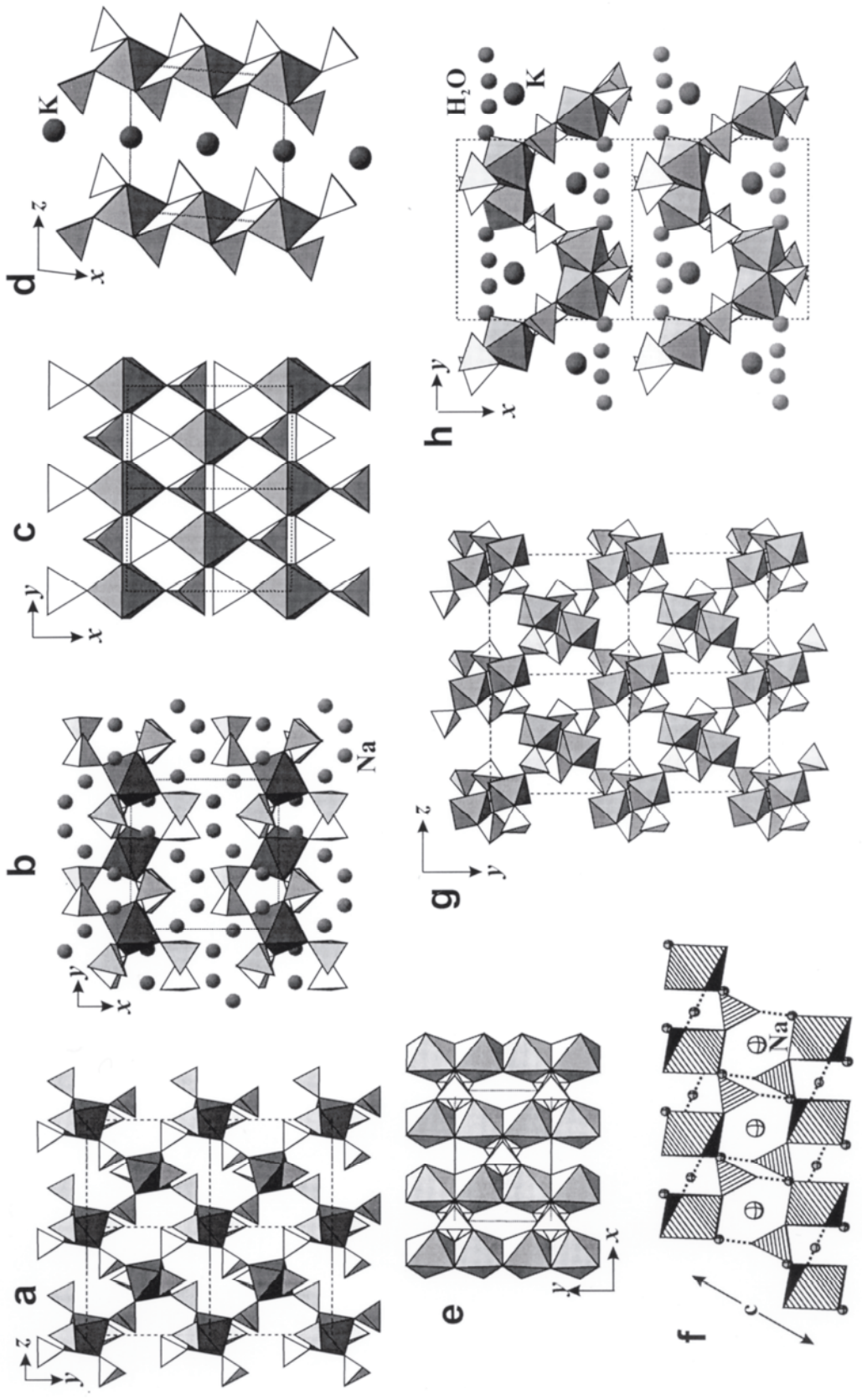

Figure 30. (a) The $[M(TØ_4)4]$ sheet in vanthoffite; (b) fitting together of the corrugated sheets in vanthoffite; (c) the $[M(TO_4)_2]$ sheet in yavapaite; (d) the structure of yavapaite projected down [010]; (e) the $[M(TØ_4)_2Ø_2]$ sheet in natrochalcite; (f) linkage of sheets in the structure of natrochalcite; (g) the $[M(TØ_4)_2Ø_2]$ sheet in goldichite; (h) packing of sheets in the structure of goldichite.

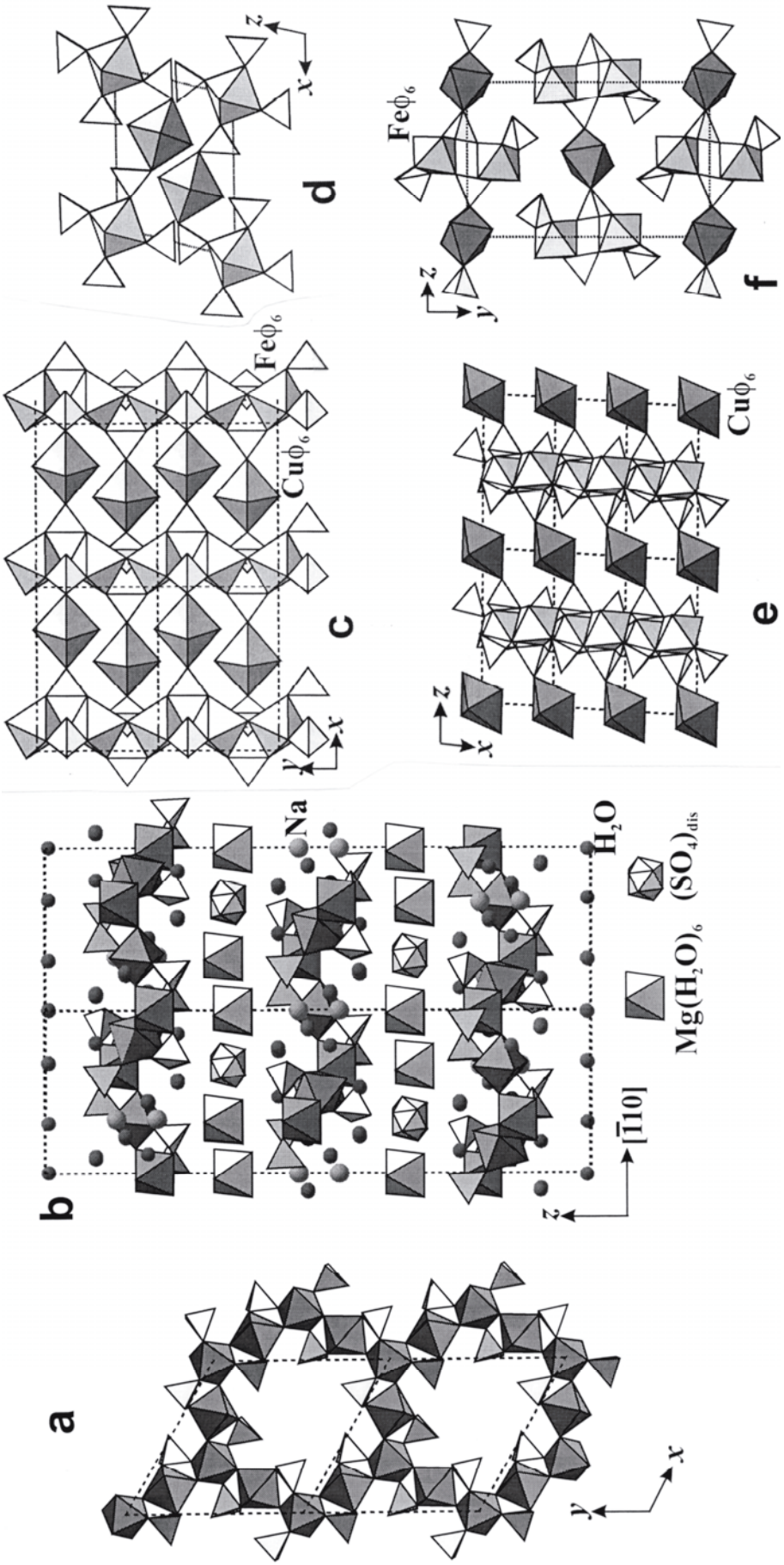

Figure 31. (a) The open sheet in slavikite; (b) the structure of slavikite projected down [110]; note that the (SO_4) tetrahedra in the interlayer are disordered; (c) the sheets in the structure of guildite; (d) the structure of guildite projected down [010]; (e) the sheet in ransomite; (f) the structure of ransomite viewed down [010].

tetrahedra. These sheets link in the [100] direction through interstitial [9]-coordinated K and a network of hydrogen bonds.

Slavikite, $Na[Fe^{3+}_5(H_2O)_6(OH)_6(SO_4)_6][Mg(H_2O)_6]_2(SO_4)(H_2O)_{15}$, is based on an unusually open sheet of corner-sharing octahedra and tetrahedra, consisting of fragments of the $[M(TO_4)Ø]$ butlerite-like 7 Å chain (Fig. 31a); the holes in the sheet are occupied by Na and (H_2O) groups. The interlayer consists of $\{Mg(H_2O)_6\}$ octahedra and disordered (SO_4) tetrahedra that are held in the structure only by hydrogen bonds (Fig. 31b). The structures of **guildite**, $[Cu^{2+}Fe^{3+}(OH)(H_2O)_4(SO_4)_2]$ (Fig. 31c,d), and **ransomite**, $[Cu^{2+}Fe^{3+}_2(SO_4)_4(H_2O)_6]$ (Fig. 31e,f), are based on sideronatrite-like and krausite-like chains, respectively, linked by Jahn-Teller-distorted $(CuØ_6)$ octahedra and by hydrogen bonding. **Poughite**, $[Fe^{3+}_2(H_2O)_3(TeO_3)_2(SO_4)]$, and **fuenzalidaite**, $K_6(Na,K)_4Na_6[Mg_{10}(H_2O)_{12}(IO_3)_{12}(SO_4)_{12}]$, are based on mixed octahedral-tetrahedral-triangular sheets. In poughite, edge-sharing octahedral dimers are linked to one (SO_4) tetrahedron each to form $[Fe^{3+}_2O_6(H_2O)_2(SO_4)_2]$ clusters that are cross-linked by (TeO_3) triangles (Fig. 32a). The sheets are held together by hydrogen bonding only (Fig. 32b). The structure of fuenzalidaite is based on the complex pinwheel sheet shown in Figures 32c,d. The pinwheels consist of $(MgØ_6)$ octahedra and both (SO_4) tetrahedra and (IO_3) triangles. These complex sheets are connected through other pinwheels that involve $(NaØ_6)$ octahedra with K in the interstices (Fig. 32e). Fuenzalidaite was discovered in Chilean nitrate deposits and is the only known natural iodate-sulfate.

Inspection of the finite clusters, chains, and sheets in sulfate minerals and their graphs shows the advantages provided by graphical representation of octahedral–tetrahedral structures. It gives a clear and simple representation of the way in which the polyhedra link together. This shows also that Nature chooses a small number of building blocks, connects them in a very simple and elegant way, and packs the resultant units (clusters, chains, or sheets) economically to use space as efficiently as possible.

Structures with infinite frameworks

The sulfate minerals in this category are listed in Table 12. Unfortunately, the topological aspects of the framework structures cannot easily be summarized in a concise graphical fashion because of the complexity that results from polymerization in three dimensions.

The structure of **bonattite**, $[Cu^{2+}(SO_4)(H_2O)_3]$, is based on a skewed arrangement of $[M(TO_4)Ø_4]$ chalcanthite-like chains (Fig. 21c) polymerized by corner-sharing of polyhedra from adjacent chains (Fig. 33a). The structure of **kieserite**, $[Mg(SO_4)(H_2O)]$, is shown in Figure 33b,c. The $[M(TØ_4)Ø]$ framework can be constructed from $[M(TØ_4)Ø_3]$ chains of the type found in butlerite, parabutlerite, and uklonskovite (Fig. 21e). The chains pack in a *C*-centered array and are cross-linked by sharing corners between octahedra and tetrahedra of adjacent chains. This is a very common arrangement in a wide variety of silicate, phosphate, arsenate, vanadate, and sulfate minerals. The structures of **millosevichite**, $[Al_2(SO_4)_3]$ and **mikasaite** $[Fe^{3+}_2(SO_4)_3]$ (Fig. 33d,e), and **langbeinite**, $K_2[Mg_2(SO_4)_3]$, are based on glaserite-ungemachite-type pinwheels linked in three dimensions (Fig. 33f). The structure of **chalcocyanite**, $[Cu^{2+}(SO_4)]$, is based on linarite-type $[M(TO_4)Ø_2]$ chains cross-linked by the tetrahedral vertices not linked to the central octahedral chain (Fig. 33g,h). In **löweite**, $Na_{12}[Mg_7(H_2O)_{12}(SO_4)_9](SO_4)_4(H_2O)_3$, there are two types of (SO_4) groups: the first type participates in formation of the open $[Mg_7(SO_4)_9(H_2O)_{12}]$ octahedral-tetrahedral framework, whereas the groups of the second type are disordered in the framework cavities (Fig. 33i). **Kainite**, $K_4[Mg_4(H_2O)_{10}(SO_4)_4](H_2O)Cl_4$, is based on kröhnkite-like $[M(TO_4)_2Ø_2]$ chains (Fig. 22e) linked into sheets parallel to (100) (Fig. 33j);

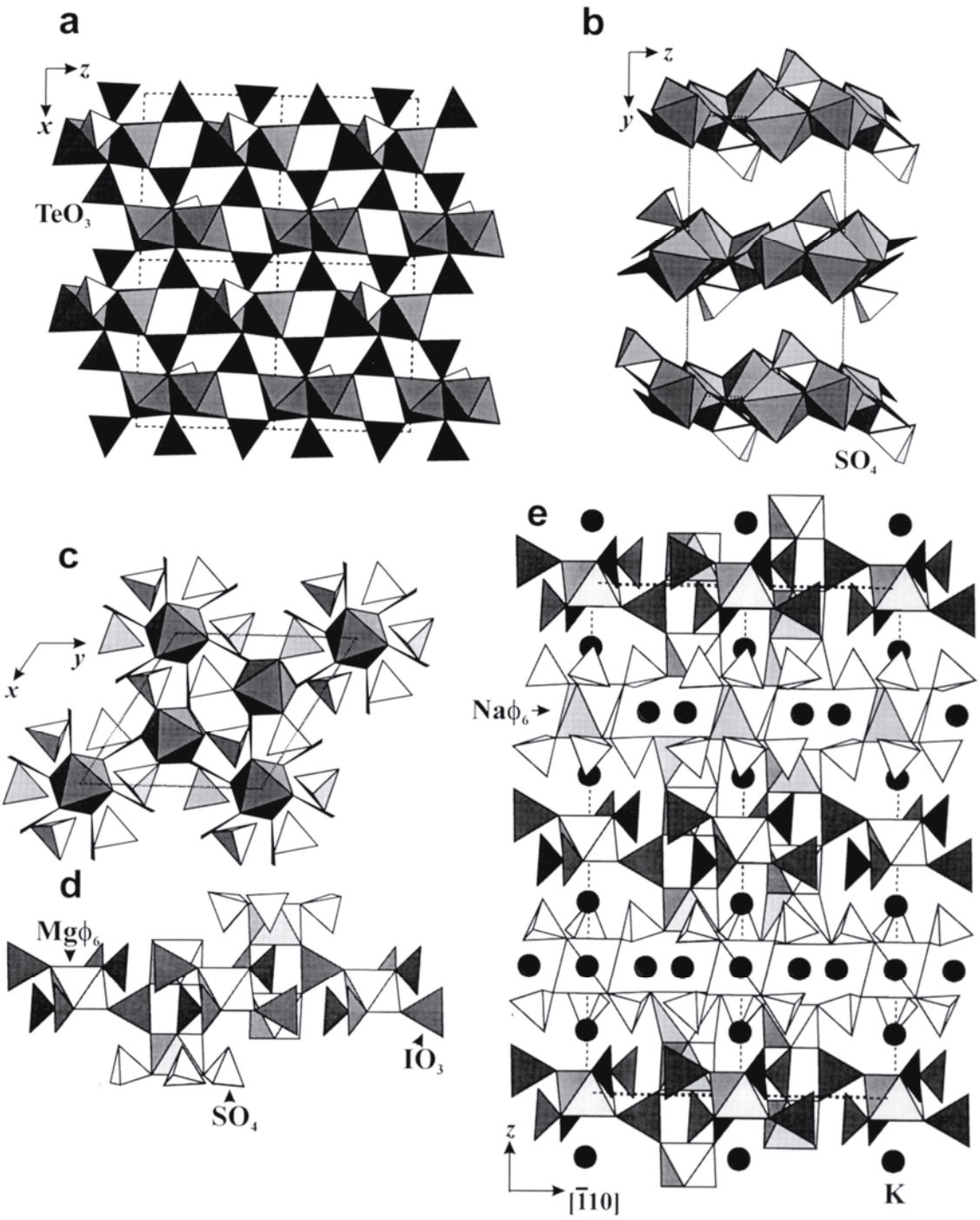

Figure 32. (a) The sheet of ($FeØ_6$) octahedra, (SO_4) tetrahedra, and (TeO_3) triangles in poughite; (b) the arrangement of sheets in poughite; (c,d) the octahedral–tetrahedral–triangle sheet in fuenzalidaite viewed (c) down [001], and (d) in the plane of the sheet; (e) the structure of fuenzalidaite projected down [110].

Table 12. Sulfate minerals with frameworks of (SO_4) tetrahedra and ($M\phi_6$) octahedra.

Name	Formula	*a* (Å)	*b* (Å)	*c* (Å)	β (°)	S. G.	Fig.	Ref.
bonattite	$[Cu^{2+}(SO_4)(H_2O)_3]$	5.592	13.029	7.341	97.1	*Cc*	33a	[1]
kieserite	$[Mg(SO_4)(H_2O)]$	6.891	7.624	7.645	117.7	*C*2/*c*	33b,c	[2]
dwornikite	$[Ni(SO_4)(H_2O)]$	6.824	7.594	7.457	117.8	*C*2/*c*	33b,c	[3]
szmikite	$[Mn^{2+}(SO_4)(H_2O)]$	7.116	7.667	7.92	118.1	*C*2/*c*	33b,c	[3]
gunningite	$[Zn(SO_4)(H_2O)]$	6.925	7.591	7.635	118.2	*C*2/*c*	33b,c	[3]
szomolnokite	$[Fe^{2+}(SO_4)(H_2O)]$	7.078	7.549	7.773	118.7	*C*2/*c*	33b,c	[3]
poitevinite[1]	$[Cu^{2+}(SO_4)(H_2O)]$	5.120	5.160	7.535	107.4	$P\bar{1}$	33b,c	[4]
millosevichite	$[Al_2(SO_4)_3]$	8.025	*a*	21.357	–	$R\bar{3}$	33d,e	[5]
mikasaite	$[Fe^{3+}{}_2(SO_4)_3]$	8.14	*a*	21.99	–	$R\bar{3}$	33d,e	(6)
langbeinite	$K_2[Mg_2(SO_4)_3]$	9.919	*a*	*a*	–	$P2_13$	33f	[7]
manganolangbeinite	$K_2[Mn^{2+}{}_2(SO_4)_3]$	10.114	*a*	*a*	–	$P2_13$	33f	(6)
efremovite	$(NH_4)_2[Mg_2(SO_4)_3]$	9.99	*a*	*a*	–	$P2_13$	33f	(6)
löweite[2]	$Na_{12}[Mg_7(H_2O)_{12}(SO_4)_9](SO_4)_4(H_2O)_3$	11.769	*a*	–	–	$R\bar{3}$	33i	[8]
chalcocyanite	$[Cu^{2+}(SO_4)]$	8.409	6.709	4.833	–	*Pnma*	33g,h	[9]
zincosite	$[Zn(SO_4)]$	8.604	6.746	4.774	–	*Pnma*	33g,h	[9]
kainite	$K_4[Mg_4(H_2O)_{10}(SO_4)_4](H_2O)Cl_4$	19.720	16.230	9.53	94.9	*C*2/*m*	33j,k	[10]
voltaite	$K_2[Fe^{2+}{}_5Fe^{3+}{}_3(H_2O)_{12}(SO_4)_{12}][Al(H_2O)_6]$	27.254	*a*	*a*	–	$Fd\bar{3}c$	33l,m	[11]
zincovoltaite	$K_2[Zn_5Fe^{3+}{}_3(H_2O)_{12}(SO_4)_{12}][Al(H_2O)_6]$	27.18	*a*	*a*	–	$Fd\bar{3}c$	33l,m	(6)
sulfoborite	$[Mg_3(OH)F(SO_4)(B(OH)_4)_2]$	10.132	12.537	7.775	–	*Pnma*	34a,b	[12]
vlodavetsite	$[Ca_2AlF_2Cl(H_2O)_4(SO_4)_2]$	6.870	*a*	13.342	–	*I*4/*m*	34c,d	[13]
tychite	$Na_6[Mg_2(CO_3)_4](SO_4)$	13.930	*a*	*a*	–	$Fd\bar{3}$	34e,f	[14]
ferrotychite	$Na_6[Fe^{2+}{}_2(CO_3)_4](SO_4)$	13.962	*a*	*a*	–	$Fd\bar{3}$	34e,f	[15]
manganotychite	$Na_6[Mn^{2+}{}_2(CO_3)_4](SO_4)$	13.995	*a*	*a*	–	$Fd\bar{3}$	34e,f	(6)
philolithite	$[Pb^{2+}{}_2O]_6[Mn^{2+}Mg_2Mn^{2+}{}_4Cl_4(OH)_{12}(SO_4)(CO_3)_4]$	12.627	*a*	12.595	–	$P4_2/nnm$	35a,b,c	[16]
brochantite	$[Cu^{2+}{}_4(OH)_6(SO_4)]$	13.087	9.835	6.015	103.3	$P2_1/a$	36a,b	[17]
antlerite	$[Cu^{2+}{}_3(OH)_4(SO_4)]$	8.244	6.043	11.987	–	*Pnma*	36c,d	[18]
mammothite	$Pb^{2+}{}_6[Cu^{2+}{}_4AlSbO_2(OH)_{16}Cl_2](SO_4)_2Cl_2$	18.390	7.330	11.350	112.4	*C*2/*m*	36e,f	[19]
caminite	$[Mg_4(SO_4)_3(OH)_2(H_2O)]$	5.242	*a*	12.995	–	$I4_1/amd$	36g-j	[20]
connellite	$[Cu^{2+}{}_{19}(OH)_{32}Cl_4](SO_4)(H_2O)_3$	15.780	*a*	9.100	–	$P\bar{6}2c$	35d	[21]

[1] α = 107.1°, γ = 92.7°; [2] rhombohedral cell: α = 106.5°

References: [1] Zahrobsky and Baur (1968), [2] Hawthorne et al. (1987), [3] Wildner and Giester (1991), [4] Giester et al. (1994), [5] Dahmen and Gruehn (1993), (6) Gaines et al. (1997), [7] Mereiter (1979), [8] Fang and Robinson (1970b), [9] Wildner and Giester (1988), [10] Robinson et al. (1972), [11] Mereiter (1972), [12] Giese and Penna (1983), [13] Starova et al. (1995), [14] Shiba and Watanabe (1931), [15] Malinovskii et al. (1979), [16] Moore et al. (2000), [17] Helliwell and Smith (1997), [18] Hawthorne et al. (1989), [19] Effenberger (1985b), [20] Keefer et al. (1981), Hochella et al. (1983), [21] McLean and Anthony (1972)

the sheets are further linked into a framework by corner-sharing through ($MgØ_6$) octahedra (Fig. 33k). The framework in **voltaite**, $K_2[Fe^{2+}{}_5Fe^{3+}{}_3(H_2O)_{12}(SO_4)_{12}]\{Al(H_2O)_6\}$, is a three-dimensional polymerization (Fig. 33l) of complex octahedral–tetrahedral chains (Fig. 33m), with K in the interstices.

Sulfoborite, $[Mg_3(OH)F(SO_4)(B(OH)_4)_2]$, is based on the complex sheets of ($MgØ_6$) octahedra and (SO_4) tetrahedra; the structure of the sheet is shown in Figure 34b. The amarantite-like octahedral tetramers (Fig. 34a) are polymerized to form octahedral chains parallel to [100] and linked by (SO_4) tetrahedra. The linkage between sheets is provided by $[B(OH)_4]$ tetrahedra (Fig. 34a). **Vlodavetsite**, $[Ca_2AlF_2Cl(H_2O)_4(SO_4)_2]$, consists of a framework of corner-sharing ($CaØ_6$), ($AlØ_6$) octahedra and (SO_4) tetrahedra (Fig. 34c). The basis of the framework is the sheet of corner-sharing ($CaØ_6$) octahedral and (SO_4) tetrahedra shown in Figure 34d. The structure of **ferrotychite**, $Na_6[Fe^{2+}{}_2(CO_3)_4](SO_4)$, is based on the octahedral–triangular framework formed by corner sharing of (FeO_6) octahedra and (CO_3) triangles (Fig. 34e). The main structural element of

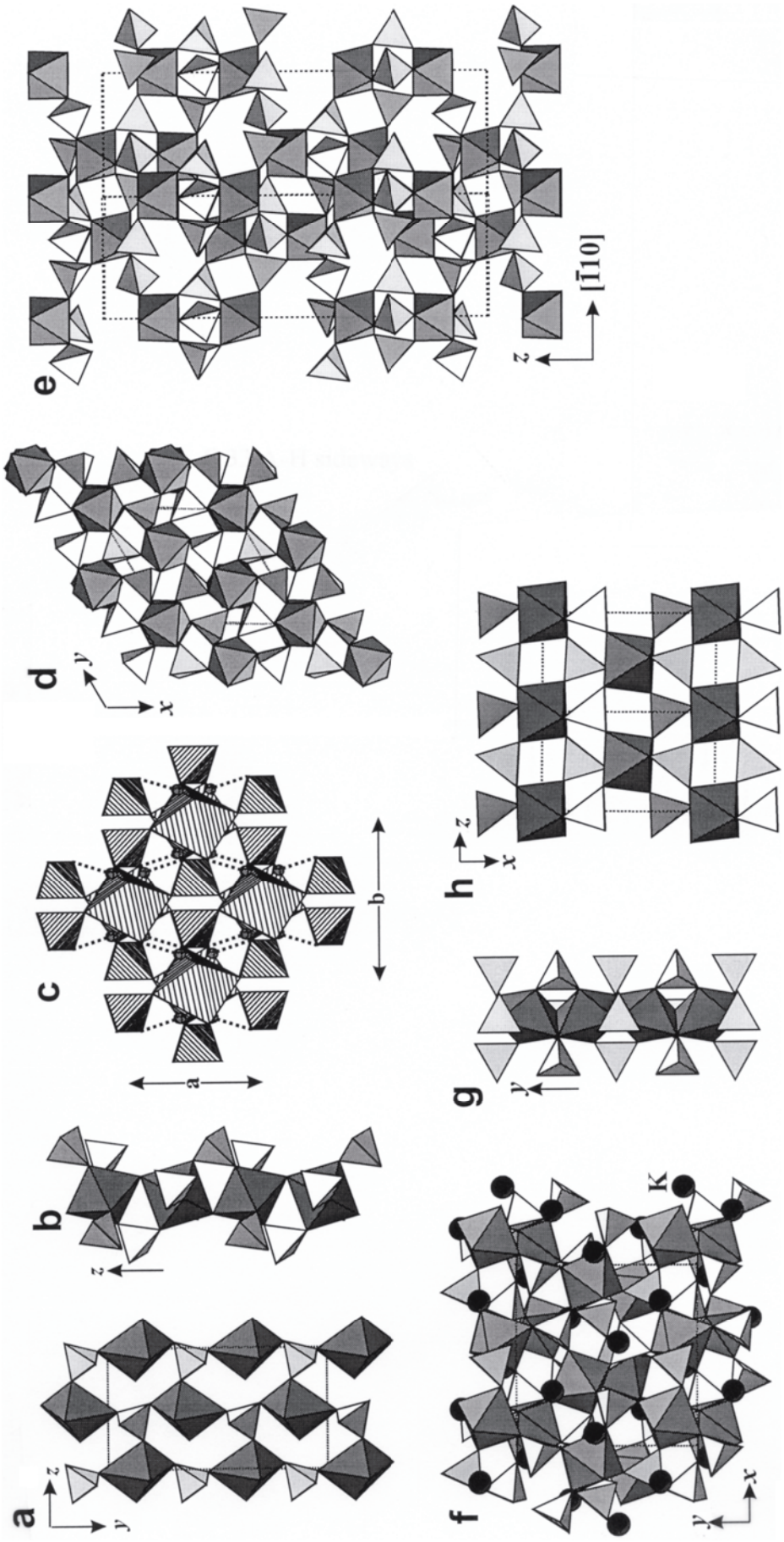

Figure 33. (a) The structure of bonattite; (b) the octahedral–tetrahedral chain in kieserite; (c) the structure of kieserite projected down [001]; (d,e) the structure of millosevichite projected down (d) [001], and (e) [110]; (f) the structure of langbeinite; (g) The octahedral–tetrahedral chain in chalcocyanite; (h) the arrangement of chains in chalcocyanite.

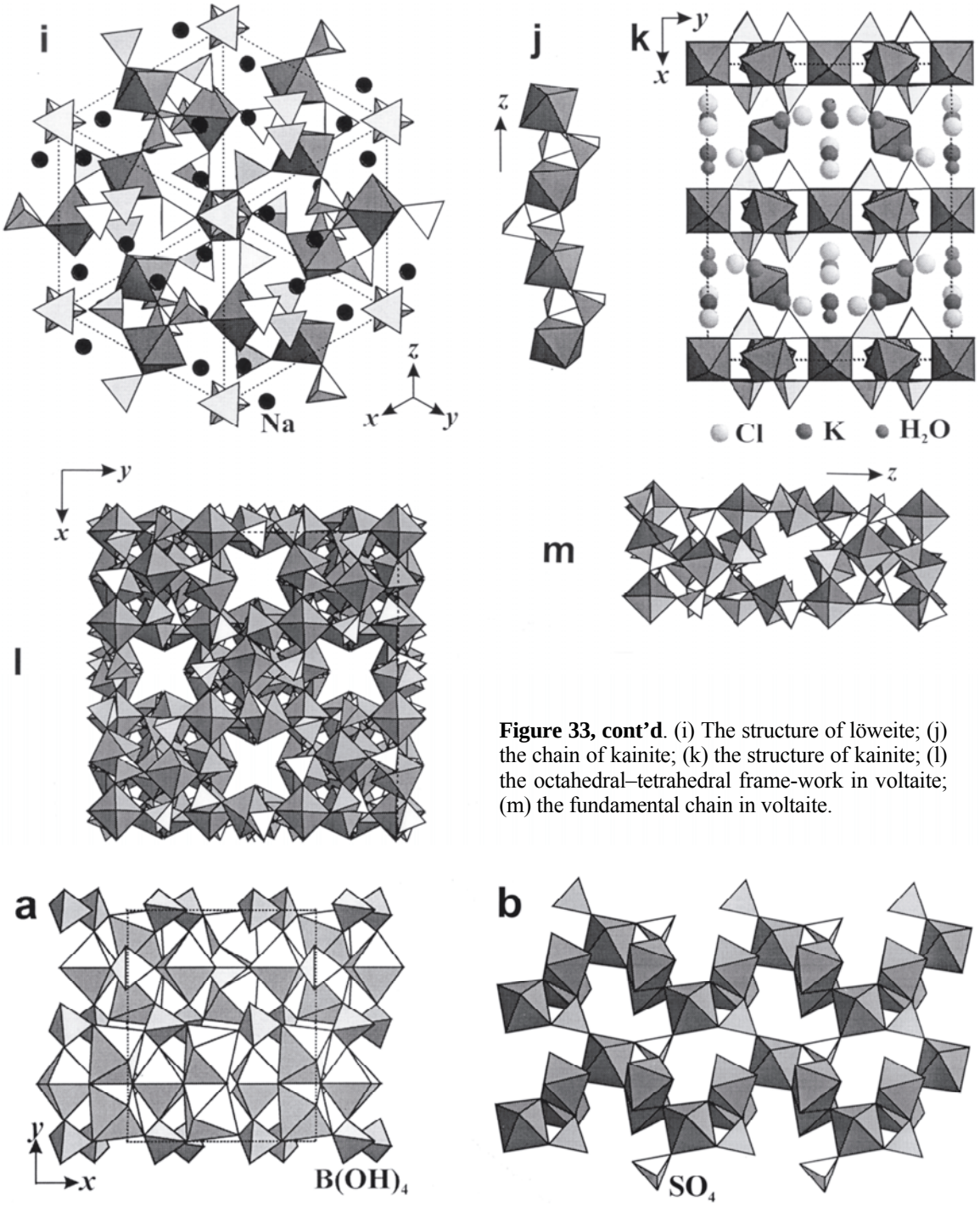

Figure 33, cont'd. (i) The structure of löweite; (j) the chain of kainite; (k) the structure of kainite; (l) the octahedral–tetrahedral frame-work in voltaite; (m) the fundamental chain in voltaite.

Figure 34. (a) The structure of sulfoborite viewed along [001]; (b) the octahedral–tetrahedral sheet in sulfoborite projected ~5° from [010].

the framework is the octahedral-triangular chain shown in Figure 34f; the (SO_4) groups are in the framework cavities.

The structure of **philolithite**, $[Pb^{2+}{}_2O]_6[Mn^{2+}(Mg,Mn^{2+})_2(Mn^{2+},Mg)_4Cl_4(OH)_{12}(SO_4)(CO_3)_4]$, consists of a trellis-like open framework based on the complex octahedral-tetrahedral-triangular chain shown in Figure 35a. The chains extend in the [110] and [$\bar{1}10$] directions and cross-link to form a trellis-like framework (Fig. 35b). The large channels of

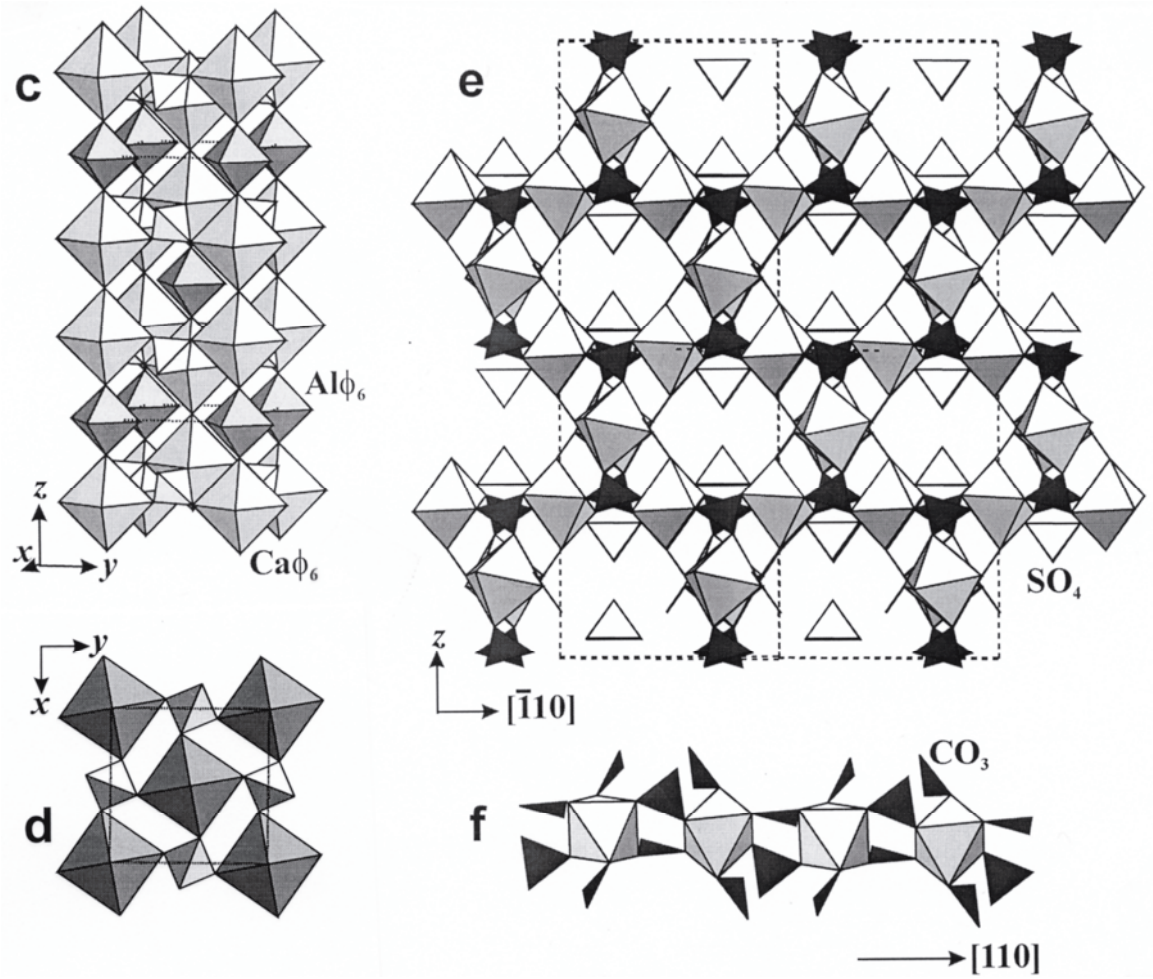

Figure 34, cont'd. (c) the structure of vlodavetsite; (d) the fundamental sheet of ($CaØ_6$) octahedra and (SO_4) tetrahedra in vlodavetsite; (e) the structure of ferrotychite projected down [110]; (f) the chain of ($MgØ_6$) octahedra and (CO_3) triangles that is an important motif in the framework of ferrotychite.

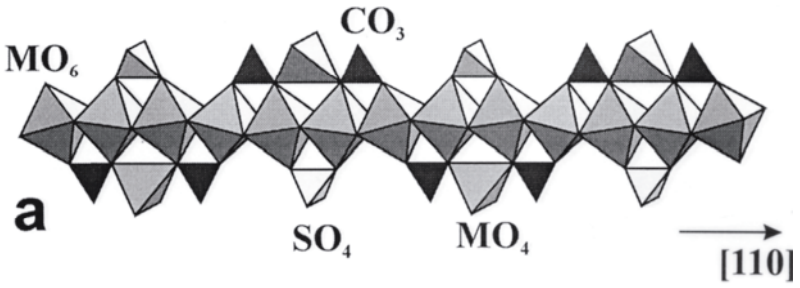

Figure 35. (a) The fundamental [$MØ_4$] chain decorated by (CO_3) triangles, (SO_4) tetrahedra, and (MO_4) tetrahedra in philolithite.

the framework are occupied by [OPb_2] chains of edge-sharing (OPb_4) tetrahedra, and Cl anions (Fig. 35c). The structure of **connellite**, $[Cu^{2+}_{19}(OH)_{32}Cl_4](SO_4)(H_2O)_3$, is based on a complex framework of ($Cu^{2+}Ø_6$) octahedra (Ø = OH, Cl) with cavities occupied by disordered (SO_4) tetrahedra (Fig. 35d).

Brochantite, $[Cu^{2+}_4(OH)_6(SO_4)]$, and **antlerite**, $[Cu^{2+}_3(OH)_4(SO_4)]$, are based on

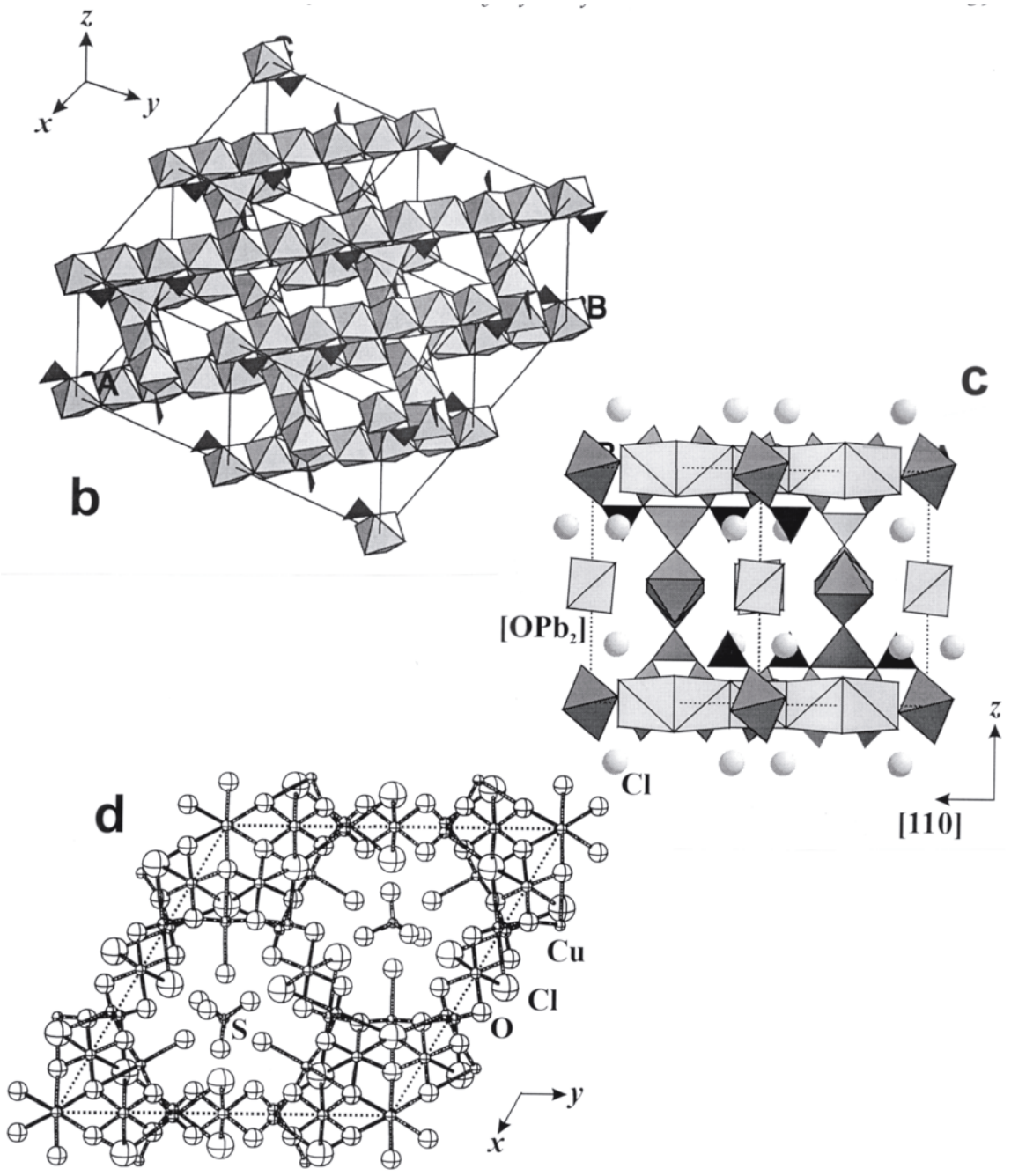

Figure 35, cont'd. (b) The trellis-like framework resulting from the intersection of the chains in (a); (c) the structure of philolithite projected down [$\bar{1}10$]; the [OPb_2] chains of edge-sharing (OPb_4) tetrahedra are shown as lightly shaded; (d) the structure of connellite projected down [001]; the (SO_4) groups are disordered in the channels of the framework of ($Cu\emptyset_6$) octahedra.

double and triple chains of ($Cu^{2+}\emptyset_6$) octahedra, respectively (Fig. 36a,c). The chains are cross-linked by (SO_4) tetrahedra to form frameworks (Figs. 36b,d). The structure of **mammothite**, $Pb^{2+}{}_6[Cu^{2+}{}_4AlSb^{5+}O_2(OH)_{16}Cl_2](SO_4)_2Cl_2$, consists of an octahedral framework based on the open-branched chain of ($Cu^{2+}\emptyset_6$) octahedra shown in Figure 36e. The chains extend parallel to [010] and are linked by ($Al\emptyset_6$) and ($Sb^{5+}\emptyset_6$) octahedra in the [100] and [001] directions, respectively (Fig. 36f). The large channels of the framework are occupied by Pb^{2+}, Cl and (SO_4) tetrahedra.

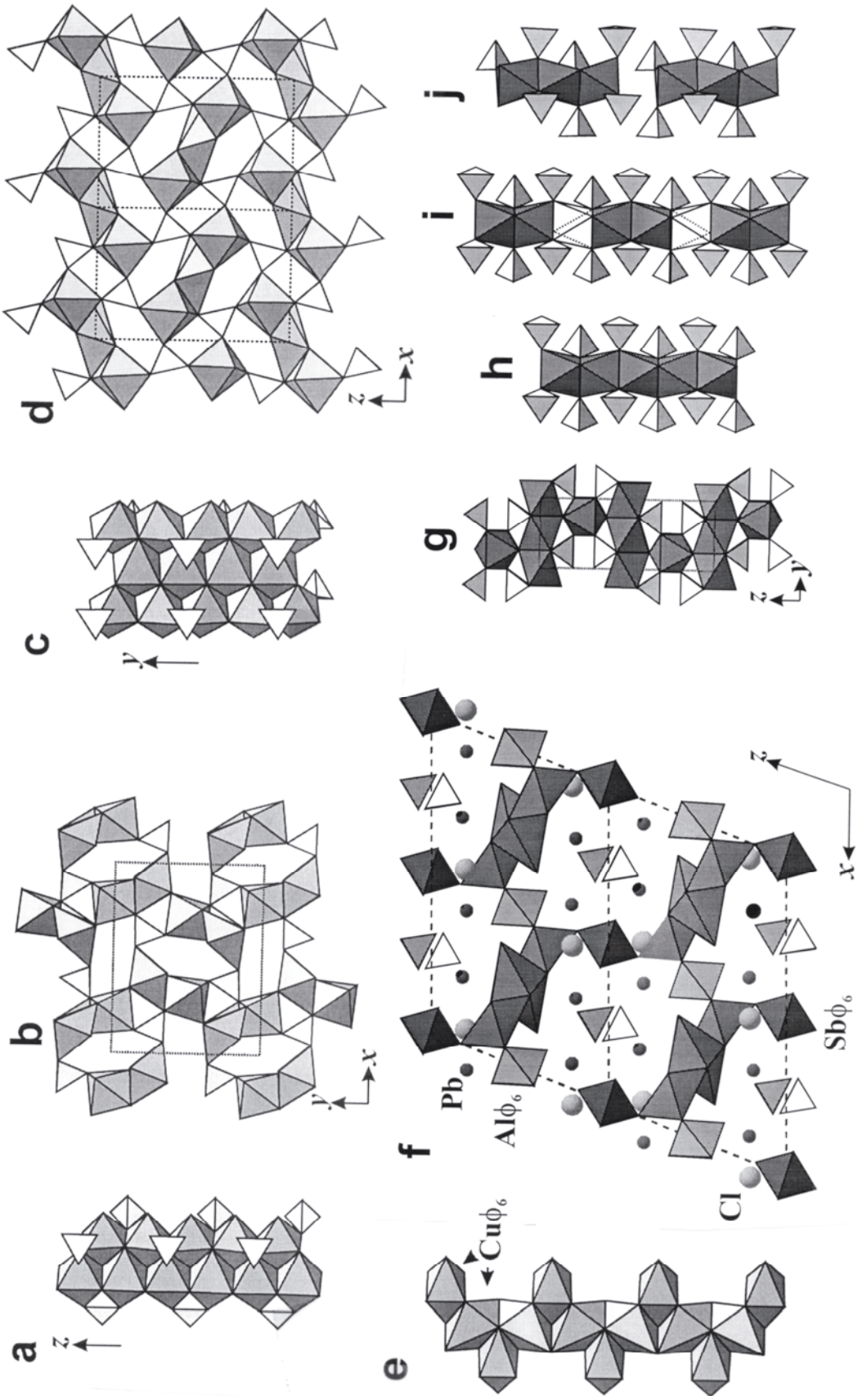

Figure 36. The double (a) and triple (c) chains of ($Cu\phi_6$) octahedra and (SO_4) tetrahedra and the frameworks in (b) brochantite and (d) antlerite; (e) the octahedral chain in mammothite; (f) the octahedral framework in mammothite; (g) the octahedral–tetrahedral framework in caminite; (h) the fundamental chain in caminite; (i) the ordered arrangement of occupied and empty octahedra in the caminite chain (as suggested by Keefer et al. 1981); (j) the ordered arrangement of occupied and empty octahedra in synthetic $Mg_3(SO_4)_2(OH)_2$ (Fleet and Knipe 1997).

Caminite, $[Mg_4(SO_4)_3(OH)_2(H_2O)]$, is the only known sulfate mineral with face-sharing divalent-metal octahedra. The ($MgØ_6$) octahedra in caminite share faces to produce chains that extend along [010] (Fig. 36g). The chains are decorated by (SO_4) tetrahedra (Fig. 36h) that provide linkage between the chains. Only two-thirds of the octahedra in the chain shown in Figure 36h are populated by Mg. Keefer et al. (1981) suggested that, in the ordered arrangement, occupied ($MgØ_6$) octahedra are associated in pairs that alternate with unoccupied octahedra (as shown in Fig. 36i). However, Fleet and Knipe (1997) determined the structure of synthetic $Mg_3(SO_4)_2(OH)_2$ with the same stoichiometry as caminite but with a different unit cell and symmetry. In this structure, the face-sharing ($MgØ_6$) octahedra occur as linear ternary groups rather than as octahedral dimers (Fig. 36j).

Table 13. Calcium-sulfate minerals.

Name	Formula	*a* (Å)	*b* (Å)	*c* (Å)	β (°)	S. G.	Fig.	Ref.
anhydrite	$[CaSO_4]$	6.993	6.995	6.245	–	*Amma*	37a-d	[1]
gypsum	$[CaSO_4(H_2O)_2]$	5.679	15.202	6.522	118.4	I2/c	37e,f,h	[2]
ardealite*	$[Ca_2(HPO_4)(SO_4)(H_2O)_4]$	5.721	30.992	6.250	117.3	Cc	37g	[3]
rapidcreekite	$[Ca_2(SO_4)(CO_3)(H_2O)_4]$	15.517	19.226	6.165	–	*Pcnb*	38a,b	[4]
bassanite	$[CaSO_4(H_2O)_{0.5}]$	6.937	*a*	6.345	–	$P3_12$	38c-f	[5]
syngenite	$K_2[Ca(SO_4)_2(H_2O)]$	6.225	7.127	9.727	104.2	$P2_1/m$	38g,h,i	[6]
görgeyite	$K_2[Ca_5(SO_4)_6(H_2O)]$	17.519	6.840	18.252	113.3	*C*2/*c*	39a,b,c	[7]
orschallite	$[Ca_3(SO_3)_2(SO_4)(H_2O)_{12}]$	11.350	*a*	28.321	–	$R\bar{3}c$	39d-g	[8]
glauberite	$[CaNa_2(SO_4)_2]$	10.129	8.306	8.533	112.2	*C*2/*c*	40a-c	[9]
ternesite	$[Ca_5(SiO_4)_2(SO_4)]$	6.863	15.387	10.181	–	*Pnma*	40d-g	[10]

* synthetic material

References: [1] Hawthorne and Ferguson (1975a), [2] Pedersen and Semmingsen (1982), [3] Sakae et al. (1978), [4] Cooper and Hawthorne (1996a), [5] Abriel and Nesper (1993), [6] Bokii et al. (1978), [7] Mukhtarova et al. (1980), Smith and Walls (1980), [8] Weidenthaler et al. (1993), [9] Araki and Zoltai (1967), [10] Irran et al. (1997)

STRUCTURES WITH NON-OCTAHEDRAL CATION-COORDINATION POLYHEDRA

Calcium-sulfate minerals

Divalent Ca has a relatively large ionic radius (1.00 Å and 1.12 Å for $^{[6]}$Ca and $^{[8]}$Ca, respectively; Shannon 1976) and is usually coordinated by more than six anions: in sulfate minerals, Ca is most often coordinated by eight or nine anions. Crystallographic parameters for Ca-sulfate minerals are given in Table 13. It is notable that most of the minerals with Ca as the dominant interstitial cation have structures closely related to that of anhydrite, $CaSO_4$.

The structure of **anhydrite**, $CaSO_4$, is based on chains of alternating edge-sharing (SO_4) tetrahedra and (CaO_8) dodecahedra (Fig. 37a,i). These chains extend in the *c* direction and are linked by edge-sharing between adjacent (CaO_8) dodecahedra and by corner-sharing between the (SO_4) tetrahedra and (CaO_8) dodecahedra (Fig. 37b). The structure contains sheets of edge-sharing chains (Fig. 37c,d) that are parallel to $(\bar{1}10)$. Similar sheets occur in the structures of **gypsum**, $CaSO_4(H_2O)_2$, and **ardealite**, $Ca_2(HPO_4)(SO_4)(H_2O)_4$. Figures 37e,f show the structure of gypsum, and Figure 37g shows the structure of ardealite. In gypsum, all sheets have the same orientation, whereas in ardealite, adjacent sheets are rotated by 62.7° relative to each other. Thus, the edge-

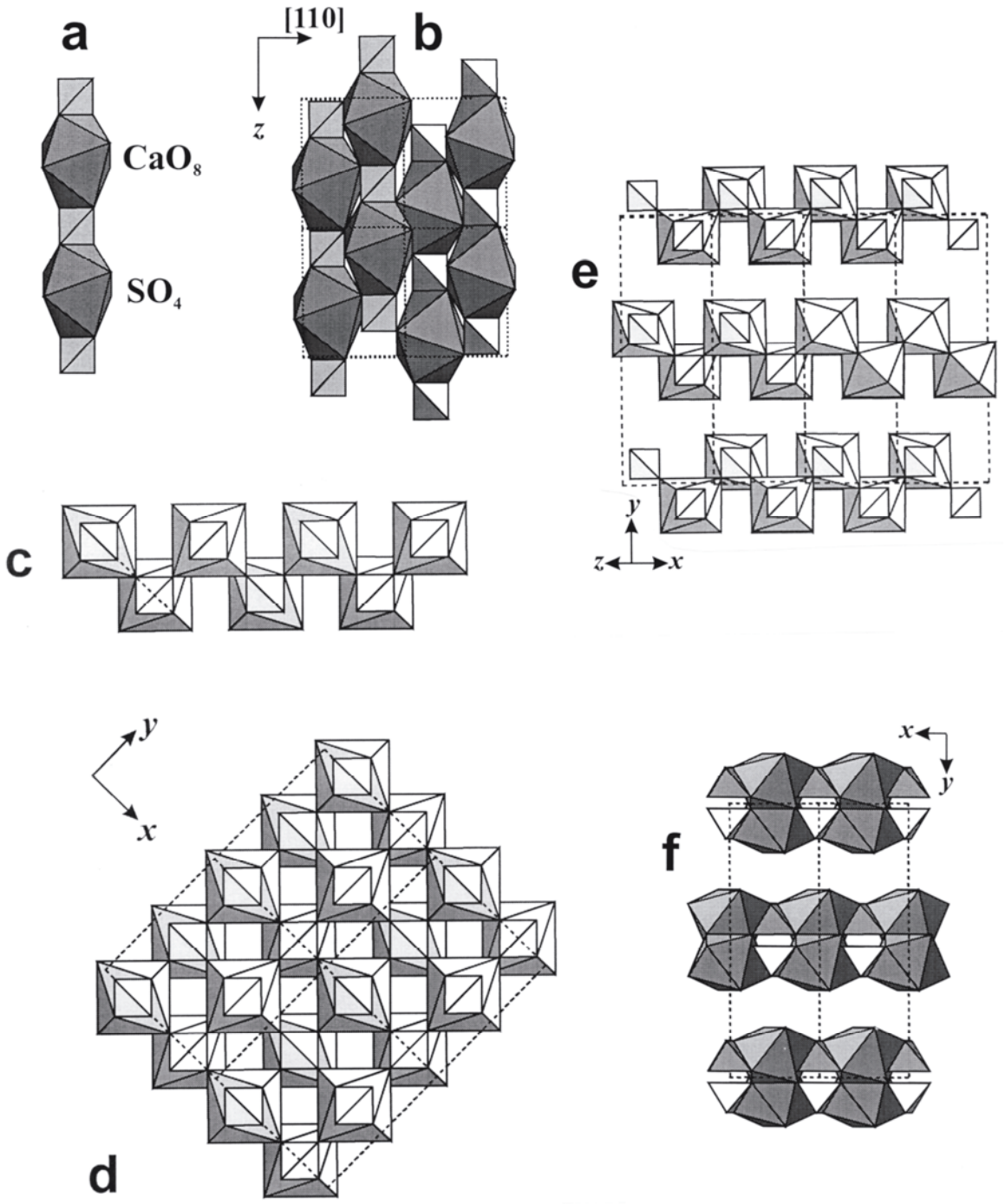

Figure 37. (a) The chain of edge-sharing CaO_8 polyhedra and (SO_4) tetrahedra in anhydrite; (b) linking of chains into layers parallel to $(1\bar{1}0)$ in anhydrite; (c) the layer viewed along [001] in anhydrite; (d) the structure of anhydrite viewed along [001]; (e,f) the structure of gypsum viewed along (e) [101] and (f) [001].

sharing chains of (SO_4) and ($CaØ_8$) polyhedra are parallel to [101] in gypsum (Fig. 37h), and to both [001] and [101] in ardealite. The chain repeats are 6.25 Å in anhydrite, 6.27 Å in gypsum, and 6.25 and 6.24 Å in ardealite.

The structure of **rapidcreekite**, $Ca_2(SO_4)(CO_3)(H_2O)_4$, can be derived from that of gypsum by twinning along alternate rows of (SO_4) groups (Fig. 38a,b). At each alternate row of (SO_4) tetrahedra, the structure is twinned by rotation of 180° about [100]. This

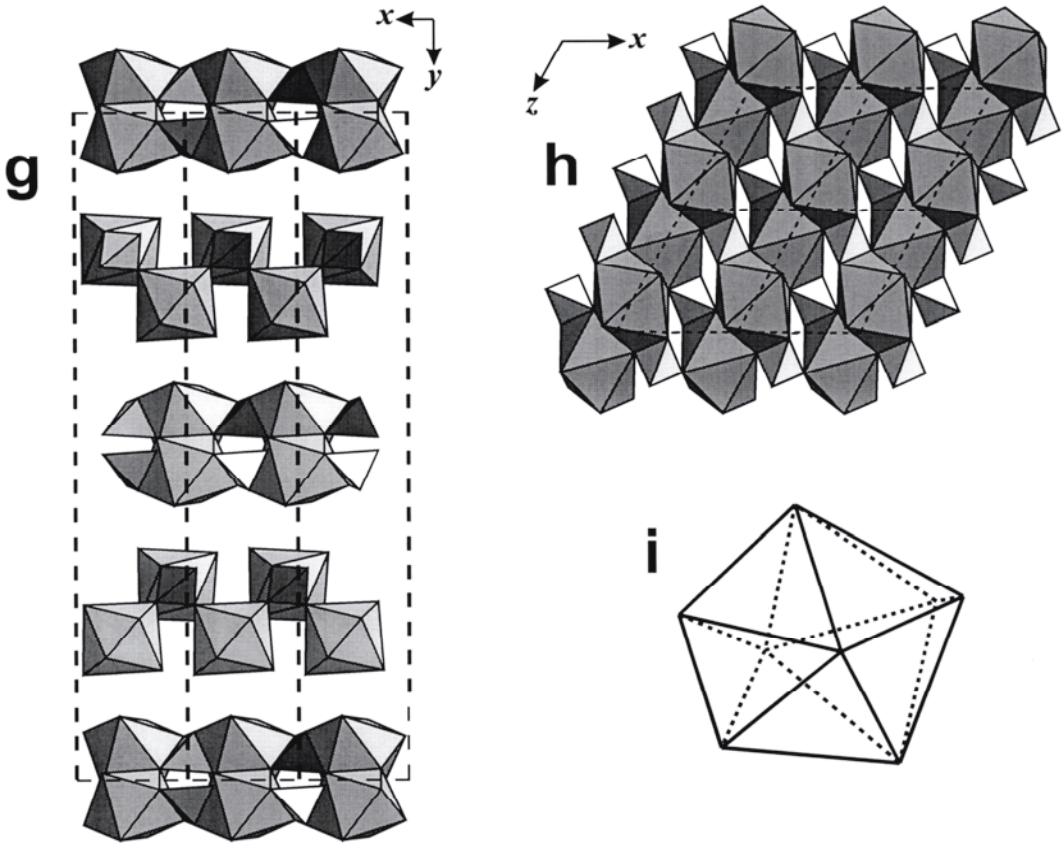

Figure 37, con't. (g) The structure of ardealite viewed along [001]; (h) the layer of chains of edge-sharing polyhedra in gypsum; (i) the ($CaØ_8$) coordination polyhedra in gypsum and ardealite.

process reverses the cant of (CaO_8) dodecahedra in adjacent chains, resulting in triangles of O atoms at the twin plane. Occupancy of these triangles by C atoms produces the (CO_3) group and the structural unit in rapidcreekite. Detailed work by Hochella et al. (1983) showed that the naturally occurring hydroxy-hydrated Mg sulfate from active hydrothermal vents on the East Pacific Rise has the general chemical composition $MgSO_4 \cdot \{Mg(OH)_2\}_x \cdot (H_2O)_{1-2x}$ where $0 \le x \le 0.5$. Thus the 'end-member' compositions are $MgSO_4(H_2O)$ and $Mg_3(SO_4)_2(OH)_2$. Keefer et al. (1981) solved the crystal structure of $Mg_4(SO_4)_3(OH)_2(H_2O)$ ($x = 0.33$), showing that it is tetragonal, $I4_1/amd$, $a = 5.242$, $c = 12.995$ Å. Haymon and Kastner (1986) described the material as caminite, focusing specifically on the composition $Mg_7(SO_4)_5(OH)_4(H_2O)_2$ ($x = 0.4$), tetragonal, $I4_1/amd$, $a = 5.239$, $c = 12.988$ Å. Presuming that one end of the 'series', $Mg(SO_4)(H_2O)$, corresponds to kieserite, the composition with $x = 0.5$ should correspond to the end-member composition for caminite: $Mg_3(SO_4)_2(OH)_2$. Fleet and Knipe (1997) have described a synthetic material similar in stoichiometry to caminite, but with a different structure.

In the structure of **bassanite**, $CaSO_4(H_2O)_{0.5}$, the ($CaØ_9$) polyhedron has nine vertices and can be described as a triaugmented trigonal prism (Fig. 38f). However, the dominant motif of the structure is a chain of alternating edge-sharing ($CaØ_8$) and (SO_4) polyhedra (Fig. 38d). These chains extend along [001] and are connected to form a framework (Fig. 38c,e). The repeat unit of the chain consists of one ($CaØ_9$) and one (SO_4) polyhedra; the period of the chain is 6.345 Å, similar to the chain-repeat distances in gypsum, anhydrite, and ardealite.

In the structure of **syngenite**, $K_2Ca(SO_4)_2(H_2O)$, bassanite-like chains are linked into sheets parallel to [100] (Fig. 38g). The sheets are linked by K in the interlayer (Fig. 38i,j).

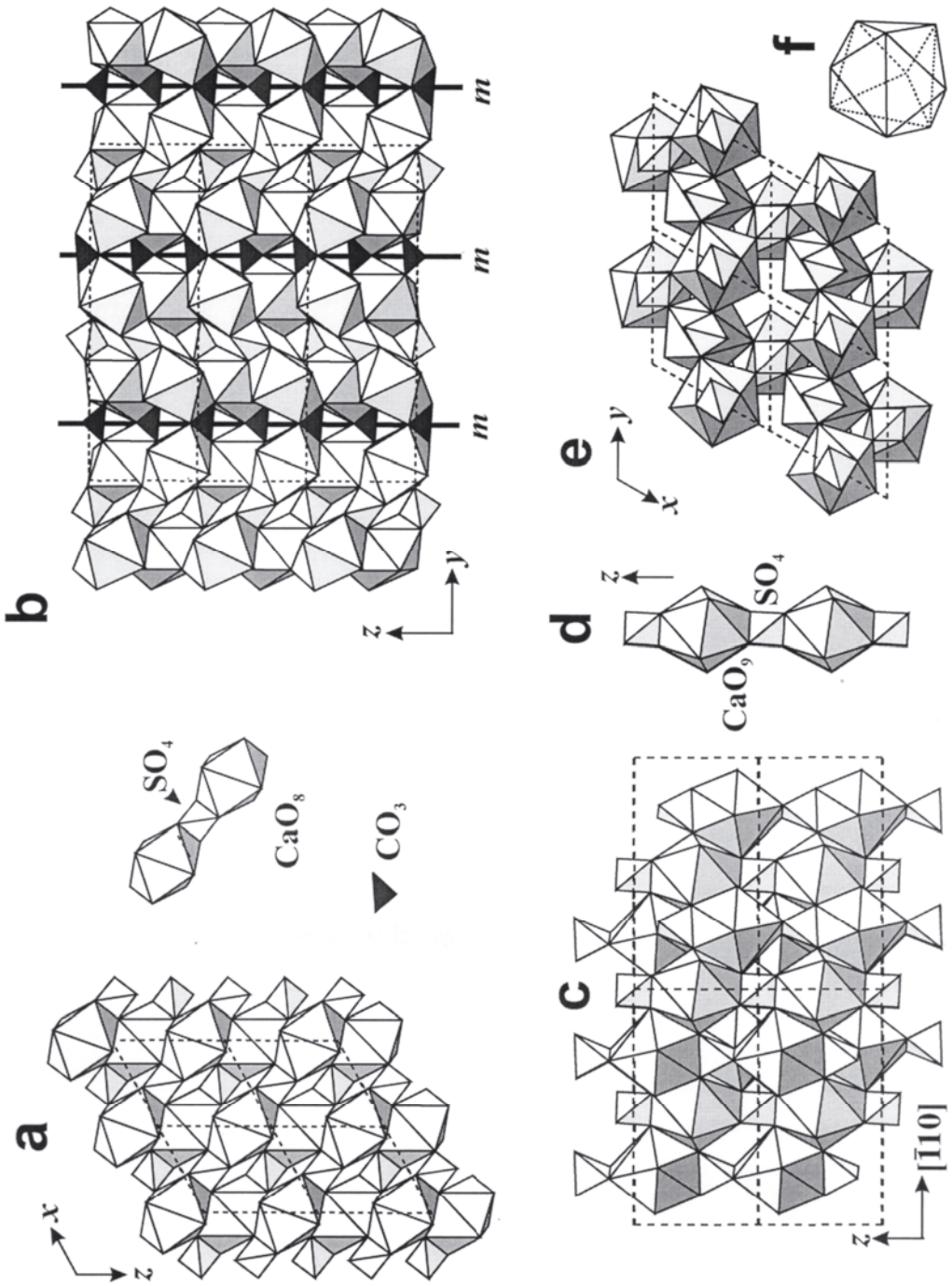

Figure 38. (a) The layer of ($CaØ_8$) polyhedra and (SO_4) tetrahedra in gypsum; (b) the layer of ($CaØ_8$) polyhedra, (SO_4) tetrahedra and (CO_3) triangles in rapidcreekite; the layer in rapidcreekite can be produced from that of gypsum by twinning along the mirror plane; (c) the structure of bassanite viewed along [110]; (d) the chain of edge-sharing ($CaØ_9$) polyhedra and (SO_4) tetrahedra in bassanite; (e) the structure of bassanite viewed along [001]; (f) the ($CaØ_9$) coordination polyhedron in bassanite.

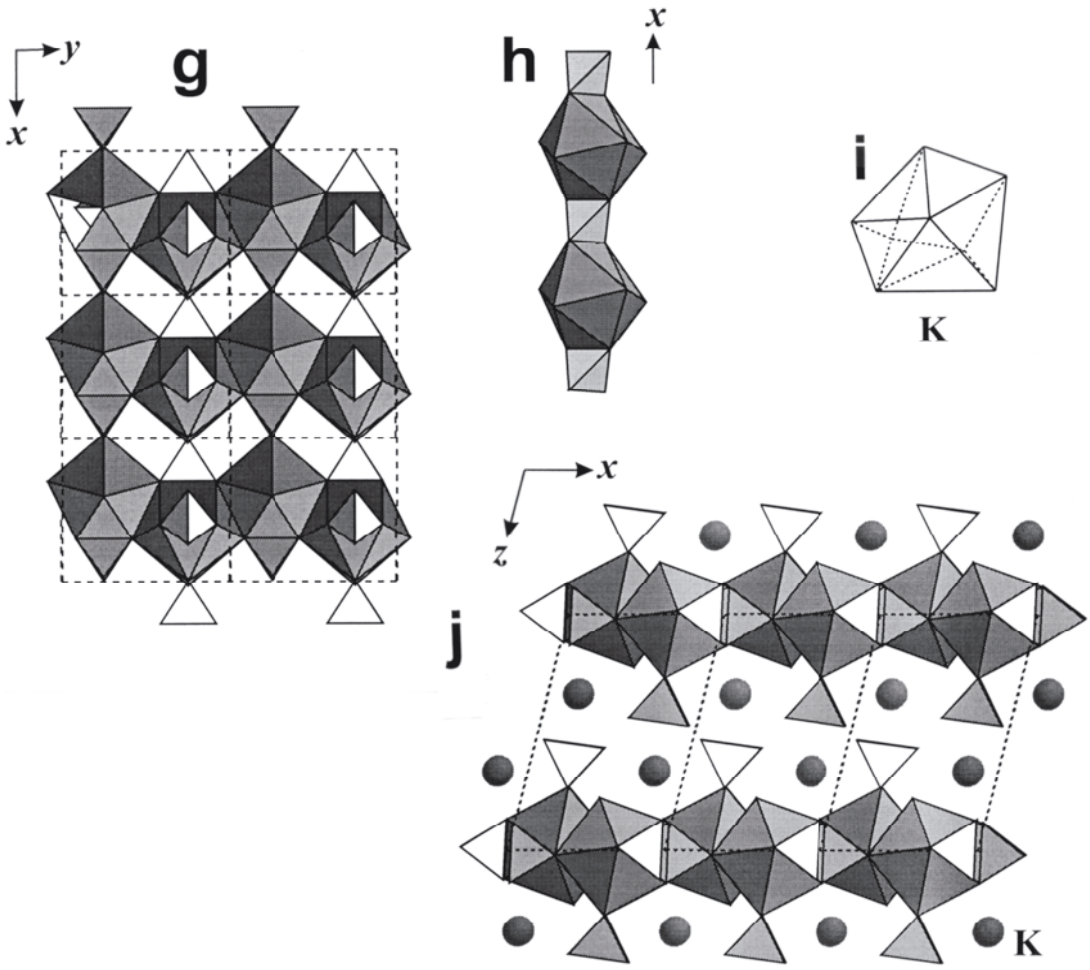

Figure 38, cont'd. (g) the structure of syngenite viewed along [001]; (h) the chain of edge-sharing ($CaØ_9$) polyhedra and (SO_4) tetrahedra in syngenite; (i) the $(KØ)_8$ coordination polyhedron in syngenite; (j) the arrangement of layers of ($CaØ_9$) polyhedra and (SO_4) tetrahedra with interstitial K in syngenite.

The repeat distance of the chains of edge-sharing polyhedra (Fig. 38h) is 6.225 Å, very close to the repeat distances of similar chains in other Ca-sulfate structures.

The structure of **görgeyite**, $K_2Ca_5(SO_4)_6(H_2O)$, is an interesting example of combinatorics of structural subunits in this class of sulfate minerals. The structure consists of slabs parallel to (010) and extending along [001] (Fig. 39a). These slabs can be built from finite bassanite-like chains consisting of five (CaO_9) polyhedra and six (SO_4) tetrahedra. These finite chains are linked by edge-sharing of (CaO_9) polyhedra to form slabs. The slabs are linked into a framework (Fig. 39b) by additional edge-sharing of coordination polyhedra (Fig. 39c). Interstitial K cations are located in channels through the framework.

The degree of condensation of edge-sharing chains in anhydrite, gypsum, ardealite, rapidcreekite, bassanite, syngenite, and görgeyite is related to the number of (H_2O) groups per Ca atom, as well as to the presence of additional alkali-metal cations. Where there are zero or 0.5 (H_2O) groups per Ca atom (anhydrite and bassanite), the chains are linked into three-dimensional frameworks. Where there are two (H_2O) groups per Ca atom (gypsum and ardealite), the result is sheet structures. With the addition of K cations, the chains condense into sheets (syngenite) or frameworks (görgeyite).

The crystal structure of **orschallite**, $Ca_3(SO_3)_2(SO_4)(H_2O)_{12}$, a rare Ca-sulfite-

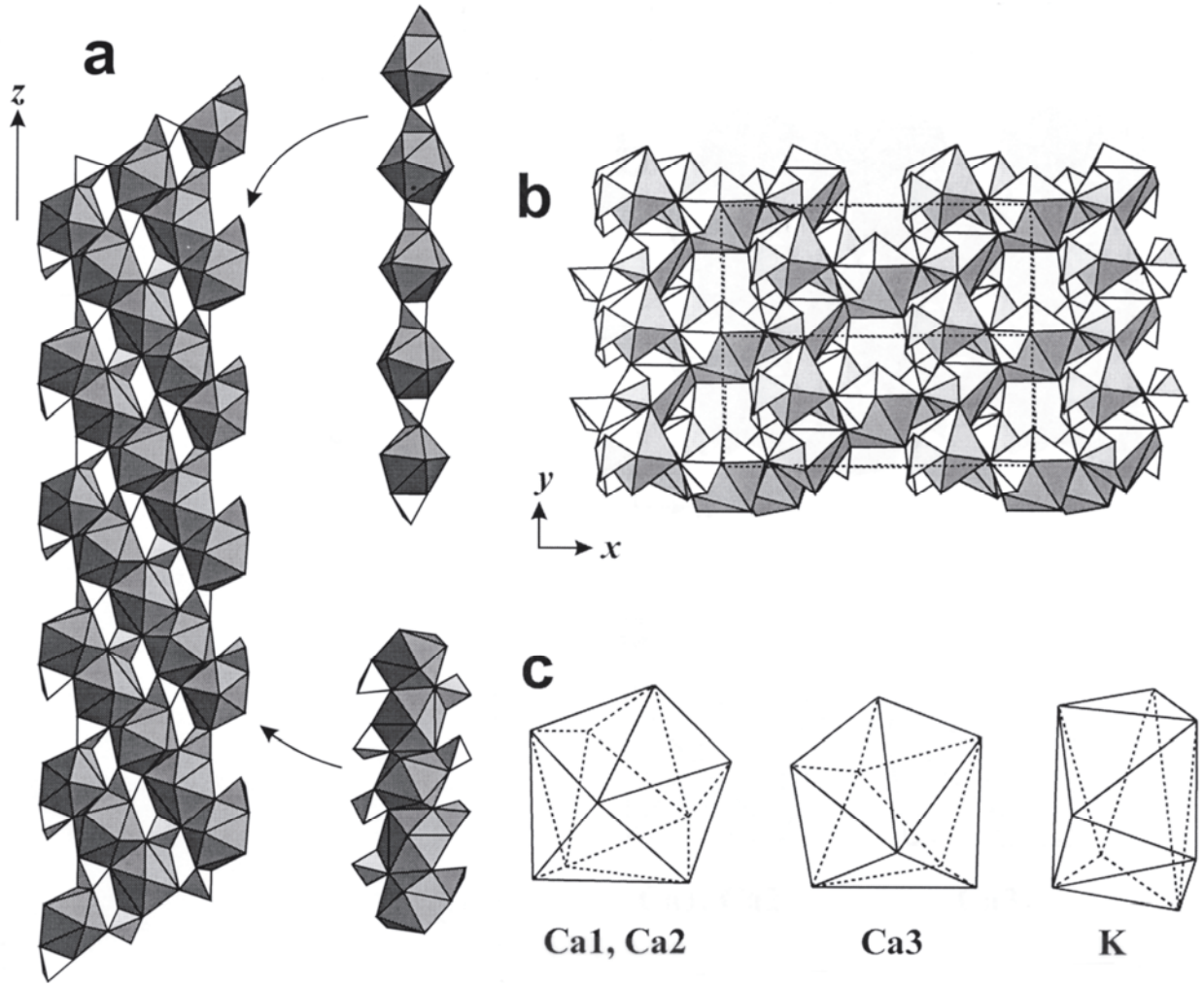

Figure 39. (a) The slab of (CaO_9) polyhedra and (SO_4) tetrahedra in görgeyite; (b) the arrangement of slabs into a framework in görgeyite; (c) coordination polyhedra of Ca and K in görgeyite.

sulfate-hydrate mineral, is based on finite $[Ca_3(SO_3)_2(H_2O)_{12}]^{2+}$ clusters consisting of three ($CaØ_8$) polyhedra and two (SO_3) groups (Fig. 39d). These clusters are arranged into sheets parallel to (001) (Fig. 39f,g) and are linked *via* hydrogen bonds to (SO_4) groups. The (SO_4) tetrahedra are held in the structure solely by hydrogen bonds and are disordered, showing two possible orientations (Fig. 39e).

The structure of **glauberite**, $CaNa_2(SO_4)_2$, is based on chains of edge-sharing (CaO_8) polyhedra decorated by edge- and corner-sharing (SO_4) tetrahedra (Fig. 40a). The chains are linked into a framework in which the channels are filled by interstitial Na cations (Fig. 40b).

The structure of **ternesite**, $Ca_5(SiO_4)_2(SO_4)$, consists of rods of edge-sharing (CaO_7) polyhedra augmented trigonal prisms, decorated by (SiO_4) and (SO_4) tetrahedra and extending along [100] (Fig. 40d). The arrangements of these rods is shown in Figure 40f. The rods are linked by additional ($CaØ_n$) polyhedra into a complex framework (Fig. 40g).

Alkali-metal- and NH_4-sulfate minerals

Glaserite-related structures. The glaserite structure-type can be selected as a parent structure-type for many sulfates, chromates, phosphates, and silicates (Table 14)

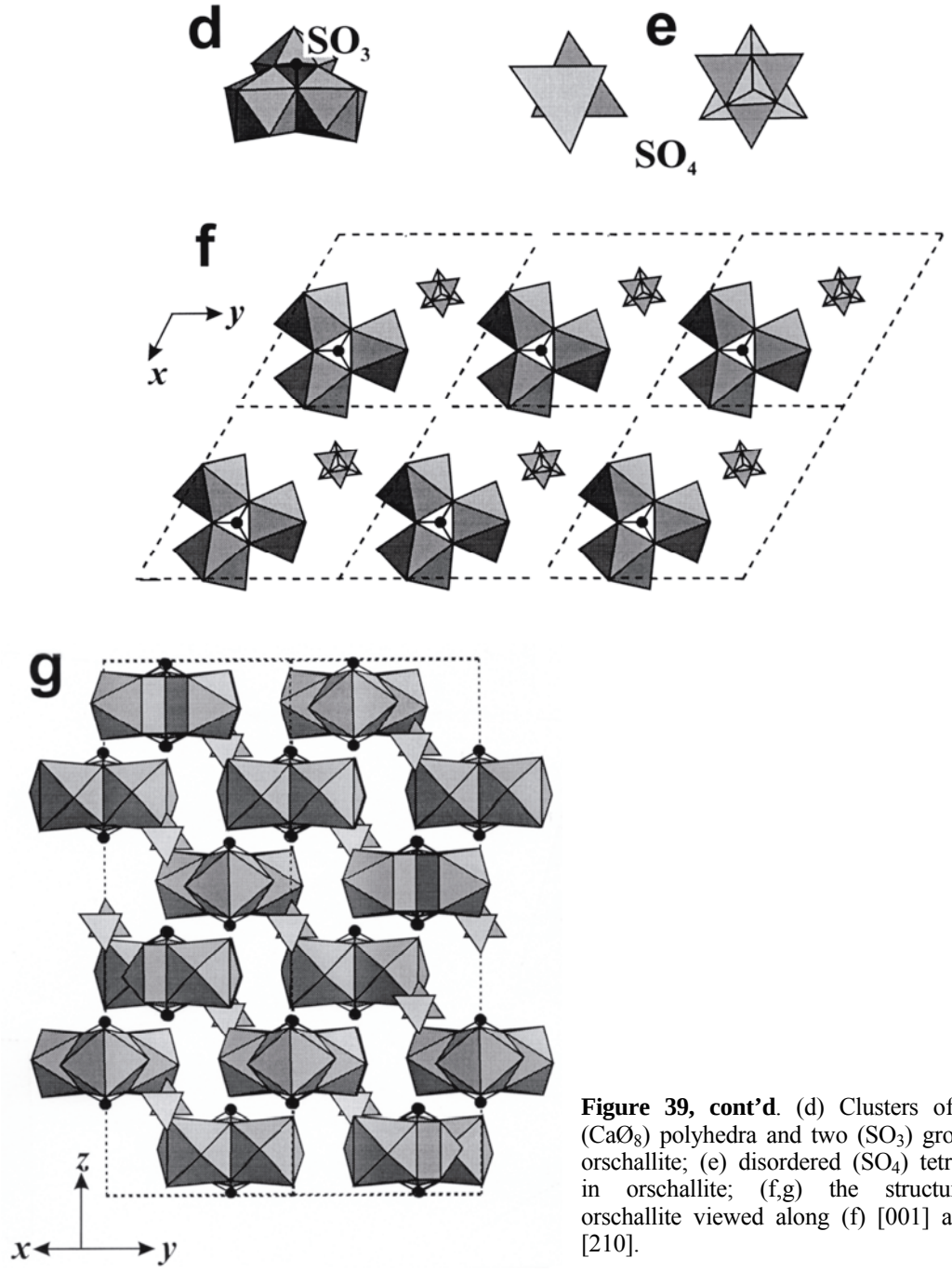

Figure 39, cont'd. (d) Clusters of three ($CaØ_8$) polyhedra and two (SO_3) groups in orschallite; (e) disordered (SO_4) tetrahedra in orschallite; (f,g) the structure of orschallite viewed along (f) [001] and (g) [210].

(Eysel 1973; Moore 1973, 1976, 1981). According to Moore (1973), the dominant structural subunit (= fundamental building block) of **glaserite**, $K_3Na(SO_4)_2$, is a pinwheel consisting of an (NaO_6) trigonal antiprism (= octahedron) that shares its six corners with (SO_4) tetrahedra (Fig. 41a). The pinwheels are linked through (SO_4) tetrahedra into layers perpendicular to [001] (Fig. 41b). The K atoms are located between the layers, and have two distinct coordinations. Both of these polyhedra are derivatives of the cuboctahedron shown in Figure 41g. The relatively large ionic radius of K allows it to form mixed cation-anion closest (or almost closest) packings with O^{2-} anions. The coordination polyhedron about K(1) in glaserite can be derived from the cuboctahedron by rotation of opposing triangular faces by 30°. Figure 41h shows the resulting polyhedron, a distorted icosahedron with ideal point symmetry $m\bar{3}5$. The $K(1)O_{12}$ icosahedra form sheets

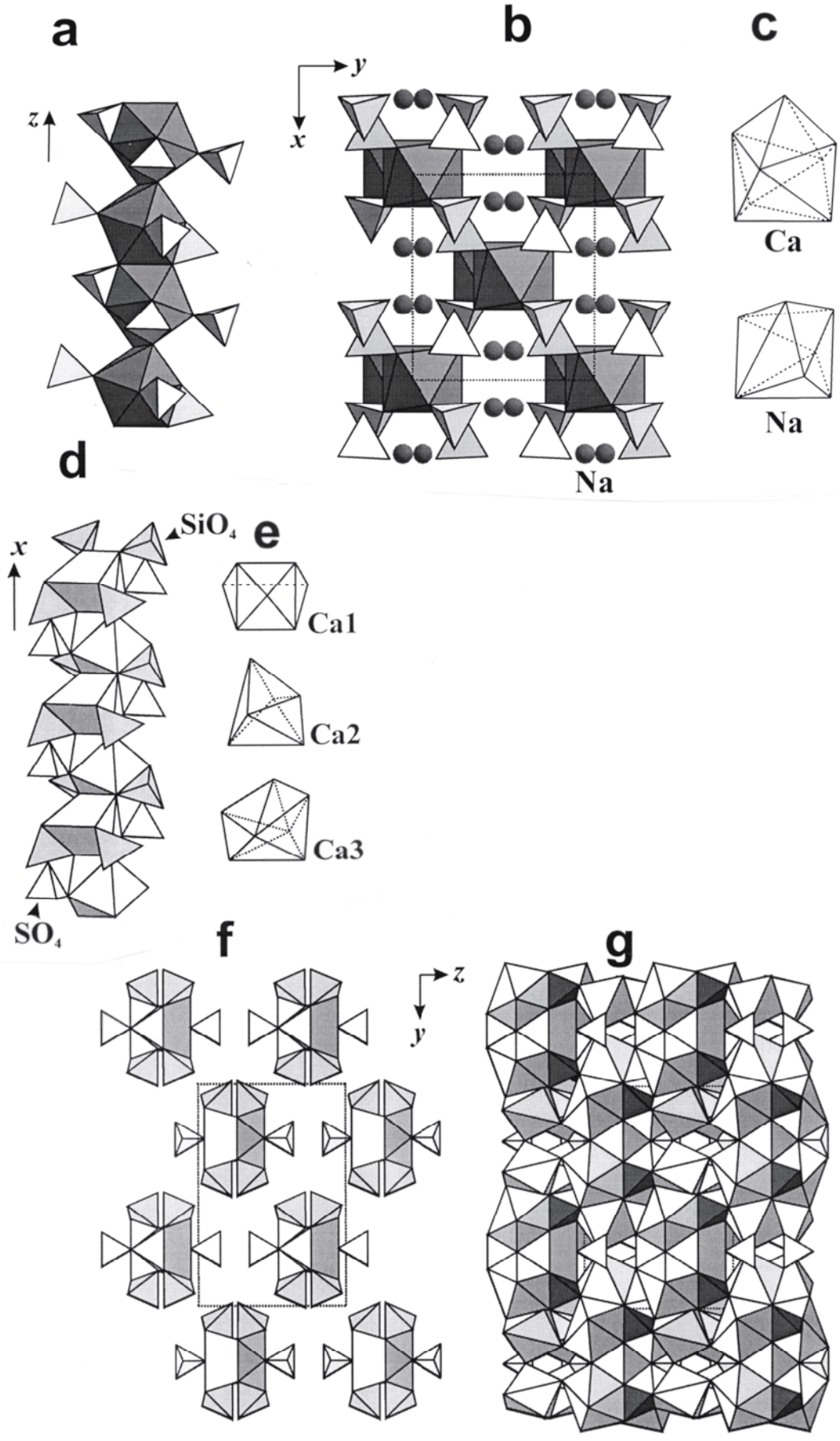
a
b
c
y
x
z
Ca
Na
Na
d
e
SiO4
x
Ca1
Ca2
Ca3
SO4
f
g
z
y

←← Figure 40 (opposite page). (a) The chain of edge-sharing ($CaØ_8$) polyhedra decorated by (SO_4) groups in glauberite; (b) linking of chains into a framework in glauberite, viewed along [001]; (c) coordination polyhedra of Ca and Na in glauberite; (d) the chain of edge-sharing {$Ca(1)O_7$} polyhedra decorated by (SO_4) and (SiO_4) tetrahedra in ternesite; (e) coordination polyhedra of Ca in ternesite; (f) the arrangement of chains of {$Ca(1)O_7$} polyhedra and tetrahedra in ternesite; (g) the structure of ternesite viewed along [100].

Table 14. Alkali-metal- and NH_4-sulfate mineral structures.

Name	Formula	*a* (Å)	*b* (Å)	*c* (Å)	β (°)	S. G.	Fig.	Ref.
glaserite	$K_3Na(SO_4)_2$	5.680	*a*	7.309	–	$P\bar{3}m$	41	[1]
arcanite	β-$K_2(SO_4)$	7.476	10.071	5.763	–	*Pnam*	41	[2]
mascagnite	$(NH_4)_2(SO_4)$	7.747	10.593	5.977	–	*Pnam*	41j,k	[3]
palmierite[1]	$K_2Pb(SO_4)_2$	7.560	*a*	–	–	$R\bar{3}m$	41c,d	[4]
kalistrontite	$K_2Sr(SO_4)_2$	*a*	*a*	–	–	$R\bar{3}m$	–	(5)
lecontite	$Na(NH_4)(SO_4)(H_2O)_2$	8.216	12.854	6.232	–	$P2_12_12_1$	42a	[6]
matteuccite	$Na(HSO_4)(H_2O)$	7.811	7.823	8.025	117.5	*Cc*	42b	[7]
mirabilite	$Na_2(SO_4)(H_2O)_{10}$	11.512	10.370	12.847	107.8	$P2_1/c$	42c,d	[8]
darapskite	$Na_3(NO_3)(SO_4)(H_2O)$	10.564	6.911	5.194	102.8	$P2_1/m$	42e-g	[9]
thenardite	Na_2SO_4	9.829	12.302	5.868	–	*Fddd*	43a-c	[10]
hanksite	$KNa_{22}[Cl(CO_3)_2(SO_4)_9]$	10.490	*a*	21.240	–	$P6_3/m$	43d-f	[11]
burkeite	$Na_4(SO_4)_{1.39}(CO_3)_{0.61}$	5.170	9.217	7.058	–	*Pmnm*	43g,h	[12]
mineevite-(Y)	$Na_{25}Ba(REE)_2(CO_3)_{11}(HCO_3)_4(SO_4)_2F_2Cl$	8.811	*a*	37.030	–	$P6_3/m$	44	[13]
mercallite	$K(HSO_4)$	8.429	9.807	18.976	–	*Pbca*	45a-d	[14]
letovicite	$(NH_4)_3H(SO_4)_2$	15.435	5.865	10.170	101.8	*C2/c*	45e,f	[15]

[1] rhombohedral; α = 42.5°

References: [1] Okada and Ossaka (1980), [2] McGinnety (1972), [3] Hasebe (1981), [4] Bachmann (1953), (5) Gaines et al. (1997), [6] Corazza et al. (1967), [7] Catti et al. (1975), [8] Levy and Lisensky (1978), [9] Sabelli (1967), [10] Hawthorne and Ferguson (1975b), [11] Kato and Saalfeld (1972), [12] Giuseppetti et al. (1988), [13] Yamnova et al. (1992), [14] Payan and Haser (1976), [15] Leclaire et al. (1985)

perpendicular to the *c* direction[1]. The $K(2)O_{10}$ polyhedron (Fig. 41i) can be obtained from the cuboctahedron by collapsing one of the opposing triangular faces into one vertex.

Moore (1973, 1976, 1981), Eysel (1973), and Egorov-Tismenko et al. (1984) reviewed the crystal chemistry of the glaserite-related structures in detail. Moore (1973) noted that the key to understanding the relation of glaserite to other structures is the disposition of the tetrahedra about the octahedron in the pinwheel. He suggested a procedure to derive all possible pinwheels from the thirteen combinatorially distinct *bracelets*, in this case, projections of octahedra with "**u**"or "**d**" symbols attached to their

[1] Moore (1976, 1981) pointed out that, due to the icosahedral geometry, the glaserite structure-type represents a super-dense-packed oxide. He noted that the glaserite-related minerals and compounds are 5 to 15% more dense that their cubic or hexagonal close-packed counterparts. The only examples he gave are $Ca_2(SiO_4)$ polymorphs. However, in the structure of 'hexagonal close-packed' (hcp) γ-$Ca_2(SiO_4)$ ('calcio-olivine'), the Ca atoms are in octahedral coordination (= fill octahedral voids in hcp), which indicates that they expand oxygen hcp packing, and therefore the structure is not ideally close-packed. In contrast, in α- and β-$Ca_2(SiO_4)$ ('silico-glaserite' and larnite, respectively), Ca participates in mixed cation–anion close packings.

vertices. The **u** and **d** designate tetrahedra pointing either up or down, respectively. Each bracelet can be symbolized as a $(\mathbf{u} + \mathbf{d})_r$ combination, where *r* is a symbol used to identify topologically distinct bracelets. The bracelet for the glaserite structure, shown in Figure 41a, corresponds to the (3 + 3)*c*′ type of Moore (1973). In contrast, the structure of **palmierite**, $K_2Pb(SO_4)_2$, is based on the bracelet (3 + 3)*c*, which is the *complement* of the glaserite bracelet (Fig. 41c) (two bracelets are complementary if the symbols **u** and **d** are interchanged). Whereas in glaserite all pinwheel-layers are located under one another, the pinwheel-layers in palmierite form a more complex three-layer packing (Fig. 41d).

According to Moore (1973), the structure of **arcanite**, β-$K_2(SO_4)$, is based on a (4 + 2)*a* pinwheel. However, Egorov-Tismenko et al. (1984) proposed a different description. Figure 41j shows the $\{K(2)O_{10}\}$ polyhedron in glaserite, decorated by edge- and corner-sharing (SO_4) tetrahedra to form a $[K(SO_4)_5]$ cluster (Fig. 41l,m). In contrast, Figures 41n,o show a similar cluster formed about the K(1) site (Fig. 41k) in arcanite. The difference between the two configurations is the orientation of one (SO_4) tetrahedron that shares an equatorial edge of the K polyhedron. The $[K(SO_4)_5]$ clusters in glaserite form a continuous layer perpendicular to the *c* direction, whereas in arcanite, the clusters initially form chains (Fig. 41q), then double chains (Fig. 41r) and, finally, a framework (Figs. 41s,t); the K(2) atoms occur in the interstices of this framework.

The description of the crystal structure of arcanite as an 'anion-stuffed' alloy has been suggested by Smirnova et al. (1967, 1968), O'Keeffe and Hyde (1985), and Hyde and Andersson (1989). They considered several sulfate-mineral structures (e.g. arcanite, barite, langbeinite) as derivatives of simple structure types, such as alloys, simple borides, and simple sulfides. For example, they noted that the arrangement of K and S cations in arcanite is similar to that of the atoms in the alloys Ca_2Sn and Ca_2Si with O atoms in the interstices. It is interesting that the high-pressure modification of K_2S is of the same arrangement, and thus arcanite can be considered as an anion-stuffed high-pressure K_2S polymorph (O'Keeffe and Hyde 1985).

Na- and NH_4-sulfates. Due to its relatively small size, Na can fill octahedral interstices in close-packed oxygen arrays, and the ($NaØ_6$) octahedron is the most common Na coordination polyhedron in mineral structures. The crystallographic parameters for sulfate minerals in which Na plays a dominant role are given in Table 14. The structures of these minerals can be described as based on structural units consisting of condensed ($NaØ_6$) octahedra.

The structure of **lecontite**, $Na(NH_4)(SO_4)(H_2O)_2$, is based on infinite chains of face-sharing ($NaØ_6$) octahedra decorated by (SO_4) tetrahedra that share corners with the ($NaØ_6$) octahedra (Fig. 42a). The chains are linked *via* NH_4 groups. The structure of **matteuccite**, $Na(HSO_4)(H_2O)$, consists of corner-sharing ($NaØ_6$) octahedra that are linked into a framework *via* (SO_4) tetrahedra (Fig. 42b). In **mirabilite**, $Na_2(SO_4)(H_2O)_{10}$, edge-sharing of $\{Na(H_2O)_6\}$ octahedra form infinite zigzag chains extending along [001] (Fig. 42c). Together with (SO_4) tetrahedra and additional (H_2O) groups, these chains form layers parallel to (100) (Fig. 42d). The structure of **darapskite**, $Na_3(NO_3)(SO_4)(H_2O)$, is based on chains of octahedra in which face- and edge-sharing alternates (Fig. 42e). These chains are linked *via* (SO_4) tetrahedra and other Na atoms into layers (Fig. 42f) that are linked into a three-dimensional structure by hydrogen bonds through (NH_4) and (H_2O) groups (Fig. 42g).

The structure of **thenardite**, $Na_2(SO_4)$, consists of a framework of (NaO_6) octahedra. Two (NaO_6) octahedra share an edge, forming $[Na_2O_{10}]$ dimers. The dimers are linked *via* edge-sharing with (SO_4) tetrahedra to form chains extended in the $[0\bar{1}2]$ direction. The chains are joined *via* corner-sharing of polyhedra to form sheets parallel to (100)

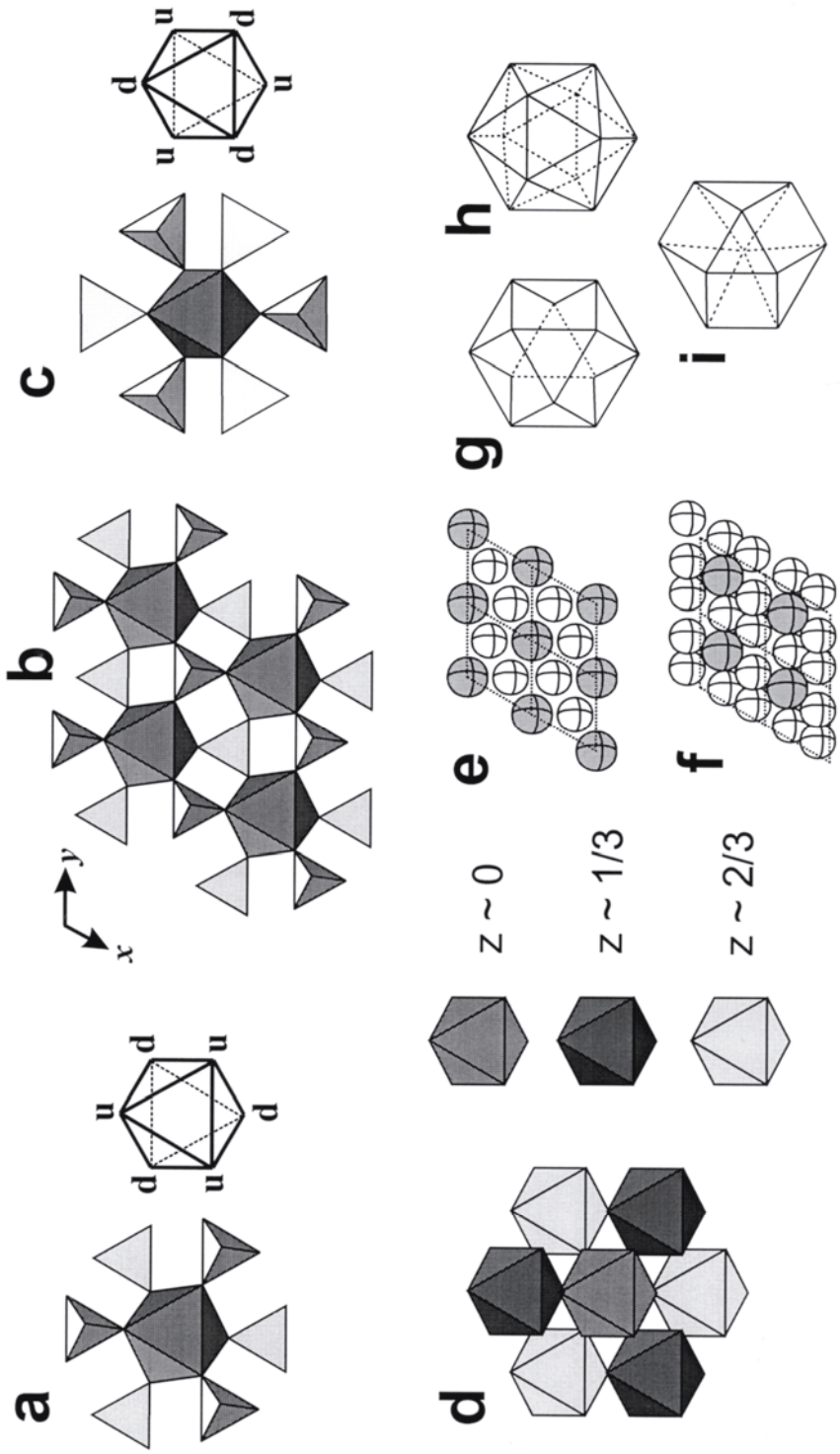

Figure 41. (a) The pinwheel in the structure of glaserite and its bracelet; (b) the pinwheel linked into layers in glaserite; (c) the pinwheel and its bracelet in palmierite; (d) the arrangement of pinwheel layers in palmierite; (e) the close-packed sheet involving the K(1) cation in glaserite; (f) the close-packed sheet involving the K(2) cation in glaserite; (g) ideal coordination polyhedron for a sphere in cubic closest packing; (h,i) coordination polyhedra of (h) K(1) and (i) K(2) in glaserite as derivatives of (g).

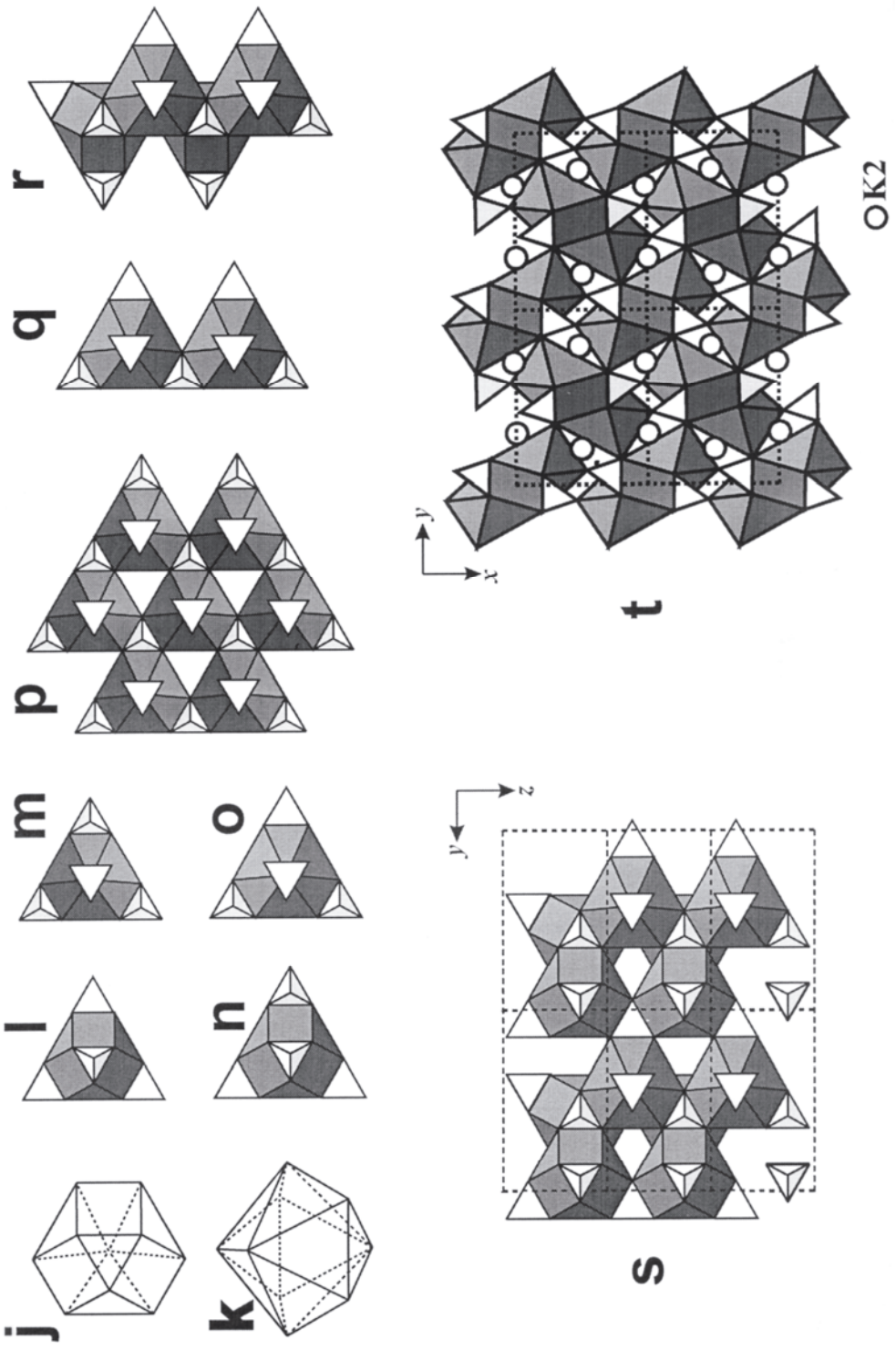

Figure 41, cont'd. (j,k) the coordination polyhedra of (j) K(1) and (k) K(2) in arcanite; (l,m) the $[K(2)(SO_4)_5]$ cluster in glaserite, viewed from (l) top and (m) bottom; (n,o) the $[K(1)(SO_4)_5]$ cluster in arcanite, viewed from (n) top and (o) bottom; (p) linking of $[K(SO_4)_5]$ clusters into a layer in glaserite; (q,r) linking of $[K(SO_4)_5]$ clusters in arcanite into (q) chains and (r) double chains; (s) the framework of double chains of $[K(SO_4)_5]$ clusters in arcanite; (t) the structure of arcanite viewed along [001]; K(2) atoms are shown as circles.

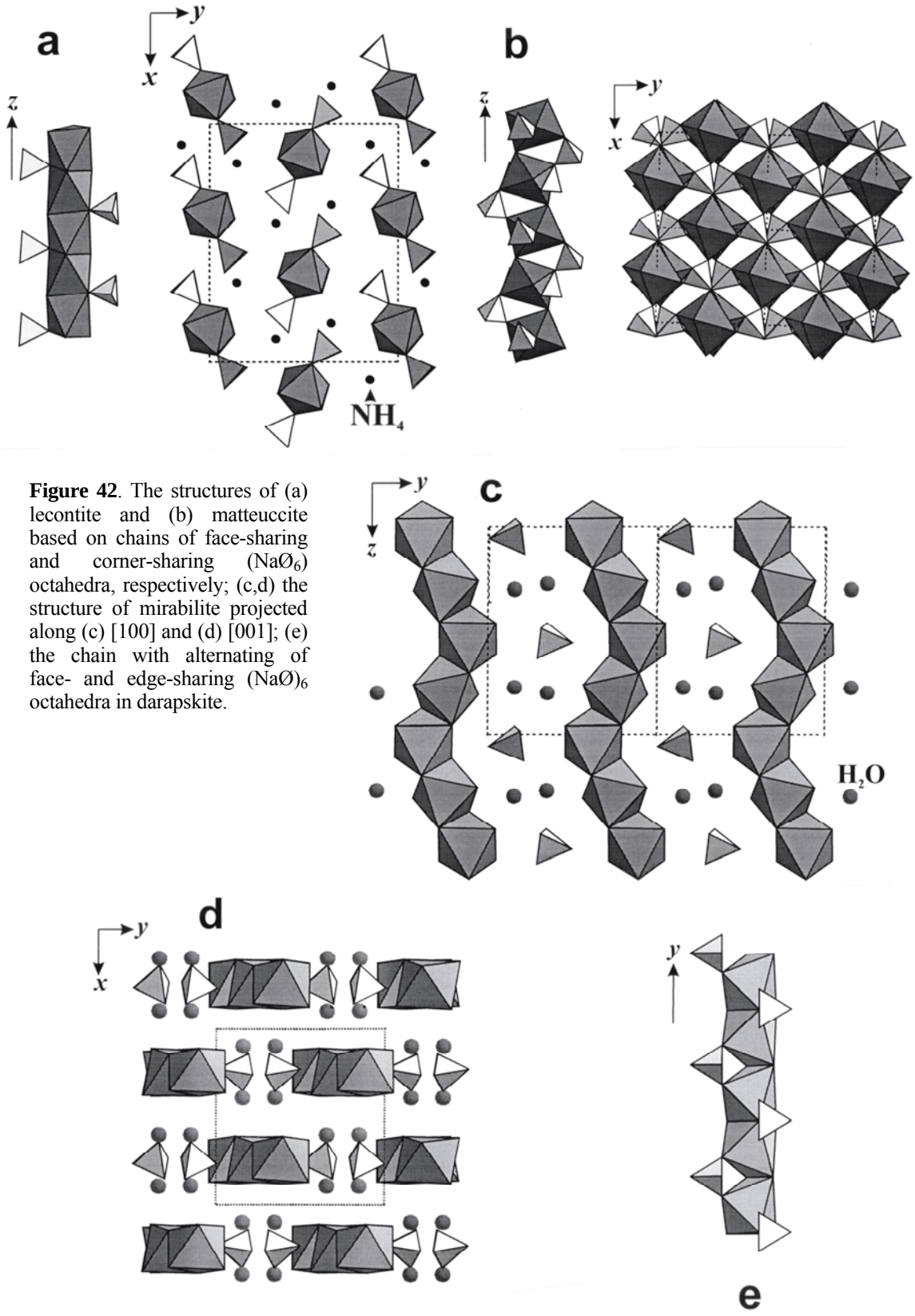

Figure 42. The structures of (a) lecontite and (b) matteuccite based on chains of face-sharing and corner-sharing ($NaØ_6$) octahedra, respectively; (c,d) the structure of mirabilite projected along (c) [100] and (d) [001]; (e) the chain with alternating of face- and edge-sharing $(NaØ)_6$ octahedra in darapskite.

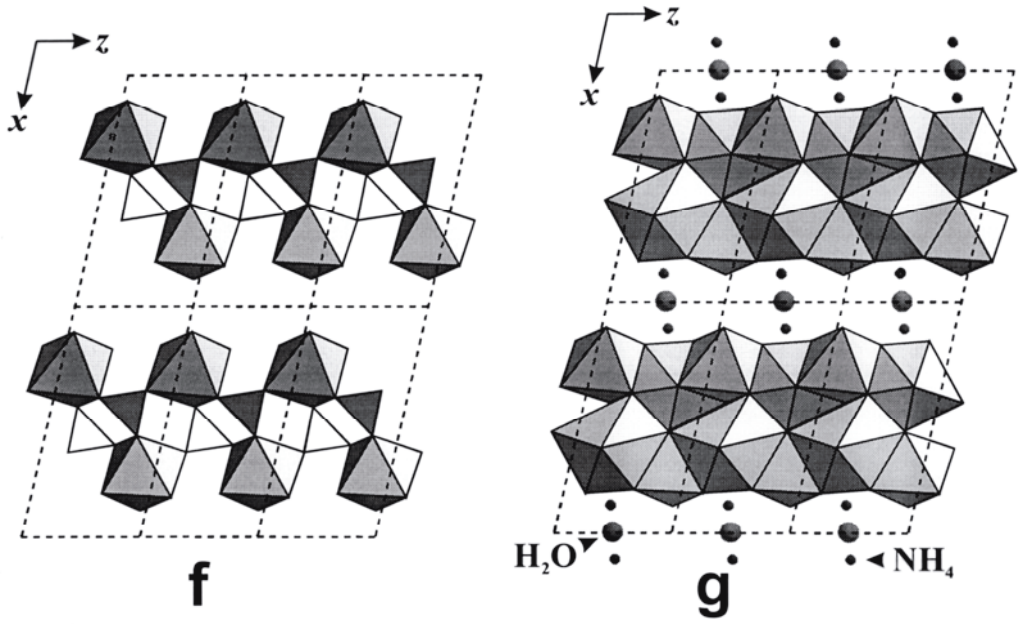

Figure 42, cont'd. (f) The arrangement of chains in darapskite to form a framework; (g) the structure of darapskite viewed along [010].

(Fig. 43a). The further linkage of the sheets into a framework results in formation of chains of edge-sharing (NaO_6) octahedra (Fig. 41c) along [100] (Fig. 43b).

The crystal structure of **hanksite**, $KNa_{22}(Cl(CO_3)_2(SO_4)_9)$, can be described as rods of face-sharing Na- and K-polyhedra-sulfate pinwheels (Fig. 43d). The orientation of the rods and their stacking are shown in Figure 43e. The remaining cation polyhedra link the rods together (Fig. 43f). The structure of **burkeite**, $Na_4(SO_4)_{1.39}(CO_3)_{0.61}$, is highly disordered, with (SO_4) tetrahedra replaced by (CO_3) triangles and vice-versa. The structure consists of complex chains of (NaO_n) polyhedra (with $n \approx 6$) (Fig. 43g) that are linked into walls parallel to (010) (Fig. 43h). The crystal structure of **mineevite-(Y)**, $Na_{25}Ba(REE)_2(CO_3)_{11}(HCO_3)_4(SO_4)_2F_2Cl$, is very complex. It consists of rods of face-sharing cation polyhedra [(NaO_6) trigonal prisms, ($REE)O_9$ polyhedra, and (BaO_{12}) icosahedra] girdled by (CO_3) triangles (Fig. 44a). The arrangement of the rods is shown in Figure 44b. Yamnova et al. (1992) described the structure as based on sheets of cation polyhedra. The sheets are of three types (*A*, *B*, and *C*; Figs. 44c,d,e, respectively). The sequence of the sheets is …*ABBACABBAC*… or (*ABBAC*) (Fig. 44f).

The structure of **mercallite**, $K(HSO_4)$, consists of (SO_4) tetrahedra linked *via* hydrogen bonds into two different substructures. The first substructure is the chain of $(HSO_4)^-$ groups that are linked *via* O···H bonds of 1.6–1.8 Å into infinite $[H(HSO_4)]^0$ chains parallel to [100] (Fig. 45a). The second substructure is composed of the finite $[H_2(SO_4)_2]^{2-}$ cluster that consists of two $(HSO_4)^-$ groups linked *via* additional O···H bonds (Fig. 45b). The hydrogen-bonded (SO_4) groups form sheets that are parallel to (001) (Fig. 45c), and these sheets are linked by K atoms, the coordinations of which are shown in Figure 45d. The structure of **letovicite**, $(NH_4)_3H(SO_4)_2$, is based on $[H(SO_4)_2]^{3-}$ groups

Figure 43. (a) The layer of edge-sharing ($NaØ_6$) octahedra and (SO_4) tetrahedra in thenardite; (b) the structure of thenardite viewed along [010]; (c) the coordination polyhedron of Na in thenardite; (d) the rod of face-sharing pinwheels in hanksite; (e) the arrangement of rods in hanksite viewed along [001]; (f) the structure of hanksite viewed along [001]; (g) the complex [$NaØ_n$] polyhedral chain decorated by (SO_4) tetrahedra and (CO_3) triangles in burkeite; (h) the structure of burkeite viewed along [100]. **Next page → →**

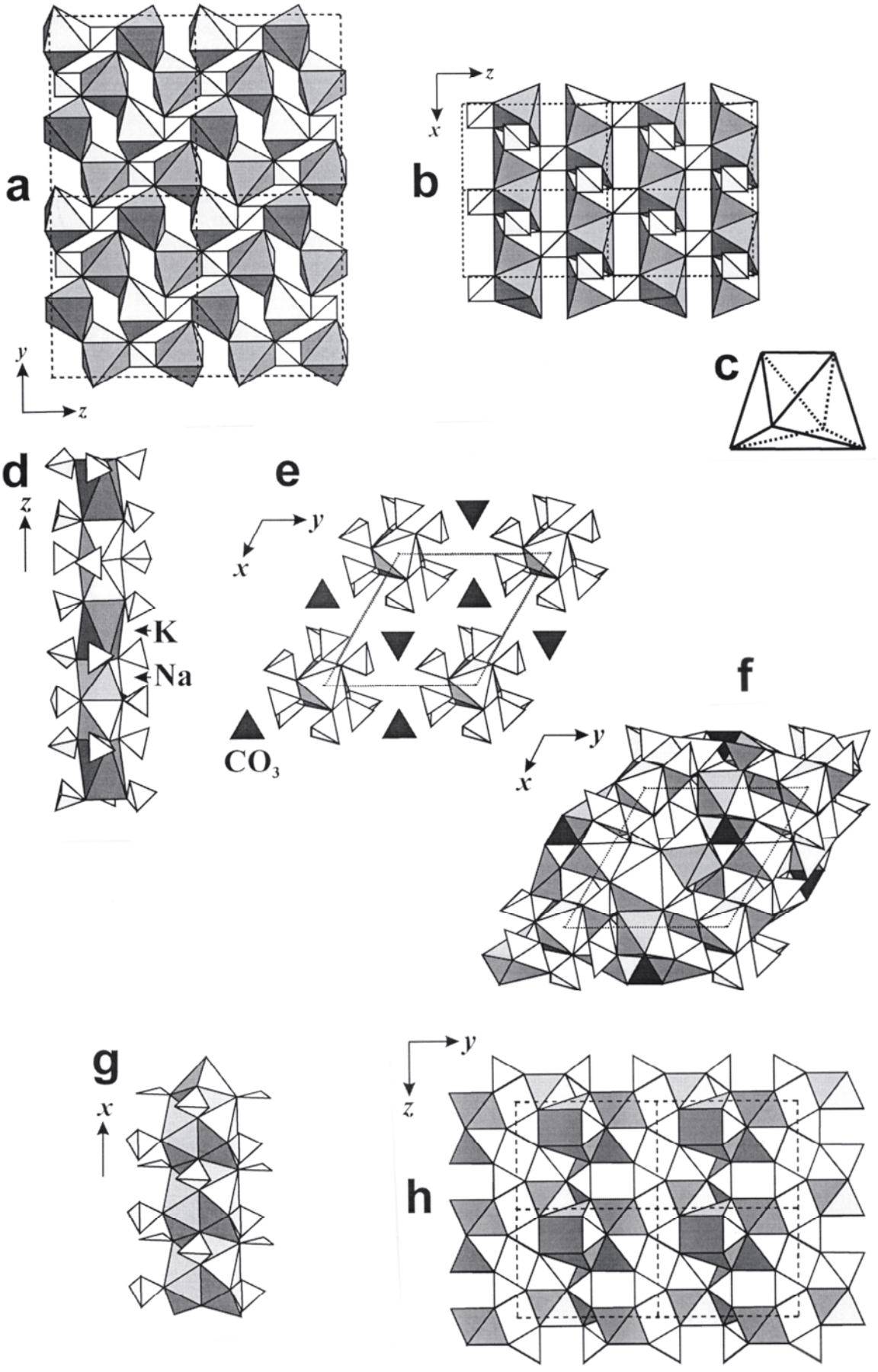
a
y
z
b
z
x
c
d
z
K
Na
e
y
x
CO_3
f
y
x
g
x
h
y
z

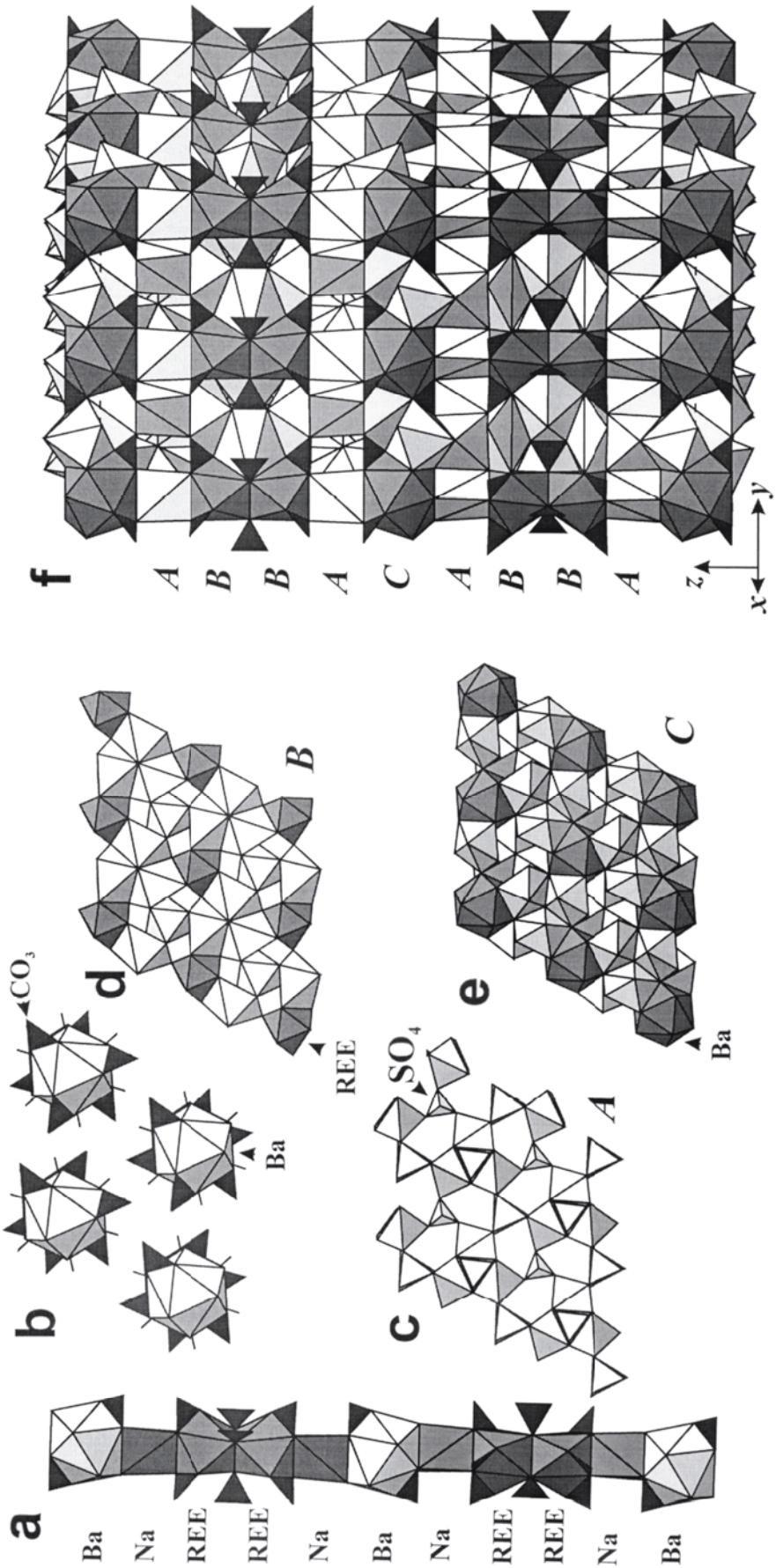

Figure 44. (a) The rod of face-sharing cation polyhedra decorated by (CO_3) triangles in mineevite-(Y); (b) the arrangement of rods viewed down [001] in mineevite-(Y); (c,d,e) *A*, *B*, and *C* sheets of cation-coordination polyhedra in mineevite-(Y), respectively; (f) the structure of mineevite-(Y) viewed along [210] (the sequence of *A*, *B*, and *C* sheets is indicated).

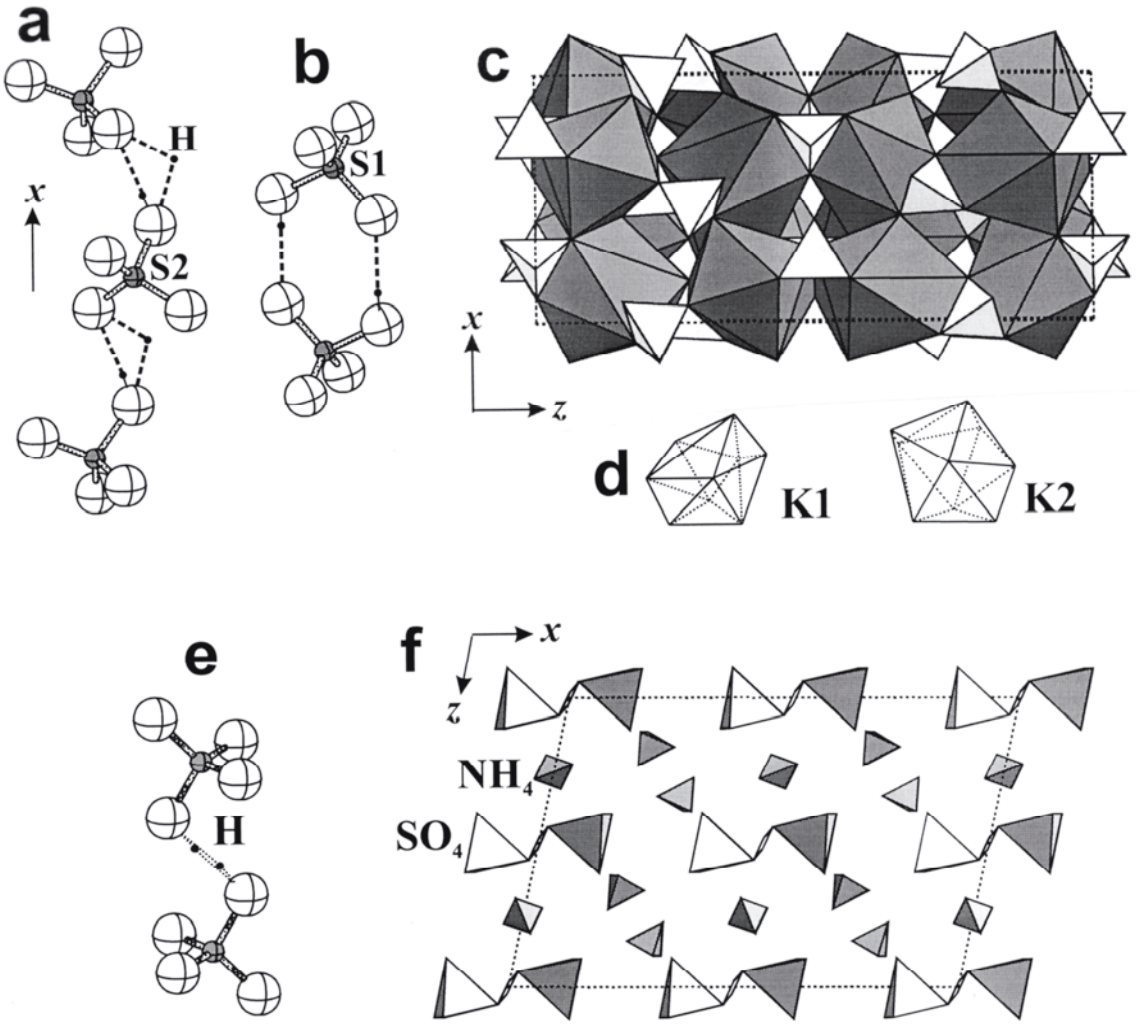

Figure 45. (a) The chain of H-bonded $(HSO_4)^-$ groups in mercallite; (b) $[(HSO_4)_2]^{2-}$ dimers in mercallite; (c) the structure of mercallite viewed along [010]; (d) the coordination polyhedra of K in mercallite; (e) the $[(SO_4)H(SO_4)]^{3-}$ cluster with the disordered H atom in letovicite; (f) the structure of letovicite viewed along [010].

consisting of two (SO_4) tetrahedra linked *via* disordered H atoms (Fig. 45e). As in mercallite, hydrogen-bonded (SO_4) groups form sheets parallel to (001) and are linked by (NH_4) groups (Fig. 45f).

Structures related to sulphohalite. There are four Na-sulfate minerals that occur as multiple salts in the system Na_2SO_4–NaF–NaCl: sulphohalite, schairerite, galeite, and kogarkoite (Table 15) (Pabst and Sharp 1973). The structure of **sulphohalite**, $Na_6ClF(SO_4)_2$, consists of a framework of clusters of $(NaØ_6)$ octahedra (Ø = O, F, Cl) (Fig. 46a,b). Each octahedron in this cluster shares four of its faces with four adjacent octahedra and one corner with a fifth octahedron (Fig. 46b). By analogy with other star-like clusters (*stella tetrangula* and *stella octangula*, O'Keeffe and Hyde 1996), this cluster should be called *stella hexangula*, a 'star with six angles.' In sulphohalite, the stellae hexangulae are linked by corner-sharing with (SO_4) tetrahedra into a three-dimensional framework (Fig. 46c).

The structures of the other three salts in this system cannot be clearly represented in terms of $(NaØ_6)$ octahedra. A more appropriate description is based on their relation to the halite structure. Both NaF and NaCl crystallize with the halite structure in which each Na

Table 15. Sulfate mineral structures related to sulphohalite, apatite, and barite.

Name	Formula	*a* (Å)	*b* (Å)	*c* (Å)	β(°)	γ(°)	S. G.	Fig.	Ref.
	Structures related to sulphohalite ($Na_2(SO_4)$ – NaF – NaCl *system*)								
sulphohalite	$Na_6ClF(SO_4)_2$	10.071	*a*	*a*	–	–	$Fm\bar{3}m$	46a-c,e	[1]
kogarkoite	$Na_3(SO_4)F$	18.079	6.958	11.443	107.7	–	$P2_1/m$	46d,f	[2]
galeite	$Na_{15}(SO_4)_5F_4Cl$	12.197	*a*	13.955	–	–	$P31m$	46d,g	[3]
schairerite	$Na_{21}(SO_4)_7F_6Cl$	12.197	*a*	19.359	–	–	$P31m$	46d,h	[4]
	Structures related to apatite								
caracolite	$Na_3Pb^{2+}_2(SO_4)_3Cl$	9.810	*a*	7.140	–	–	$P6_3/m$	47a-e	[5]
ecsanite	$Ca_{1.31}Na_{4.32}(OH)_{0.94}(SO_4)_3$	9.446	*a*	6.895	–	–	$P6_3/m$	47f	[6]
ellestadite	$Na_3Ca_2(SO_4)_3(OH)$	9.526	9.506	6.922	–	120.0	$P2_1$	–	[7]
chloroellestadite	$Ca_5(SiO_4)_{1.5}(SO_4)_{1.5}Cl$	9.530	*a*	6.914	–	–	$P6_3/m$	–	(8)
fluorellestadite	$Ca_5(SiO_4)_{1.5}(SO_4)_{1.5}F$	9.485	*a*	6.916	–	–	$P6_3/m$	–	(9)
hydroxylellestadite	$Ca_5(SiO_4)_{1.5}(SO_4)_{1.5}(OH)$	9.522	9.527	6.909	–	119.9	$P2_1/m$	–	[10]
mattheddleite	$Pb^{2+}_5(SiO_4)_{1.5}(SO_4)_{1.5}Cl$	9.963	*a*	7.464	–	–	$P6_3/m$	–	(11)
	Structures related to barite								
barite	$[Ba(SO_4)]$	7.154	8.879	5.454	–	–	*Pbnm*	47g-j	[12]
celestine	$[Sr(SO_4)]$	6.867	8.355	5.346	–	–	*Pbnm*	47g-j	[12,13]
anglesite	$[Pb^{2+}(SO_4)]$	6.955	8.472	5.397	–	–	*Pbnm*	47g-j	[12]
hashemite	$[Ba(CrO_4)]$	9.113	5.536	7.340	–	–	*Pnma*	47g-j	[14]
olsacherite	$[Pb^{2+}_2(SO_4)(SeO_4)]$	8.42	10.96	7.00	–	–	$P22_12$	47g-j	(15)

References: [1] Sakamoto (1968), [2] Fanfani et al. (1980), [3] Fanfani et al. (1975a), [4] Fanfani et al. (1975b), [5] Schneider (1967), [6] Deganello (1983), [7] Organova et al. (1994), [8] Rouse and Dunn (1982), (9) Chesnokov et al. (1987a), [10] Hughes and Drexler (1991), (11) Livingstone et al. (1987), [12] Jacobsen et al. (1998), [13] Hawthorne and Ferguson (1975b), [14] Pasero and Davoli (1987), (15) Hurlbut and Aristarain (1969)

atom is octahedrally coordinated by halogen atoms, *X*, and vice-versa. Thus, the halite structure can be considered as built from cation-centered (NaX_6) octahedra or anion-centered (XNa_6) octahedra. In terms of (XNa_6) octahedra, the structure of sulphohalite represents a corner-linked octahedral framework (Fig. 46c). In the structures of **kogarkoite**, $Na_3(SO_4)F$, **galeite**, $Na_{15}(SO_4)_5F_4Cl$, and **schairerite**, $Na_{21}(SO_4)_7F_6Cl$, there are clusters of three face-sharing (XNa_6) octahedra (Fig. 46d). The structures of these minerals are built from layers of *single* (FNa_6) octahedra (S_F layers), layers of *single* ($ClNa_6$) octahedra (S_{Cl} layers), and layers of *triple* octahedra (*T* layers). The layers are linked into frameworks by corner-sharing of single and triple octahedra. The sequences of layers are shown in Figures 46eBh. Sulphohalite has a sequence …$S_FS_{Cl}S_FS_{Cl}$… (Fig. 46e), and thus is built from single layers only, whereas the sequence …*TT*… (Fig. 46f) in kogarkoite indicates that it consists only of layers of triple octahedra. The structures of galeite (…$S_{Cl}S_FT$…; Fig. 46g) and schairerite (…TTS_{Cl}…; Fig. 46h) are built from both single and triple octahedra. As each Na atom in *X*-centered octahedra belongs to two such octahedra in all structures, the ratio Na : *X* is invariably 3:1.

Figure 46. (a) (NaO_6) octahedra and (SO_4) tetrahedra in the structure of sulphohalite; (b) a *stella hexangula* formed by linkage of six (NaO_6) octahedra; (c) sulphohalite viewed as built from (XNa_6) octahedra (*X* = F, Cl); (d) triplet of octahedra from the structures of kogarkoite, galeite, and schairerite; (e,f,g,h) the structures of (e) sulphohalite; (f) kogarkoite; (g) galeite; (h) schairerite, as based on a framework of (XNa_6) octahedra (*X* = F, Cl) (see text for details).

Next page → →

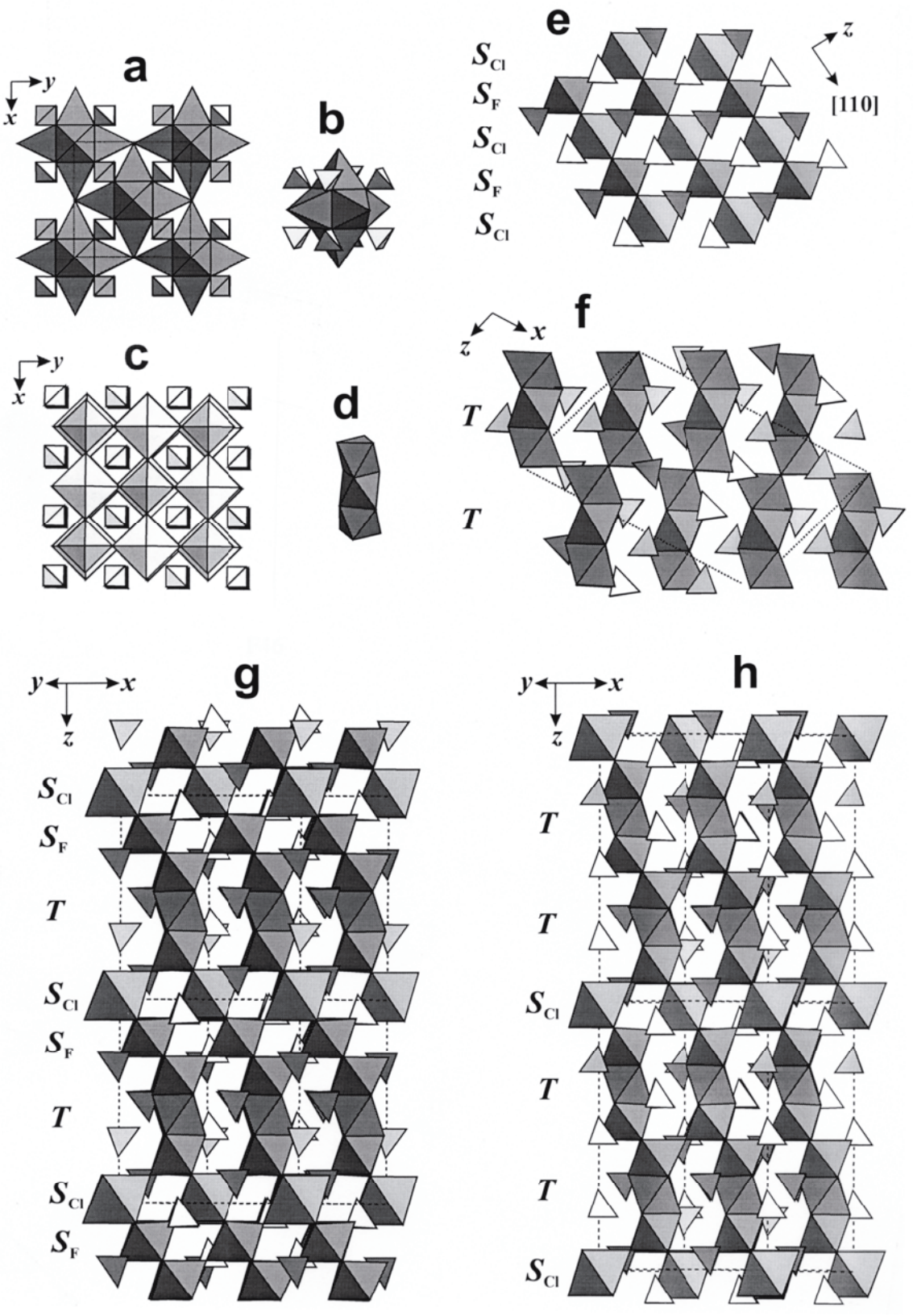
a
y
x
b
c
y
x
d
e
z
[110]
S_{Cl}
S_F
S_{Cl}
S_F
S_{Cl}
f
z
x
T
T
g
y
x
z
S_{Cl}
S_F
T
S_{Cl}
S_F
T
S_{Cl}
S_F
h
y
x
z
T
T
S_{Cl}
T
T
S_{Cl}

Apatite-like structures

The apatite-related sulfate minerals (Table 15, above) consist of frameworks of infinite rods of face-sharing cation polyhedra (Fig. 47b) that are decorated by (SO_4) tetrahedra (Fig. 45a). These rods are linked into frameworks that contain large channels (Fig. 47c), typically extending along [001]. These channels can be occupied by a variety of cations and anions. In the structure of **caracolite**, $Na_3Pb_2(SO_4)_3Cl$, the channels are occupied (Fig. 47e) by infinite chains of face-sharing (ClA_6) octahedra (A = Na, Pb) (Fig. 47d), whereas in **cesanite**, $Ca_{1.31}Na_{4.32}(OH)_{0.94}(SO_4)_3$, **ellestadite**, $Ca_4(Ca_{5.94}(OH)_{1.2}O_{0.5}Cl_{0.32})(SiO_4)_2(SO_4)_2(Si_{0.5}S_{0.5}O_4)_2$, and **hydroxylellestadite**, $Ca_{10}(SiO_4)_3(SO_4)_3(F_{0.16}Cl_{0.48}(OH)_{1.36})$, the channels are occupied by (XCa_3) triangles (X = Cl, OH) (Fig. 47f). The channel species are usually disordered and can be exchanged with other cations and/or anions.

Sulfates with the barite structure

Anhydrous sulfate minerals with the **barite**, $BaSO_4$, structure are listed in Table 15. The Ba cations are in [12]-coordination, forming irregular coordination polyhedra that are linked into a framework (Fig. 47g). Considering only the six nearest O neighbors, the Ba coordination can be described as a distorted octahedron and the structure as built from chains of edge-sharing octahedra linked by (SO_4) groups into sheets (Fig. 47h). These sheets are linked into a framework by corner-sharing between (BaO_6) polyhedra and (SO_4) tetrahedra from adjacent sheets (Fig. 47i). The presence of sheets results in the perfect cleavage of barite parallel to (001). An alternative description of the barite structure-type has been given by Smirnova et al. (1967) and O'Keeffe and Hyde (1985). The BaS cation array in barite is the same as that of the alloy FeB, with Ba in place of Fe, and S in place of B; O atoms are 'inserted' into SBa_3 tetrahedra of the BaS array, and barite can be regarded as an O-stuffed BaS array of the Fe– B type.

$Pb_4(SO_4)(CO_3)_2(OH)_2$ polymorphs

The structures of the $Pb^{2+}{}_4(SO_4)(CO_3)_2(OH)_2$ polymorphs (Table 16: **susannite**, **leadhillite**, and **macphersonite**) are based on the complex $[Pb^{2+}{}_4(OH)_2(CO_3)_2]^{2+}$ layer. The basis of this layer is the close-packed arrangement of Pb^{2+} atoms (Fig. 48a). Four of these cation sheets form a layer that is filled by (OH) and (CO_3) triangles (Fig. 48b). The resultant $[Pb^{2+}{}_4(OH)_2(CO_3)_2]^{2+}$ layers are separated in the structures by a single layer of (SO_4) tetrahedra (Figs. 48c,d,e). The difference between polymorphs is primarily in the relative positions of the (SO_4) tetrahedra (Steele et al. 1999).

Uranyl sulfates

There are three uranyl-sulfate minerals (Table 16) in the structural hierarchy for uranyl minerals given by Burns et al. (1996) and Burns (1999). In this scheme, **schröckingerite**, $NaCa_3[(U^{6+}O_2)(CO_3)_3](SO_4)F(H_2O)_{10}$, consists of a complex sheet of $(U^{6+}O_2)(CO_3)_3$ uranyl-carbonate clusters, ($NaØ_6$) octahedra, and trimers of ($CaØ_8$) polyhedra capped by (SO_4) groups (Fig. 49a). Note the similarity of the Ca-polyhedral trimer to the clusters in despujolsite (Fig. 16f) and orschallite (Fig. 39f). Linkage between sheets is provided by hydrogen bonding involving interlayer (H_2O) groups (Fig. 49b). The structure of **johannite**, $Cu^{2+}[(U^{6+}O_2)_2(OH)_2(SO_4)_2](H_2O)_8$, is based on an open sheet of $\{(U^{6+}O_2)O_5\}$ dimeric pentagonal bipyramids (Fig. 49c). Cross-linking between the sheets is *via* Jahn-Teller-distorted ($Cu^{2+}Ø_6$) octahedra and hydrogen bonds involving interlayer (H_2O) groups (Fig. 49d). **Zippeite**, $K[(U^{6+}O_2)_2(SO_4)(OH)_3](H_2O)$, and its analogs $M^{2+}{}_2[(UO_2)_6(SO_4)_3(OH)_{10}]\ (H_2O)_{16}$, M^{2+} = Co, Mg, Ni, Zn (Burns 1999), are based on the sheet shown in Figure 49e. The structure consists of chains of edge-sharing $\{(U^{6+}O_2)O_5\}$ pentagonal bipyramids linked by corner sharing with (SO_4) tetrahedra (Fig. 49f). Note that, in johannite and zippeite, (SO_4) tetrahedra and uranyl polyhedra polymerize only by corner-sharing.

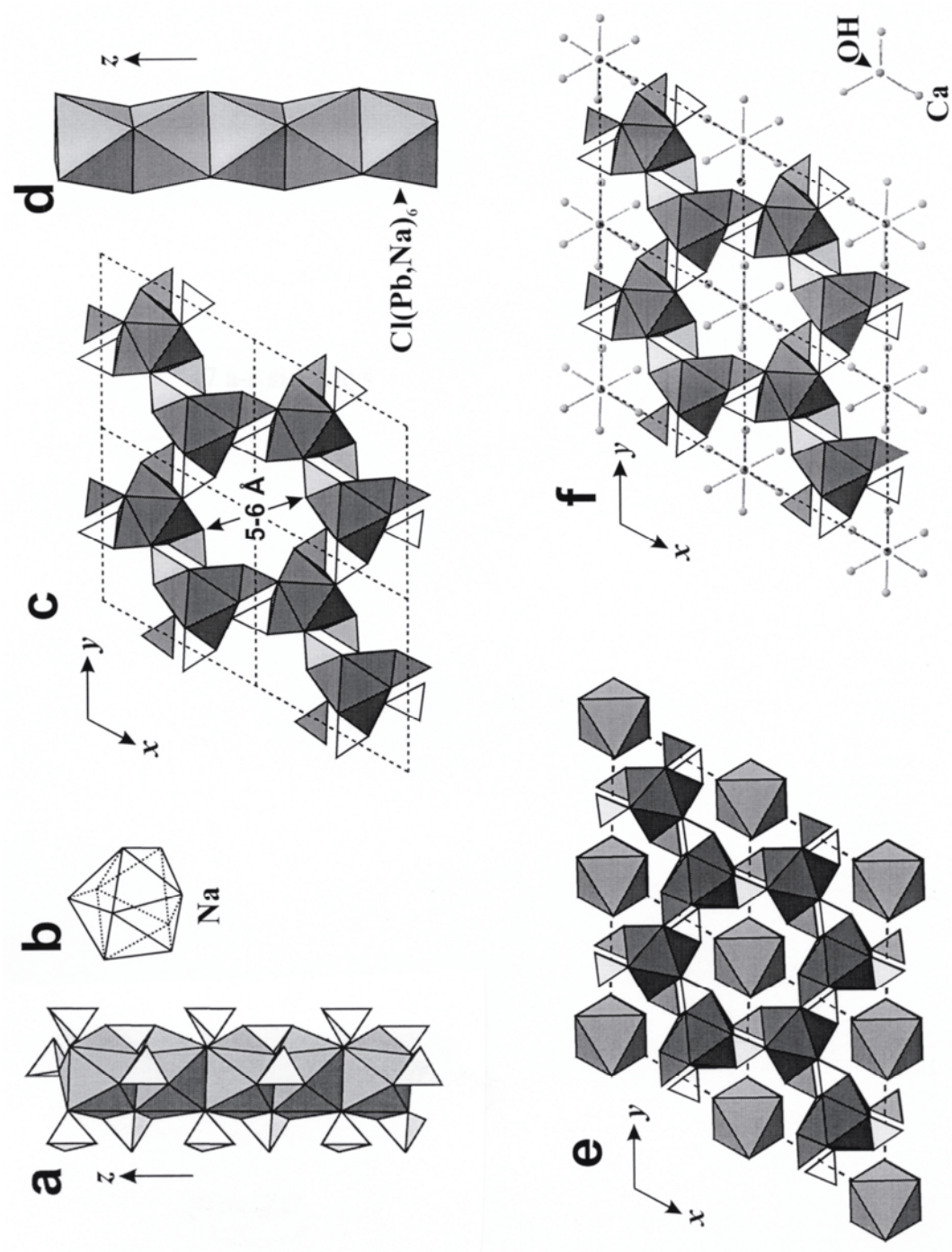

Figure 47. The structures of apatite-related sulfate minerals: (a) rods of face-sharing ($NaØ_9$) polyhedra in caracolite; (b) the ($NaØ_9$) polyhedron in caracolite; (c) the arrangement of rods in caracolite; note the large channels parallel to [001]; (d) the chain of face-sharing [Cl(Pb,Na)$_6$] octahedra in caracolite; (e) the structure of caracolite viewed along [001]; (f) the structure of cesanite viewed along [001]; the structures of ellestadite and hydroxylellestadite closely resemble that of cesanite.

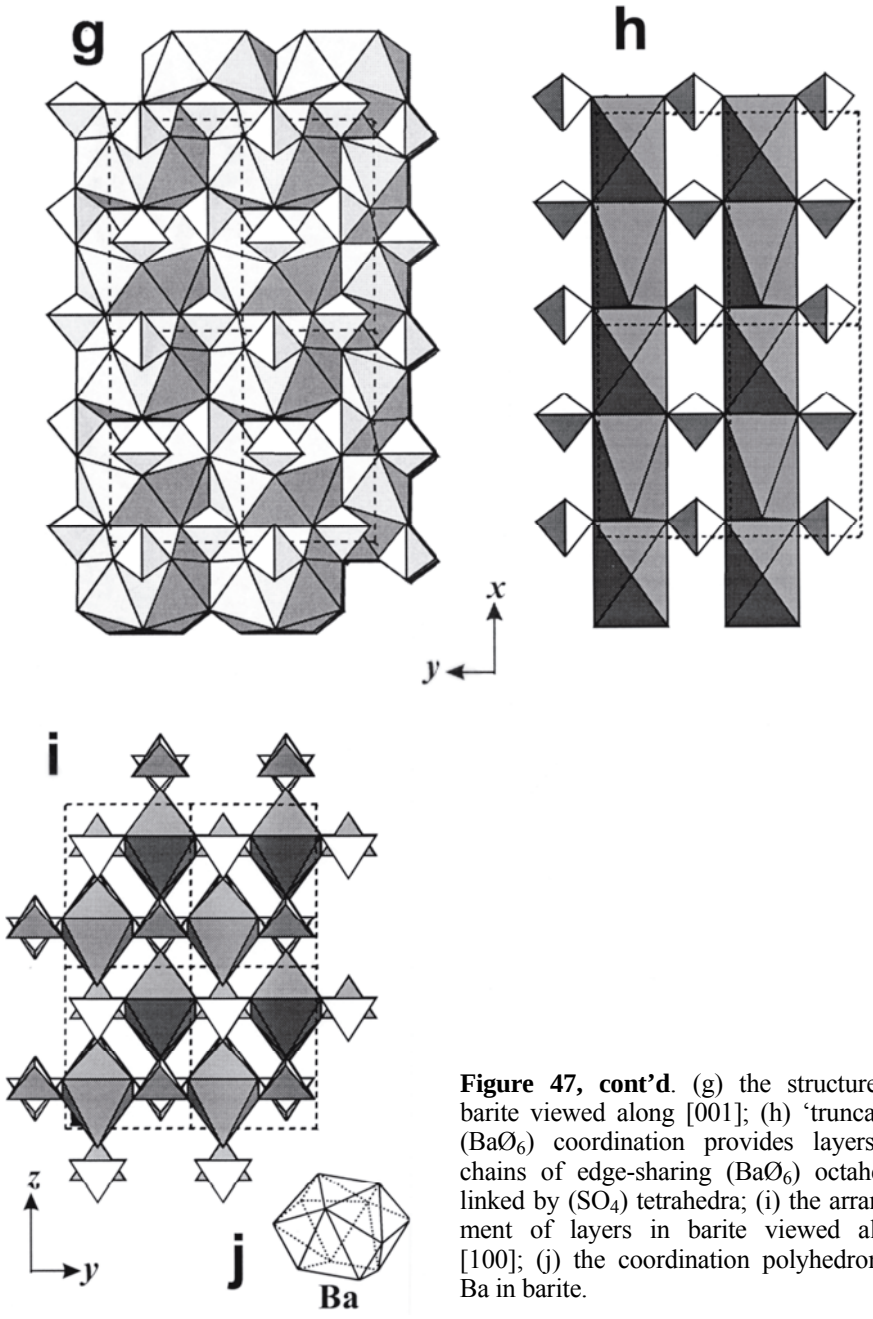

Figure 47, cont'd. (g) the structure of barite viewed along [001]; (h) 'truncated' ($BaØ_6$) coordination provides layers of chains of edge-sharing ($BaØ_6$) octahedra linked by (SO_4) tetrahedra; (i) the arrangement of layers in barite viewed along [100]; (j) the coordination polyhedron of Ba in barite.

Sulfates with non-sulfate tetrahedral sheets or frameworks

The crystallographic parameters for sulfate minerals of this class are given in Table 16. The structure of **heidornite**, $Na_2Ca_3[B_5O_8(OH)_2](SO_4)_2Cl$, consists of $[B_5O_8(OH)_2]$ sheets of ($BØ_3$) triangles and ($BØ_4$) tetrahedra (Fig. 50c). The ($NaØ_6$) octahedra, ($CaØ_8$) polyhedra, and (SO_4) tetrahedra are in the interlayer (Fig. 50a,b). The structures of **tuscanite**, $KCa_{5.8}[(Si,Al)_{10}O_{22}](SO_4)_{1.9}$, **latiumite**, $KCa_3[(Al,Si)_5O_{11}](SO_4)_{0.7}(CO_3)_{0.3}$, and **quietite**, $Pb^{2+}{}_4[Zn_2(SiO_4)(Si_2O_7)](SO_4)$, are based on the $[T_{10}O_{22}]$ double-tetrahedral sheet shown in Figure 50e. Some large cations (K, Ca, Pb^{2+}) occur within the sheet, whereas others are in the interlayer, together with (SO_4) tetrahedra (Fig. 50d). The dominant structural motif of the structure of **roeblingite**, $Pb^{2+}{}_2Ca_6(SO_4)_2(OH)_2$-$[Mn^{2+}(Si_3O_9)_2](H_2O)_4$, is the $[Mn^{2+}(Si_3O_9)_2]$ sheet formed by polymerization of ($Mn^{2+}O_6$) octahedra and (Si_3O_9) silicate rings (Fig. 50g). In heidornite, tuscanite, latiumite, and

Table 16. Sulfate minerals with non-octahedral cation coordination polyhedra.

Name	Formula	*a* (Å)	*b* (Å)	*c* (Å)	β (°)	S. G.	Fig.	Ref.
susannite	$Pb^{2+}_4(SO_4)(CO_3)_2(OH)_2$	9.0718	*a*	11.570	–	*P*3	48a,b,c	[1]
leadhillite	$Pb^{2+}_4(SO_4)(CO_3)_2(OH)_2$	9.110	20.820	11.590	90.5	$P2_1/a$	48a,b,d	[2]
macphersonite	$Pb^{2+}_4(SO_4)(CO_3)_2(OH)_2$	9.242	23.050	10.383	–	*Pcab*	48a,b,e	[3]
schröckingerite[1]	$NaCa_3[(U^{6+}O_2)(CO_3)_3](SO_4)F(H_2O)_{10}$	9.634	9.635	14.391	92.3	$P\bar{1}$	49a,b	[4]
johannite[2]	$Cu^{2+}[(U^{6+}O_2)_2(OH)_2(SO_4)_2](H_2O)_8$	8.903	9.499	6.812	112.0	$P\bar{1}$	49c,d	[5]
zippeite	$K[(U^{6+}O_2)_2(SO_4)(OH)_3](H_2O)$	8.755	13.987	17.730	104.1	*C*2/*c*	49e,f	[6]
heidornite	$Na_2Ca_3[B_5O_8(OH)_2](SO_4)_2Cl$	10.210	7.840	18.790	93.5	*C*2/*c*	50a,b,c	[8]
tuscanite	$KCa_{5.8}[(Si,Al)_{10}O_{22}](SO_4)_{1.9}$	24.030	5.110	10.880	106.9	$P2_1/a$	50d,e	[9]
latiumite	$KCa_3[(Al,Si)_5O_{11}](SO_4)_{0.7}(CO_3)_{0.3}$	12.060	5.080	10.810	106.0	$P2_1$	–	[10]
queitite	$Pb^{2+}_4[Zn_2(SiO_4)(Si_2O_7)](SO_4)$	11.362	5.266	12.655	108.2	$P2_1$	–	[11]
roeblingite	$Pb^{2+}_2Ca_6(SO_4)_2(OH)_2[Mn^{2+}(Si_3O_9)_2](H_2O)_4$	13.208	8.287	13.089	106.7	*C*2/*m*	50f,g	[12]
klebelsbergite	$Sb^{3+}_4O_4(OH)_2(SO_4)$	5.766	11.274	14.887	–	$Pca2_1$	51a,b	[16]
peretaite	$CaSb^{3+}_4O_4(OH)_2(SO_4)_2(H_2O)_2$	24.665	5.601	10.185	96.0	*C*2/*c*	51c,d	[17]
cannonite	$Bi^{3+}_2O(OH)_2(SO_4)$	7.692	13.870	5.688	109.0	$P2_1/c$	51e,f	[18]
d'ansite	$(Na_6Cl)_3[(Na_{0.75}Zn_{0.25})_2(SO_4)_5]_2$	15.913	*a*	*a*	–	$I\bar{4}3d$	52a,b,c	[7]
coskrenite-(Ce)[3]	$Ce_2(SO_4)_2(C_2O_4)(H_2O)_8$	6.007	8.368	9.189	105.6	$P\bar{1}$	52d,e	[13]
zircosulfate	$[Zr(SO_4)_2(H_2O)_4]$	25.920	11.620	5.532	–	*Fddd*	52f,g	[14]
vonbezingite	$Ca_6Cu^{2+}_3(SO_4)_3(OH)_{12}(H_2O)_2$	15.122	14.358	22.063	108.7	$P2_1/c$	52h	[15]

[1] $\alpha = 91.4°$, $\gamma = 120.3°$; [2] $\alpha = 109.9°$, $\gamma = 100.4°$; [3] $\alpha = 99.9°$, $\gamma = 107.7°$.

References: [1] Steele et al. (1999), [2] Giuseppetti et al. (1990), [3] Steele et al. (1998), [4] Mereiter (1986), [5] Mereiter (1982), [6] Vochten et al. (1995), [7] Lange and Burzlaff (1995), [8] Burzlaff (1967), [9] Mellini and Merlino (1977), [10] Canillo et al. (1973), [11] Hess and Keller (1980), [12] Moore and Shen (1984), [13] Peacor et al. (1999b), [14] Singer and Cromer (1959), [15] Dai and Harlow (1992), [16] Menchetti and Sabelli (1980a), [17] Menchetti and Sabelli (1980b), [18] Golic et al. (1982)

Table 17. Framework-silicate minerals with (SO_4) tetrahedra in cavities.

Name	Formula	*a* (Å)	*c* (Å)	S. G.	Fig.	Ref.
	Cancrinite group					
liottite	$(Ca_{11}Na_9K_4)[(Al_{18}Si_{18})O_{72}](SO_4)_4(CO_3)_2Cl_3(OH)_4(H_2O)_2$	12.870	16.096	$P\bar{6}$	50h	[1]
microsommite	$(Na,Ca,K)_{7-8}[(Al,Si)_{12}O_{24}](Cl,SO_4,CO_3)_{2-3}$	22.138	5.248	$P6_3$	–	[2]
pitiglianoite	$Na_6K_2[Al_6Si_6O_{24}](SO_4)(H_2O)_2$	22.121	5.221	$P6_3$	–	[3]
davyne	$CaNa_{4.26}K_{1.74}[Al_6Si_6O_{24}]Cl_{2.67}(SO_4)_{0.67}$	12.705	5.368	$P6_3/m$	–	[4]
afghanite	$(Na,K,Ca)_8(Si,Al)_{12}O_{24}(SO_4,Cl,CO_3)_3(H_2O)$	12.801	21.412	*P*31*c*	–	[5]
franzinite	$(Na,Ca)_7[(Si,Al)_{12}O_{24}](SO_4,CO_3,OH,Cl)_3(H_2O)$	12.861	26.45	?	–	(6)
giuseppettite	$(Na,Ca)_{7-8}[(Si,Al)_{12}O_{24}](SO_4,Cl)_{1-2}$	12.850	42.22	?	–	(6)
sacrofanite	$(Na,Ca,K)_9[Si_6Al_6O_{24}](OH,SO_4,CO_3Cl)_4(H_2O)_n$	12.865	74.240	$P6_3/mmc$	–	(6)
tounkite	$(Na,Ca,K)_8[Si_6Al_6O_{24}](SO_4)_2Cl(H_2O)$	12.843	32.239	$P6_222$	–	(6)
vishnevite	$(Na,K)_8[Si_6Al_6O_{24}](SO_4)(H_2O)_2$	12.685	5.179	$P6_3$	–	[7]
	Sodalite group					
haüyne	$(Na,K,Ca)_8[Si_6Al_6O_{24}](SO_4)_2$	9.118	*a*	$P\bar{4}3n$	50i	[8]
nosean	$Na_8[Si_6Al_6O_{24}](SO_4)(H_2O)$	9.084	*a*	$P\bar{4}3n$	50i	[9]

References: [1] Ballirano et al. (1996), [2] Klaska and Jarchow (1977), [3] Merlino et al. (1991), [4] Bonaccorsi et al. (1990), [5] Ballirano et al. (1997), (6) Gaines et al. (1997), [7] Hassan and Grundy (1984), [8] Evsyunin et al. (1996), [9] Hassan and Grundy (1989)

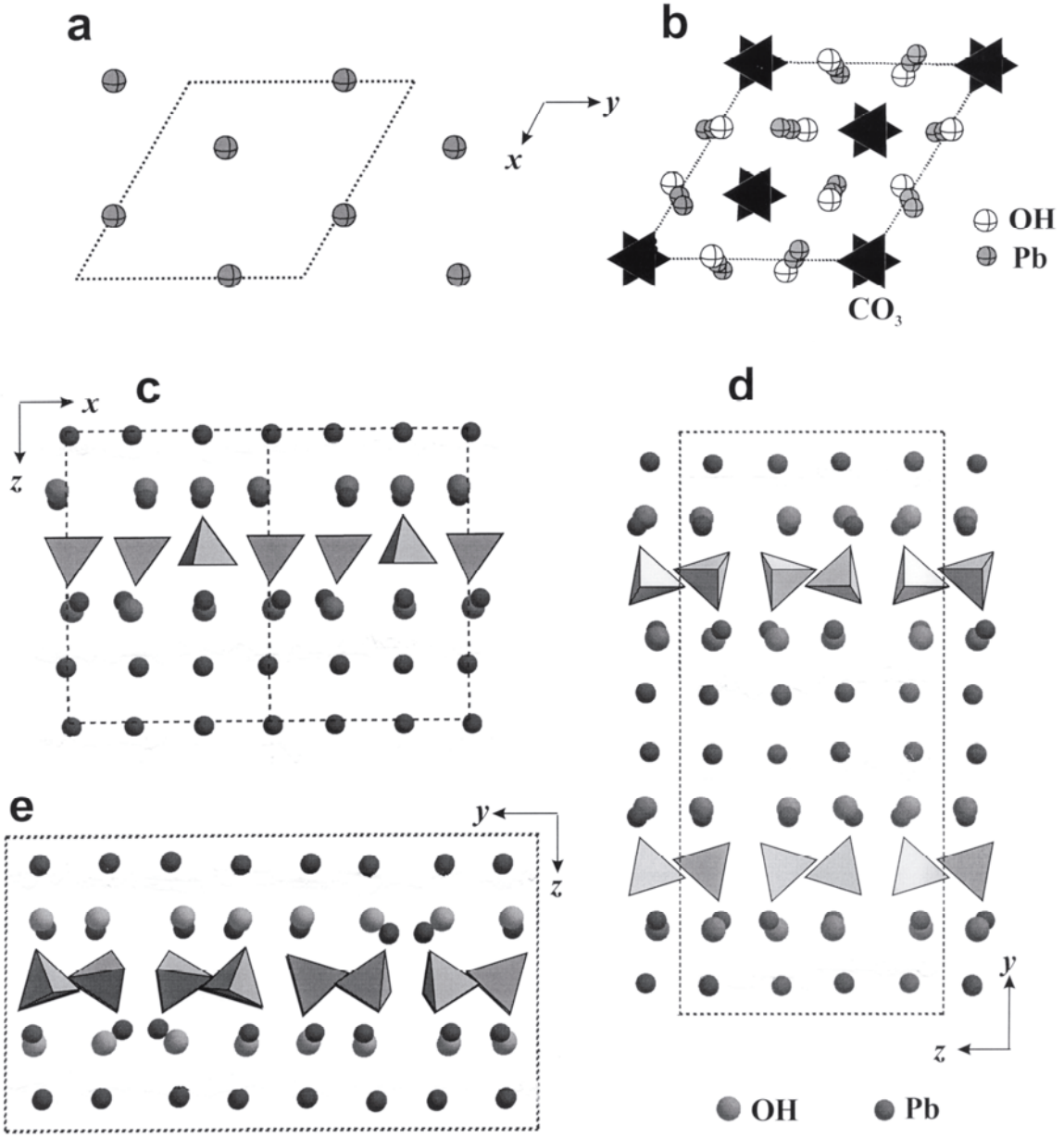

Figure 48. (a) The sheet of eutactically arranged Pb atoms in the $Pb_4(OH)_2(SO_4)(CO_3)_2$ polymorphs; (b) the $[Pb_4(OH)_2(CO_3)_2]$ layer present in all $Pb_4(OH)_2(SO_4)(CO_3)_2$ polymorphs; (c,d,e) the structures of (c) susannite, (d) leadhillite, and (e) macphersonite viewed along the extension of the sheets. The polymorphs differ in the positions of the interlayer (SO_4) tetrahedra.

quietite, the other structural subunits [Ca and Pb^{2+} cations, (SO_4) groups, and (OH) groups] act as connectors of the sheets in three dimensions (Fig. 50f).

Table 17 (above) lists framework silicate minerals that contain (SO_4) tetrahedra encapsulated in cavities. Two examples, **liottite**, $(Ca_{11}Na_9K_4)[(Al_{18}Si_{18})O_{72}](SO_4)_4(CO_3)_2Cl_3(OH)_4(H_2O)_2$, and **haüyne**, $(Na,K,Ca)_8[Si_6Al_6O_{24}](SO_4)_2$, are shown in Figures 50h and 50i, omitting the interframework cations for clarity.

Basic sulfates of Sb^{3+} and Bi^{3+}

Table 16 lists crystallographic parameters for the minerals of this group. The structures of **klebelsbergite**, $Sb^{3+}{}_4O_4(OH)_2(SO_4)$, **peretaite**, $CaSb^{3+}{}_4O_4(OH)_2(SO_4)_2(H_2O)_2$, and **cannonite**, $Bi^{3+}{}_2O(OH)_2(SO_4)$, are strongly influenced by the s^2 lone-

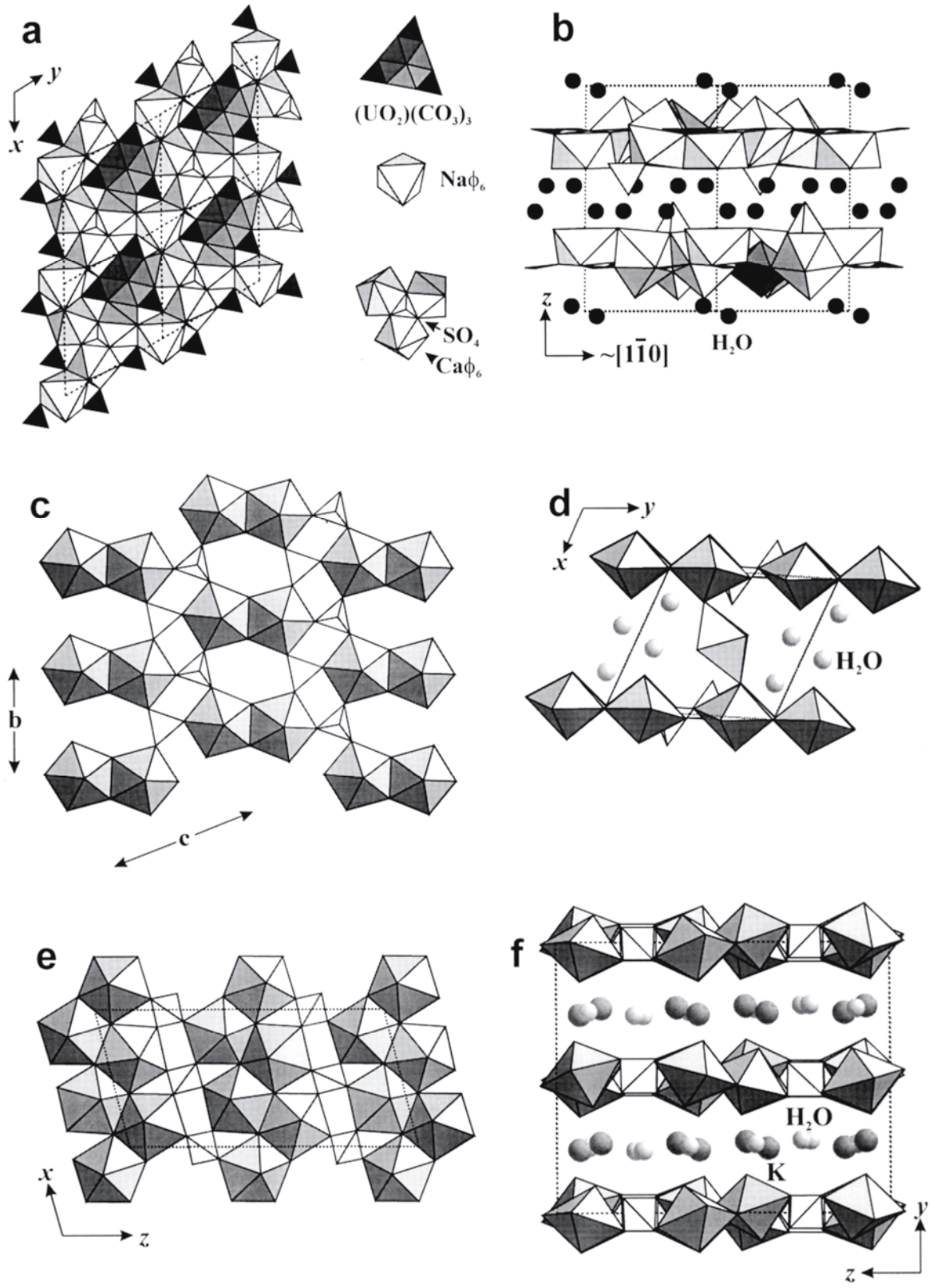

Figure 49. (a) The polyhedral sheet in schröckingerite; (b) the arrangement of sheets in the structure of schröckingerite; (c,d,e,f) the sheets of $\{(UO_2)O_5\}$ pentagonal bipyramids and (SO_4) tetrahedra and the structures of (c,d) johannite and (e,f) zippeite.

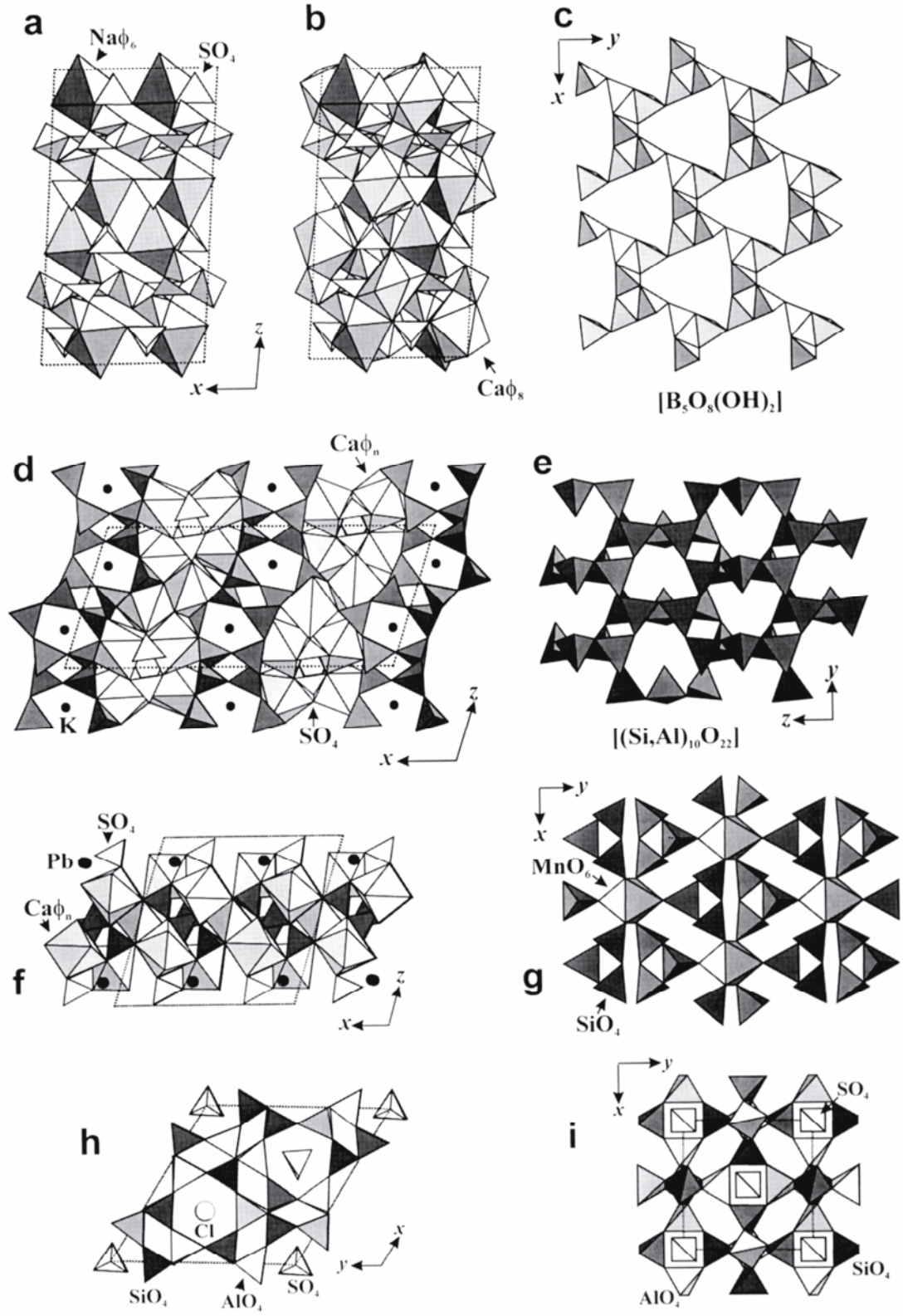

Figure 50. (a) The linkage of $[B_5O_8(OH)_2]$ sheets, (SO_4) tetrahedra, and $(NaØ_6)$ octahedra in heidornite viewed down [010]; (b) the same view of heidornite with the addition of $(CaØ_8)$ polyhedra; (c) the $[B_5O_8(OH)_2]$ sheet in heidornite viewed down [001]; (d) the structure of tuscanite viewed along [010]; (e) the aluminosilicate tetrahedral sheet in tuscanite viewed down [100]; (f) the structure of roeblingite viewed down [010]; (g) the $[Mn(Si_3O_9)_2]$ sheet in roeblingite viewed down [100]; (h,i) the structures of framework silicates with (SO_4) tetrahedra in cavities: (h) liottite and (i) haüyne; interframework cations are omitted for clarity.

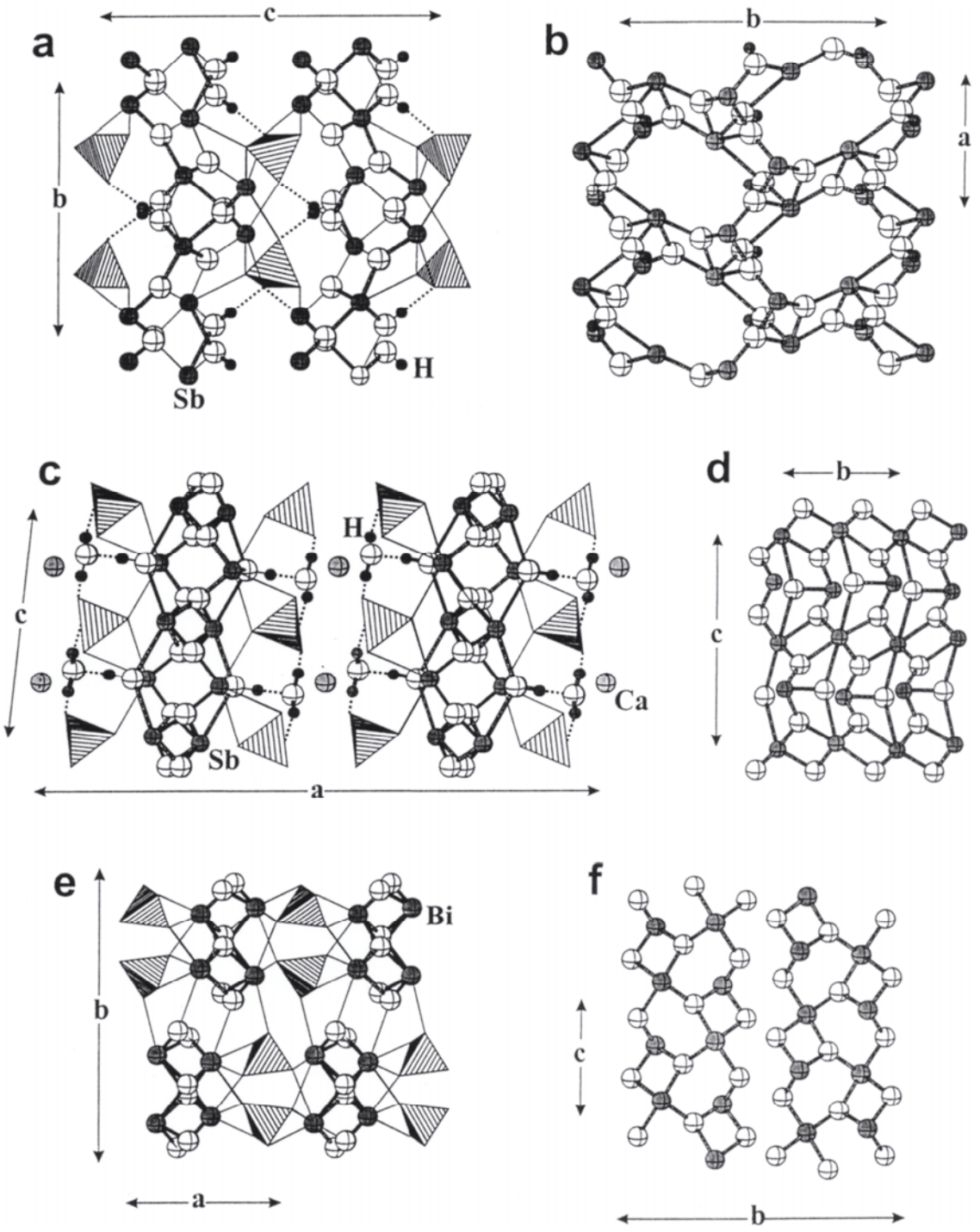

Figure 51. The structures and basic elements of the Sb and Bi sulfates: (a) klebelsbergite viewed along [100]; (b) klebelsbergite viewed down [001]; (c) peretaite viewed along [010]; (d) peretaite viewed down [100]; (e) cannonite viewed down [001]; (f) cannonite viewed down [100].

electron pairs on Sb^{3+} and Bi^{3+}. The coordination polyhedra of these cations are highly irregular and the structures are better understood in the terms of motifs of metal–oxygen bonds rather than in terms of coordination polyhedra. **Klebelsbergite** is based on the $[Sb^{3+}{}_4O_4(OH)_2]$ sheet parallel to (001); bonding within the sheet is between Sb^{3+} cations and O and (OH) anions not linked to S. The structure of the sheet is shown in Figure 51b. The two Sb^{3+} cations are [3]- and [5]-coordinated, respectively; O anions are [3]-coordinated and (OH) anions are [2]-coordinated (Fig. 51a). The structure of **peretaite**

consists of sheets of the same stoichiometry as the sheet in klebelsbergite, but with a rather different structure (Fig. 51d) and linkage (Fig. 51c). In **cannonite** (Fig. 51e,f), Bi^{3+}, O and (OH) form $[Bi^{3+}_2O(OH)_2]$ chains extending along [001] (Fig. 51f). In all three structures, (SO_4) tetrahedra are between the structural units, participating in long cation–oxygen bonds to the trivalent cations (Figs. 51a,c,e). The structures of klebelsbergite, peretaite, and cannonite are examples of the strong tendency of cations with lone-electron pairs to form complexes with O and (OH) anions. These complexes should play an essential role not only in minerals, but also as complexes involved in fluid transport of metals in natural processes.

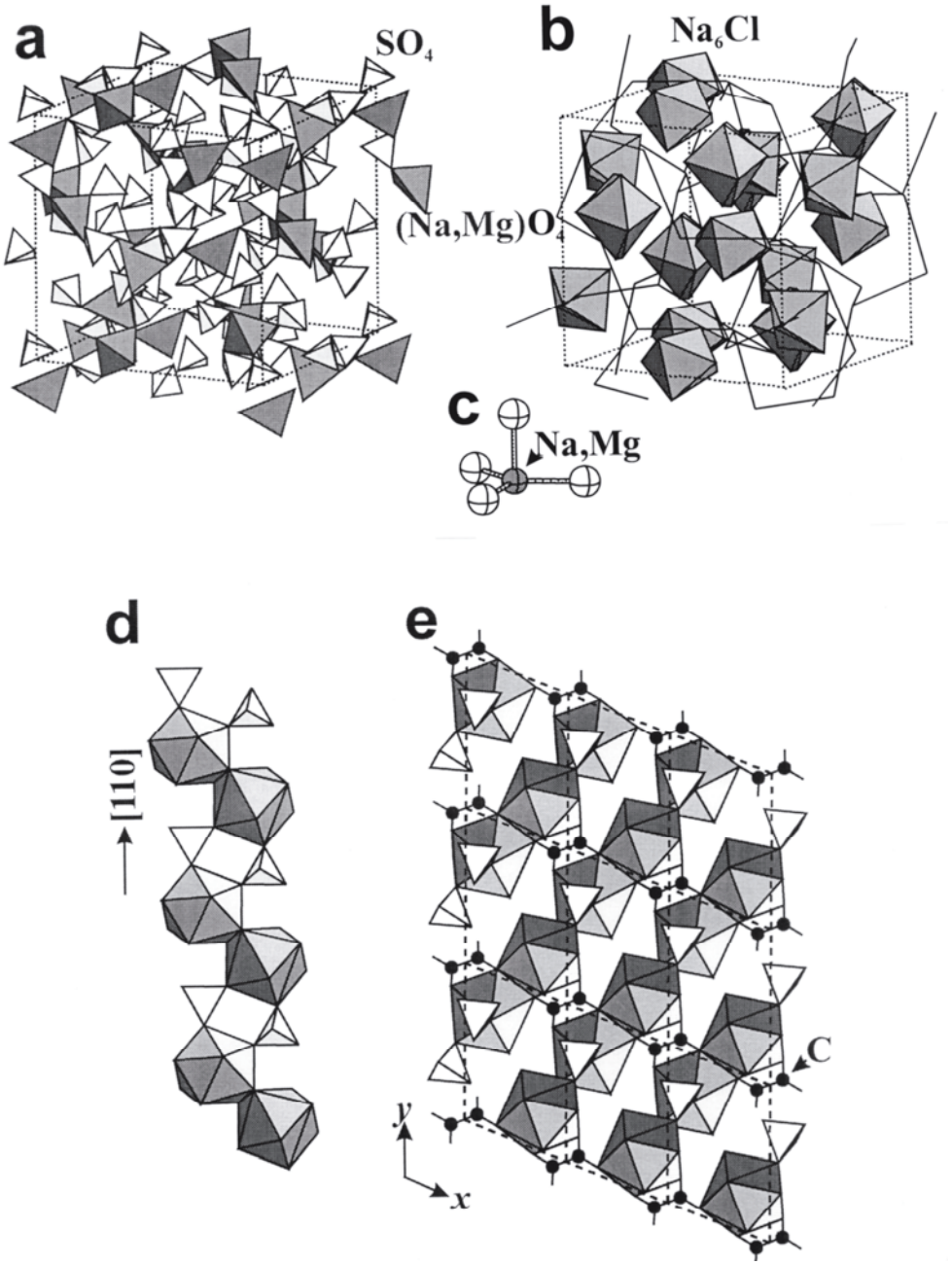

Figure 52. (a) The framework of $[(Na,Mg)O_4]$ trigonal pyramids and (SO_4) tetrahedra in d'ansite; (b) the positions of (Na_6Cl) octahedra in the framework of d'ansite, with the latter shown as a net; (c) coordination of the (Na,Mg) position in d'ansite; (d) the chain of $(REE)O_9$ polyhedra and (SO_4) tetrahedra in coskrenite-(Ce); (e) the chains in coskrenite-(Ce) cross-linked by (C_2O_4) groups to form a sheet.

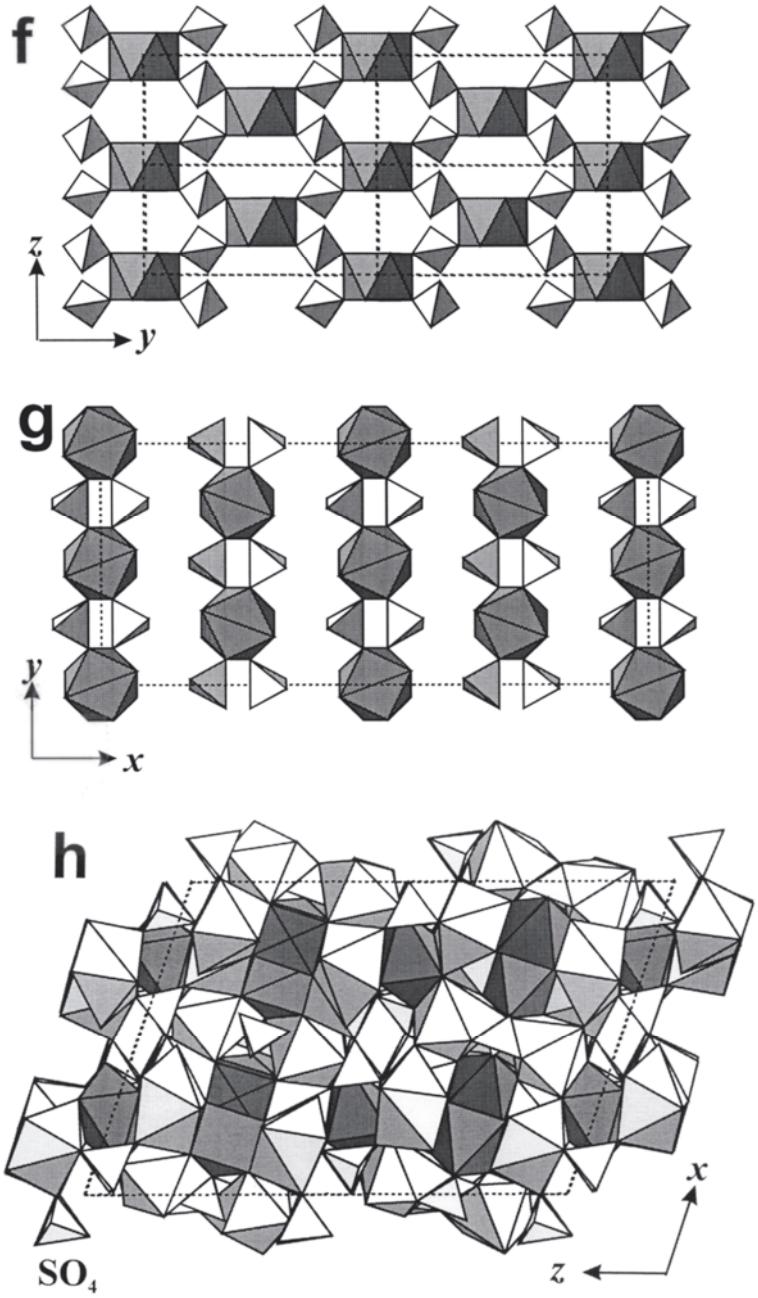

Figure 52, cont'd. (f) The sheet of ($ZrØ_8$) polyhedra and (SO_4) tetrahedra in zircosulfate; (g) packing of the sheets in the structure of zircosulfate; (h) the structure of vonbezingite projected down [010].

Miscellaneous sulfates

D'ansite, $(Na_6Cl)_3[(Na_{0.75}Zn_{0.25})_2(SO_4)_5]_2$, is based on a framework of corner-sharing [$(Na,Mg)O_4$] trigonal pyramids and (SO_4) tetrahedra (Figs. 52a,b,c). The cavities in the framework are occupied by ($ClNa_6$) octahedra.

The structure of **coskrenite-(Ce)**, $(Ce,Nd,La)_2(SO_4)_2(C_2O_4)(H_2O)_8$, the only sulfate-oxalate mineral of known structure, is based on the chain shown in Figure 52d. Edge-sharing dimers of (REE)$Ø_9$ polyhedra are linked by corner-sharing with (SO_4) tetrahedra, forming a chain extending along [110]. These chains are further linked through oxalate anions, $(C_2O_4)^{2-}$, into sheets parallel to (001) (Fig. 52e). Other sulfate–oxalate

Table 18. Sulfate minerals with anion-centered [XA_4] tetrahedra. *

Name	Formula	*a* (Å)	*b* (Å)	*c* (Å)	β (°)	S. G.	Graph	Fig.	Ref.
euchlorine	$NaK[Cu^{2+}_3O](SO_4)_3$	18.410	9.430	14.210	113.7	*C*2/*c*	53a	–	[1]
fedotovite	$K_2[Cu^{2+}_3O](SO_4)_3$	19.037	9.479	14.231	111.0	*C*2/*c*	53a	54a	[2]
kamchatkite	$K[Cu^{2+}_3O]Cl(SO_4)_2$	9.741	12.858	7.001	–	$Pna2_1$	53b	54b	[3]
vergasovaite	$[Cu^{2+}_3O][(Mo,S)O_4SO_4]$	7.421	6.754	13.624	–	*Pnma*	53b	54c	[4]
piypite	$K_4[Cu^{2+}_4O_2](SO_4)_4MCl$	13.600	*a*	4.980	–	*I*4	53c	54d	[5]
klyuchevskite	$K_3[Cu^{2+}_3(Fe,Al)O_2](SO_4)_4$	18.667	4.940	18.405	–	*I*2	53c	–	[6]
alumoklyu-chevskite	$K_3[Cu^{2+}_3AlO_2](SO_4)_4$	–	–	–	–	*I*2	53c	–	(7)
lanarkite	$[Pb^{2+}_2O](SO_4)$	13.769	5.698	7.079	115.9	*C*2/*m*	53c	54e	[8]
sidpietersite[1]	$[Pb^{2+}_4O_2](OH)_2(SO_3S)$	7.455	6.496	11.207	89.65	$P\bar{1}$	53d	–	[9]
synthetic[2]	$[Pb^{2+}_4O_2](OH)_2(SO_4)$	6.378	7.454	10.308	79.37	$P\bar{1}$	53d	–	[10]
nabokoite	$KCu^{2+}[Cu^{2+}_6TeO_4](SO_4)_5Cl$	9.833	*a*	20.591	–	*P*4/*ncc*	53e	55a	[11]
atlasovite	$KFe^{3+}Cu^{2+}_6Bi^{3+}O_4(SO_4)_5Cl$	9.86	*a*	20.58	–	*P*4/*ncc*	53e	–	(12)
dolerophanite	$[Cu^{2+}_2O](SO_4)$	9.370	6.319	7.639	122.3	*C*2/*m*	53f	55b	[13]
grandreefite	$[Pb^{2+}_2F_2](SO_4)$	8.667	4.442	14.242	107.4	*A*2/*a*	53g	55c	[14]
kleinite	$[Hg_2N](SO_4,Cl,H_2O)$	6.762	*a*	11.068	–	$P6_3/m$	53h	–	[15]
mosesite	$[Hg_4N_2](SO_4)(H_2O)$	9.503	*a*	*a*	–	$F\bar{4}3m$	53i	–	[16]
gianellaite	$[Hg_4N_2](SO_4)$	9.521	*a*	*a*	–	$F\bar{4}3m$	53i	–	(7)
schuetteite	$[Hg_3O_2](SO_4)$	7.044	*a*	10.000	–	$P3_121$	53j	–	[17]

* X = O, F, N; A = Cu^{2+}, Pb^{2+}, Hg, Te, Fe^{3+}, Al; M = Na, K; [1] α = 114.33°, γ = 88.69°; [2] α = 75.26°, γ = 88.16°.

References: [1] Scordari and Stasi (1990), [2] Starova et al. (1991), [3] Varaksina et al. (1990), [4] Berlepsch et al. (1999), [5] Effenberger and Zemann (1984), [6] Gorskaya et al. (1992), (7) Gaines et al. (1997), [8] Sahl (1970), [9] Cooper and Hawthorne (1999), [10] Steele et al. (1997), [11] Pertlik and Zemann (1988), (12) Popova et al. (1987), [13] Effenberger (1985a), [14] Kampf (1991), [15] Giester et al. (1996), [16] Airoldi and Magnano (1967), [17] Nagorsen et al. (1962)

minerals, **levinsonite-(Y)**, $(Y,Nd,Ce)Al(SO_4)_2(C_2O_4)\cdot 12H_2O$, and **zugshunstite-(Ce)**, $(Ce,Nd,La)Al(SO_4)_2(C_2O_4)\cdot 12H_2O$, are known (Peacor et al. 1999b), but complete descriptions and crystal-structure data are not yet published. The crystal structure of **zircosulfate**, $[Zr(SO_4)_2(H_2O)_4]$, is based on sheets of corner-sharing ($ZrØ_8$) tetragonal antiprisms and (SO_4) tetrahedra (Fig. 52f). The sheets are parallel to (100) and are held together by hydrogen bonds only (Fig. 52g). **Vonbezingite**, $Ca_6Cu^{2+}_3(SO_4)_3(OH)_{12}(H_2O)_2$, consists of thick heteropolyhedral slabs parallel to (001) (Fig. 52h).

STRUCTURES WITH ANION-CENTERED TETRAHEDRA

The structures of most of the minerals described in the preceding sections are based on *cation-centered* coordination polyhedra. However, application of the hierarchical principle (Hawthorne 1983a) to some sulfate minerals shows that they should be considered as based on *anion-centered* polyhedra rather than on cation-centered polyhedra (Krivovichev and Filatov 1999a). Recently, Krivovichev et al. (1998a) reported a structural hierarchy of minerals and inorganic compounds based on oxocentered (OM_4) tetrahedra and described their general crystal-chemical features. The importance of anion-centered tetrahedra in minerals has been noted in a number of previous works (e.g. Bergerhoff and Paeslack 1968; O'Keeffe and Bovin 1978; Effenberger 1985a; Hyde and Andersson 1989), but has not been extensively developed until recently.

Table 18 lists sulfate minerals based on anion-centered metal tetrahedra; Figure 53 shows various types of anion-centered tetrahedral units occurring in sulfate minerals. By analogy with other minerals, those in Table 18 can be subdivided into finite-cluster, infinite-chain, infinite-sheet and infinite-framework minerals.

The structures of **euchlorine**, $NaK[Cu^{2+}_3O](SO_4)_3$, and **fedotovite**, $K_2[Cu^{2+}_3O](SO_4)_3$, are based on the $[O_2Cu^{2+}_6]$ edge-sharing tetrahedral dimer linked through (SO_4) groups into infinite sheets parallel to (100) (Fig. 54a). **Kamchatkite**, $K[Cu^{2+}_3O]Cl(SO_4)_2$ (Fig. 54b), and **vergasovaite**, $[Cu^{2+}_3O][(Mo,S)O_4SO_4]$ (Fig. 54c), are based on the $[O_2Cu^{2+}_6]$ infinite chain of corner-sharing (OCu^{2+}_4) tetrahedra of the type shown in Figure 53b; more details about the crystal chemistry of minerals and synthetic compounds based on this chain are given by Krivovichev et al. (1998b). The structures of **piypite**, $K_4[Cu^{2+}_4O_2](SO_4)_4{\cdot}M$Cl, M = (Na,K), **klyuchevskite**, $K_3[Cu^{2+}_3(Fe^{3+})O_2]$-$(SO_4)_4$, and **lanarkite**, $[Pb^{2+}_2O](SO_4)$, are based on $[O_2M_4]$ chains of *edge*-sharing $[OM_4]$ tetrahedra (Fig. 53c). In piypite (Fig. 54d) and klyuchevskite, these chains are connected through (SO_4) groups into frameworks, whereas in lanarkite (Fig. 54e), they form infinite sheets parallel to $(\bar{1}01)$. **Nabokoite**, $KCu^{2+}[Cu^{2+}_6TeO_4](SO_4)_5Cl$, consists of $[O_4Cu^{2+}_6Te]$ sheets based on the tetrahedral tetramers shown in Figure 53e. The sheets are decorated by (SO_4) tetrahedra and are linked together through $(Cu^{2+}O_4Cl)$ tetragonal pyramids and interlayer K atoms (Fig. 55a). **Dolerophanite**, $[Cu^{2+}_2O](SO_4)$, is based on the $[O_2Cu^{2+}_4]$ sheet (Fig. 53f); the sheets are cross-linked by (SO_4) tetrahedra to form a three-dimensional framework (Fig. 55b). The structure of **grandreefite**, $[Pb^{2+}_2F_2](SO_4)$, consists of $[F_2Pb^{2+}_2]$ sheets of the type observed in the structure of tetragonal PbO (Fig. 53g). The (SO_4) tetrahedra are located between the sheets, linking them together (Fig. 55c).

The $[NHg_2]$ frameworks of the nitrogen-centered (NHg_4) tetrahedra in **kleinite**, $[Hg_2N](SO_4,Cl,H_2O)$ (Fig. 53h), and **mosesite**, $[Hg_4N_2](SO_4)(H_2O)$ (Fig. 53i), show striking similarity to the $[SiO_2]$ frameworks in tridymite and cristobalite, respectively. It should be noted that N-centered tetrahedra are well-known in trivalent rare-earth compounds (Schleid 1996). The $[O_2Hg_3]$ framework in **schuetteite**, $[Hg_3O_2](SO_4)$, is built by corner-sharing of the $[O_2Hg_6]$ tetrahedral dimers of the euchlorine-fedotovite type (Fig. 53j).

Inspection of the list of the sulfate minerals with anion-centered tetrahedra (Table 18) shows that their most common metals are Cu, Pb, and Hg. It is of interest that all the Cu minerals possessing (OCu^{2+}_4) tetrahedra are of fumarolic origin, occurring in the exhalation deposits of the Vesuvio (Italy) and Tolbachik (Russia) volcanoes. There are several other examples of fumarolic Cu-chloride, vanadate, arsenate, and selenite minerals with (OCu^{2+}_4) tetrahedra (Krivovichev et al. 1998a; Krivovichev and Filatov 1999a,b). Filatov et al. (1992) suggested that oxocentered tetrahedra play an important role as a form of Cu transport in fumarolic processes. Both Pb^{2+} and Hg^{2+} show a strong tendency to form complex polycations with O anions; these also could act as agents in metal transport in natural and anthropogenic processes.

THIOSULFATE MINERALS

There are a few thiosulfate minerals known (Table 19). Only the structure of sidpietersite is known, although bazhenovite has a synthetic orthorhombic polymorph, the structure of which has been determined (Chesnokov et al. 1987b). Thiosulfates are not highly represented among minerals, but they are of potential environmental importance because they can form as weathering products of anthropogenic materials such as slags (e.g. Braithwaite et al. 1993).

Sidpietersite, $Pb^{2+}_4(S^{6+}O_3S^{2-})O_2(OH)_2$, is a lead hydroxy-thiosulfate, the structure

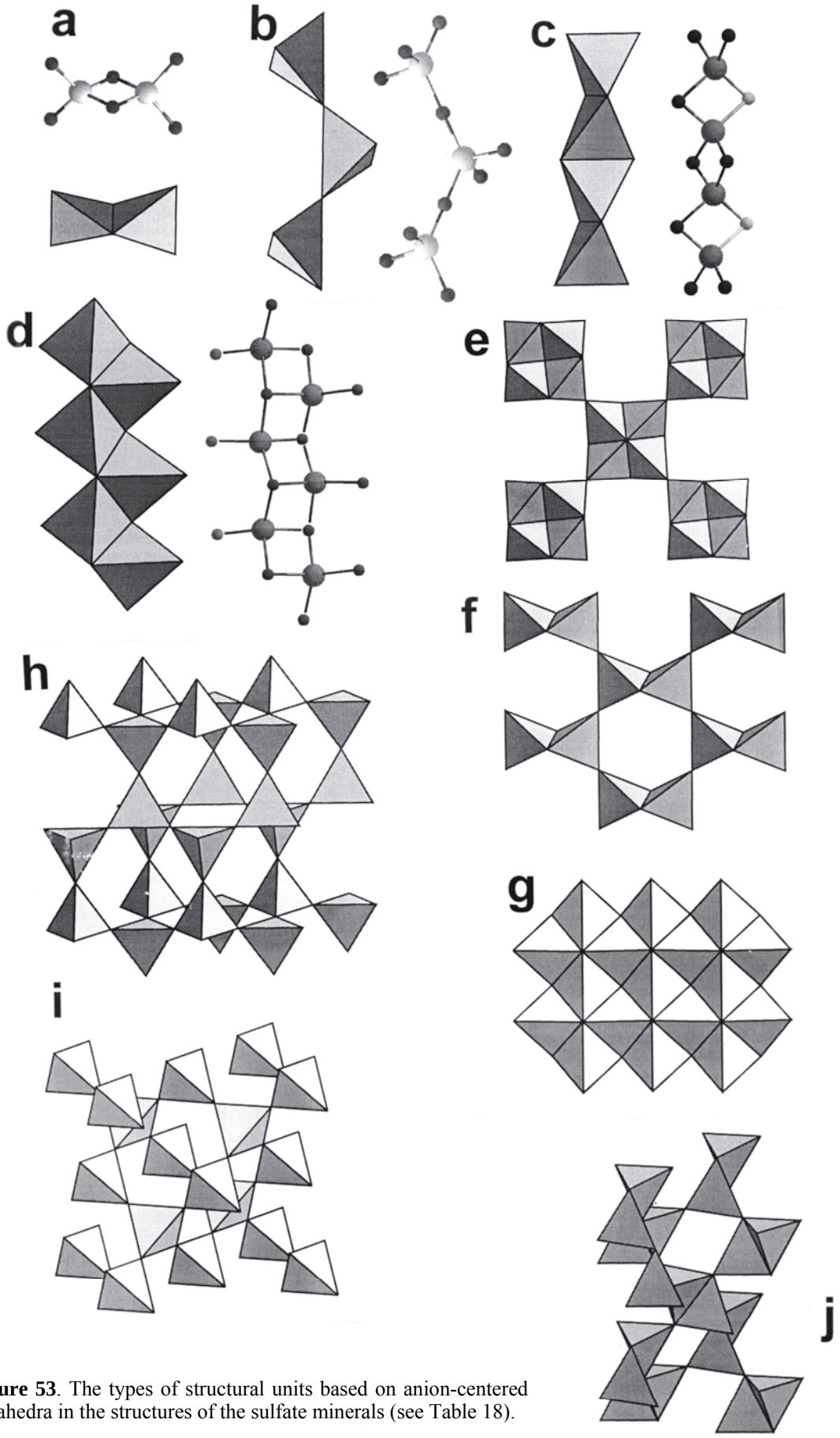

Figure 53. The types of structural units based on anion-centered tetrahedra in the structures of the sulfate minerals (see Table 18).

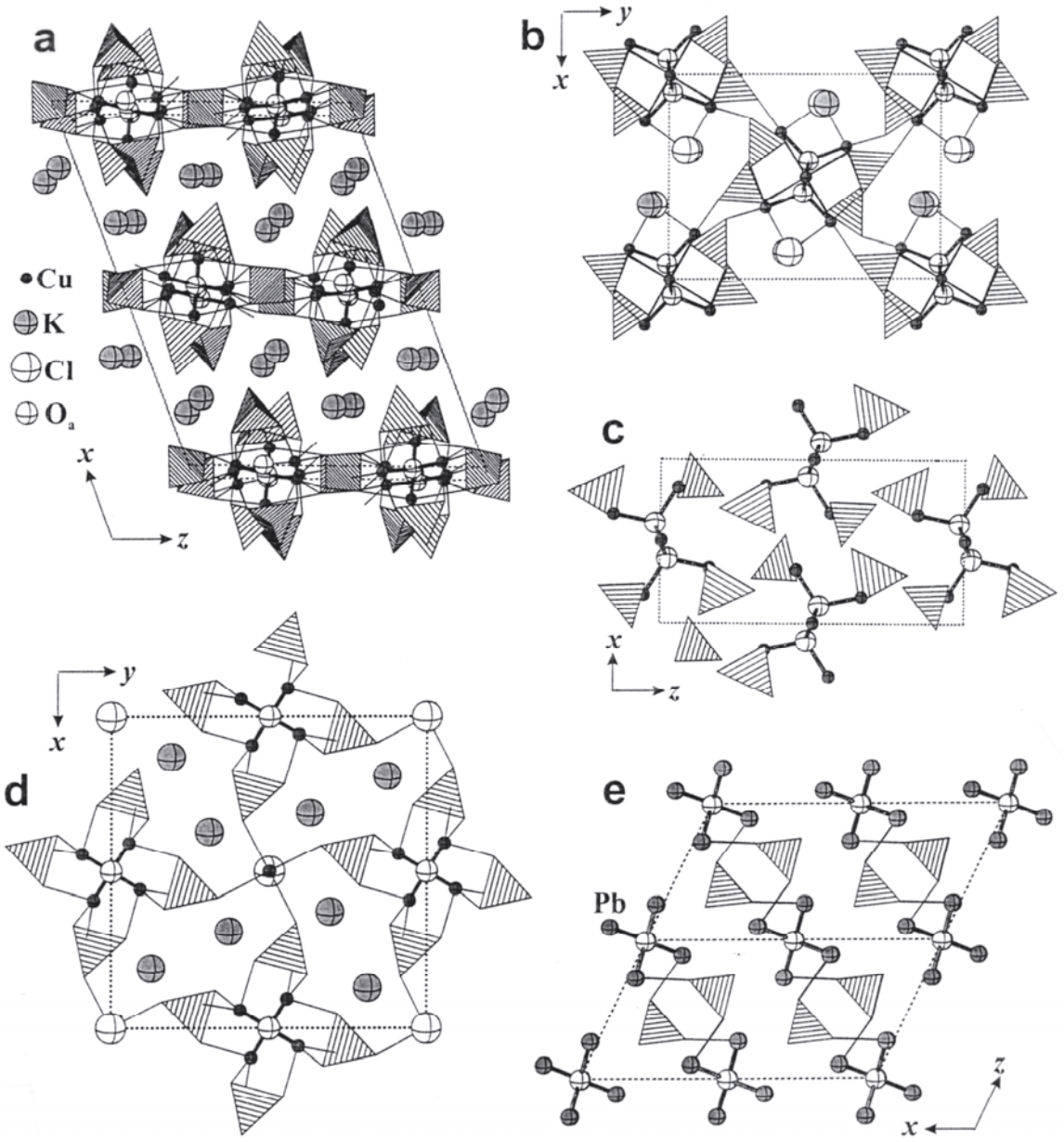

Figure 54. The structure of sulfate minerals containing anion-centered tetrahedra: (a) fedotovite; (b) kamchatkite; (c) vergasovaite; (d) piypite; (e) lanarkite. The anion atoms in the centers of tetrahedra are shown as large unshaded circles.

of which is shown in Figure 56. A ladder of Pb [*Pb*(1) and *Pb*(4)] and O atoms extends along the *a* axis; note that this is a motif from the PbO structure. This ladder is decorated on either side by a staggered arrangement of Pb^{2+} [*Pb*(2) and *Pb*(3)] and O atoms to form a ribbon that extends along the *a* axis. These ribbons are linked in the *c* direction by ($S^{6+}O_3S^{2-}$) groups such that the S^{2-} anions [*S*(2)] form an almost linear array in projection (Fig. 56a). This linkage forms thick slabs orthogonal to [001]. In Figure 56b, the '*Pb*–O' ladders are seen 'end-on'; they are linked into slabs orthogonal to [001] by thiosulfate groups and *Pb*–O bonds. These slabs are linked in the *c* direction by long weak *Pb*–*S*(2) bonds; note that, in this orientation, the *Pb*(2), *Pb*(3) and *S*(2) atoms form a ladder resembling the *Pb*–O ladder in Figure 56a.

Sidpietersite is a unique structure both with regard to minerals and to synthetic

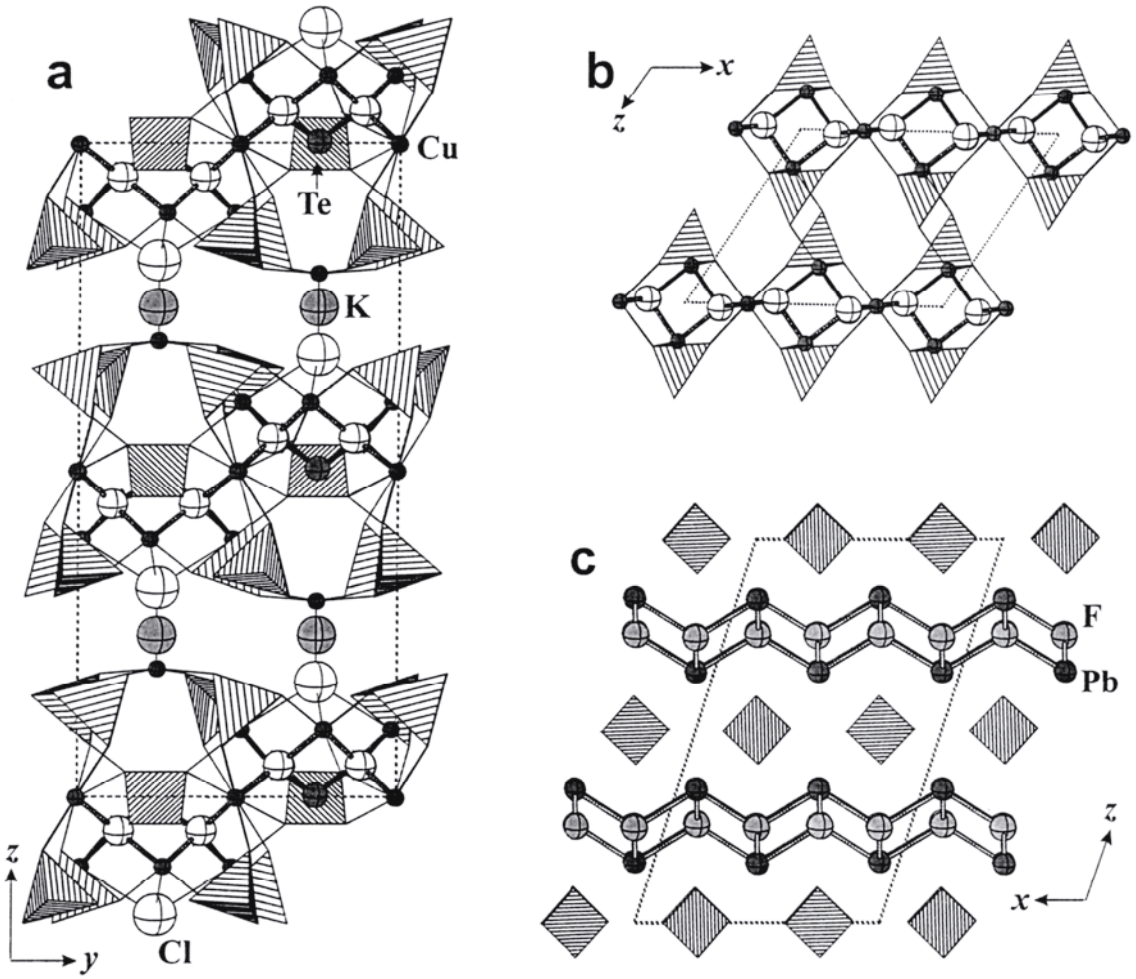

Figure 55. The structure of sulfate minerals containing anion-centered tetrahedra: (a) nabokoite; (b) dolerophanite; (c) grandreefite. The anion atoms in the centers of tetrahedra are shown as large unshaded circles.

compounds. Inspection of Table 2 shows that all the known synthetic thiosulfates have cation:S_2O_3 ratios between 1 and 2, and all of the structural arrangements involve thiosulfate tetrahedra in a network of weak cation–oxygen bonds, usually involving H or alkali cations. Sidpietersite has a cation:S_2O_3 ratio of 4, and contains relatively strongly bonded and polymerized fragments of the PbO structure. However, there does not seem to be anything particularly exotic about the structure of sidpietersite, except for the occurrence of the thiosulfate group in a mineral, and there seems to be no intrinsic reason why structures with cation:S_2O_3 ratios higher than 2 should not be common.

SULFITE MINERALS

The few sulfite minerals known are listed in Table 19 and are illustrated in Figure 57. **Hannebachite**, $Ca(S^{4+}O_3)(H_2O)_{0.5}$, is based on chains of edge-sharing ($CaØ_8$) polyhedra, decorated by ($S^{4+}O_3$) triangles, that extend along the *z* axis (Fig. 57a). Seen 'end-on' in Figure 57b, these chains are arranged in a checkerboard fashion, linking through shared edges of the ($CaØ_8$) polyhedra. **Scotlandite**, $Pb^{2+}(S^{4+}O_3)$, consists of sheets of edge-sharing ($Pb^{2+}Ø_9$) polyhedra decorated by ($S^{4+}O_3$) triangles and parallel to (001) (Fig. 57c). The ($Pb^{2+}Ø_9$) polyhedra from adjacent sheets share edges to form a fairly dense framework (Fig. 57d). **Gravegliaite**, $Mn^{2+}(S^{4+}O_3)(H_2O)_3$, consists of chains of ($Mn^{2+}Ø_6$) octahedra and

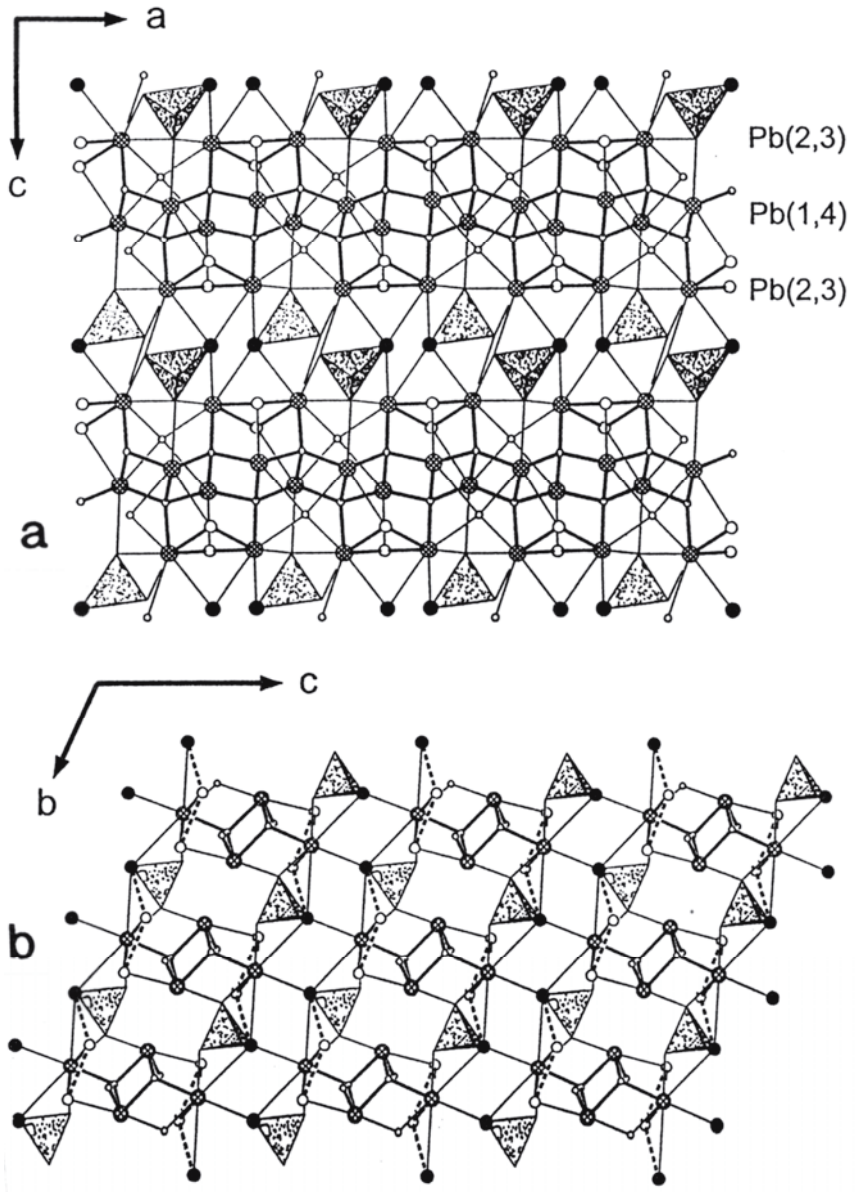

Figure 56. The structure of sidpietersite: (a) viewed down an axis 5° from [010]; (b) viewed down an axis 3° from [100]; the thiosulfate anion is random-dot-shaded, the S^{2-} anion is shown as a large black circle, Pb^{2+} cations are shown as cross-hatched circles, OH anions and O anions are shown as medium-sized and small unshaded circles, respectively, and H bonds are shown as broken lines. After Cooper and Hawthorne (1999).

($S^{4+}O_3$) triangles (Fig. 57e). The chain can be considered as being built from [$M_2(TO_3)Ø_6$] clusters which link by sharing corners between triangles and octahedra; the graph of this chain is shown in Figure 57f. Viewed along [010] (Fig. 57g), these chains are arranged, end-on, at the vertices of a centered plane square lattice, with adjacent chains canted to each other. The chemical formula of the chain is the same as that of the mineral, and the chains are linked only by hydrogen bonds. **Orschallite**, $Ca_3(S^{4+}O_3)_2(S^{6+}O_4)(H_2O)_{12}$, is a mixed sulfite–sulfate mineral. The structure is discussed in the section on calcium-sulfate minerals. **Abenakiite-(Ce)**, $Na_{26}Ce_6(SiO_3)_6(PO_4)_6(CO_3)_6(S^{4+}O_3)$, has a structure similar to that of mineevite-(Y) (Fig. 44) and hanksite (Figs. 43d,e,f). The structure is based on complex chains and columns that are arranged at and around the

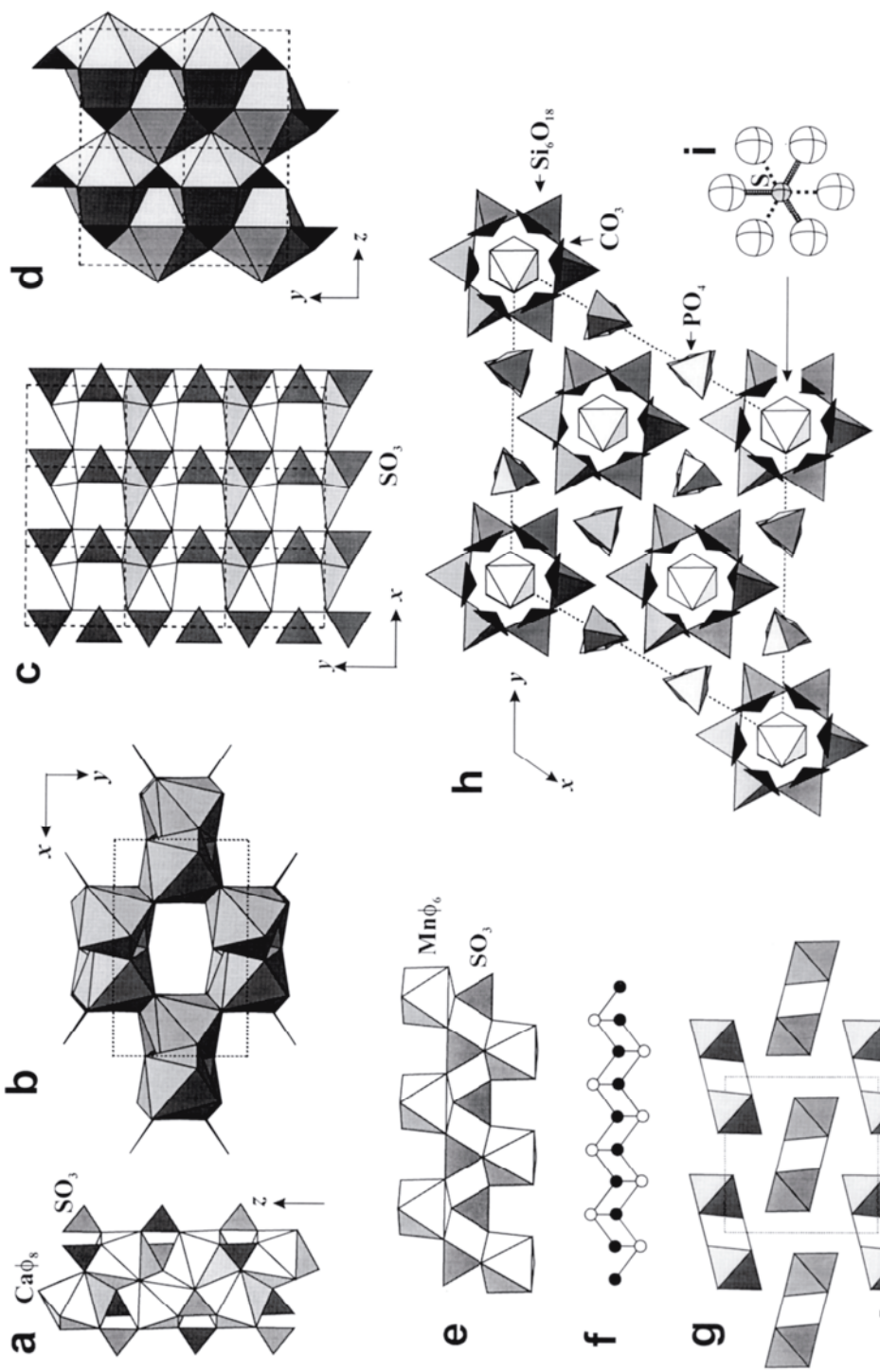

Figure 57. The structure of the sulfite minerals: (a) the chain of ($CaØ_8$) polyhedra and (SO_3) triangles in hannebachite; (b) the structure of hannebachite projected down [001]; (c) the sheet of ($PbØ_9$) polyhedra and (SO_3) triangles in scotlandite; (d) the structure of scotlandite projected down [100]; (e) the chain of ($MnØ_6$) octahedra and (SO_3) triangles in gravegliaite; (f) the graph of the chain shown in (e); (g) the structure of gravegliaite projected down [010]; (h) the structure of abenakiite-(Ce) projected down [001]; cations are omitted for clarity; (i) the disordered ($S^{4+}O_3$) group in abenakiite-(Ce); the two preferential positions are shown as solid and dashed, respectively.

Table 19. Thiosulfate, sulfite, and fluorosulfate minerals.

Mineral	Formula	*a* (Å)	*b* (Å)	*c* (Å)	S. G.	Fig.	Ref.
			Thiosulfate minerals				
sidpietersite	$Pb^{2+}{}_4(S^{6+}O_3S^{2-})O_2(OH)_2$		see Table 18			56a,b	[1]
bazhenovite	$CaS_5Ca(S^{6+}O_3S^{2-})Ca_6(OH)_{12}(H_2O)_{20}$					–	(2)
viaeneite	$(Fe,Pb)(S_2)_{11}(S^{6}O_3S^{2-})$					–	(3)
			Sulfite minerals				
hannebachite	$Ca(S^{4+}O_3)(H_2O)_{0.5}$	10.664(1)	6.495(1)	9.823(1)	*Pbcn*	57a,b	[4]
scotlandite	$Pb^{2+}(S^{4+}O_3)$	4.505(2)	5.333(2)	6.405(6)	$P2_1/m$	57c,d	[5]
gravegliaite	$Mn^{2+}(S^{4+}O_3)(H_2O)_3$	9.763(1)	5.635(1)	9.558(1)	*Pnma*	57e,f,g	[6]
orschallite	$Ca_3(S^{4+}O_3)_2(SO_4)(H_2O)_{12}$	11.350(1)	*a*	28.321(2)	$R\bar{3}c$	39d-g	[7]
abenakiite-(Ce)	$Na_{26}Ce_6(SiO_3)_6(PO_4)_6(CO_3)_6(S^{4+}O_3)$	16.018(2)	*a*	19.761(4)	$R\bar{3}$	57h,i	[8]
			Fluorosulfate minerals				
reederite-(Y)	$Na_{15}Y_2(CO_3)_9(SO_3F)Cl$	8.763(1)	*a*	10.736(2)	$P\bar{6}$	58a,b,c	[9]

*β = 106.24(3)°

References: [1] Roberts et al. (1999), Cooper and Hawthorne (1999), (2) Chesnokov et al. (1987b), (3) Kucha et al. (1996), [4] Matsuno et al. (1984), Schröpfer (1973), [5] Pertlik and Zemann (1985), [6] Basso et al. (1991), [7] Weidenthaler et al. (1993), [8] McDonald and Chao (1994), [9] Grice et al. (1995)

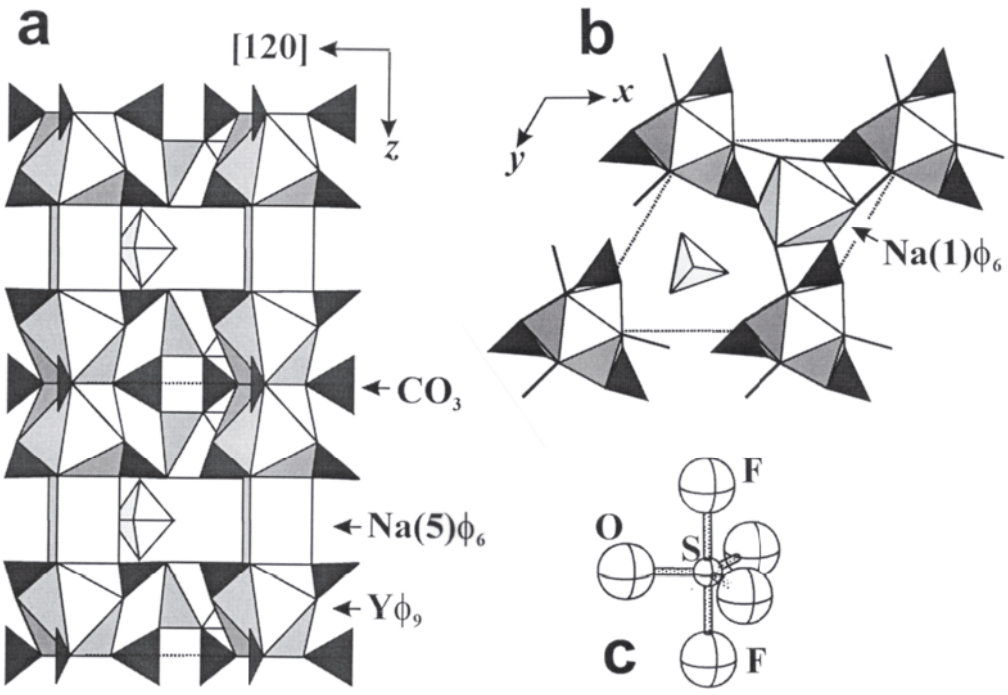

Figure 58. The structure of the fluorosulfate mineral reederite-(Y): (a) projected along [100]; (b) projected along [001]; the Na(2), Na(3) and Na(4) cations are omitted for clarity; the disordered (SO_3F) fluorosulfate anion is shown.

vertices of a plane hexagonal net (Fig. 57h). Prominent six-membered rings of (SiO_4) tetrahedra (Fig. 57h) are linked in the [001] direction by rings of ($NaØ_7$) and ($CeØ_9$) polyhedra to form hollow tubes; within these tubes are (CO_3) groups, ($NaØ_6$) octahedra, and orientationally disordered ($S^{4+}O_3$) groups (Fig. 57i). These filled tubes are linked in the (001) plane by chains of ($NaØ_7$) and (PO_4) polyhedra.

FLUOROSULFATE MINERALS

Only one fluorosulfate mineral is known (Table 19). **Reederite-(Y)**, ideally $Na_{15}Y_2(CO_3)_9(SO_3F)Cl$, is layered on {001}, similar to many other REE carbonates (Grice et al. 1994). The Y occupies a [9]-coordinated site that links to (CO_3) groups arranged both parallel to {001} and at an oblique angle to [001] (Fig. 58a). The ($YØ_9$) and ($NaØ_6$) groups form columns parallel to [001] that occur at the nodes of a plane hexagonal net (Fig. 58b), and are linked by columns of ($NaØ_n$) polyhedra and (SO_3F) groups (Fig. 58c). Note that the ideal formula has one excess positive charge; it is not clear how this is actually compensated in the observed structure.

ACKNOWLEDGMENTS

This work was funded by Natural Sciences and Engineering Research Council of Canada Grants to FCH, by the Environmental Management Sciences Program of the United States Department of Energy grant DE-FG07-97ER14820 to PCB, and by the National Science Foundation NATO Fellowship in Science and Engineering DGE99-03354 to SVK and PCB.

APPENDIX

Index of mineral names and the table numbers in which they appear

Appendix cont'd

lautenthallite (9)
lawsonbauerite (9)
leadhillite (16)
lecontite (14)
leightonite (7)
leonite (7)
letovicite (14)
linarite (8)
liottite (17)
lonecreekite (6)
löweite (12)
macphersonite (16)
magnesioaubertite (5)
magnesiocopiapite (8)
mallardite (5)
mammothite (12)
manganolangbeinite (12)
manganotychite (12)
mascagnite (14)
matteuccite (14)
melanterite (5)
mendozite (6)
mercallite (14)
mereiterite (7)
metasideronatrite (8)
metavoltine (7)
microsommite (17)
mikasaite (12)
millosevichite (12)
minamiite (10)
minasragrite (7)
mineevite-(Y) (14)
mirabilite (14)
mohrite (6)
mooreite (9)
moorhouseite (5)
morenosite (5)
mosesite (18)
motukoreaite (9)
mountkeithite (9)
nabokoite (18)
namuwite (9)
natroalunite (10)
natrochalcite (11)
natrojarosite (10)
nickelblödite (7)
nickelboussingaultite (6)
niedermayrite (9)
nickelhexahydrite (5)
nosean (17)
olsacherite (15)
orschallite (13,19)
orthoserpierite (9)
osarizawaite (10)
palmierite (14)
parabutlerite (8)
paracoquimbite (7)
pentahydrite (8)
peretaite (16)
philolithite (12)
pickeringite (7)
picromerite (6)
pitiglianoite (17)
piypite (18)
plumbojarosite (10)
poitevinite (12)
polyhalite (7)
posnjakite (9)
potassium alum (6)
poughite (11)
queitite (16)
quenstedtite (7)
ramsbeckite (9)
ransomite (11)
rapidscreekite (13)
reederite-(Y) (19)
retgersite (5)
rhomboclase (11)
roeblingite (16)
roemerite (7)
rozenite (7)
sarcofanite (17)
schairerite (15)
schaurteite (6)
schlossmacherite (10)
schröckingerite (16)
schuetteite (18)
schulenbergite (9)
scotlandite (19)
serpierite (9)
shigaite (9)
sideronatrite (8)
siderotil (8)
sidpietersite (18,19)
slavikite (10)
sodium alum (6)
spangolite (9)
starkeyite (7)
sturmanite (6)
svanbergite (10)
sulphohalite (15)
susannite (16)
svyazhinite (5)
syngenite (13)
szmikite (12)
szomolnokite (12)
tamarugite (6)
ternesite (13)
thaumasite (6)
thenardite (14)
torreyite (9)
tounkite (17)
tschermigite (6)
tsumebite (8)
tuscanite (16)
tychite (12)
uklonskovite (8)
ungemachite (7)
vanthoffite (11)
vergasovaite (18)
vishnevite (17)
viaeneite (12)
vlodavetsite (12)
voltaite (12)
vonbenzingite (16)
walthierite (10)
wermlandite (9)
wherryite (8)
woodhouseite (10)
woodwardite (9)
wroewolfeite (9)
wupatkiite (7)
xitieshanite (7)
yavapaite (11)
zincobotryogen (8)
zincocopiapite (8)
zincosite (12)
zincovoltaite (12)
zippeite (16)
zircosulfate (16)
zinc-melanterite (5)

REFERENCES

Abdeen AM, Will G, Schaefer W, Kirfel A, Bargouth MO, Recker K, Weiss A (1981) X-ray and neutron diffraction study of alums: III. The crystal structure of ammonium aluminium alum. Z Kristallogr 157:147-166

Abriel W, Nesper R (1993) Bestimmung der Kristallstruktur von $CaSO_4(H_2O)_{0.5}$ mit Röntgen-beugungsmethoden und mit Potentialprofil-Rechnungen. Z Kristallogr 205:99-113

Adams DC, Birchall T, Faggiani R, Gillespie RJ, Vekris JE (1991) The ^{119}Sn Mössbauer and solid-state NMR and the crystal and molecular structure of tin(II) bisfluorosulfate, $Sn(OSO_2F)_2$. Can J Chem 69:2122-2126

Adiwidjaja G, Friese K, Klaska K-H, Schlüter J (1996) The crystal structure of christelite $Zn_3Cu_2(SO_4)_2(OH)_6{\cdot}4(H_2O)$. Z Kristallogr 211:518-521

Adiwidjaja G, Friese K, Klaska K-H, Schlüter J (1997) The crystal structure of gordaite $NaZn_4SO_4(OH)_6Cl_6(H_2O)$. Z Kristallogr 212:704-707

Airoldi R, Magnano G (1967) Sulla struttura del solfato (di)mercurioammonico. Rassegna Chimica 5: 181-189

Aka Y, Armağan N, Uraz AA (1980) An X-ray diffraction study of barium thiosulphate monohydrate, $BaS_2O_3{\cdot}H_2O$. Z Kristallogr 151:61-66

Allmann R (1977) Refinement of the hybrid layer structure $(Ca_2Al(OH)_6)^+(0.5SO_4{\cdot}3H_2O)^-$. N Jahrb Mineral Monatsh 136-144

Allred AL, Rochow E (1958) A scale of electronegativity based on electrostatic force. J Inorg Nucl Chem 5:264-268

Araki T, Zoltai T (1967) Refinement of the crystal structure of a glauberite. Am Mineral 52:1272-1277

Bachmann HG (1953) Beiträge zur Kristallchemie natürlicher und künstlicher Schwermetallvanadate: III. Das Bleiorthovanadat, seine Darstellung, Kristallstruktur und Isotypiebeziehungen. N Jahrb Mineral Monatsh 209-223

Bacon GE, Titterton DH (1975) Neutron diffraction studies of $CuSO_4(H_2O)_5$ and $CuSO_4(D_2O)_5$. Z Kristallogr 141:330-341

Baggio S, Pardo MI, Baggio R, Gonzalez O (1997) Cadmium thiosulfate dihydrate. Acta Crystallogr C53:1521-1523

Balic Zunic T, Moëlo Y, Loncar Z, Micheelsen H (1994) Dorallcharite, $Tl_{0.8}K_{0.2}Fe_3$ $(SO_4)_2(OH)_6$, a new member of the jarosite-alunite family. Eur J Mineral 6:255-263

Ballhorn R, Brunner H, Schwab RG (1989) Artificial compounds of the crandallite type: a new material for separation and immobilization of fission products. Sci Basis Nucl Waste Manag 12:249-252

Ballirano P, Merlino S, Bonaccorsi E, Maras A (1996) The crystal structure of liottite, a six-layer member of the cancrinite group. Can Mineral 34:1021-1030

Ballirano P, Bonaccorsi E, Maras A, Merlino S (1997) Crystal structure of afghanite, the eight-layer member of the cancrinite-group: evidence for long-range Si, Al ordering. Eur J Mineral 9:21-30

Bartell LS, Su LS, Yow H (1970) Lengths of phosphorus-oxygen and sulfur-oxygen bonds. An extended Hückel molecular orbital examination of Cruickshank's d_π–p_π picture. Inorg Chem 9:1903-1912

Bartlett N, Wechsberg M, Jones GR, Burbank RD (1972) The crystal structure of xenon(II) fluoride fluorosulfate, $FXeOSO_2F$. Inorg Chem 11:1124-1127

Bartmann K, Mootz D (1990) Structures of two strong broensted acids: (I) fluorosulfuric acid and (II) trifluoromethanesulfonic acid. Acta Crystallogr C46:319-320

Basso R, Lucchetti G, Palenzona A (1991) Gravegliaite, $MnSO_3{\cdot}2H_2O$, a new mineral from Val Graveglia (Northern Apennines, Italy). Z Kristallogr 197:97-106

Baur WH (1960) Die Kristallstruktur von $FeSO_4{\cdot}4H_2O$. Naturwiss 47:467

Baur WH (1962) Zur Kristallchemie der Salzhydrate. Die Kristallstrukturen von $MgSO_4{\cdot}4H_2O$ (Leonhardtit) und $FeSO_4{\cdot}4H_2O$ (Rozenit). Acta Crystallogr 15:815-826

Baur WH (1964) On the crystal chemistry of salt hydrates: III. The determination of the crystal structure of $FeSO_4{\cdot}7H_2O$ (melanterite). Acta Crystallogr 17:1167-1174

Baur WH, Rolin JL (1972) Salt hydrates. IX. The comparison of the crystal structure of magnesium sulfate pentahydrate with copper sulfate pentahydrate and magnesium chromate pentahydrate. Acta Crystallogr B28:1448-1455

Bayliss P, Atencio D (1985) X-ray powder-diffraction data and cell parameters for copiapite-group minerals. Can Mineral 23:53-56

Bergerhoff G, Paeslack (1968) Sauerstoff als Koordinationszentrum in Kristallstrukturen. Z Kristallogr 126:112-123

Berlepsch P, Armbruster Th, Brugger J, Bykova EY, Kartashov PM (1999) The crystal structure of vergasovaite $Cu_3O[(Mo,S)O_4SO_4]$, and its relation to synthetic $Cu_3O[MoO_4]_2$. Eur J Mineral 11: 101-110

Birchall T, Denes G, Faggiani R, Frampton CS, Gillespie RJ, Kapoor R, Vekris JE (1990) Crystal and molecular structure and Raman and ^{127}I Mössbauer spectra of iodine(III) bis(fluorosulfate) iodide $I(OSO_2F)_2I$. Inorg Chem 29:1527-1530

Blades AT, Kebarle P (1994) Study of the stability and hydration of doubly charged ions in the gas phase: SO_4^{2-}, $S_2O_6^{2-}$, $S_2O_8^{2-}$, and some related species. J Amer Chem Soc 116:10761-10766

Bokii GB, Gorogotskaya LI (1965) The crystal structure of chukhrovite. Dokl Akad Nauk SSSR 163: 183-185 (in Russian)

Bokii GB, Gorogotskaya LI (1969) Crystal chemical classification of sulfates. Zhurnal Strukt Khim 10:624-632 (in Russian)

Bokii GB, Pal'chik NA, Antipin MYu (1978) More precise determination of syngenite crystal structure. Trudy Inst Geol Geofiz Akad Nauk SSSR, Sibir Otd 385:3-7 (in Russian)

Boldyrev A, Simons J (1994) Isolated SO_4^{2-} and PO_4^{3-} do not exist. J Phys Chem 98:2298-2300

Bonaccorsi E, Merlino S, Pasero M (1990) Davyne: Its structural relationships with cancrinite and vishnevite. N Jahrb Mineral Monatsh 97-112

Bookin AS, Drits VA (1993) Polytype diversity of the hydrotalcite-like minerals. I. Possible polytypes and their diffraction features. Clays Clay Minerals 41:551-557

Bookin AS, Cherkashin VI, Drits VA (1993) Polytype diversity of the hydrotalcite-like minerals. II. Determination of the polytypes of experimentally studied varieties. Clays Clay Minerals 41:558-564

Borene J (1970) Structure cristalline de la parabutlerite. Bull Soc franc Minéral Cristallogr 93:185-189

Bowen NL (1928) The evolution of igneous rocks. Princeton University Press, Princeton, New Jersey

Bragg WL (1930) The structure of silicates. Z Kristallogr 74:237-305

Braithwaite RSW, Kampf AR, Pritchard RG, Lamb RPH (1993) The occurrence of thiosulfates and other unstable sulfur species as natural weathering products of old smelting slags. Mineral Petrol 47:255-261

Breidenstein B, Schlüter J, Gebhard G (1992) On beaverite: new occurrence, chemical data and crystal structure. N Jahrb Mineral Monatsh 213-220

Brese NE, O'Keeffe M (1991) Bond-valence parameters for solids. Acta Crystallogr B47:192-197

Brown ID (1981) The bond-valence method: an empirical approach to chemical structure and bonding. *In* O'Keeffe M, Navrotsky A (Eds) Structure and bonding in crystals. Academic Press, New York, 2:1-30

Brown ID, Shannon RD (1973) Empirical bond strength—bond length curves for oxides. Acta Crystallogr A29:266-282

Burdett JK, Hawthorne FC (1993) An orbital approach to the theory of bond valence. Am Mineral 78: 884-892

Burns PC (1999) The crystal chemistry of uranium. Rev Mineral 38:23-90

Burns PC, Hawthorne FC (1994) The crystal structure of humberstonite, a mixed sulfate-nitrate mineral. Can Mineral 32:381-385

Burns PC, Grice JD, Hawthorne FC (1995) Borate minerals: I. Polyhedral clusters and fundamental building blocks. Can Mineral 33:1131-1151

Burns PC, Miller ML, Ewing RC (1996) U^{6+} minerals and inorganic phases: a comparison and hierarchy of structures. Can Mineral 34:845-880

Burns PC, Roberts AC, Nikischer AJ (1998) The crystal structure of $Ca[Zn_8(SO_4)_2(OH)_{12}Cl_2](H_2O)_9$, a new phase from slag dumps at Val Varenna, Italy. Eur J Mineral 10:923-930

Burzlaff H (1967) Die Struktur des Heidornit, $Ca_3Na_2Cl(SO_4)_2B_5O_8(OH)_2$. N Jahrb Mineral Monatsh 157-169

Calleri M, Gavetti A, Ivaldi G, Rubbo M (1984) Synthetic epsomite, $MgSO_4(H_2O)_7$: Absolute configuration and surface features of the complementary (111) forms. Acta Crystallogr B40:218-222

Cannillo E, dal Negro A, Rossi G (1973) The crystal structure of latiumite, a new type of sheet silicate. Am Mineral 58:466-470

Catti M, Ferraris G, Franchini-Angela M (1975) Hydrogen bonding in the crystalline state. $NaHSO_4H_2O$ (matteuccite), a pseudo-symmetric crystal structure. Atti Accad Sci Torino Fis Matem Natur 109:531-545

Chesnokov BV, Bazhenova LF, Bushmakin AF (1987a) Fluorellestadite $Ca_{10}[(SO_4),(SiO_4)]_6F_2$—a new mineral. Zapiski Vses Mineral Obshch 116:743-746 (in Russian)

Chesnokov BV, Polyakov VO, Bushmakin AF (1987b) Bazhenovite $CaS_5 \cdot CaS_2O_3 \cdot 6Ca(OH)_2 \cdot 20H_2O$: A new mineral. Zapiski Vses Mineral Obshch 116:737-743 (in Russian)

Christidis PC, Rentzeperis PJ (1985) Experimental charge density in polythionate anions I. X-ray study of electron density distribution in potassium trithionate, $K_2S_3O_6$. Z Kristallogr 173:59-74

Christidis P, Rentzeperis PJ, Kirfel A, Will G (1983) X-ray determination of the electron density distribution in monoclinic ferric sulfate. Z Kristallogr 164:219-236

Collins MJ, Gillespie RJ, Sawyer JF, Schrobilgen GJ (1986) Decaselenium bis(fluorosulfate). Acta Crystallogr C42:13-16

Cooper MA, Hawthorne FC (1994) The crystal structure of wherryite, $Pb_7Cu_2(SO_4)_4(SiO_4)_2(OH)_2$, a mixed sulfate–silicate with $(M(TO_4)Ø_2)$ chains. Can Mineral 32:373-380

Cooper MA, Hawthorne FC (1996a) The crystal structure of rapidcreekite, $Ca_2(SO_4)(CO_3)(H_2O)_4$, and its relation to the structure of gypsum. Can Mineral 34:99-106

Cooper MA, Hawthorne FC (1996b) The crystal structure of shigaite, $(AlMn^{2+}{}_2(OH)_6)_3(SO_4)_2 Na(H_2O)_6(H_2O)_6$, a hydrotalcite-group mineral. Can Mineral 34:91-97

Cooper MA, Hawthorne FC (1999) The structure topology of sidpietersite, $Pb^{2+}{}_4(S^{6+}O_3S^{2-})O_2(OH)_2$, a novel thiosulfate structure. Can Mineral 37:1275-1282

Corazza E, Sabelli C, Giuseppetti G (1967) The crystal structure of lecontite, $NaNH_4SO_4(H_2O)_2$. Acta Crystallogr 22:683-687

Cromer DT, Kay MI, Larson AC (1967) Refinement of the alum structures. II. X-ray and neutron diffraction of $NaAl(SO_4)_2{\cdot}(H_2O)_{12}$, γ-alum. Acta Crystallogr 22:182-187

Cruickshank DWJ (1961) The role of 3d-orbitals in p-bonds between (a) silicon, phosphorus, sulfur, or chlorine to (b) oxygen or nitrogen. J Chem Soc 1961:5486-5504

Cruickshank DWJ (1985) A reassessment of d-p bonding in the tetrahedral oxyanions of second-row atoms. J Mol Struct 130:177-91

Cruickshank DWJ, Eisenstein M (1985) The role of d functions in *ab initio* calculations. Part 1. The deformation densities of sulfamic acid and SO_3^-. J Mol Struct 130:143-56

Cruickshank DWJ, Eisenstein M (1987) The role of d functions in *ab initio* calculations. II. The deforma-tion densities of sulfur dioxide, nitrogen dioxide, and their ions. J Comput Chem 8:6-27

Dahmen T, Gruehn R (1993) Beitrage zum thermischen Verhalten von Sulfaten. IX. Einkristall-strukturverfeinerung der Metall(III)-sulfate $Cr_2(SO_4)_3$ und $Al_2(SO_4)_3$. Z Kristallogr 204:57-65

Dai Y, Harlow GE (1992) Description and crystal structure of vonbezingite, a new Ca-Cu-SO_4-H_2O mineral from the Kalahari manganese field, South Africa. Am Mineral 77:1292-1300

Deganello S (1983) The crystal structure of cesanite at 21 and 263°C. N Jahrb Mineral Monatsh 305-313

Duesler EN, Foord EE (1986) Crystal structure of hashemite, $BaCrO_4$, a barite structure type. Am Mineral 71:1217-1220

Eby RK, Hawthorne FC (1993) Structural relations in copper oxysalt minerals. I. Structural hierarchy. Acta Crystallogr B49:28-56

Effenberger H (1985a) $Cu_2O(SO_4)$, dolerophanite: refinement of the crystal structure with a comparison of $OCu(II)_4$ tetrahedra in inorganic compounds. Monatsh Chem 116:927-931

Effenberger H (1985b) The crystal structure of mammothite, $Pb_6Cu_4AlSbO_2(OH)_{16}Cl_4(SO_4)_2$. Tschermaks mineral petrogr Mitt 34:279-288

Effenberger H (1987) Crystal structure and chemical formula of schmiederite, $Pb_2Cu_2(OH)_4(SeO_3)(SeO_4)$, with a comparison to linarite $PbCu(OH)_2(SO_4)$. Mineral Petrol 36:3-12

Effenberger H (1988) Ramsbeckite, $(Cu,Zn)_{15}(OH)_{22}(SO_4)_4(H_2O)_6$: Revision of the chemical formula based on a structure determination. N Jahrb Mineral Monatsh 38-48

Effenberger H, Zemann J (1984) The crystal structure of caratiite. Mineral Mag 48:541-546

Effenberger H, Pertlik F, Zemann J (1986) Refinement of the crystal structure of krausite: a mineral with an interpolyhedral oxygen-oxygen contact shorter than the hydrogen bond. Am Mineral 71:202-205

Egorov-Tismenko YuK, Sokolova EV, Smirnova NL, Yamnova NA (1984) Crystal chemical features of minerals related to the glaserite structure type. Mineral Zhurnal 6(6):3-9

Elerman Y, Uraz AA, Armagan N (1978) An X-ray diffraction study of nickel thiosulphate hexahydrate. Acta Crystallogr B34:3330-3332

Elerman Y, Bats JW, Fuess H (1983) Deformation density in complex anions: IV. Magnesium thiosulfate hexahydrate, $MgS_2O_3{\cdot}6H_2O$. Acta Crystallogr C39:515-518

Evsyunin VG, Sapozhnikov AN, Rastsvetaeva RK, Kashaev AA (1996) Crystal structure of the potassium-rich hauyne from Arissia (Italy). Kristallografiya 41:659-662 (in Russian)

Eysel W (1973) Crystal chemistry of the system Na_2SO_4–K_2SO_4–K_2CrO_4–Na_2CrO_4 and of the glaserite phase. Am Mineral 58:736-747

Fanfani L, Zanazzi PF (1967) Structural similarities of some secondary lead minerals. Mineral Mag 36: 522-529

Fanfani L, Nunzi A, Zanazzi PF (1970) The crystal structure of roemerite. Am Mineral 55:78-89

Fanfani L, Nunzi A, Zanazzi PF (1971) The crystal structure of butlerite. Am Mineral 56:751-757

Fanfani L, Nunzi A, Zanazzi PF, Zanzari AR (1973) The copiapite problem: the crystal structure of a ferrian copiapite. Am Mineral 58:314-322

Fanfani L, Nunzi A, Zanazzi PF, Zanzari AR, Sabelli C (1975a) The crystal structure of schairerite and its relationship to sulphohalite. Mineral Mag 40:131-139

Fanfani L, Nunzi A, Zanazzi PF, Zanzari AR (1975b) The crystal structure of galeite, $Na_{15}(SO_4)_5F_4Cl$. Mineral Mag 40:357-361

Fanfani L, Giuseppetti G, Tadini C, Zanazzi PF (1980) The crystal structure of kogarkoite, Na_3SO_4F. Mineral Mag 43:753-759

Fang JH, Robinson PD (1970a) Crystal structures and mineral chemistry of hydrated ferric sulfates. I. The crystal structure of coquimbite. Am Mineral 55:1534-1540

Fang JH, Robinson PD (1970b) Crystal structures and mineral chemistry of double-salt hydrates. I. The crystal structure of loeweite. Am Mineral 55:378-386

Fang JH, Robinson PD (1972) Crystal structures and mineral chemistry of double-salt hydrates: II. The crystal structure of mendozite, $NaAl(SO_4)_2(H_2O)_{11}$. Am Mineral 57:1081-1088

Farkas L, Pertlik F (1997) Crystal structure determinations of felsöbányaite and basaluminite, $Al_4(SO_4)(OH)_{10}\cdot 4H_2O$. Acta Mineral Petrogr Szeged 38:5-15

Figgis BN, Kepert CJ, Kucharski ES, Reynolds PA (1992) Charge-density study of deuterated ammonium ferrous Tutton salt at 85 K and comparison with Cr(II) and Cu(II) salts. Acta Crystallogr B48:753-761

Filatov SK, Semenova TF, Vergasova LP (1992) Types of polymerization of $[OCu_4]^{6+}$ tetrahedra in compounds with 'additional' oxygen atoms. Proc Acad Sci USSR 322:536-539 (in Russian)

Fischer W, Hellner E (1964) Über die Struktur des Vanthoffits. Acta Crystallogr 17:1613

Fleet ME, Knipe SW (1997) Structure of magnesium hydroxide sulfate $[2MgSO_4\cdot Mg(OH)_2]$ and solid solution in magnesium hydroxide sulfate hydrate and caminite. Acta Crystallogr B53:358-363

Gaines RV, Skinner HCW, Foord EE, Mason B, Rosenzweig A, King VT (1997) Dana's new mineralogy. Wiley, New York

Galy J, Jaud J, Pulou R, Sempere R (1984) Structure cristalline de la langite, $Cu_4(SO_4(OH)_6H_2O)H_2O$. Bull Minéral 107:641-648

Gaudefroy C, Granger MM, Permingeat F, Protas J (1968) La despujolsite, une nouvelle espece minerale. Bull Soc franc Minéral Cristallogr 91:43-50

Giacovazzo C, Menchetti S (1969) Sulla struttura della amarantite. Rend Soc Ital Mineral Petrol 25:399-406

Giacovazzo C, Menchetti S, Scordari F (1973) The crystal structure of caledonite, $CuPb_5(SO_4)_3CO_3(OH)_6$. Acta Crystallogr B29:1986-1990

Giacovazzo G, Scordari F, Todisco A, Menchetti S (1976a) Crystal structure model for metavoltine from Sierra Gorda. Tschermaks mineral petrogr Mitt 23:155-166

Giacovazzo C, Scandale E, Scordari F (1976b) The crystal structure of chlorothionite $CuK_2Cl_2SO_4$. Z Kristallogr 144:226-237

Gibbs GV (1982) Molecules as models for bonding in solids. Am Mineral 67:421-450

Gibbs GV, Hamil MM, Louisnathan SJ, Bartell LS, Yow H (1972) Correlations between SiBO bond length, SiBOBSi angle and bond overlap populations calculated using extended Hückel molecular orbital theory. Am Mineral 57:1578-1613

Giese RF Jr, Penna G (1983) The crystal structure of sulfoborite, $Mg_3SO_4(B(OH)_4)_2(OH)F$. Am Mineral 68:255-261

Giester G, Rieck B (1995) Mereiterite, $K_2Fe(SO_4)_2\cdot 4(H_2O)$, a new leonite-type mineral from the Lavrion Mining District, Greece. Eur J Mineral 7:559-566

Giester G, Rieck B (1996) Bechererite, $(Zn,Cu)Zn_2(OH)_{13}((S,Si)(O,OH)_4)_2$, a novel mineral species from the Tonopah-Belmont mine, Arizona. Am Mineral 81:244-248

Giester G, Zemann J (1987) The crystal structure of the natrochalcite-type compounds $(Me^+)Cu_2(OH)(ZO_4)_2\cdot H_2O$ (Me^+ = Na, K, Rb; Z = S, Se), with special reference to the hydrogen bonds. Z Kristallogr 179:431-442

Giester G, Lengauer CL, Redhammer G (1994) Characterization of the $FeSO_4\cdot(H_2O)$–$CuSO_4\cdot(H_2O)$ solid-solution series, and the nature of poitevinite, $(Cu,Fe)SO_4\cdot(H_2O)$. Can Mineral 32:873-884

Giester G, Mikenda W, Pertlik F (1996) Kleinite from Terlingua, Brewster County, Texas: investigations by single crystal X-ray diffraction, and vibrational spectroscopy. N Jahrb Mineral Monatsh 49-56

Giester G, Rieck B, Brandstatter F (1998) Niedermayrite, $Cu_4Cd(SO_4)_2(OH)_6\cdot 4H_2O$, a new mineral from the Lavrion Mining District, Greece. Mineral Petrol 63:19-34

Gillespie RJ, Schrobilgen GJ, Slim DR (1977) Crystal structure of mue-fluorosulphato-bis(fluoroxenon(II)-hexafluoroarsenate(V). J Chem Soc Dalton Trans 1977:1003-1006

Gillespie RJ, Kent JP, Sawyer JF, Slim DR, Tyrer JD (1981a) Reactions of S_4N_4 with $SbCl_5$, SbF_5, AsF_5, PF_5 and HSO_3F. Preparation and crystal structures of salts of the $S_4N_4^{2+}$ cation. Inorg Chem 20: 3799-3812

Gillespie RJ, Kent JP, Sawyer JF (1981b) Monomeric and dimeric thiodithiazyl cations, S_3N^{2+} and $(S_6N_4)^{2+}$: Preparation and crystal structure of $(S_3N_2)(AsF_6)$, $(S_6N_4)(S_2O_2F)_2$ and $(S_6N_4)(SO_3F)_2$. Inorg Chem 20:3784-3799

Ginderow D, Cesbron F (1979) Structure cristalline de l'aubertite, $AlCuCl(SO_4)_2(H_2O)_{14}$. Acta Crystallogr B35:2499-2502

Giuseppetti G, Tadini C (1980) The crystal structure of osarizawaite. N Jahrb Mineral Monatsh 401-407

Giuseppetti G, Tadini C (1983) Structural analysis and refinement of Bolivian creedite, $Ca_3Al_2F_8(OH)_2(SO_4)\cdot(H_2O)_2$. The role of the hydrogen atoms. N Jahrb Mineral Monatsh 69-78

Giuseppetti G, Tadini C (1987) Corkite, $PbFe_3(SO_4)(PO_4)(OH)_6$, its crystal structure and ordered arrangement of the tetrahedral cations. N Jahrb Mineral Monatsh 71-81

Giuseppetti G, Mazzi F, Tadini C (1988) The crystal structure of synthetic burkeite. N Jahrb Mineral Monatsh 203-221

Giuseppetti G, Mazzi F, Tadini C (1990) The crystal structure of leadhillite: $Pb_4(SO_4)(CO_3)_2(OH)_2$. N Jahrb Mineral Monatsh 255-268

Gjerrestad K, Marøy K (1973) The crystal structure of barium telluropentathionate trihydrate. Acta Chem Scand 27:1653-1666

Golic L, Graunar M, Lazarini F (1982) Catena-di-mue-hydroxo-$_3$-oxo-dibismuth(III) sulfate. Acta Crystallogr B38:2881-2883

Gorskaya MG, Filatov SK, Rozhdestvenskaya IV, Vergasova LP (1992) The crystal structure of klyuchevskite, $K_3Cu_3(Fe,Al)O_2(SO_4)_4$, a new mineral from Kamchatka volcanic sublimates. Mineral Mag 56:411-416

Graeber EJ, Rosenzweig A (1971) The crystal structures of yavapaiite, $KFe(SO_4)_2$, and goldichite, $KFe(SO_4)_2(H_2O)_4$. Am Mineral 56:1917-1933

Granger MM (1969) Determination et etude de la structure cristalline de la jouravskite $Ca_3Mn(SO_4)(CO_3)(OH)(H_2O)_{12}$. Acta Crystallogr B25:1943-1951

Grice JD, Van Velthuizen J, Gault RA (1994) Petersenite-(Ce), a new mineral from Mont Saint-Hilaire, and its structural relationship to other REE carbonates. Can Mineral 32:405-414

Grice JD, Gault RA, Chao GY (1995) Reederite-(Y), a new sodium rare-earth carbonate mineral with a unique fluorosulfate anion. Am Mineral 80:1059-1064

Grice JD, Burns PC, Hawthorne FC (1999) Borate minerals: II. A hierarchy of structures based upon the borate fundamental building block. Can Mineral 37:731-762

Griffen DT, Ribbe PH (1979) Distortions in the tetrahedral oxyanions of crystalline substances. Neues Jahrb Mineral Abh 137:54-73

Groat LA (1996) The crystal structure of namuwite, a mineral with Zn in tetrahedral and octahedral coordination, and its relationship to the synthetic basic zinc sulfates. Am Mineral 81:238-243

Groat LA, Hawthorne FC (1986) Structure of ungemachite, $K_3Na_8Fe^{3+}(SO_4)_6(NO_3)_2(H_2O)_6$ a mixed sulfate-nitrate mineral. Am Mineral 71:826-829

Hasebe K (1981) Studies of the crystal structure of ammonium sulfate in connection with its ferroelectric phase transition. J Phys Soc Japan 50:1266-1274

Hassan I, Grundy HD (1984) The character of the cancriniteBvishnevite solid-solution series. Can Mineral 22:333-340

Hassan I, Grundy HD (1989) The structure of nosean, ideally $Na_8(Al_6Si_6O_{24})SO_4H_2O$. Can Mineral 27: 165-172

Hawthorne FC (1979) The crystal structure of morinite. Can Mineral 17:93-102

Hawthorne FC (1983a) Graphical enumeration of polyhedral clusters. Acta Crystallogr A39:724-736

Hawthorne FC (1983b) The crystal structure of tancoite. Tschermaks mineral petrogr Mitt 31:121-135.

Hawthorne FC (1984) The crystal structure of stenonite, and the classification of the aluminofluoride minerals. Can Mineral 22:245-251

Hawthorne FC (1985a) Towards a structural classification of minerals: The $^{VI}M^{IV}T_2O_n$ minerals. Am Mineral 70:455-473

Hawthorne FC (1985b) Refinement of the crystal structure of blödite: structural similarities in the $[^{VI}M(^{IV}T\Ø_4)_2\Ø_n]$ finite-cluster minerals. Can Mineral 23:669-674

Hawthorne FC (1986) Structural hierarchy in $^{IV}M_x^{III}T_y\Ø_z$ minerals. Can Mineral 24:625-642

Hawthorne FC (1990) Structural hierarchy in $M^{[6]}T^{[4]}\Ø_n$ minerals. Z Kristallogr 192:1-52

Hawthorne FC (1992) The role of OH and H_2O in oxide and oxysalt crystals. Z Kristallogr 201:183-206

Hawthorne FC (1994) Structural aspects of oxide and oxysalt crystals. Acta Crystallogr B50:481-510

Hawthorne FC (1997) Structural aspects of oxide and oxysalt minerals. *In* Merlino (Ed) Modular aspects of minerals. EMU (European Mineralogical Union) Notes in Mineralogy 1:373-429

Hawthorne FC, Ferguson RB (1975a) Anhydrous sulfates. II. Refinement of the crystal structure of anhydrite. Can Mineral 13:289-292

Hawthorne FC, Ferguson RB (1975b) Anhydrous sulphates. I. Refinement of the crystal structure of celestite with an appendix on the structure of thenardite. Can Mineral 13:181-187

Hawthorne FC, Ferguson RB (1975c) Refinement of the crystal structure of kroehnkite. Acta Crystallogr B31:1753-1755

Hawthorne FC, Groat LA (1985) The crystal structure of wroewolfeite, a mineral with $[(Cu_4(OH)_6(SO_4)(H_2O)]$ sheets. Am Mineral 70:1050-1055

Hawthorne FC, Schindler MS (2000) Topological enumeration of decorated $[Cu^{2+}Ø_2]_N$ sheets in hydroxy-hydrated copper oxysalt minerals. Can Mineral 38 (in press)

Hawthorne FC, Groat LA, Raudsepp M, Ercit TS (1987) Kieserite, $MgSO_4(H_2O)$, a titanite-group mineral. N Jahrb Mineral Abh 157:121-132

Hawthorne FC, Groat LE, Eby RK (1989) Antlerite, $Cu_3SO_4(OH)_4$, a heteropolyhedral wallpaper structure. Can Mineral 27:205-209

Hawthorne FC, Kimata M, Eby RK (1993) The crystal structure of spangolite, a complex copper sulfate sheet mineral. Am Mineral 78:649-652

Hawthorne FC, Burns PC, Grice JD (1996) The crystal chemistry of boron. *In* Grew ES, Anobitz LM (Eds) Boron: Mineralogy, petrology and geochemistry. Rev Mineral 33:41-115

Haymon RM, Kastner M (1986) Caminite: A new magnesium-hydroxide-sulfate-hydrate mineral found in a submarine hydrothermal deposit, East Pacific Rise, 21EN. Am Mineral 71:819-825

Helliwell M, Smith JV (1997) Brochantite. Acta Crystallogr C53:1369-1371

Hess H, Keller P (1980) Die Kristallstruktur von Queitit, $Pb_4Zn_2(SO_4)(SiO_4)(Si_2O_7)$. Z Kristallogr 151:287-299

Hess H, Keller P, Riffel H (1988) The crystal structure of chenite, $Pb_4Cu(OH)_6(SO_4)_2$. N Jahrb Mineral Monatsh 259-264

Hesse W, Leutner B, Boehn KH, Walker NPC (1993) Structure of a new sodium thiosulfate hydrate. Acta Crystallogr C49:363-365

Hexiong Y, Pingqiu F (1988) Crystal structure of zincobotryogen. Kuangwu Xuebao 8:1-12

Hill RJ (1980) The structure of mooreite. Acta Crystallogr B36:1304-1311

Hill FC, Gibbs GV, Boisen MBJr (1997) Critical point properties of electron density distributions for oxide molecules containing first and second row cations. Phys Chem Minerals 24:582-596

Hochella MFJr, Keefer KD, de Jong BHWS (1983) The crystal chemistry of a naturally occuring magnesium hydroxide sulfate hydrate, a precipitate of heated seawater. Geochim Cosmochim Acta 47:2053-2058

Hoenle W (1991) Crystal structure of $H_2S_2O_7$ at 298 K. Z Kristallogr 196:279-288

Hoffmann C, Armbruster T, Giester G (1997) Acentric structure (*P*3) of bechererite, $Zn_7Cu(OH)_{13}(SiO(OH)_3SO_4)$. Am Mineral 82:1014-1018

Hughes JM, Drexler JW (1991) Cation substitution in the apatite tetrahedral site: Crystal structures of type hydroxylellestadtite and type fermorite. N Jahrb Mineral Monatsh 327-336

Hyde B, Andersson S (1989) Inorganic crystal structures. Wiley, New York

Hurlbut CS Jr, Aristarain LF (1969) Olascherite, $Pb_2(SO_4)(SeO_4)$, a new mineral from Bolivia. Am Mineral 54:1519-1527

Irran E, Tillmanns E, Hentschel G (1997) Ternesite, $Ca_5(SiO_4)_2SO_4$, a new mineral from the Ettringer Bellerberg/Eifel, Germany. Mineral Petrol 60:121-132

Iskhakova LD, Dubrovinskii LS, Charushnikova IA (1991) Crystal structure, calculation of parameters of atomic interaction potential and thermochemical properties of $NiSO_4 \cdot nH_2O$ (n = 7,6). Kristallografiya 36:650-655 (in Russian)

Jacobsen SD, Smyth JR, Swope RJ, Downs RT (1998) Rigid-body character of the SO_4 groups in celestine, anglesite and barite. Can Mineral 36:1053-1060

Jambor JL (1999) Nomenclature of the alunite supergroup. Can Mineral 37:1323-1341

Jambor JL, Owens DR, Grice JD, Feinglos MN (1996) Gallobeudantite, $PbGa_3[(AsO_4),(SO_4)](OH)_6$, a new mineral species from Tsumeb, Namibia, and associated new gallium analogues of the alunite-jarosite family. Can Mineral 34:1305-1315

Jarosch D (1985) Kristallstruktur des Leonits; $K_2Mg(SO_4)_2(H_2O)_4$. Z Kristallogr 173:75-79

Jolly JH, Foster HL (1967) X-ray diffraction data of aluminocopiapite. Am Mineral 52:1220-1223

Kampf AR (1991) Grandreefite, $Pb_2F_2SO_4$: Crystal structure and relationship to the lanthanide oxide sulfates, $Ln_2O_2SO_4$. Am Mineral 76:278-282

Kannan KK, Viswamitra MA (1965) Crystal structure of magnesium potassium sulfate hexahydrate $MgK_2(SO_4)_2(H_2O)_6$. Z Kristallogr 122:161-174

Kato T (1977) Further refinement of the woodhouseite structure. N Jahrb Mineral Monatsh 54-58

Kato T, Miura Y (1977) The crystal structure of jarosite and svanbergite. Mineral J (Japan) 8:419-430

Kato K, Saalfeld H (1972) The crystal structure of hanksite, $KNa_{22}(Cl(CO_3)_2(SO_4)_9)$ and its relation to the K_2SO_4 I structure type. Acta Crystallogr B28:3614-3617

Keefer KD, Hochella MFJr, de Jong BHWS (1981) The structure of magnesium hydroxide sulfate hydrate $MgSO_4 \cdot 1/3Mg(OH)_2 \cdot 1/3H_2O$. Acta Crystallogr B37:1003-1006

Kellersohn T (1992) Structure of cobalt sulfate tetrahydrate. Acta Crystallogr C48:776-779

Kellersohn T, Delaplane RG, Olovsson I (1991) Disorder of a trigonally planar coordinated water molecule in cobalt sulfate heptahydrate, $CoSO_4 \cdot 7D_2O$ (bieberite). Z Naturforsch B46:1635-1640

Kemnitz E, Werner C, Trojanov SI (1996a) Structural chemistry of alkaline metal hydrogen sulfates. A review of new structural data. Part I. Synthesis, metal and sulfur polyhedra. Eur J Solid State Inorg Chem 33:563-580

Kemnitz E, Werner C, Trojanov SI (1996b) Structural chemistry of alkaline metal hydrogen sulfates. A review of new structural data. Part II. Hydrogen bonding systems. Eur J Solid State Inorg Chem 33:581-596

Kemnitz E, Werner C, Trojanov SI (1996c) Reinvestigation of crystalline sulfuric acid and oxonium hydrogensulfate. Acta Crystallogr C52:2665-2668

Kirfel A, Will G (1980) Charge density distribution in anhydrite, $CaSO_4$, from X-ray and neutron diffraction measurements. Acta Crystallogr B36:2881-2890

Klaska R, Jarchow O (1977) Synthetischer Sulfat-hydrocancrinit vom Mikrosommit-Typ. Naturwiss 64:93

Kolitsch U, Tiekink ERT, Slade PG, Taylor MR, Pring A (1999) Hinsdalite and plumbogummite, their atomic arrangements and disordered lead sites. Eur J Mineral 11:513-520

Konnert JA, Evans HTJr, McGee JJ, Ericksen GE (1994) Mineralogical studies of the nitrate deposits of Chile: VII. Two new saline minerals with the composition $K_6(Na,K)_4Na_6Mg_{10}(XO_4)_{12}(IO_3)_{12}\cdot 12H_2O$: fuenzalidaite (X = S) and carlosruizite (X = Se). Am Mineral 79:1003-1008

Krivovichev SV, Filatov SK (1999a) Structural principles for minerals and inorganic compounds containing anion-centered tetrahedra. Am Mineral 84:1099-1106

Krivovichev SV, Filatov SK (1999b) Metal arrays in structural units based on anion-centered metal tetrahedra. Acta Crystallogr B55:664-676

Krivovichev SV, Filatov SK, Semenova TF (1998a) Types of cationic complexes on the base of oxocentered tetrahedra $[OM_4]$ in crystal structures of inorganic compounds. Russ Chem Rev 67: 137-155

Krivovichev SV, Filatov SK, Semenova TF, Rozhdestvenskaya IV (1998b) Crystal chemistry of inorganic compounds based on chains of oxocentered tetrahedra. I. Crystal structure of chloromenite, $Cu_9O_2(SeO_3)_4Cl_6$. Z Kristallogr 213:645-649

Kucha H, Osuch W, Elsen J (1996) Viaeneite, $(Fe,Pb)_4S_8O$, a new mineral with mixed sulphur valences from Engis, Belgium. Eur J Mineral 8:93-102

Ladd MFC, Palmer RA (1994) Structure determination by X-ray crystallography. Plenum Press, New York

Lange J, Burzlaff H (1995) Single-crystal data collection with a Laue diffractometer. Acta Crystallogr A51:931-936

Larson AC, Cromer DT (1967) Refinement of the alum structures: III. X-ray study of the α-alums, K, Rb and $NH_4Al(SO_4)_2(H_2O)_{12}$. Acta Crystallogr 22:793-800

Leclaire A, Ledesert M, Monier JC, Daoud A, Damak M (1985) Structure du disulfate acide de triammonium. Une redetermination. Relations des chaines de liaisons hydrogene avec la morphologie et la conductivite eletrique. Acta Crystallogr B41:209-213

Lengauer CL, Giester G, Irran E (1994) $KCr_3(SO_4)_2(OH)_6$: Synthesis, characterization, powder diffraction data, and structure refinement by the Rietveld technique and a compilation of alunite-type compounds. Powder Diffraction 9:265-271

Levy AH, Lisensky GC (1978) Crystal structures of sodium sulfate decahydrate (Glauber's salt) and sodium tetraborate decahydrate (borax). Redetermination by neutron diffraction. Acta Crystallogr B34:3502-3510

Li G, Peacor DR, Essene EJ, Brosnahan DR, Beane RE (1992) Walthierite, $Ba_{0.5}\square_{0.5}[Al_3(OH)_6(SO_4)_2]$, and huangite, $Ca_{0.5}\square_{0.5}[Al_3(OH)_6(SO_4)_2]$, two new minerals of the alunite group from the Coquimbo region, Chile. Am Mineral 77:1275-1284

Li JJ, Zhou JL, Dong W (1990) The structure of amarillite. Chinese Sci Bull 35:2073-2075

Liebau F (1985) Structural chemistry of silicates. Springer-Verlag, Berlin

Lima-de-Faria J (1994) Structural mineralogy. Kluwer, Dordrecht, the Netherlands

Lima-de-Faria J, Hellner E, Liebau F, Makovicky E, Parthé E (1990) Nomenclature of inorganic structure types. Acta Crystallogr A46:1-11

Lindsay CG, Gibbs GV (1988) A molecular orbital study of bonding in sulfate molecules: implications for sulfate crystal structures. Phys Chem Mineral 15:260-270

Liu Tiegeng, Gong Guohong, Ye Lin (1995) Discovery and investigation of zinc-melanterite in nature. Acta Mineral Sinica 15:286-290 (in Chinese)

Livingstone A, Ryback G, Fejer EE, Stanley CJ (1987) Mattheddleite, a new mineral of the apatite group from Leadhills, Strathclyde region. Scottish J Geol 23:1-8

Louisnathan SJ, Gibbs GV (1972a) The effect of tetrahedral angles on SiBO bond overlap populations for isolated tetrahedra. Am Mineral 57:1614-1642

Louisnathan SJ, Gibbs GV (1972b) Bond length variation in TO^{n-}_4 tetrahedral oxyanions of the third row elements: T = Al, Si, P, S and Cl. Mat Res Bull 7:1281-1292

Louisnathan SJ, Hill RJ, Gibbs GV (1977) Tetrahedral bond length variations in sulfates. Phys Chem Minerals 1:53-69

Lynton H, Truter MR (1960) An accurate determination of the crystal structure of potassium pyrosulfate. J Chem Soc 5112-5118

Malinovskii YuA, Baturin SV, Belov NV (1979) The crystal structure of the Fe-tychite. Dokl Akad Nauk SSSR 249:1365-1368 (in Russian)

Marøy K (1971) The crystal structure of potassium pentathionate hemitrihydrate. Acta Chem Scand 25:2580-2590

Maslen EN, Ridout SC, Watson KJ, Moore FH (1988) The structures of Tuttons's salts. I. Diammonium hexaaqua magnesium(II) sulfate. Acta Crystallogr C44:409-412

Mathew M, Takagi S, Waerstad KR, Frazier AW (1981) The crystal structure of synthetic chukhrovite, $Ca_4AlSi(SO_4)F_{13}(H_2O)_{10}$. Am Mineral 66:392-397Matsuno T, Takayanagi H, Furuhata K, Koishi M, Ogura H (1984) The crystal structure of calcium sulfite hemihydrate. Bull Chem Soc Japan 57: 1155-1156

McDonald AM, Chao GY (1994) Abenakiite-(Ce), a new silicophosphate carbonate mineral from Mont Saint-Hilaire, Quebec: description and structure determination. Can Mineral 32:843-854

McGinnety JA (1972) Redetermination of the structures of potassium sulphate and potassium chromate: the effect of electrostatic crystal forces upon observed bond lengths. Acta Crystallogr B28:2845-2852

McKee ML (1996a) Computational study of the mono- and dianions of SO_2, SO_3, SO_4, S_2O_3, S_2O_4, S_2O_6 and S_2O_8. J Phys Chem 100:3473-3481

McKee ML (1996b) Additions and corrections: Computational study of the mono- and dianions of SO_2, SO_3, SO_4, S_2O_3, S_2O_4, S_2O_6 and S_2O_8. J Phys Chem 100:16444

McLean WJ, Anthony JW (1972) The disordered, zeolite-like structure of connellite. Am Mineral 57: 426-438

Medenbach O, Gebert W (1993) Lautenthalite, $PbCu_4[(OH)_6|(SO_4)_2]\cdot 3H_2O$, the Pb analogue of devillite: A new mineral from the Harz mountains, Germany. N Jahrb Mineral Monatsh 401-407

Mellini M, Merlino S (1977) The crystal structure of tuscanite. Am Mineral 62:1114-1120

Mellini M, Merlino S (1978) Ktenasite, another mineral with $((Cu,Zn)_2(OH)_3O)^{1-}$ octahedral sheets. Z Kristallogr 147:129-140

Mellini M, Merlino S (1979) Posnjakite. $(Cu_4(OH)_6(H_2O)O)$ octahedral sheets in its structure. Z Kristallogr 149:249-257

Menchetti S, Sabelli C (1974) Alunogen. Its structure and twinning. Tshchermaks mineral petrogr Mitt 21:164-178

Menchetti S, Sabelli C (1976a) Crystal chemistry of the alunite series: Crystal structure refinement of alunite and synthetic jarosite. N Jahrb Mineral Monatsh 406-417

Menchetti S, Sabelli C (1976b) The halotrichite group: The crystal structure of apjohnite. Mineral Mag 40:599-608

Menchetti S, Sabelli C (1980a) The crystal structure of klebelsbergite $Sb_4O_4(OH)_2SO_4$. Am Mineral 65:931-935

Menchetti S, Sabelli C (1980b) Peretaite, $CaSb_4O_4(OH)_2(SO_4)_2(H_2O)_2$: Its atomic arrangement and twinning. Am Mineral 65:940-946

Menchetti S, Sabelli C (1982) Campigliaite, $Cu_4Mn(SO_4)_2(OH)_6(H_2O)_4$, a new mineral from Campiglia Marittima, Tuscany, Italy. Am Mineral 67:385-393

Mereiter K (1972) Die Kristallstruktur des Voltaits, $K_2Fe^{2+}{}_5Fe^{3+}{}_3Al(SO_4)_{12}(H_2O)_{18}$. Tschermaks mineral petrogr Mitt 18:185-202

Mereiter K (1974) Die Kristallstruktur von Rhomboklas $(H_5O_2)^+(Fe(SO_4)_2(H_2O)_2)$. Tschermaks mineral petrogr Mitt 21:216-232

Mereiter K (1976) Die Kristallstruktur des Ferrinatrits, $Na_3Fe(SO_4)_3(H_2O)_3$. Tshchermaks mineral petrogr Mitt 23:317-327

Mereiter K (1979) Refinement of the crystal structure of langbeinite $K_2Mg_2(SO_4)_3$. N Jahrb Mineral Monatsh 182-188

Mereiter K (1982) Die Kristallstruktur des Johannits, $Cu(UO_2)_2(OH)_2(SO_4)_2(H_2O)_8$. Tschermaks mineral petrogr Mitt 30:47-57

Mereiter K (1986) Crystal structure and crystallographic properties of a schroeckingerite from Joachimsthal. Tschermaks mineral petrogr Mitt 35: 1-18

Merlino S, Mellini M, Bonaccorsi E, Pasero M, Leoni L, Orlandi P (1991) Pitiglianoite, a new feldspathoid from southern Tuscany, Italy: chemical composition and crystal structure. Am Mineral 76:2003-2008

Merlino S, Pasero M, Sabelli C, Trosti-Ferroni R (1992) Crystal structure refinements of spangolite, a hydrated basic sulphate of copper and aluminium, from three different occurrences. N Jahrb Mineral Monatsh 349-357

Moore AE, Taylor HFW (1970) Crystal structure of ettringite. Acta Crystallogr B26:386-393
Moore PB (1965) A structural classification of Fe–Mn orthophosphate hydrates. Am Mineral 50:2052-2062
Moore PB (1970) Structural hierarchies among minerals containing octahedrally coordinated oxygen. I. Stereoisomerism among corner-sharing octahedral and tetrahedral chains. N Jahrb Mineral Monatsh 163-173
Moore PB (1973) Bracelets and pinwheels: A topological-geometrical approach to the calcium orthosilicate and alkali sulfate structures. Am Mineral 58:32-42
Moore PB (1976) The glaserite, $K_3Na[SO_4]_2$, structure type as a 'super' dense-packed oxide: Evidence for icosahedral geometry and cation-anion mixed layer packings. N Jahrb Mineral Abh 127:187-196
Moore PB (1981) Complex crystal structures related to glaserite, $K_3Na(SO_4)_2$: Evidence for very dense packings among oxysalts. Bull Minéral 104:536-547
Moore PB, Shen J (1984) Roeblingite, $Pb_2Ca_6(SO_4)_2(OH)_2(H_2O)_2(Mn(Si_3O_9)_2)$: Its crystal structure and comments on the lone pair effect. Am Mineral 69:1173-1179
Moore PB, Kampf AR, Sen Gupta PK (2000) The crystal structure of philolithite, a trellis-like open framework based on cubic closest-packing of anions. Am Mineral 85:810-816
Mootz D, Bartmann K (1991) Hydrate der Fluorsulfonsaeure: Das Schmelzdiagramm des Systems FSO_3H-H_2O und die Kristallstruktur des Monohydrats $(H_3O)FSO_3$. Z Anorg Allg Chem 592:171-178
Mukhtarova NN, Kalinin VR, Rastsvetaeva RK, Ilyukhin VV, Belov NV (1980) The crystal structure of görgeyite $K_2Ca_5(SO_4)_6H_2O$. Dokl Akad Nauk SSSR 252:102-105
Mumme WG, Sarp H, Chiappero PJ (1994) A note on the crystal structure of schulenbergite. Arch Sci Geneve 47:117-124
Nagorsen G, Lyng S, Weiss A, Weiss A (1962) Zur Konstitution von $HgSO_4(HgO)_2$. Angew Chem 74:119
Okada K, Ossaka J (1980) Structures of potassium sodium sulphate and tripotassium sodium disulphate. Acta Crystallogr B36:919-921
Okada K, Hirabayashi J, Ossaka J (1982) Crystal structure of natroalunite and crystal chemistry of the alunite group. N Jahrb Mineral Monatsh 534-540
O'Keeffe M, Bovin JO (1978) The crystal structure of paramelaconite, Cu_4O_3. Am Mineral 63:180-185
O'Keeffe M, Hyde B (1985) An alternative approach to non-molecular crystal structures with emphasis on the arrangements of cations. Struct Bond 61:77-144
O'Keeffe M, Hyde B (1996) Crystal structures: I. Patterns and symmetry. Mineralogical Society of America, Washington, DC
O'Keeffe M, Domenges B, Gibbs GV (1985) Ab initio molecular orbital calculations on phosphates: comparison with silicates. J Phys Chem 89:2304-2309
Organova NI, Rastsvetaeva RK, Kuz'mina OV, Arapova GA, Litsarev MA, Fin'ko VI (1994) Crystal structure of low-symmetry ellestadite in comparison with other apatite-like structures. Kristallografiya 39:278-282 (in Russian)
Ossaka J, Hirabayashi J, Okada K, Kobayashi R, Hayashi T (1982) Crystal structure of minamiite, a new mineral of the alunite group. Am Mineral 67:114-119
O'Sullivan K, Thompson RC, Trotter J (1970) Crystal structure of ammonium fluorosulfate. J Chem Soc A:1814-1817
Otto HH (1975) Die Kristallstruktur von Fleischerite, $Pb_3Ge(OH)_6(SO_4)_2(H_2O)_3$ sowie kristallchemische Untersuchungen an isotypen Verbindungen. N Jahrb Mineral Abh 123:160-190
Pabst A, Sharp WN (1973) Kogarkoite, a new natural phase in the system Na_2SO_4–NaF–NaCl. Am Mineral 58:116-127
Pasero M, Davoli P (1987) Structure of hashemite, $Ba(Cr,S)O_4$. Acta Crystallogr C43:1467-1469
Payan F, Haser R (1976) On the hydrogen bonding in potassium hydrogen sulphate. Comparison with a previous crystal structure determination. Acta Crystallogr B32:1875-1879
Peacor DR, Rouse RC, Coskren TD, Essene EJ (1999a) Destinezite ('diadochite'), $Fe_2(PO_4)(SO_4)(OH)\cdot 6H_2O$: its crystal structure and role as a soil mineral at Alum Cave Bluff, Tennessee. Clays Clay Minerals 47:1-11
Peacor DR, Rouse RC, Essene EJ, Lauf RJ (1999b) Coskrenite-(Ce), $(Ce,Nd,La)_2(SO_4)_2(C_2O_4)\cdot 8H_2O$, a new rare-earth oxalate mineral from Alum Cave Bluff, Tennessee: characterization and crystal structure. Can Mineral 37:1453-1462
Pedersen BF, Semmingsen D (1982) Neutron diffraction refinement of the structure of gypsum, $CaSO_4(H_2O)_2$. Acta Crystallogr B38:1074-1077
Pertlik F (1971) Die Kristallstruktur von Poughit, $Fe_2(TeO_3)_2(SO_4)(H_2O)_3$. Tschermaks mineral petrogr Mitt 15:279-290
Pertlik F, Zemann J (1985) The crystal structure of scotlandite, $PbSO_3$. Tschermaks mineral petrogr Mitt 34:289-295
Pertlik F, Zemann J (1988) The crystal structure of nabokoite, $Cu_7TeO_4(SO_4)_5KCl$: The first example of a $Te(IV)O_4$ pyramid with exactly tetragonal symmetry. Mineral Petrol 38:291-298

Pollmann H, Witzke T, Kohler H (1997) Kuzelite ($Ca_4Al_2(OH)_{12}$)((SO_4)·$6H_2O$), a new mineral from Maroldweisach/Bavaria, Germany. N Jahrb Mineral Monatsh 423-432

Popova VI, Popov VA, Rudashevsky NS, Glavatskikh SF, Polyakov VO, Bushmakin AF (1987) Nabokoite, $Cu_7TeO_4(SO_4)_5$·KCl, and atlasovite, $Cu_6Fe^{3+}Bi^{3+}O_4(SO_4)_5$·KCl: new minerals of volcanic exhalations. Zap Vses Mineral Obshch 116:358-367 (in Russian)

Ptasiewicz-Bak H, McIntyre GJ, Olovsson I (1983) Structure of monoclinic nickel sulphate hexadeuterate, $NiSO_4(D_2O)_6$. Acta Crystallogr C39:966-968

Pushcharovsky DYu, Lima-de-Faria J, Rastsvetaeva RK (1998) Main structural subdivisions and structural formulas of sulphate minerals. Z Kristallogr 213:141-150

Ramondo F, Bencivenni L, Caminiti L, Sadun C (1991) Ab initio SCF study on lithium perchlorate and lithium sulfate molecules: geometries and vibrational frequencies. Chem Phys 151:179-186

Rastsvetaeva RK, Pushcharovsky DYu (1989) Kristallokhimiya sulfatov (= Crystal chemistry of sulfates). Itogi Nauki I Tekhniki, ser Kristallokhimiya Vol 23 (= Advances in Science and Technology, ser Crystal Chemistry) (in Russian)

Rius J, Allmann R (1984) The superstructure of the double layer mineral wermlandite ($Mg_7AlFe(OH)_{18}$)($Ca(H_2O)_6(SO_4)_2(H_2O)_6$. Z Kristallogr 168:133-144

Rius J, Plana F (1986) Contribution to the superstructure resolution of the double layer mineral motukoreaite. N Jahrb Mineral Monatsh 263-272

Roberts AC, Cooper MA, Hawthorne FC, Criddle AJ, Stanley CJ, Key CL, Jambor JL (1999) Sidpietersite, $Pb^{2+}{}_4(S^{6+}O_3S^{2-})O_2(OH)_2$, a new thiosulfate mineral from Tsumeb, Namibia. Can Mineral 37:1269-1273

Robinson DJ, Kennard CHL (1972) Potassium hexa-aquacopper(II) sulfate, $CuH_{12}K_2O_{14}S_2$. Cryst Struct Comm 1:185-188

Robinson PD, Fang JH (1969) Crystal structures and mineral chemistry of double-salt hydrates. I. Direct determination of the crystal structure of tamarugite. Am Mineral 54:19-30

Robinson PD, Fang JH (1971) Crystal structures and mineral chemistry of hydrated ferric sulphates: II. The crystal structure of paracoquimbite. Am Mineral 56:1567-1571

Robinson PD, Fang JH (1973) Crystal structures and mineral chemistry of hydrated ferric sulphates. III. The crystal structure of kornelite. Am Mineral 58:535-539

Robinson PD, Fang JH, Ohya Y (1972) The crystal structure of kainite. Am Mineral 57:1325-1332

Rouse RC, Dunn PJ (1982) A contribution to the crystal chemistry of ellestadite and the silicate sulfate apatites. Am Mineral 67:90B96

Ruben H, Zalkin A, Faltens MO, Templeton DH (1974) Crystal structure of sodium gold(I) thiosulfate dihydrate, $Na_3Au(S_2O_3)_2·2H_2O$. Inorg Chem 13:1836-1839

Rumanova IM, Malitskaya GI (1959) Revision of the structure of astrakhanite by weighted phase projection methods. Kristallografiya 4:510-525 (in Russian)

Sabelli C (1967) La struttura della Darapskite. Atti della Accad Naz Sci Fis Mat Natur Rend Ser 8 42: 874-887

Sabelli C (1980) The crystal structure of chalcophyllite. Z Kristallogr 151:129-140

Sabelli C (1985a) Refinement of the crystal structure of jurbanite, $Al(SO_4)(OH)(H_2O)_5$. Z Kristallogr 173:33-39

Sabelli C (1985b) Uklonskovite, $NaMg(SO_4)F(H_2O)_2$: New mineralogical data and structure refinement. Bull Minéral 108:133-138

Sabelli C, Ferroni T (1978) The crystal structure of aluminite. Acta Crystallogr B34:2407-2412

Sabelli C, Trosti-Ferroni R (1985) A structural classification of sulfate minerals. Per Mineral 54:1-46

Sabelli C, Zanazzi PF (1968) The crystal structure of serpierite. Acta Crystallogr B24:1214-1221

Sabelli C, Zanazzi PF (1972) The crystal structure of devillite. Acta Crystallogr B28:1182-1189

Sahl K (1970) Zur Kristallstruktur von Lanarkit, $Pb_2O(SO_4)$. Z Kristallogr 132:99-117

Sakae T, Nagata H, Sudo T (1978) The crystal structure of synthetic calcium phosphate sulfate hydrate, $Ca_2(HPO_4)(SO_4)(H_2O)_4$, and its relation to brushite and gypsum. Am Mineral 63:520-527

Sakamoto Y (1968) The size, atomic charges, and motion of the sulfate radical of symmetry 4-3m in the crystal of sulfohalite, $Na_6ClF(SO_4)_2$. J Sci Hiroshima Univ A32:101-108

Sandomirsky PA, Belov NV (1984) Crystal chemistry of mixed anionic radicals. Nauka, Moscow (in Russian)

Schindler M, Hawthorne FC, Baur WH (2000a) Crystal chemical aspects of vanadium: Polyhedral geometries, characteristic bond-valences and polymerization of (VO_n) polyhedra. Chem Mater 12:1248-1259

Schindler MC, Hawthorne FC, Baur WH (2000b) A crystal-chemical approach to the composition and occurrence of vanadium minerals. Can Mineral (accepted)

Schlatti M, Sahl K, Zemann A, Zemann J (1970) Die Kristallstruktur des Polyhalits, $K_2Ca_2Mg(SO_4)_4(H_2O)_2$. Tschermaks mineral petrogr Mitt 14:75-86

Schleid Th (1996) [NM_4] tetrahedra in nitride sulfides and chlorides of the trivalent lanthanides. Eur J Solid State Inorg Chem 33:227-240

Schlüter J, Klaska K-H, Gebhard G (1999) Changoite, $Na_2Zn(SO_4)_2{\cdot}4H_2O$, the zinc analogue of blödite, a new mineral from Sierra Gorda, Antofagasta, Chile. N Jahrb Mineral Monatsh 97-103

Schneider W (1967) Caracolit, das $Na_3Pb_2(SO_4)_3Cl$ mit Apatitstruktur. N Jahrb Mineral Monatsh 284-289

Schröpfer L (1973) Strukturelle Untersuchungen an $Ca(SO_3)(H_2O)_{0.5}$. Z Anorg Allg Chem 401:1-14

Scordari F (1977) The crystal structure of ferrinatrite, $Na_3(H_2O)_3(Fe(SO_4)_3)$ and its relationship to Maus's salt, $(H_3O)_2K_2(K_{0.5}(H_2O)_{0.5})_6(Fe_3O(H_2O)_3(SO_4)_6)(OH)_2$. Mineral Mag 41:375-383

Scordari F (1978) The crystal structure of hohmannite, $Fe_2(H_2O)_4((SO_4)_2)(H_2O)_4$ and its relationship to amaranite, $Fe_2(H_2O)_4((SO_4)_2O)(H_2O)_3$. Mineral Mag 42:144-146

Scordari F (1981a) Fibroferrite: a mineral with a $(Fe(OH)(H_2O)_2(SO_4))$ spiral chain and its relationship to $Fe(OH)(SO_4)$, butlerite and parabutlerite. Tschermaks mineral petrogr Mitt 28:17-29

Scordari F (1981b) Sideronatrite: a mineral with a $(Fe_2(SO_4)_4(OH)_2)$ guildite type chain? Tschermaks mineral petrogr Mitt 28:315-319

Scordari F (1981c) Crystal chemical implications on some alkali hydrated sulphates. Tschermaks mineral petrogr Mitt 28:207-222

Scordari F, Stasi F (1990) The crystal structure of euchlorine, $NaKCu_3O(SO_4)_3$. N Jahrb Mineral Abh 161:241-253

Scordari F, Stasi F, Milella G (1982) Concerning metasideronatrite. N Jahrb Mineral Monatsh 341-347

Scordari F, Stasi F, Schingaro E, Comunale G (1994) Analysis of the $(Na_{1/3},(H_2O)_{2/3})_{12}$-$(NaFe^{3+}{}_3O(SO_4)_6(H_2O_3))$ compound: Crystal structure, solid-state transformation and its relationship to some analogues. Z Kristallogr 209:43-48

Shannon RD (1976) Revised effective ionic radii and systematic studies of interatomic distances in halides and chalcogenides. Acta Crystallogr A32:751-767

Shiba H, Watanabe T (1931) Les structures des cristaux de northupite, de northupite bromee et de tychite. Comptes Rend Hebd Acad Sci 193:1421-1423

Singer J, Cromer DT (1959) The crystal structure analysis of zirconium sulphate tetrahydrate. Acta Crystallogr 12:719-723

Sliznev VV, Solomonik VG (1996) The structure and vibrational spectra of M_2SO_4 (M = Li, Na, K) molecules: ab initio SCF MO LCAO calculations with effective core potentials and with account taken of all electrons. Russ J Coord Chem 22:655-660

Smirnova NL, Akimova NV, Belov NV (1967) Crystal chemistry of the sulfates. J Struct Chem 8:65-68

Smirnova NL, Akimova NV, Belov NV (1968) Crystal chemistry of the sulfates. II. J Struct Chem 9:724-726

Smith GW, Walls R (1980) The crystal structure of görgeyite $K_2(SO_4)(Ca(SO_4))_5(H_2O)$. Z Kristallogr 151:49-60

Stadnicka K, Glazer AM, Koralewski M (1987) Structure, absolute configuration and optical activity of α-nickel sulfate hexahydrate. Acta Crystallogr B43:319-325

Starova GL, Filatov SK, Fundamensky VS, Vergasova LP (1991) The crystal structure of fedotovite, $K_2Cu_3O(SO_4)_3$. Mineral Mag 55:613-616

Starova GL, Filatov SK, Matusevich GL, Fundamensky VS (1995) The crystal structure of vlodavetsite, $AlCa_2(SO_4)_2F_2Cl{\cdot}4H_2O$. Mineral Mag 59:159-162

Steele IM, Pluth JJ, Richardson JW Jr (1997) Crystal structure of tribasic lead sulfate ($3PbO{\cdot}PbSO_4{\cdot}H_2O$) by X-rays and neutrons: An intermediate phase in the production of lead acid batteries. J Solid State Chem 132:173-181

Steele IM, Pluth JJ, Livingstone A (1998) Crystal structure of macphersonite ($Pb_4SO_4(CO_3)_2(OH)_2$): Comparison with leadhillite. Mineral Mag 62:451-459

Steele IM, Pluth JJ, Livingstone A (1999) Crystal structure of susannite, Pb_4SO_4 $(CO_3)_2(OH)_2$): A trimorph with macphersonite and leadhillite. Eur J Mineral 11:493-499

Süsse P (1967) Crystal structure of amarantite. Naturwiss 54:642-643

Süsse P (1968) Die Kristallstruktur des Botryogens. Acta Crystallogr B24:760-767

Süsse P (1970) The crystal structure of copiapite. N Jahrb Mineral Monatsh 286-287

Süsse P (1973) Slavikit: Kristallstruktur und chemische Formel. N Jahrb Mineral Monatsh 93-95

Szymanski JT (1985) The crystal structure of plumbojarosite $Pb(Fe_3(SO_4)_2(OH)_6)_2$. Can Mineral 23:659-668

Szymanski JT (1988) The crystal structure of beudantite, $Pb(Fe,Al)_3((As,S)O_4)_2(OH)_6$. Can Mineral 26:923-932

Tachez M, Theobald F, Watson KJ, Mercier R (1979) Redetermination de la structure du sulfate de vanadyle pentahydrate $VOSO_4(H_2O)_5$. Acta Crystallogr B35:1545-1550

Tahirov TH, Lu T-H, Huang C-C, Chung C-S (1994) A precise structure redetermination of nickel ammonium sulfate hexahydrate, $Ni(H_2O)_6{\cdot}2NH_4{\cdot}2SO_4$. Acta Crystallogr C50:668-669

Teng ST, Fuess H, Bats JW (1984) Refinement of sodium thiosulfate, $Na_2S_2O_3$ at 120K. Acta Crystallogr C40:1785-1787

Thomas JN, Robinson PD, Fang JH (1974) Crystal structures and mineral chemistry of hydrated ferric sulfates: IV. The crystal structure of quenstedtite. Am Mineral 59:582-586

Tossell JA, Vaughan DJ (1992) Theoretical geochemistry. Oxford University Press, New York

Treiman AH, Peacor DR (1982) The crystal structure of lawsonbauerite, $(Mn,Mg)_9Zn_4(SO_4)_2(OH)_{22}\cdot 8(H_2O)$, and its relation to mooreite. Am Mineral 67:1029-1034

Uraz AA, Armağan N (1977) An X-ray diffraction study of sodium thiosulfate pentahydrate, $Na_2S_2O_3\cdot 5H_2O$. Acta Crystallogr B33:1396-1399

Vairavamurthy A, Manowitz B, Luther GW, Jeon Y (1993) Oxidation state of sulfur in thiosulfate and implications for anaerobic energy metabolism. Geochim Cosmochim Acta 57:1619-1623

Varaksina TV, Fundamensky VS, Filatov SK, Vergasova LP (1990) The crystal structure of kamchatkite, a new naturally occuring oxychloride sulphate of potassium and copper. Mineral Mag 54:613-616

Vochten R, Van Haverbeke L, Van Springel K, Blaton N, Peeters OM (1995) The structure and physicochemical characteristics of synthetic zippeite. Can Mineral 33:1091-1101

Wan C, Ghose S, Rossman GR (1978) Guildite, a layer structure with a ferric hydroxy-sulphate chain and its optical absorption spectra. Am Mineral 63:478-483

Wang C-Q, Willner H, Bodenbinder M, Batchelor RJ, Einstein FWB, Aubke F (1994) Formation of cis-bis(carbonyl)palladium(II) fluorosulfate, cis-$Pd(CO)_2(SO_3F)_2$, and its crystal and molecular structure. Inorg Chem 33:3521-3525

Wang C-Q, Lewis AR, Batchelor RJ, Einstein FWB, Willner H, Aubke F (1996) Synthesis, molecular structure, and vibrational spectra of mer-tris(carbonyl)iridium(III) fluorosulfate, mer-$Ir(CO)_3(SO_3F)_3$. Inorg Chem 35:1279-1285

Wang X-B, Ding C-F, Nicholas JB, Dixon DA, Wang L-S (1999) Investigation of free singly and doubly charged alkali metal sulfate ion pairs: $M^+(SO_4^{2-})$ and $[M^+(SO_4^{2-})]_2$ (M = Na, K). J Phys Chem A103:3423-3429

Weidenthaler C, Tillmanns E, Hentschel G (1993) Orschallite, $Ca_3(SO_3)_2(SO_4)\cdot 12(H_2O)$, a new calcium-sulfite-sulfate-hydrate mineral. Mineral Petrol 48:167-177

Wildner M, Giester G (1988) Crystal structure refinements of synthetic chalcocyanite ($CuSO_4$) and zincosite ($ZnSO_4$). Mineral Petrol 39:201-209

Wildner M, Giester G (1991) The crystal structures of kieserite-type compounds: I. Crystal structures of $Me(II)SO_4\cdot H_2O$ (Me = Mn, Fe, Co, Ni, Zn). N Jahrb Mineral Monatsh 296-306

Willner H, Rettig SJ, Trotter J, Aubke F (1991) The crystal and molecular structure of gold tris(fluorosulfate). Can J Chem 69:391-396

Witzke T (1999) Hydrowoodwardite, a new mineral of the hydrotalcite group from Königswalde near Annaberg, Saxony/Germany and other localities. N Jahrb Mineral Monatsh 75-86

Wood MM (1970) The crystal structure of ransomite. Am Mineral 55:729-734

Yamnova NA, Pushcharovskii DYu, Vyatkin SV, Khomyakov AP (1992) Crystal structure of a new natural sulfatocarbonate $Na_{25}BaTR_2(CO_3)_{11}(HCO_3)_4(SO_4)_2F_2Cl$. Kristallografiya 37:1396-1402 (in Russian)

Zahrobsky RF, Baur WH (1968) On the crystal chemistry of salt hydrates. V. The determination of the crystal structure of $CuSO_4.3H_2O$ (bonattite). Acta Crystallogr B24:508-513

Zak Z, Kosicka M (1978) The crystal structure of lithium fluorosulphate $LiSO_3F$. Acta Crystallogr B34: 38-40

Zalkin A, Ruben H, Templeton DH (1964) The crystal structure and hydrogen bonding of magnesium sulfate hexahydrate. Acta Crystallogr 17:235-240

Zemann J, Zobetz E (1981) Do the carbonate groups in thaumasite have anomalously large deviations from coplanarity. Kristallografiya 26:1215-1217 (in Russian)

Zhang D, Rettig SJ, Trotter J, Aubke F (1996) Superacid anions: Crystal and molecular structures of $(H_3O)(Sb_2F_{11})$, $Cs(SO_3F)$, $Cs(H(SO_3F)_2)$, $Cs(Au(SO_3F)_4)$, $Cs_2(Pt(SO_3F)_6)$, and $Cs(Sb(SO_3F)_6)$. Inorg Chem 35:6113-6130

Zhou J, Li J, Dong W (1988) The crystal structure of xitieshanite. Kexue Tongbao 33:502-505

Zoltai T (1960) Classification of silicates and other minerals with tetrahedral structures. Am Mineral 45:960-973